This project was supported by the Centre for Global Eco-Innovation and is part financed by the European Regional Development Fund.

Innovation to increase the head for hydropower applications

By

Neil Barker

Academic Supervisor: Professor G. Aggidis
Industrial Supervisor: Professor D. McMinn

In collaboration with

Ocean Current Power Limited

European Union
European Regional Development Fund

Signed Declaration

Lancaster University

Faculty of Science and Technology

Engineering Department

Signed Declaration on the submission of a dissertation

"I declare that this dissertation is my own work and has not been submitted in substantially the same form towards the award of a degree or other qualification. Acknowledgement is made in the text of assistance received and all major sources of information have been appropriately referenced. I confirm that I have read and understood the publication Guidance on Writing Technical Reports published by the Department."

Signed ……

20th September 2019

Date ……

Abstract

This project investigated the potential power output using a Ram pump to artificially increase the pressure of water entering a turbine. Ocean Current Power Limited had a Patent detailing how this Ram pump power generator was constructed. The Centre for Global Innovation along with the European Union Development Fund commissioned for this Patent to be researched.

MATLAB computational software was used to build a simple model using the governing fluid equations. With a static head of 10m and an average fluid velocity of 1 ms^{-1} this managed to produce 150 kW of power. A more complicated 3D system model was produced and with the aid of ANSYS, a computational fluid dynamics program, a second mathematical model was completed. Using the same variables as the first model, 82 kW of power was generated. Finally, a third model was produced using a Kaplan bulb turbine the most recent state of the art turbines used in low head situations. This model was completed to confirm whether the Ram pump power generator was a viable option. Using the same variables and volumetric flow rates, the Kaplan bulb generated 330 kW of power. The Ram pump power generation system has the ability to generate power; however, turbines currently available on the market offer a greater power output for similar volumetric flow rates as they are more efficient.

Acknowledgements

I would like to express my great appreciation to my project supervisor, Professor George Aggidis. His ability to continually offer recommendations when it was assumed no further work could be achieved were invaluable. My thanks are also extended to Mr. Simeon Doyle (PhD Student) for all his assistance with the ANSYS modelling and Mr. Simon Baker (MRes student) for his help in the MATLAB modelling. I would also like to thank Professor Derek McMinn of Ocean Current Power Limited for allowing me to work on his Patent.

A sincere thank you to Dr. Louise Innes from Learning Development at the University of Lancaster for her constant support and for proofreading this dissertation. Her continued assistance throughout the year has been greatly appreciated.

Finally, I would like to thank my wife Kim and my children Holly and Sonny. Without their constant interjection, this project would have probably been completed two months earlier.

Contents

List of figures

List of tables

Notation

ASG- Archimedes screw generators

CFD-Computational Fluid Dynamics

CGE-Centre for Global Eco-innovation

ERDF-European Regional Development Fund

FF-Friction Factor

GHG-Greenhouse gasses

GWh-Gigawatt hours

HEC- High End Computing cluster at the University of Lancaster

IPO-Intellectual Property Office

MtCO2e-Million tonnes of equivalent Carbon Dioxide

N-S Navier-Stokes

OCPL-Ocean Current Power Limited

Ø-Internal pipe diameter

OWC- Oscillating water column

RANS-Reynolds Averaged Navier Stokes

RoR-Run of River

RP-Ram pump

TWh-Terawatt hours

UDF-User Defined Function

UK-United Kingdom

1. Introduction

The UK government's commitment to reducing greenhouse gasses began with the Kyoto Protocol in 1997 and was legislated through the Climate Change Act 2008. This act of parliament gave a firm commitment to reduce carbon emissions by 80% of the 1990 levels by 2050 (Department of Energy, 2008). A 2019 report by the Department of Energy and Climate Change stated a total of 364.1 $MtCO_2e$ (Million tonnes of carbon dioxide equivalent) was produced in the UK in 2018, with an estimated 87.4 $MtCO_2e$ of which was as a result of power generation. This gave power generation a 24% share of all greenhouse gasses produced in the UK (Department for Business, 2019).

To reduce these greenhouse gasses (GHG) within the power generation sector, clean, renewable energy has been invested in and subsidised by the UK government. As shown in Figure 1, the amount of renewable electricity generated in the UK in 2018 was 33% of the total amount. The breakdown of the type of renewable electricity generation is shown in Figure 2 (Department for Business, 2019).

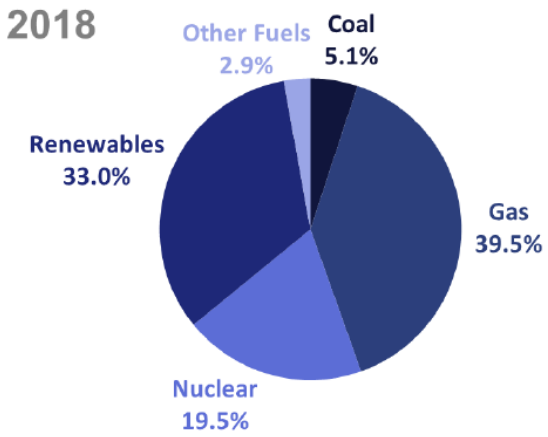

Figure 1 2018 UK share of electricity generation by fuel (Department for Business, 2019)

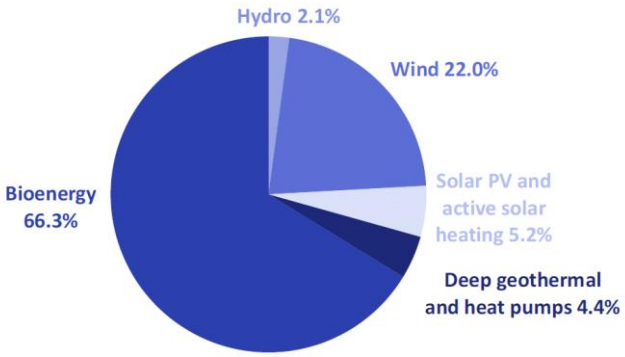

Figure 2 2018 UK Renewable use breakdown (Department for Business, 2019)

In addition to reducing greenhouse gasses in the developed world, 22% of the world's population is without electricity. Therefore, finding a way to generate clean, renewable and sustainable power would assist both causes. The commonest form of renewable power throughout the world is hydropower. It accounts for 16% of global electricity production (Kaya et al., 2015). The UK generated 8 TWh of electricity in 2018 from hydroelectric schemes. This is broken down to 5.5 TWh from storage/run-of-river and the remaining 2.5 TWh from pumped storage schemes. This hydroelectric power came from a total installed hydroelectric capacity of 1676MW (Department for Business, 2019). According to the UK government guidance notes published in 2013, there is between 850 to 1550 MW of hydroelectric untapped potential remaining within the UK (Department for Buisiness, 2013)

There are three main types of hydroelectric schemes: storage, run-of-river and pumped storage. Storage schemes use a dam to impound the fluid, creating a head differential between the dam wall and the penstock. This fluid is then used to generate electricity in the powerhouse as shown in Figure 3.

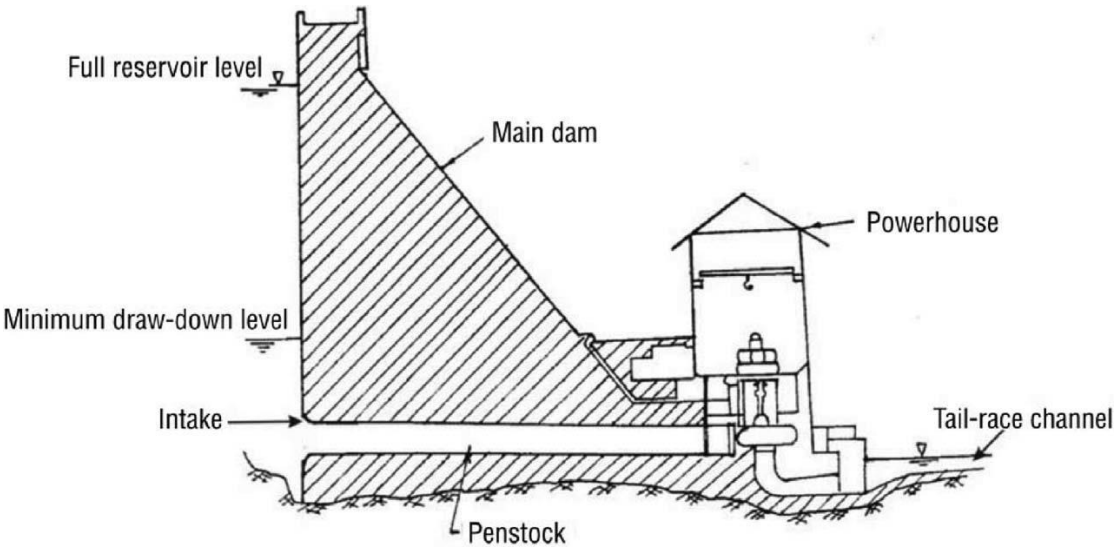

Figure 3 Typical hydropower scheme (Varun et al., 2010)

Pumped storage hydropower is used to regulate the peak power demands of the national grid. There are normally two reservoirs at differing heights which generate power via a turbine when the fluid is flowing from the upper to the lower reservoir. A schematic of the system is shown in Figure 4. When the peak power demand has been fulfilled, the turbines are used to pump the fluid back to the upper reservoir. The filling of the upper reservoir occurs using off-peak cheaper electricity and the generation happens during the peak times expensive electricity (Zhang et al., 2018)

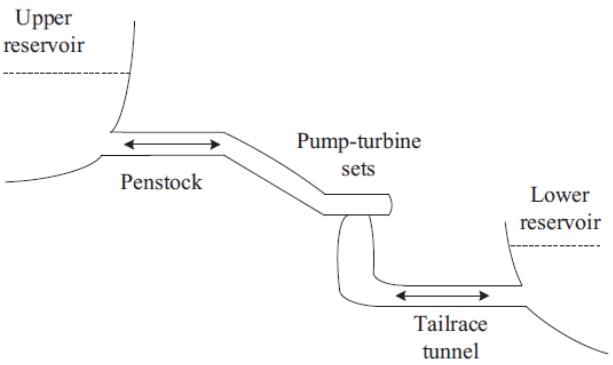

Figure 4 Pumped storage schematic model (Zhang et al., 2018)

Run-of-river schemes use the flow of the river to turn a low head fluid turbine. These schemes do not require a large dam to be constructed and are generally classed as more environmentally friendly. As they use the kinetic flow of the river and a small head to produce power, they are typically less than one megawatt in size. The small head usually comes from bypassing a weir already established within the river. As the fluid is not stored, they are also subject to seasonal changes in river flow patterns. A typical run of river set up is shown in Figure 5 where some of the river is diverted into a tank where it then flows through the penstock to the turbine (Paish, 2002).

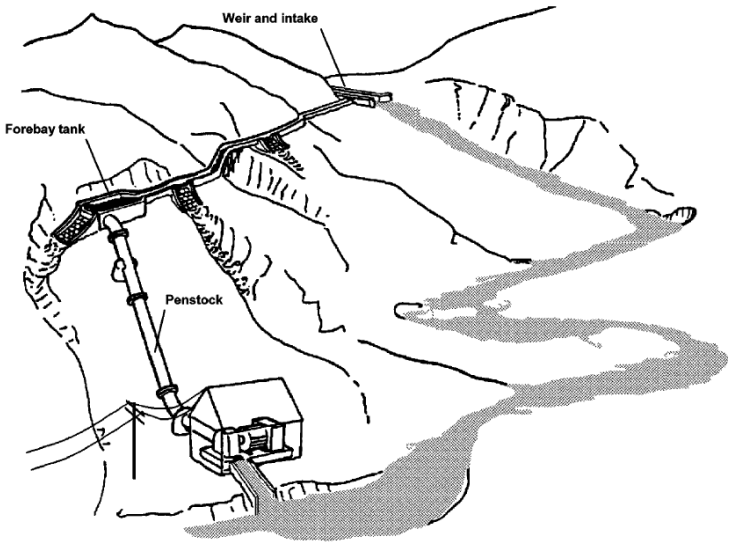

Figure 5 Run of river hydroelectric layout (Paish, 2002)

Ocean Current Power Limited (OCPL) are a new start-up company from Kingswinford in the West Midlands specialising in generating electricity through the movement of fast flowing water. OCPL created a concept design for a run-of-river power generation system. This concept used the water hammer effect to produce additional pressure that would be converted into electrical power. OCPL applied for a Patent through the Intellectual Property Office (IPO) and offered it to the University of Lancaster's Centre for Global Eco-innovation

(CGE) for further investigation. CGE gained additional funding through the European Regional Development Fund (ERDF) for the yearlong project and it commenced on the 1st October 2018.

1.1 Aims and Objectives

The overall aim of this project was to construct a model of the Patent that would be able to calculate the electrical power generated by the run-of-river system. To accomplish this, the following tasks were completed:

- Review the current literature on Ram pumps
- Review the current literature on Fluid turbines
- Review the Patent and all calculations associated with it
- Develop a mathematical model using MATLAB and confirm the power generated
- Construct a 3D model in SOLIDWORKS with the information from the MATLAB model
- Develop a computational fluid dynamic model using ANSYS and confirm the power generated
- Investigate the latest state of the art fluid power generating system currently available in the hydropower market
- Review all the models to confirm the viability of Ram pump power generation

2. Literature review

The literature review is split into two sections, the first examined the latest ram pump technology and the second reviewed the different types of fluid turbines available.

2.1. Ram pumps

Hydraulic ram pumps are a type of cyclic pump that lift water to a higher elevation. These types of pumps were first developed over 200 years ago as they do not require an external energy source to work. In addition, they are cheap, easy to maintain and simple to construct. They are still used today in remote parts of the world that do not have a reliable electricity supply to pump water (Young, 1995).

Ram pumps work by forcing a fraction of the fluid from an initial head to a higher head. Water flows through a pipe and is suddenly stopped using a valve. This increases the pressure in the pipe due to the momentum of the fluid abruptly changing. This additional pressure surge transfers the fluid into an exit pipe via a pressure vessel. Once the excess pressure has subsided, the valve opens and the cycle starts again. This pressure surge is known as “water hammer” (Young, 1995).

Since hydraulic ram pumps do not use fossil fuels to increase the head, such pump may be used to generate clean reliable electricity. Research into this area was undertaken by Roberts (2007), his work demonstrated how electricity can be extracted from a hydraulic ram pump.

2.1.1. Basic operation of a ram pump

The basic ram pump elements are shown Figure 6. These elements are as follows:

(a) Header tank
(b) Inlet pipe
(c) Impulse valve
(d) delivery valve
(e) Air chamber
(f) Exit pipe

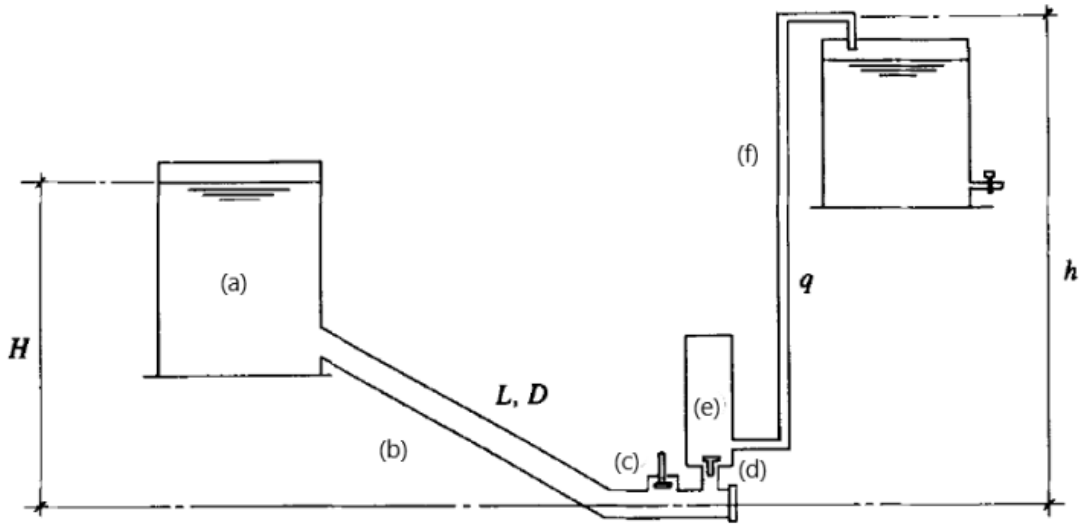

Figure 6 Ram pump elements (Young, 1995)

The operation of the ram pump can be divided into 3 separate sections:

1. Acceleration
2. Pumping
3. Recoil

Acceleration occurs when the impulse valve (c) is open and the delivery valve is closed. The fluid flows from the inlet tank (a), along the delivery pipe (b) and exits through the impulse valve to atmospheric pressure.

Once the velocity of the water has reached the set point (critical velocity), the impulse valve (c) is rapidly closed. Pumping is now present as the water hammer effect is now taking place. The induced shock wave propagates throughout the system moving at the speed of sound. This shock wave forces open the delivery valve and the fluid flows into the air chamber (d).

Once the pressure impulse has subsided, the recoil of the system occurs. This reduction in pressure closes the delivery valve and opens the impulse valve allowing the fluid to flow from the inlet tank again.

The velocity of the fluid through the three stages of pumping is shown in Figure 7. Each of the three coloured lines represents the velocity at sections (c), (d) and (f) in Figure 6.

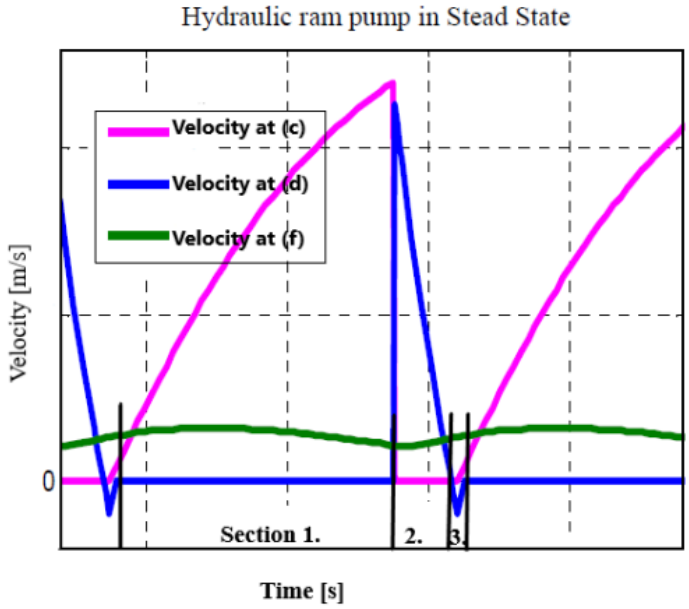

Figure 7 Ram pump velocity profile (de Carvalho et al., 2012)

2.1.2. Ram pumps used for pumping

Ram pump technology is still being researched for irrigation of farm land in remote areas. Inthachot et al, recently researched the construction of a ram pump in Thailand. Their idea was to build a robust ram pump out of locally sourced, off-the-shelf materials within Thailand and test it on the university campus (Inthachot et al., 2015).

Materials used:

- Supply head tank with a head of 3.5m
- Delivery head tank raised to a head of 9m
- Drive pipe with 30mm internal diameter PVC
- Three different pressure vessels were used: 0.6, 2.3 and 3.6 litre
- Four different valves were used for the impulse valve
    - 1” check (clap) valve Brass
    - 1” brazen valve brass
    - 3/4” PVC valve
    - 1 1/2” PVC valve

The arrangement of the valves, tanks, pressure vessel and pipes were arranged as shown in Figure 8.

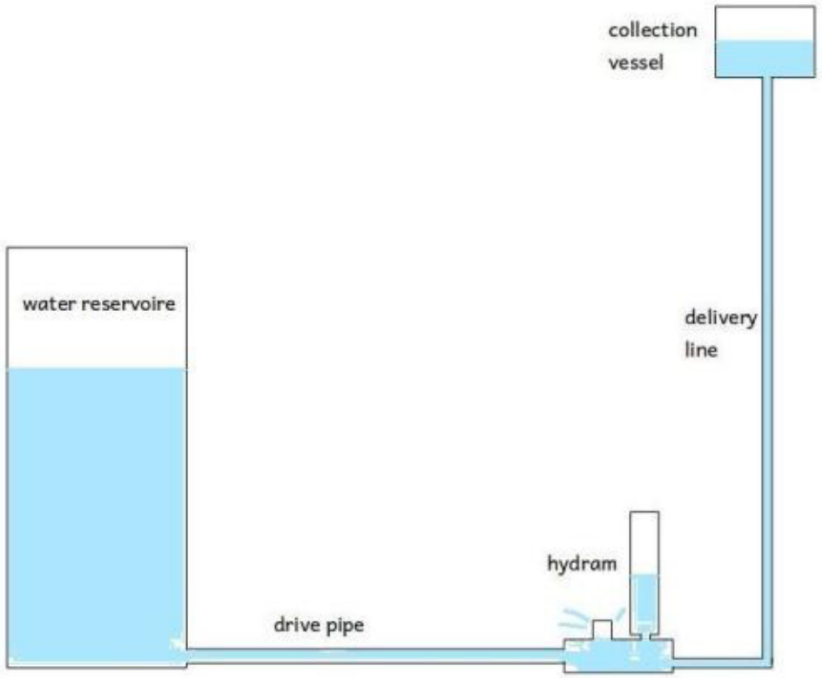

Figure 8 Schematic layout of the ram pump (Inthachot et al., 2015)

Inthachot et al, stated the installation was easy to assemble at a cost of US$20. Three sizes of pressure chamber were used: small (0.6l), medium (2,3l) and large (3.6l). It was observed that the small pressure chamber did not pump the water, however, the medium and larger pressure chambers performed reasonably with the efficiencies being 32.6% for the medium and 33.1 for the large pressure chamber. The valves worked in a similar fashion to each other, however, it was found that the PVC valves were receiving “visible shocks” from the water hammer effect. Trials were undertaken and the system ran continuously for 6 weeks before heavy rainfall caused a failure. This was due to the strainer at the inlet not being fixed in place during the initial trials allowing debris into the pump. Once the strainer was in place the pump ran for 8 weeks unhindered (Inthachot et al., 2015).

This study indicated that ram pumps may be built with limited funds for pumping fluids without the need of an electrical supply in remote areas. The efficiencies are low compared to standard devices for lifting water. However, as the power required to pump the fluid is generated by the river/stream, these efficiencies are not a major concern.

2.1.3. Ram pumps used for generating electricity

Roberts (2017) research on the hydrodynamics of the water hammer energy system considered extracting energy using ram pump technology. There were three ways considered for the power extraction and these are shown in Figure 9. Figure 9a uses the oscillating water column (OWC) to drive a Wells turbine, Figure 9b uses the pressure surges to drive a piston that is connected to a crankshaft and Figure 9c the pressure surge drives a floating magnet which induces a current in a coil of wire around the float.

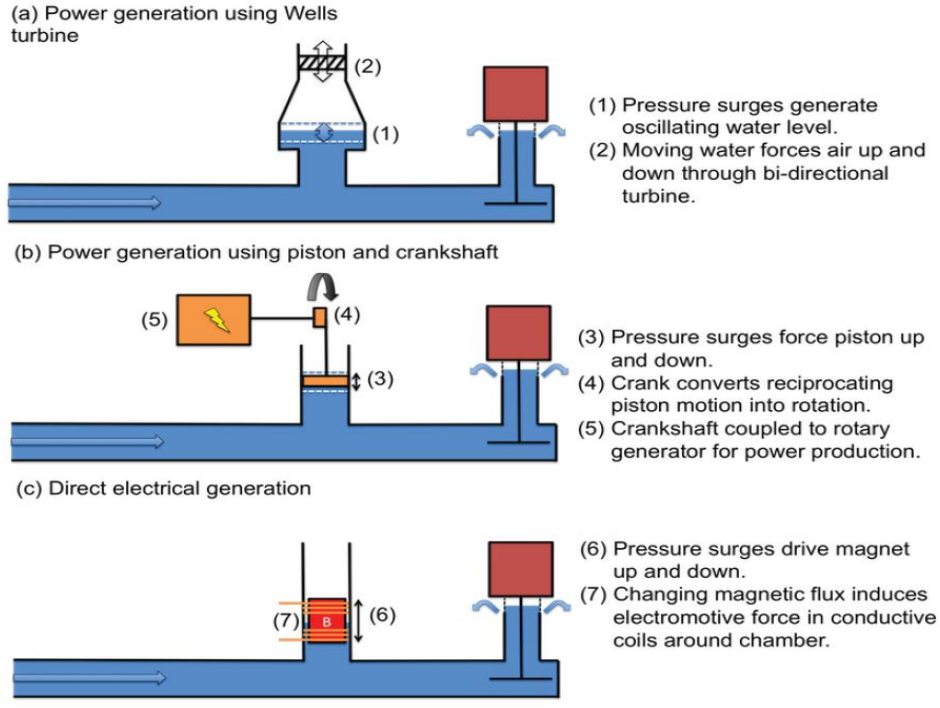

Figure 9 Three methods used for generating power using a hydraulic ram pump (Roberts, 2017)

Roberts (2017) examined the power density, scalability, durability, maintainability, economic potential and the environmental impact of a hydraulic ram pump used to create electricity.

Experiments were performed using a test rig comprising of a moving float to simulate the drive magnet in Figure 9c above. The scalability was calculated by constructing a mathematical model that mimicked the experimental results. This program was completed in MATLAB and the comparison results are shown in Figure 10.

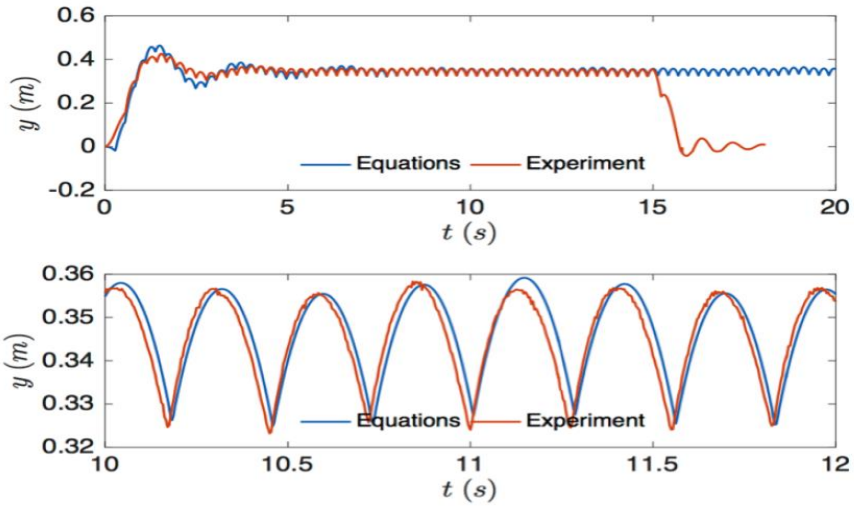

Figure 10 Comparison of mathematical and experimental results (Roberts, 2017)

The parameters in the program were altered to imitate sections of sea in Poole harbour. A cross sectional area of $1m^2$ was used for the drive pipe with a mean velocity of 0 to $2ms^{-1}$. The maximum theoretical hydrodynamic efficiency of the system was met when the impulse valve was operated at 0.5 Hz and the operating velocity of the impulse valve operated at 0.4 ms^{-1}. The mean power output was estimated at 0.77 to 3.81 kW across the sites and this equates to a total of 25 houses supplied with electricity used for power, lighting and heating. However, this took the ebb and flood of the tide into consideration. Using a theoretical constant flow, the mathematical model calculated there was enough energy to power 180 homes.

Conversion of the hydrodynamic energy of the mathematical model into electricity required an additional efficiency factor to be applied. An arbitrary 30% factor was applied to encompass all the loss associated with power generation and transmission. This brings the total number of houses that could be powered by the 7 ram pumps to 54 (Roberts, 2017).

One of the engineering challenges associated with the design was operating the impulse valve. A cam was used to operate the valve as shown in Figure 11 and was altered to find the most efficient frequency of operation (Roberts, 2017). This can be up scaled to larger valves by using the cam to fire larger electrically operated valves.

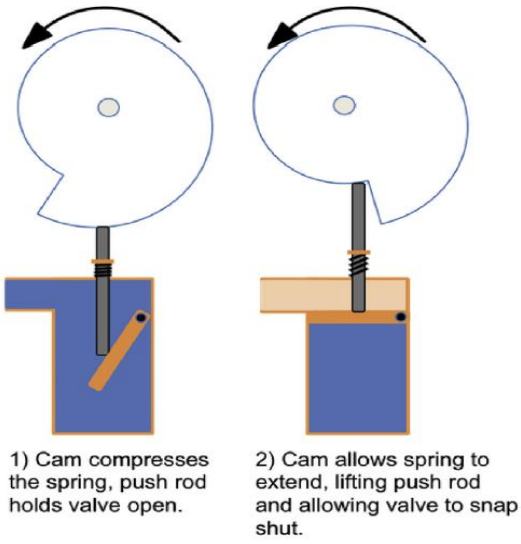

Figure 11 Cam for opening and closing the impulse valve (Roberts et al., 2018)

2.1.4. Ram pump Conclusion

Using ram pumps in remote areas to lift water looked to be a viable option. However, the test cases only used small ram pumps and it was not discussed if the system could be scaled up. PVC and Brass valves were used in the small-scale ram pumps and the PVC valves did not last as long as the brass equivalent valves. The force acting on the valves were not recorded so it

was not clear if the pressure on the valve exceeded the manufacturers specifications or there was a fault in the valve.

Roberts (2017) demonstrated that mechanical power can be developed by the use of water hammer, although the mean efficiency was low (0.3% to 1.7%) however, the peak efficiency was 25% at the instant when the valve was closed. This was using input data comparable to the data used in the Ocean Current Power Patent inlet.

The scalability of the PhD thesis was only conducted using the mathematical model; however, this model imitated the experimental data within acceptable tolerances. Therefore, the model may be scaled up to increase the power output of the system.

2.2. Fluid turbines

The mathematical models in subsequent sections calculate mechanical power. To obtain the electrical power, the efficiency of the turbine, transformer and transmission lines needed be taken into account. This section looked at the latest state of the art hydraulic turbines and their efficiencies.

There are two main types of water turbine: reaction and impulse. The reaction type does not change the direction of the water flow as much as the impulse, however it imparts a force on the angled blade as the fluid passes through. Impulse turbines change the velocity of the fluid as it hits the blade resulting in a change of momentum causing the blade to spin. In addition to the reaction and impulse there are two other types of fluid turbines: Archimedes screw and waterwheel. The turbine family tree is shown in Figure 12.

The various types of turbine offer differing hydraulic power outputs depending on volumetric flow rate (m^3s^{-1}) and head (m). The types of turbine and their hydraulic power output are shown in Figure 13. As shown in this figure, the Kaplan turbines are more suitable with low

head. Pelton turbines are more suitable with high head, and the Francis turbine works well at medium to high heads. At this project worked with low heads, only the crossflow, Kaplan and Francis were reviewed.

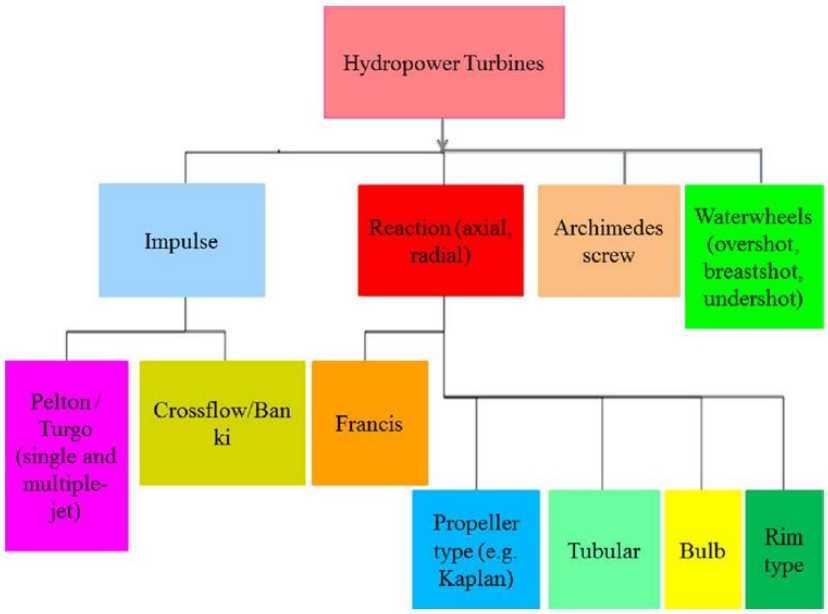

Figure 12 Turbine classifications (Kadier et al., 2018)

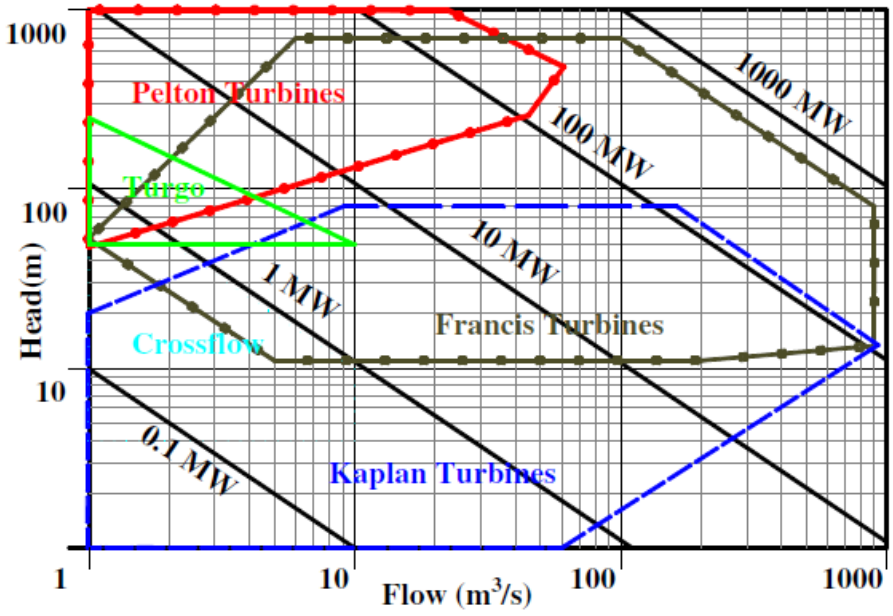

Figure 13 Turbine application range (Chen et al., 2013)

2.2.1. Crossflow turbines

The Crossflow turbine was originally invented by Mitchell and further developed by Bánki in the early twentieth century (Reihani et al., 2014). The main difference between the crossflow and other impulse turbines is that the fluid passes through the turbine blades twice. The efficiency is not as good as other impulse turbines, but is increased with this second pass through the blades. Crossflow turbines have low manufacturing costs as well as low maintenance costs which make them ideal for remote places with low to medium head. The setup of a single crossflow turbine is shown in Figure 14. The flow of the fluid through stages 1 and 2 in a crossflow turbine is shown in Figure 15 (Kaya et al., 2015).

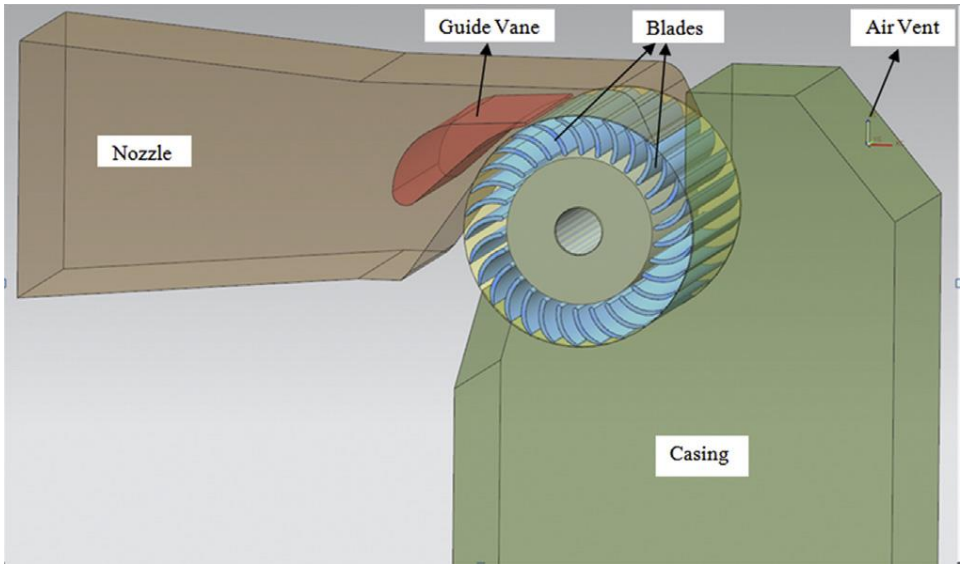

Figure 14 Crossflow turbine set up (Acharya et al., 2015)

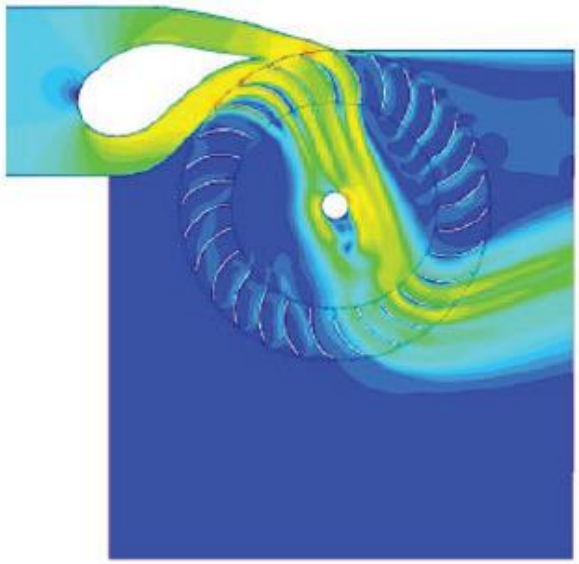

Figure 15 Crossflow turbine fluid flow (Aliman et al., 2018)

Changing the angle of the blades, velocity of the fluid entering the turbine (C1) and the velocity of the runner (U1) affects the efficiency of the turbine. (Aliman et al 2018), confirmed the highest efficiency rating of a crossflow turbine was approximately 83% and their work is shown in Figure 16.

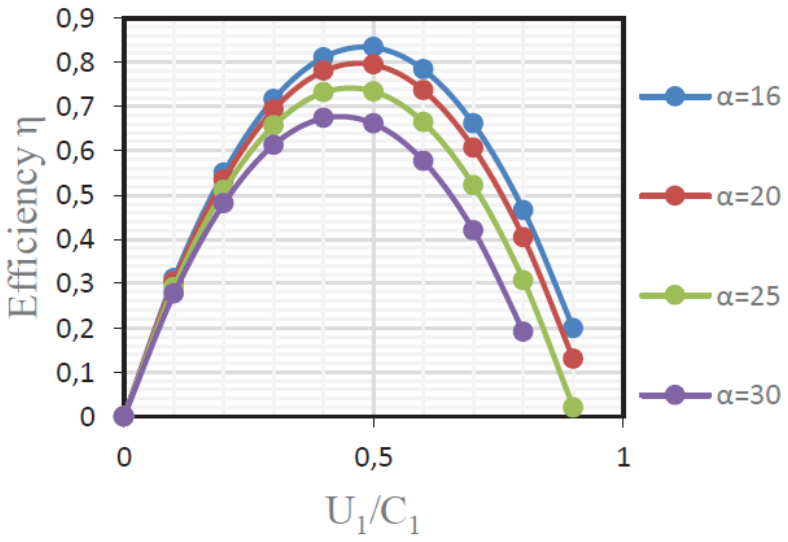

Figure 16 Efficiency with various crossflow blade angles (Aliman et al., 2018)

Introduction of air into the draft tube to increase efficiency was investigated by Chen and Choi (2015). Holes A and B shown in Figure 17 allowed air to be sucked into the chamber. The computational fluid dynamic model suggested there would be in increase from 77.8% to 81.3% in overall efficiency with the additional of this air flow (Chen and Choi, 2015).

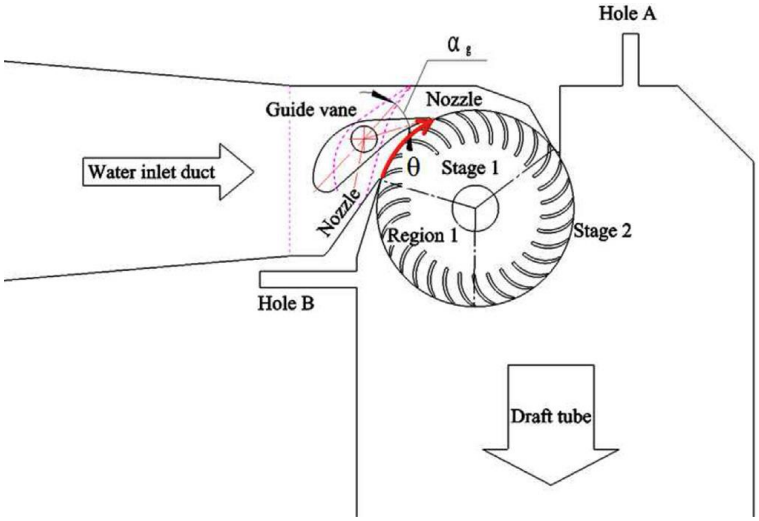

Figure 17 Cross flow turbine set up with air inlet (Chen and Choi, 2015)

2.1.5. Kaplan turbines

The Kaplan turbine was first developed in the early 20th century. Kaplan combined the adjustable guide vanes with adjustable runner blades to make the turbine (Karwata, 2003). The angle of the runner blades is adjusted by a control system located within the hub of the turbine as shown in Figure 18. Altering the guide vane reduces the amount of fluid entering the turbine and is shown in Figure 20. Therefore, by altering the pitch of the runner blades and the fluid entering the turbine, the system can be regulated. Furthermore, the regulation of these devices happens during operation, allowing the setup to be altered with changing head, flow and load on the turbine (Zhang et al., 2019).

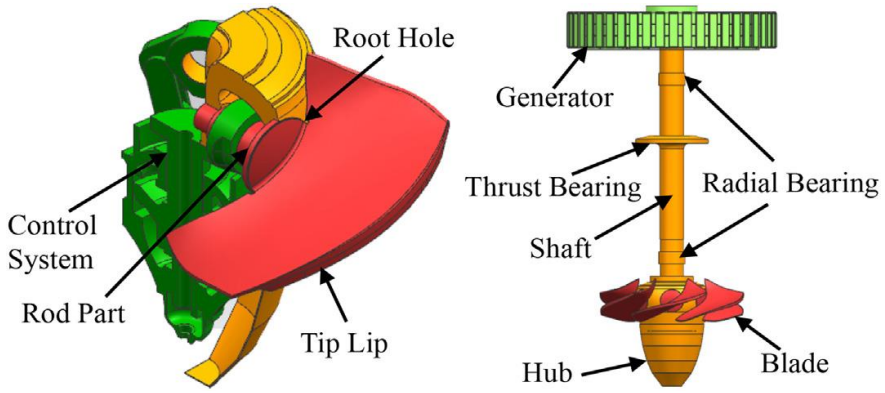

Figure 18 Typical Kaplan assembly (Zhang et al., 2019)

The Kaplan turbine and generator can be coupled together in two distinctive ways by the rim generator and the bulb generator. The rim generator is where the stator and rotor are located externally to the turbine. These require more room and are generally more expensive than the bulb type. They have slightly higher efficiencies due to the inertia generated from the additional rotor mass. The bulb system is where the generator is located directly on the rotor shaft. Figure 19 shows how a rim turbine is connected and Figure 20 a bulb connection.

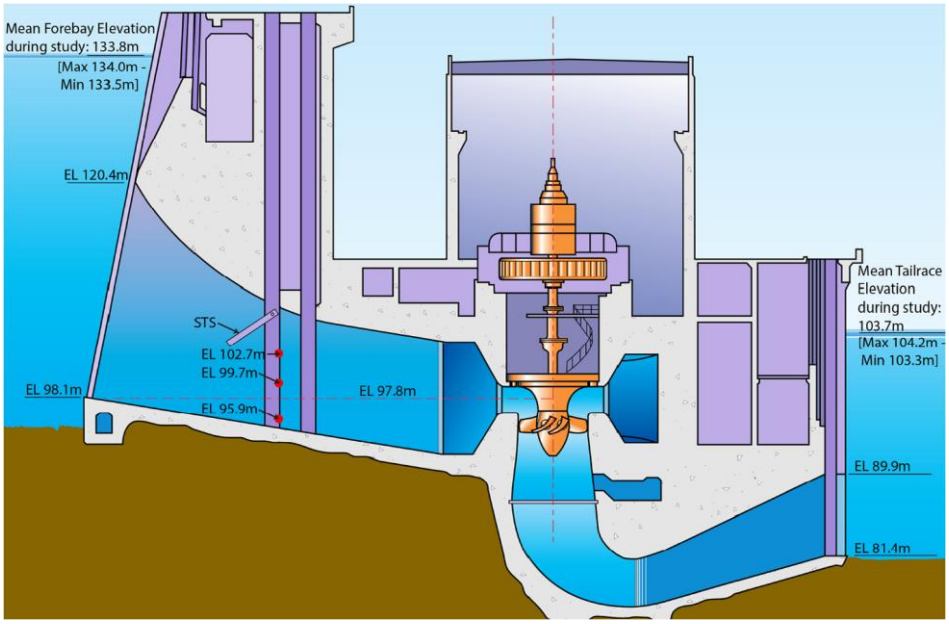

Figure 19 The Rim type Kaplan turbine (Martinez et al., 2019)

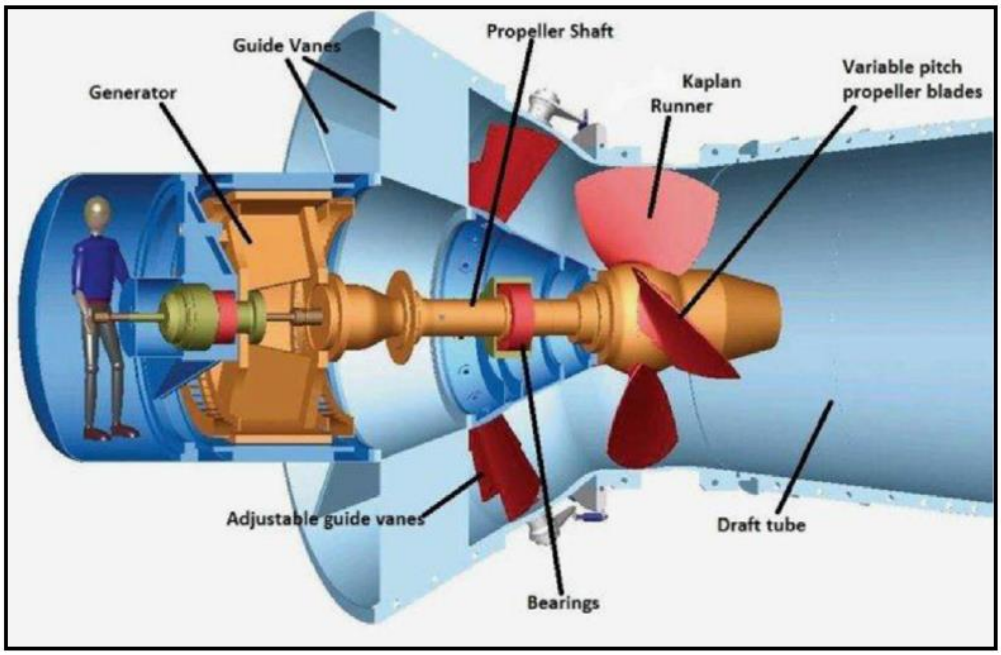

Figure 20 The Bulb Kaplan Turbine (Waters and Aggidis, 2016)

Using the latest Kaplan bulb turbine hill charts from manufacturer Andritz Hydro, the maximum efficiency is approximately 88%. This maximum efficiency is discussed further in chapter 7 Current state of the art technology. The Kaplan turbine works well at low heads and extremely versatile with varying output conditions. However, the capital expenditure is higher than most of the other fluid turbine installations which makes is difficult to justify in emerging markets (Kougias et al., 2019).

2.2.2. Francis turbines

The Francis turbine is another reaction turbine, first developed in the mid-19th century. It works in a similar way to the Kaplan; however, the runner blades are fixed as shown in Figure 21. Without this additional level of flexibility in the vanes, the Francis turbine is regulated by the guide vanes only. These vanes restrict the flow of the fluid entering the runner which in turn restricts the power output. The maximum power output is reached when the guide vanes are opened fully (Viollet, 2017).

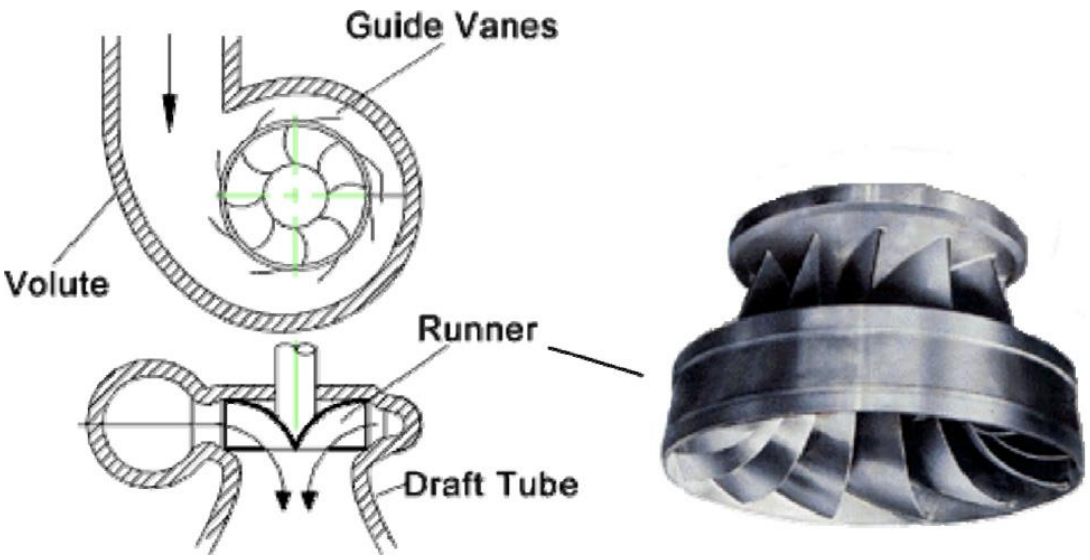

Figure 21 Francis turbine (Okot, 2013)

When the guide vanes are fully open, the maximum power output is limited to 95%. This is due to cavitation around the runner blades at these increased fluid velocities. The cavitation is reduced by installing a draft tube, which diffuses the exiting fluid, however these cavitation's are still present at high velocities. A non-dimensional 'hill chart' was produced using empirical data from small scale models and published by Guo et al (2017) with the results shown in Figure 22. This included the cavitation boundaries to find the optimal efficiency. With a head of 100m the optimal efficiency of their turbine was 94% (Guo et al., 2017).

Throughout the world the Francis turbine is the most used turbine for generating electricity with over 60% of the total power generation turbines being this type (Goyal and Gandhi, 2018).

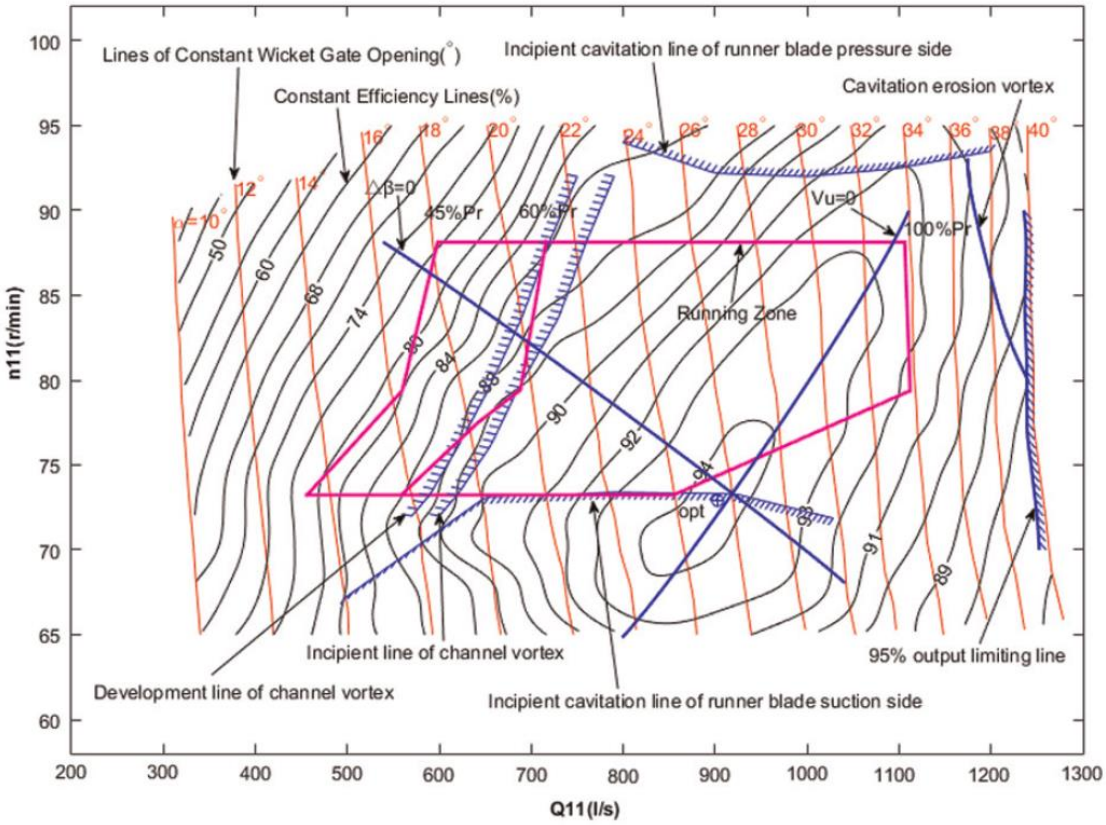

Figure 22 Francis turbine 'hill chart' with 100m of head (Guo et al., 2017)

2.2. Turbine conclusion

Using ram pump technology to generate electricity is a relatively new concept. The most recent research was undertaken by Roberts in 2018. However, there has been research in the last 5 years on using ram pumps in remote areas for irrigation and lifting water. As these remote areas are normally void of electricity, the ram pump is ideal for pumping water. In addition, they are cheap to manufacture, construct and maintain. Once the commissioning teething troubles have been ironed out, they are extremely reliable.

Depending on the head and flow rates available there is a turbine that will offer over 75% efficiency. Recent interest in turbine efficiency has resulted in a number of studies applying CFD to all available types of turbine. As computing power is becoming cheaper, bigger CFD models are being produced looking to increase the efficiency of all turbines.

Combining a ram pump with a highly efficient turbine could result in a viable, cost effective system for use in remote areas to generate electricity. However, this would require the ram pump to adequately increase the pressure enough to compensate for the acceleration phase of the system.

3. Patent review

The patent supplied by Ocean Current Power Limited (OCPL) is confidential and not in the public domain at present. This section explored the patent and the fluid calculations contained within it to confirm its accuracy. The full patent is located in Appendix A.

3.1. Ram pump stages

The patent consists of 5 stages as shown in Figure 23. Stage 1 is the inlet that funnels the fluid increasing the velocity. The fluid then passes through the ram valve in stage 2 with the accelerated fluid passing up through the air pressure tanks (stage 3) to the turbine in stage 4. Finally, stage 5 where the turbine is connected to a generator. As well as the straight inlet, there was also a drop inlet designed to increase the velocity within the patent and this is shown in Figure 24.

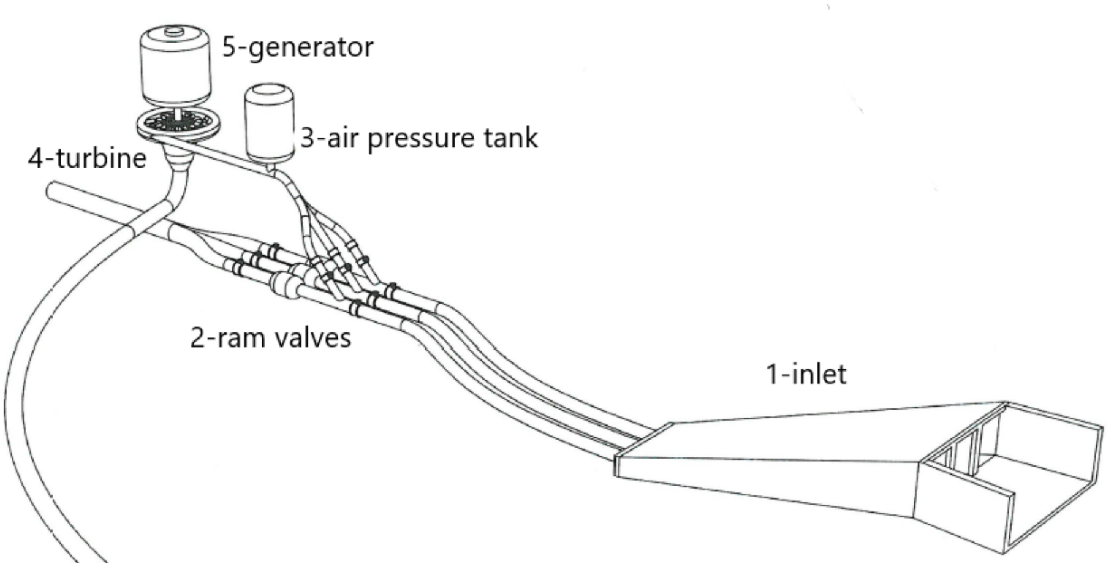

Figure 23 The five stages of the ram pump generation system patent

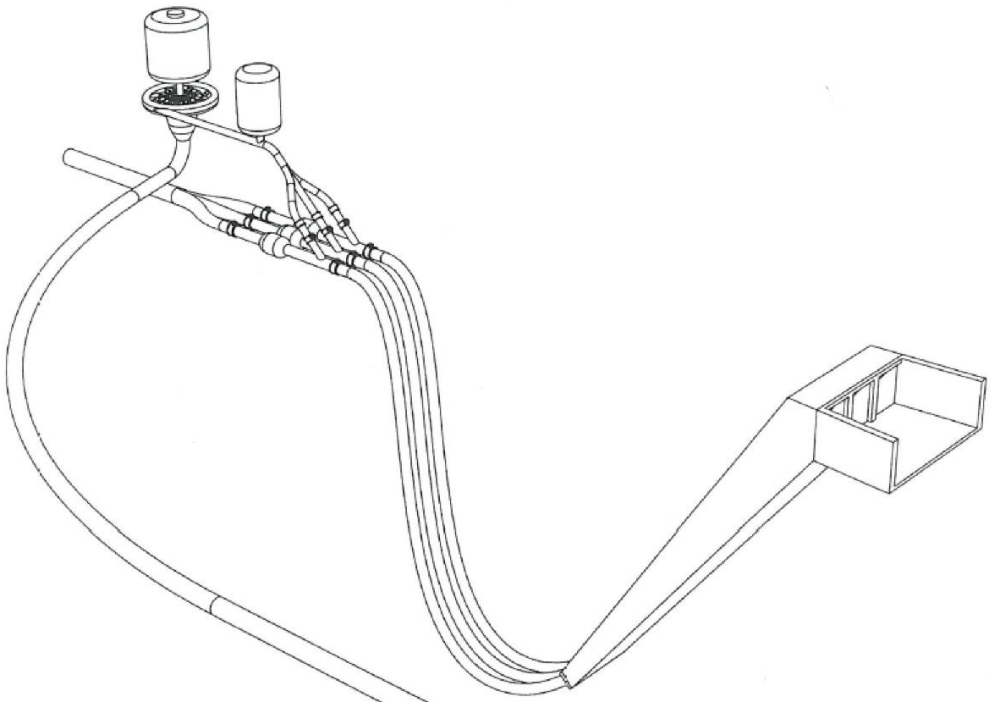

Figure 24 Patent drop inlet

3.2. Straight inlet

Stage one of the patent concentrated on the inlet from the river. The varying river heights and velocities in the patent revolve around the River Seven in an area of Worcester. However, the calculations have been extended to incorporate additional pressures that may be present in other rivers around the world.

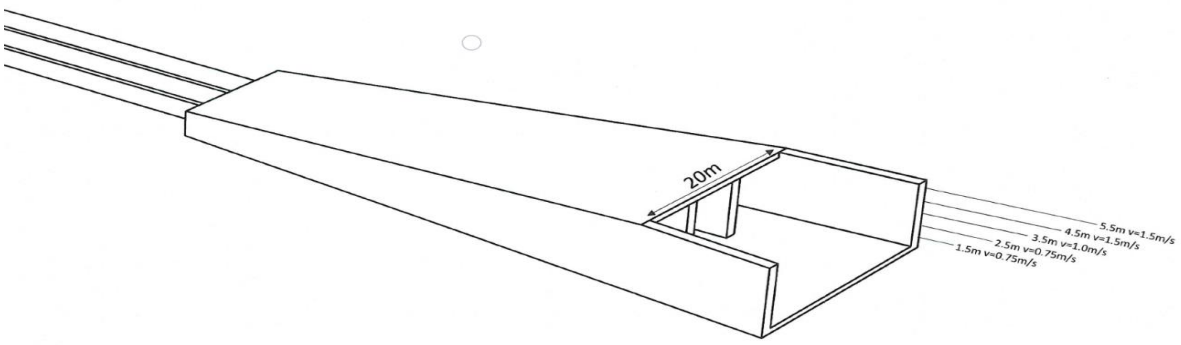

Figure 25 Patent straight inlet

The straight inlet as shown in Figure 25 has a width of 20m and a height of 5.5m. The height of the fluid varies from 1.5 to 5.5m depending on the flow of the river. The velocity is also dependant on this and is set between 0.75 and 1.5 ms^{-1}. The outlet consists of 3 pipes that have an internal diameter of 1.3m. These pipes can be operated to use either 1, 2 or all 3 of them in parallel.

Using this information, a matrix was constructed with all the various river heights, velocities and outlet pipes used and is shown in Table 1. The patent calculated the exit velocities of some of the permutations using the conservation of mass continuity equation (3.1). However, this does not calculate the pressure within the system. Therefore, Bernoulli's equation was used to calculate the pressures required to achieve these velocities.

$$\rho A_1 V_1 = \rho A_2 V_2 \qquad (3.1)$$

ρ – Density of water ($kg \cdot m^{-3}$)
A_1 – Inlet surface area (m^2)
V_1 – inlet velocity (ms^{-1})
A_2 – outlet surface area (m^2)
V_2 – outlet velocity (ms^{-1})

Table 1 Calculations from the patent

Model Number	Patent	Inlet width (m)	River height (m)	Inlet surface area (m^2)	Inlet velocity (ms^{-1})	Outlet Internal diameter (m)	Number of pipes	Outlet surface area (m^2)	Patent outlet velocity (ms^{-1})
1	fig 13	20	1.5	30	0.75	1.3	1	1.33	16.95
2		20	1.5	30	0.75	1.3	2	2.65	8.48
3		20	1.5	30	0.75	1.3	3	3.98	5.65
4	fig 21	20	2.5	50	0.75	1.3	1	1.33	28.25
5		20	2.5	50	0.75	1.3	2	2.65	14.13
6		20	2.5	50	0.75	1.3	3	3.98	9.42
7	fig 22	20	3.5	70	1	1.3	1	1.33	52.74
8		20	3.5	70	1	1.3	2	2.65	26.37
9		20	3.5	70	1	1.3	3	3.98	17.58
10	fig 23	20	4.5	90	1.5	1.3	1	1.33	101.71
11		20	4.5	90	1.5	1.3	2	2.65	50.85
12		20	4.5	90	1.5	1.3	3	3.98	33.90
13	fig 24	20	5.5	110	1.5	1.3	1	1.33	124.31
14		20	5.5	110	1.5	1.3	2	2.65	62.16
15		20	5.5	110	1.5	1.3	3	3.98	41.44

Hand calculations were performed using the full form of Bernoulli's equation. The dynamic pressure of the river water was calculated using equation (3.2). This was added to the static pressure to give a total inlet pressure. For the first set of calculations, 0m of static pressure was used. However, a further 4 sets of studies were completed with various static heads of 5m, 10m, 15m and 20m applied and these are shown in full in Appendix B.

$$p = \frac{\rho * V^2}{2} \qquad (3.2)$$

p – Dynamic Pressure (Pa)
ρ – Density of water ($kg \cdot m^{-3}$)
V – Fluid velocity (ms^{-1})

Due to the inlet being horizontal, Bernoulli's equation (3.3) was simplified to that shown in equation (3.4). The total inlet pressure was calculated by adding the dynamic pressure of the flowing fluid to the static pressure. Using the inlet pressure, inlet velocity and outlet velocity

the outlet pressure was calculated for all 15 studies and are shown in appendix B. The negative outlet pressures in the table confirmed a suction pressure was required to generate the velocities calculated in the patent. The negative pressures were converted into additional head that was required to achieve the velocities.

In order to calculate the actual maximum outlet velocity, a pressure of 1Pa was applied to the outlet in equation (3.4). In reality this pressure would not be ideal to use in hydraulic power generation and was incorporated into the table to show the maximum velocity only.

$$P_1 + \frac{1}{2}\,\rho\, v_1^2 + \rho g h_1 = P_2 + \frac{1}{2}\,\rho\, v_2^2 + \rho g h_2 \qquad (3.3)$$

$$P_1 - P_2 = \frac{1}{2}\,\rho(\, v_2^2 - \, v_1^2) \qquad (3.4)$$

P_1 – total inlet pressure (Pa)
P_2 – total outlet pressure (Pa)
v_1 – inlet velocity (ms^{-1})
v_2 – outlet velocity (ms^{-1})
g – acceleration due to gravity (ms^{-2})
h_1 – inlet height (m)
h_2 – outlet height (m)

Supplementary static head was applied to the calculations to establish if the original velocities could have been reached. The additional 5, 10, 15 and 20m of static head was added to the hand calculations and are shown in Appendix B.

3.2.1. Validation of the hand calculations

ANSYS CFX was used to complete the steady state computational fluid dynamic calculations for each of the models. This software required a solid model of the fluid. A simple cone was constructed with the inlet and outlet dimensions of all 15 studies shown in Table 2. The cones were constructed in SOLIDWORKS with funnel 1 as shown in Figure 26.

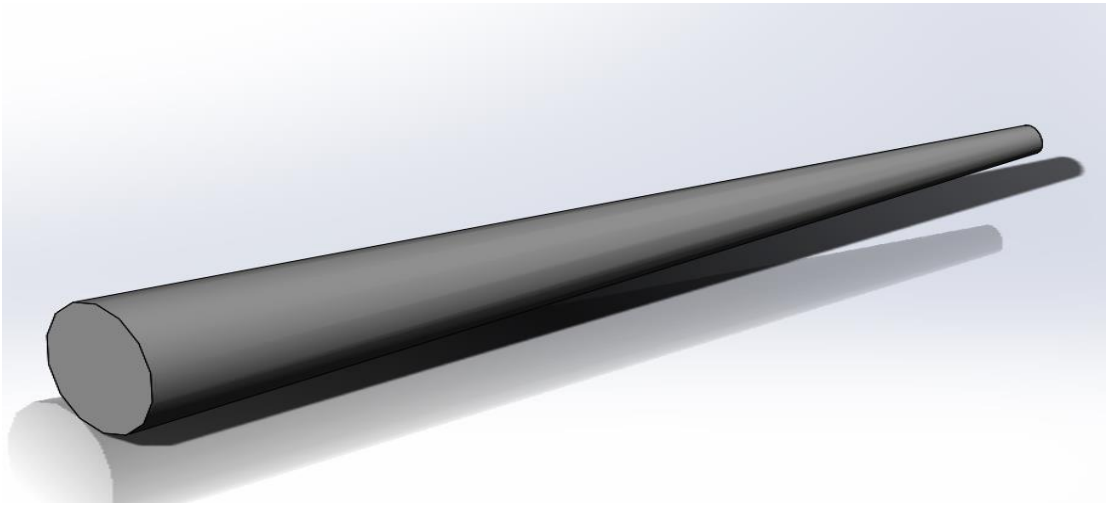

Figure 26 Simplified model of the inlet

Table 2 Model inlet and outlet dimensions

Funnel Number	Patent	Inlet width (m)	River height (m)	Inlet surface area (m^2)	inlet Radius	Outlet int. dia. (m)	Number of pipes	Outlet surface area (m^2)	SOLIDWORKS outlet radius
1	fig 13	20	1.5	30	3.090	1.3	1	1.33	0.650
2		20	1.5	30	3.090	1.3	2	2.65	0.919
3		20	1.5	30	3.090	1.3	3	3.98	1.126
4	fig 21	20	2.5	50	3.989	1.3	1	1.33	0.650
5		20	2.5	50	3.989	1.3	2	2.65	0.919
6		20	2.5	50	3.989	1.3	3	3.98	1.126
7	fig 22	20	3.5	70	4.720	1.3	1	1.33	0.650
8		20	3.5	70	4.720	1.3	2	2.65	0.919
9		20	3.5	70	4.720	1.3	3	3.98	1.126
10	fig 23	20	4.5	90	5.352	1.3	1	1.33	0.650
11		20	4.5	90	5.352	1.3	2	2.65	0.919
12		20	4.5	90	5.352	1.3	3	3.98	1.126
13	fig 24	20	5.5	110	5.917	1.3	1	1.33	0.650
14		20	5.5	110	5.917	1.3	2	2.65	0.919
15		20	5.5	110	5.917	1.3	3	3.98	1.126

Once the models were imported into ANSYS, a simple mesh was constructed (shown in Figure 27) and the boundary conditions were applied as per Table 4. The outlet boundary condition was the proposed outlet velocity provided by the patent which were in dispute. The inlet boundary condition was the total pressure applied to the inlet. The total pressure is equal to the dynamic pressure (fast flowing water) plus the static head. The total pressure in the first 15 studies was with 0m static head.

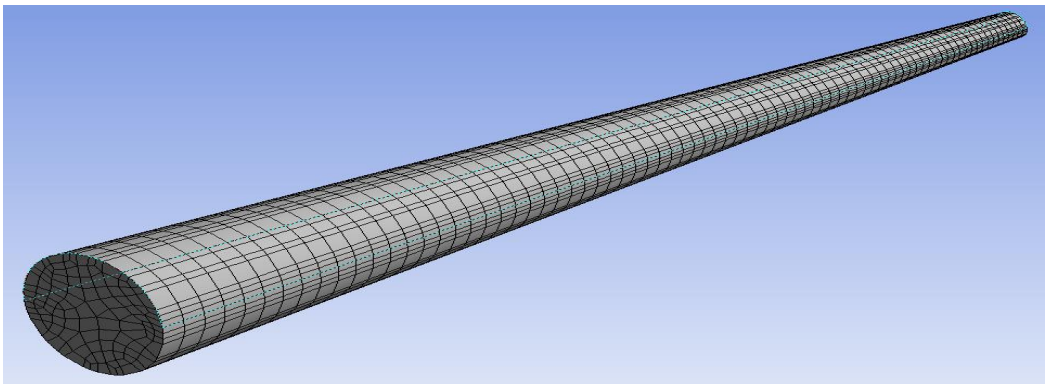

Figure 27 ANSYS CFX meshing

The mesh quality metrics for the simple funnel are shown in Table 3 and these results are within acceptable tolerances. These metrics are discussed in greater detail in chapter 5.

Table 3 Mesh sensitivity analysis

Mesh metric	Element quality	Aspect ratio	Skewness	Orthogonal quality
Minimum	0.16276	1.1839	0.0018	0.13847
Maximum	0.9033	9.873	0.86153	0.98938
Average	0.78042	2.0333	0.29771	0.70134
Standard deviation	0.11572	0.59322	0.13049	0.12908
Ansys manual maximum value to obtain accuracy	N/A	35	0.95	>0.01
Ansys manual average value to obtain accuracy	>0.75	5	0.33	N/A

Table 4 ANSYS CFX Boundary conditions with 0m static head

Boundary conditions set in ANSYS	
Outlet velocity (ms^{-1})	**Total inlet pressure (Pa)**
16.95	281.25
8.48	281.25
5.65	281.25
28.25	281.25
14.13	281.25
9.42	281.25
52.74	500
26.37	500
17.58	500
101.71	1125
50.85	1125
33.90	1125
124.31	1125
62.16	1125
41.44	1125

To determine if the fluid flowing through the funnel was turbulent or laminar, the Reynolds number was calculated using the equation shown in (3.5). If the Reynolds number is below 2100 the flow is classed as laminar and if the Reynolds number is greater than 4000 the flow is classed as turbulent. If the Reynolds number is between 2100 and 4000, the flow is in the transitional region.

$$Re = \frac{\rho V D}{\mu} \qquad (3.5)$$

Re-Reynolds number
ρ-Density of the fluid (kg·m-3)
V-Average fluid velocity (m·s-1)
D-Pipe diameter (m)
μ-Dynamic viscosity (Pa·s)

If the fluid viscosity was 1.308 Pa·s (water at 10°C), mean velocity was 4 m/s, pipe diameter at the outlet 1.5 m and the density of the fluid was 1000 $kg{\cdot}m^{-3}$ the Reynolds number would be

4587 and classed as a turbulent flow. Therefore, any flow in excess of 4 m/s within the 1.5 m diameter pipe would be turbulent. Bernoulli's principle is used for laminar flows and therefore may give errors when higher levels of turbulence are introduced to the flow.

A sample from of the ANSYS solution is shown in Figure 28. A probe within ANSYS CFX was used to confirm the velocities and pressures at the outlet with the results recorded. All the results from the 15 studies with 0, 5, 10, 15 and 20m of additional static head applied are shown in Appendix B.

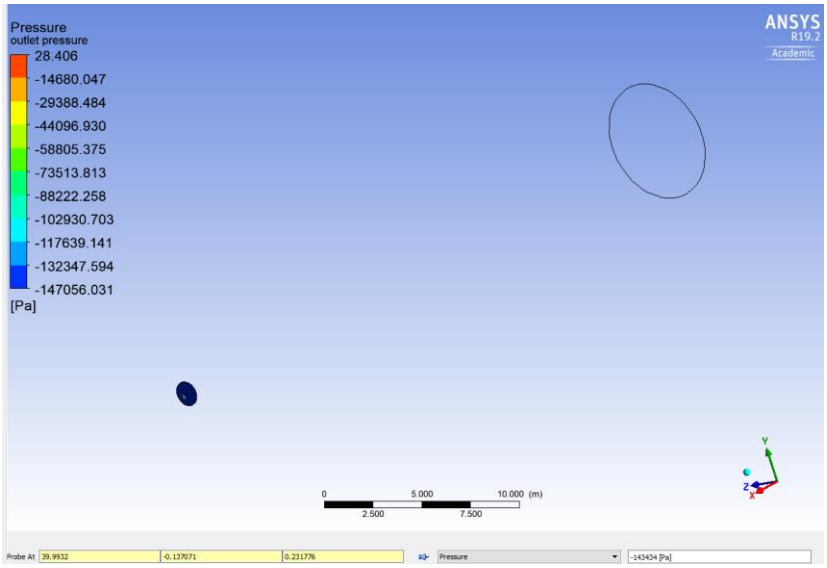

Figure 28 Sample of ANSYS CFX output

As a validation method, the outlet pressure from the hand calculation and the CFD were compared and the results are shown in Table 5.

Table 5 Comparison between Hand calculations and the CFD results

Validation of CFD/Hand calculations				
Outlet pressure CFD	**Outlet pressure hand calculation**	**Pressure difference (Pa)**	**Pressure difference (m)**	**% difference**
-145421.00	-143112.96	-2308.04	-0.24	1.59
-35571.00	-35356.37	-214.63	-0.02	0.60
-15663.00	-15401.44	-261.56	-0.03	1.67
-393658.00	-398536.01	4878.01	0.50	-1.24
-98700.00	-99212.13	512.13	0.05	-0.52
-43818.00	-43781.78	-36.22	0.00	0.08
-1367110.00	-1389636.57	22526.57	2.30	-1.65
-343098.00	-346659.14	3561.14	0.36	-1.04
-152565.00	-153515.17	950.17	0.10	-0.62
-5068070.00	-5170066.63	101996.63	10.40	-2.01
-1272910.00	-1290829.16	17919.16	1.83	-1.41
-566420.00	-572451.85	6031.85	0.61	-1.06
-7552540.00	-7724297.07	171757.07	17.51	-2.27
-1899000.00	-1929386.77	30386.77	3.10	-1.60
-845014.00	-856255.23	11241.23	1.15	-1.33

The percentage difference between the CFD output pressure and the hand calculations was approximately ± 2%. The above data came from the 15 studies where 0m of static head was applied. As per the patent, depending on where the outlet is in relation to the river, there may be an additional static head available. Therefore the 15 models were run again with 5m, 10m, 15m and 20m of static head in addition to the dynamic head generated by the fast-flowing river.

A total of 75 studies were completed on the inlet. The graph in Figure 29 shows all the models that managed a positive outlet pressure with various additional static heads applied. The models that did not manage a positive outlet pressure had smaller outlet surface areas compared to their inlet surface areas. Increasing the outlet surface area, reduced the outlet velocity, but gave a positive pressure when the additional head was applied. Finally, Figure 30 shows the mean outlet velocity calculated using Bernoulli's equation.

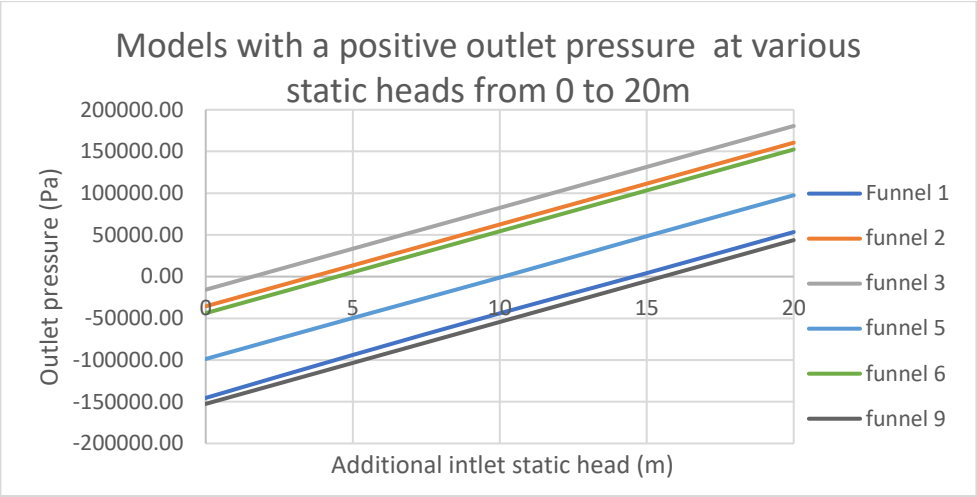

Figure 29 The outlet pressure with varying static heads applied to the dynamic head

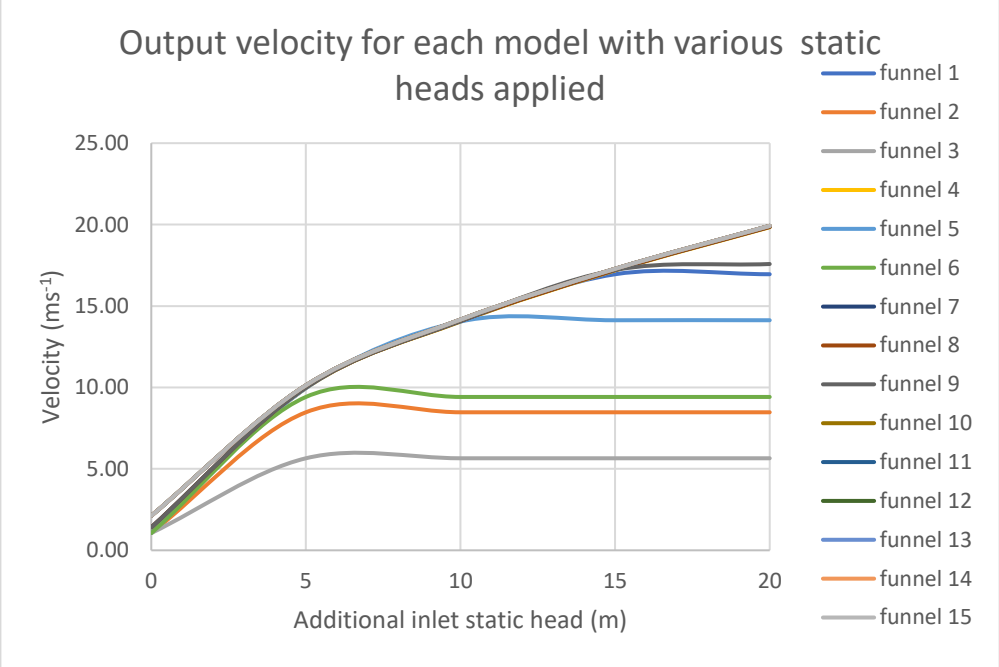

Figure 30 The outlet velocity with the varying static head applied to the dynamic head

As shown in Figure 30, the greater the static head applied, the greater the outlet velocity. These velocities are calculated using the governing equations and do not take the inlet geometry into account or any turbulence generated within the inlet. The pressure required to obtain the outlet velocities shown in the patent could only be gained by having significant

additional head. The patent calculations were proved to be invalid and a new type of outlet was offered by OCPL to increase the velocity.

3.3. Inlet variation

The inlet variation shown in Figure 24 was issued with the patent and OCPL. However, this was revised by OCPL and the sketch in appendix C was produced and issued to calculate the outlet velocity. This sketch was used to produce a 3D model in SOLIDWORKS and is also shown in appendix C. OCPL intended this revised variation to increase the velocity flowing through the inlet.

As with the straight inlet, ANSYS CFX was used to complete the steady state computational fluid dynamic calculations. The fluid region was generated in SOLIDWORKS as shown in Figure 31 with the ANSYS simple tetrahedron mesh shown in Figure 32.

The mesh quality metrics of the simple funnel are shown Table 6. This are well within acceptable tolerances. These metrics are discussed in greater detail in chapter 5.

Table 6 Mesh sensitivity analysis

Mesh metric	Element quality	Aspect ratio	Skewness	Orthogonal quality
Minimum	0.0059	1.1848	0.0027	0.0409
Maximum	0.9999	26.662	0.95911	0.9820
Average	0.76263	2.1889	0.32	0.678864
Standard deviation	0.14393	1.1388	0.15472	0.15311
Ansys manual maximum value to obtain accuracy	N/A	35	0.95	>0.01
Ansys manual average value to obtain accuracy	>0.75	5	0.33	N/A

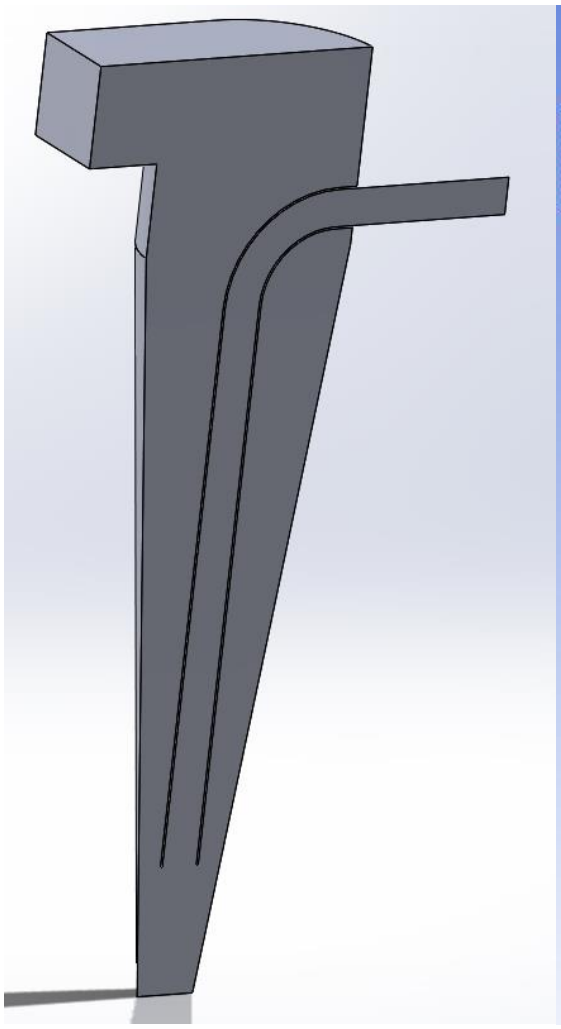

Figure 31 Sectional view of the fluid in the 40m inlet drop variation

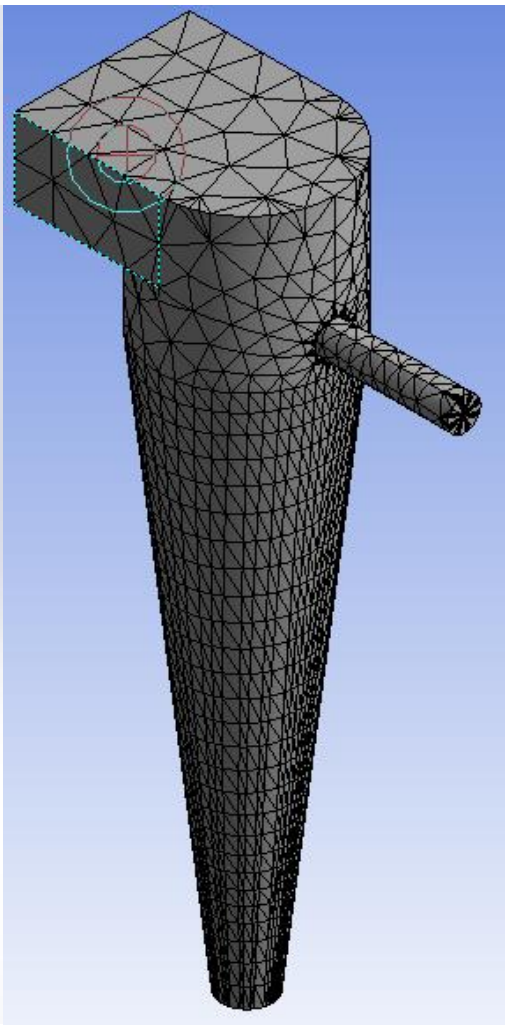

Figure 32 ANSYS mesh layout

3.3.1. Inlet boundary conditions

Using the previous data, the inlet boundary conditions were spit into 3 types: Velocity, Dynamic pressure and Mass flow rate. The dynamic pressure is calculated using equation (3.6) and the mass flow rate is calculated using equation (3.7). Using these equations, the three inlet boundary conditions are shown in Table 7.

$$\text{Dynamic Pressure} = \frac{\rho * v^2}{2} \qquad (3.6)$$

$$Mass\ flow\ rate = \rho * A * v \qquad (3.7)$$

ρ = density of fluid ($kg \cdot m^{-3}$)
v = Velocity of fluid (ms^{-1})
A = Cross sectional area (m^2)

Table 7 Inlet boundary conditions

Condition	Set value	Unit
Velocity	0.75	ms^{-1}
Dynamic Pressure	1125	Pa
Mass flow rate	99825	$kg \cdot s^{-1}$

Gravity was applied to all studies by applying momentum to the source. The acceleration due to gravity is multiplied by the fluid density. This gave the boundary condition of 9810 $kg*m^{-2}*s^{-2}$. To confirm gravity was applied correctly, an analysis was performed with and without gravity applied and these are shown in Figure 33 and Figure 34.

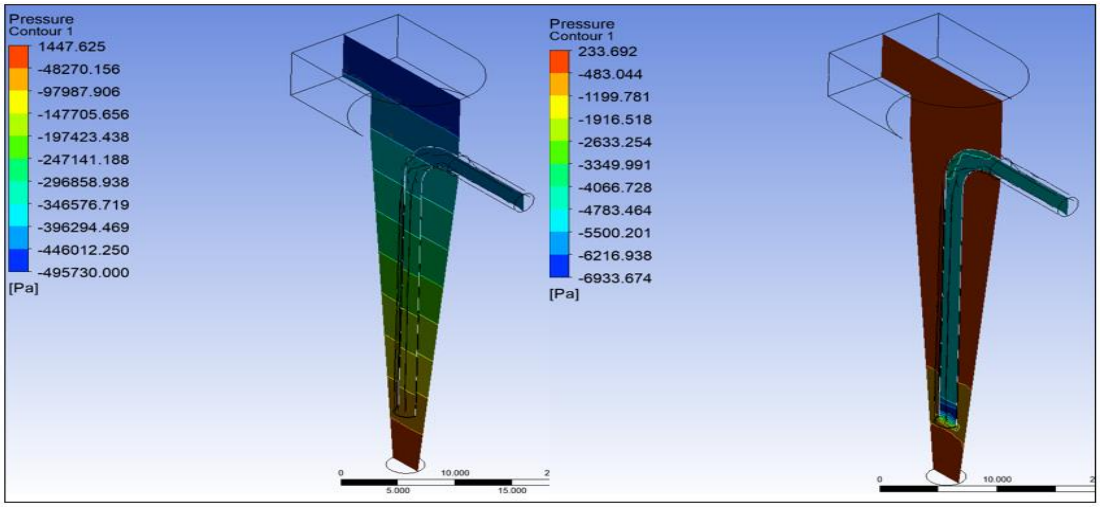

Figure 33 ANSYS snapshot with gravity applied

Figure 34 ANSYS snapshot without gravity applied

As a way of verifying the gravity equation was correct, a steady state study was completed on the SOLIDWORKS flow simulator. This software has a dedicated gravity function incorporated into the initial conditions of the fluid model. With the input of 0.75 ms^{-1} and an output of 1Pa

the pressure gradient is shown in Figure 35 and had equivalent pressures to the ANSYS model throughout the depth of the model.

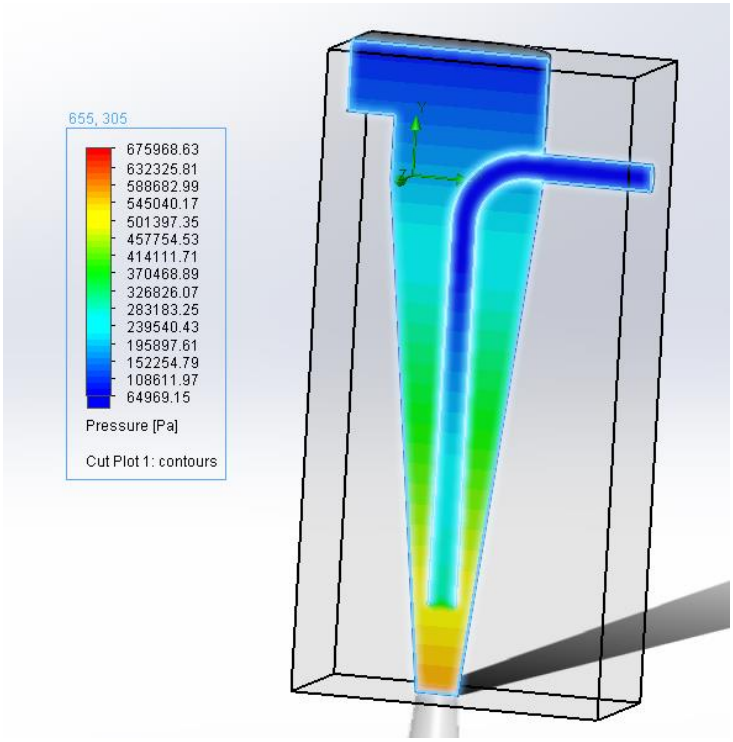

Figure 35 SOLIDWORKS CFD with input of 0.95 ms^{-1} output of 1Pa with gravity applied

3.3.2. Outlet boundary conditions

For a steady state internal flow, ANSYS required a boundary condition for the outlet. As this was not known, various outlet boundary conditions were applied. The outlet velocity was altered from 1 ms^{-1} to 10 ms^{-1} for each of the 3 inlet conditions. In addition, the outlet pressure was also applied from 1 to 10000 Pa. This resulted in 30 studies being performed and are shown along with the inlet boundary conditions in Table 8. The results of these inputs are shown in Table 9.

Table 8 Inlet and outlet boundary conditions

	Boundary conditions			
Study Number	**Inlet**	**Units**	**Outlet**	**Units**
1	0.75	ms^{-1}	1	ms^{-1}
2	0.75	ms^{-1}	2	ms^{-1}
3	0.75	ms^{-1}	3	ms^{-1}
4	0.75	ms^{-1}	4	ms^{-1}
5	0.75	ms^{-1}	5	ms^{-1}
6	0.75	ms^{-1}	6	ms^{-1}
7	0.75	ms^{-1}	7	ms^{-1}
8	0.75	ms^{-1}	8	ms^{-1}
9	0.75	ms^{-1}	9	ms^{-1}
10	0.75	ms^{-1}	10	ms^{-1}
11	1125	Pa	1	ms^{-1}
12	1125	Pa	2	ms^{-1}
13	1125	Pa	3	ms^{-1}
14	1125	Pa	4	ms^{-1}
15	1125	Pa	5	ms^{-1}
16	1125	Pa	6	ms^{-1}
17	1125	Pa	7	ms^{-1}
18	1125	Pa	8	ms^{-1}
19	1125	Pa	9	ms^{-1}
20	1125	Pa	10	ms^{-1}
21	99825	$kg{\cdot}s^{-1}$	1	ms^{-1}
22	99825	$kg{\cdot}s^{-1}$	4	ms^{-1}
23	99825	$kg{\cdot}s^{-1}$	6	ms^{-1}
24	99825	$kg{\cdot}s^{-1}$	8	ms^{-1}
25	99825	$kg{\cdot}s^{-1}$	10	ms^{-1}
26	1125	Pa	1	Pa
27	1125	Pa	10	Pa
28	1125	Pa	100	Pa
29	1125	Pa	1000	Pa
30	1125	Pa	10000	Pa

Table 9 40m Inlet drop ANSYS results

	ANSYS results					
Study Number	**Inlet**	**Units**	**Outlet**	**Units**		
1	-462314	Pa	-416112	Pa		
2	-466726	Pa	-416917	Pa		
3	-463297	Pa	-426582	Pa		
4	-459348	Pa	-433502	Pa		
5	-464584	Pa	-444520	Pa		
6	-461148	Pa	-458628	Pa		
7	-462371	Pa	-477649	Pa		
8	-464794	Pa	-492205	Pa		
9	-465789	Pa	-516187	Pa		
10	-464421	Pa	-538561	Pa	**Inlet**	**Units**
11	2.4	ms^{-1}	72001	Pa	15151	Pa
12	2.3	ms^{-1}	70578	Pa	15965	Pa
13	1.9	ms^{-1}	66862	Pa	18910	Pa
14	1.8	ms^{-1}	58657	Pa	21222	Pa
15	1.7	ms^{-1}	46728	Pa	19681	Pa
16	1.5	ms^{-1}	28792	Pa	25639	Pa
17	1.1	ms^{-1}	12373	Pa	16623	Pa
18	0.6	ms^{-1}	-5935	Pa	14821	Pa
19	0.3	ms^{-1}	-30780	Pa	11189	Pa
20	0.8	ms^{-1}	-54013	Pa	14510	Pa
21	1.3	ms^{-1}	-423730	Pa	-463415	Pa
22	1.2	ms^{-1}	-443481	Pa	-465142	Pa
23	1.5	ms^{-1}	-471902	Pa	-463150	Pa
24	1.5	ms^{-1}	-507147	Pa	-464627	Pa
25	1.5	ms^{-1}	-549519	Pa	-464914	Pa
26	1.02	ms^{-1}	1381	pa	12865	Pa
27	1.02	ms^{-1}	1182	Pa	13827	Pa
28	1.7	ms^{-1}	112	Pa	17835	Pa
29	1.26	ms^{-1}	3517	Pa	37677	Pa
30	1.76	ms^{-1}	11102	Pa	20091	Pa

To show a comparison, another SOLIDWORKS model was created without the 40m drop variation. Figure 36 shows the SOLIDWORKS model, the internal fluid section for ANSYS and the ANSYS general mesh ready for analysis. The only head created was the 3m from the inlet to the outlet. This was chosen for comparison to confirm if the 40m drop generated any additional velocities.

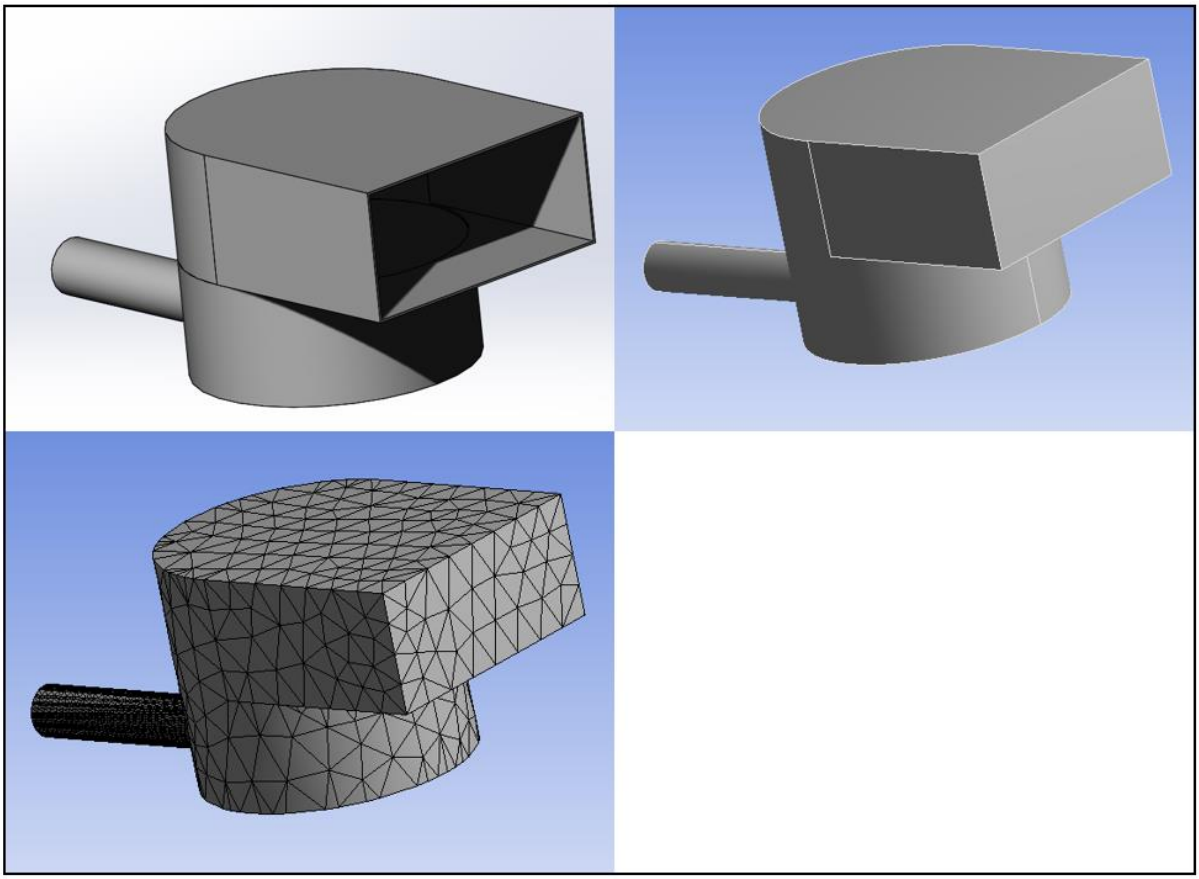

Figure 36 SOLIDWORKS model, Fluid model and ANSYS mesh of 3m drop variation

The boundary conditions that were applied to the 40m model were applied to the 3m model and the results are shown in Table 10.

Table 10 3m inlet drop variation ANSYS results

	ANSYS results					
Study Number	**Inlet**	**Units**	**Outlet**	**Units**		
1	-42046	Pa	14511	Pa		
2	-38515	Pa	14474	Pa		
3	-37873	Pa	14370	Pa		
4	-34911	Pa	14709	Pa		
5	-29790	Pa	14666	Pa		
6	-22141	Pa	14722	Pa		
7	-10710	Pa	15003	Pa		
8	-5142	Pa	16192	Pa		
9	6883	Pa	14842	Pa		
10	19179	Pa	15863	Pa	**inlet**	**units**
11	1.99	ms^{-1}	88059	Pa	13592	Pa
12	2.3	ms^{-1}	87911	Pa	19705	Pa
13	1.8	ms^{-1}	84576	Pa	21739	Pa
14	1.49	ms^{-1}	77433	Pa	24346	Pa
15	1.1	ms^{-1}	68012	Pa	20258	Pa
16	1.2	ms^{-1}	62090	Pa	20589	Pa
17	1.47	ms^{-1}	53908	Pa	16636	Pa
18	1.46	ms^{-1}	43689	Pa	16964	Pa
19	1.34	ms^{-1}	28532	Pa	14723	Pa
20	0.94	ms^{-1}	17139	Pa	12126	Pa
21	1.45	ms^{-1}	43727	Pa	-5689	Pa
22	1.45	ms^{-1}	48981	Pa	15898	Pa
23	1.42	ms^{-1}	49247	Pa	32398	Pa
24	1.44	ms^{-1}	54127	Pa	48410	Pa
25	1.43	ms^{-1}	53210	Pa	74828	Pa
26	0.97	ms^{-1}	612	pa	17011	Pa
27	0.91	ms^{-1}	629	Pa	14704	Pa
28	1.27	ms^{-1}	519	Pa	17817	Pa
29	1.28	ms^{-1}	3517	Pa	16000	Pa
30	1.28	ms^{-1}	10106	Pa	15683	Pa

The 3 different types of inlet boundary conditions for both the 40m and 3m inlet drop variation were studied. Both the 3m and 40m drop were compared for all studies. The inlet velocities were compared when a constant mass flow rate was applied and these are shown in Figure 37. The inlet velocities were also compared when a constant pressure was applied and are shown in Figure 38.

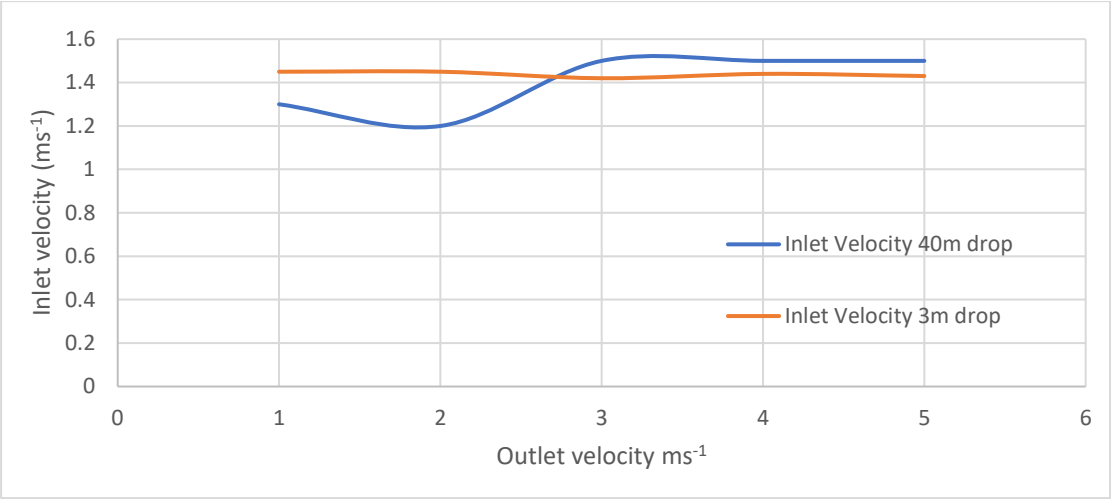

Figure 37 Inlet velocity at various outlet velocities with an inlet mass flow rate boundary of 99825 kg·s^{-1}

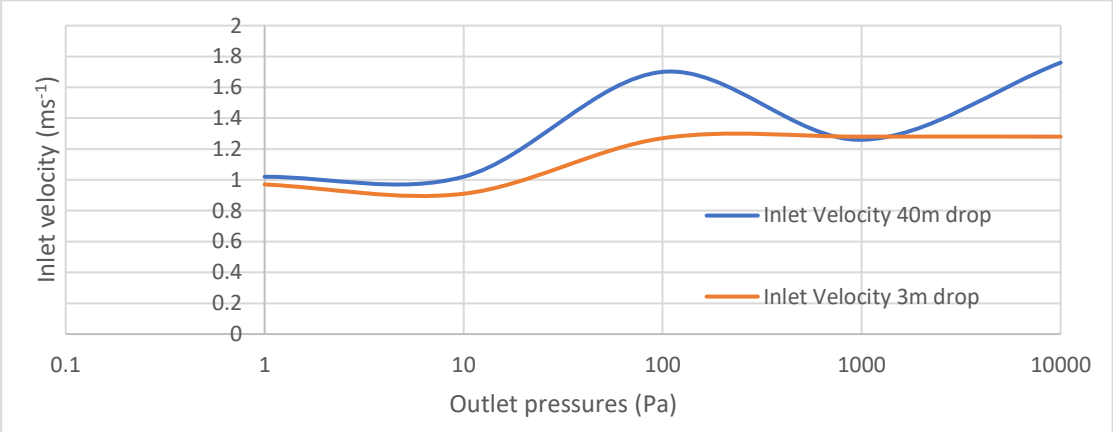

Figure 38 Inlet velocity at various outlet pressures with an inlet pressure boundary of 1125 Pa

3.3.3. Hand calculations using Bernoulli's principle

To calculate the velocity of the outlet pipe, the head form of Bernoulli's equation (3.3) was used with both the inlet and outlet shown in equation (3.8). The dynamic pressure on the inlet is given by equation (3.9).

$$\frac{P_{inlet}}{\rho * g} + \frac{v_{inlet}^2}{2 * g} + z_{inlet} = \frac{P_{outlet}}{\rho * g} + \frac{v_{outlet}^2}{2 * g} + z_{outlet} \quad (3.8)$$

P-Pressure (Pa)
v-Velocity (ms^{-1})
z-distance from a fixed point (m)
ρ-Density of fluid ($kg \cdot m^{-3}$)
g-acceleration due to gravity (ms^{-2})

$$\text{Dynamic pressure} = \frac{\rho * v^2}{2} \quad (3.9)$$

The inlet dynamic pressure using velocity of 1 ms^{-1} = 1000*1²*0.5 = 500 Pa

Assuming the inlet is the fixed point with a pressure of 500Pa (dynamic pressure) and the outlet has a pressure of 1Pa. Therefore, populating equation (3.8) in equation (3.10) we calculate that the outlet velocity will be 13 ms^{-1}

$$\frac{500}{1000 * 9.81} + \frac{1^2}{2 * 9.81} + 0 = \frac{1}{1000 * 9.81} + \frac{v_{outlet}^2}{2 * 9.81} + 10 \quad (3.10)$$

This can be used at any length of drop and pipe size. This does not take into consideration the losses in the pipe. If you increase the pipe length and drop, this only decreases the outlet velocity and pressure.

3.4. Patent review conclusion

Using the straight inlet as shown in the patent, velocities of 2 ms^{-1} were achieved in both the hand calculations and the funnel CFD. This was significantly lower than the calculations OCPL shown in their patent. Using additional static head did increase the exit velocity of the fluid. If 20m of static head was applied, the majority of the studies would have achieved the outlet velocity stated in the patent.

OCPL located several places around the United Kingdom where there was approximately 10m of static head available. Using this static head along with the kinetic head of the flowing river, the outlet velocity was calculated at 14 ms^{-1}. To reduce computational time of this model, three calculation factors were removed: The geometry was reduced to a simple cone, there was no turbulence equations in the CFD solver and the friction factor of the model was removed. Therefore, the 14 ms^{-1} would not be achieved in practice.

In the alternative inlet, the 40m drop did not significantly increase the outlet velocity compared to the 3m drop in the ANSYS CFX model. The fluid gained pressure at the foot of the 40m inlet, however during the rise of the fluid to the outlet, it lost all the pressure it gained. The friction of the fluid moving through the 40m drop would reduce the velocity compared to the 3m drop. This was not clear in the studies as the friction of the inlet walls was not applied to save on computer calculation time.

To perform a steady state model for an internal flow, ANSYS CFX required both an inlet and outlet boundary condition. This meant once the conditions were met, negative pressures were required to achieve these boundary conditions. Therefore, an external flow transient CFD model was require with a single inlet boundary of the river flow. This was completed and is shown in chapter 5 where more computational time was allowed.

In light of the calculations completed on the patent review, OCPL suggested a number of case studies that could potentially increase the velocity of the fluid entering the Ram pump section from the inlet. A 50-mile tunnel was proposed that would originate at the River Severn just outside of Birmingham heading southwards to the Bristol Channel. This route had a height difference of 26m. Using Moody charts, the friction factor of the pipe itself meant that the majority of the head would be used counter acting friction losses of the pipe.

4. Computational model (MATLAB)

MATLAB is a computer programming language that is mainly used in numerical computing. This was ideal for manipulating the governing equations to calculate the estimated hydraulic power output of the system.

4.1. Model from Literature review

The MATLAB code from the research carried out by Roberts (2017) was used to model a ram pump. As discussed in the literature review, this computational model had an oscillating column of water which was used to calculate the hydraulic power generated. This original model used experimental data with a set up as shown in Figure 39. Once the valve was closed, the water in the Y direction oscillated as shown in Figure 40. This allowed for extraction of energy without consuming the fluid in the reservoir. If no flow was allowed through the ram valve (Qv = 0) after the initial closure, the oscillations would continue as shown by the purple line in Figure 40.

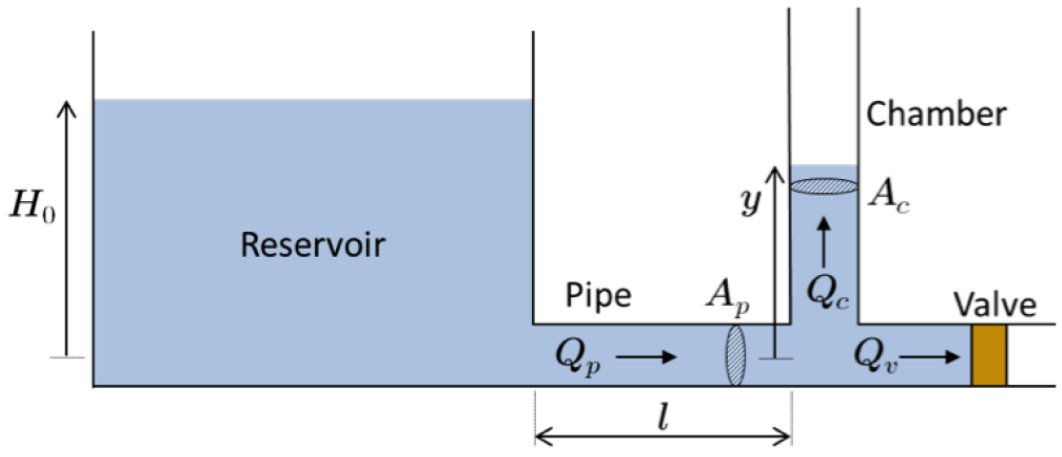

Figure 39 Ram pump from the Thiess (Roberts, 2017)

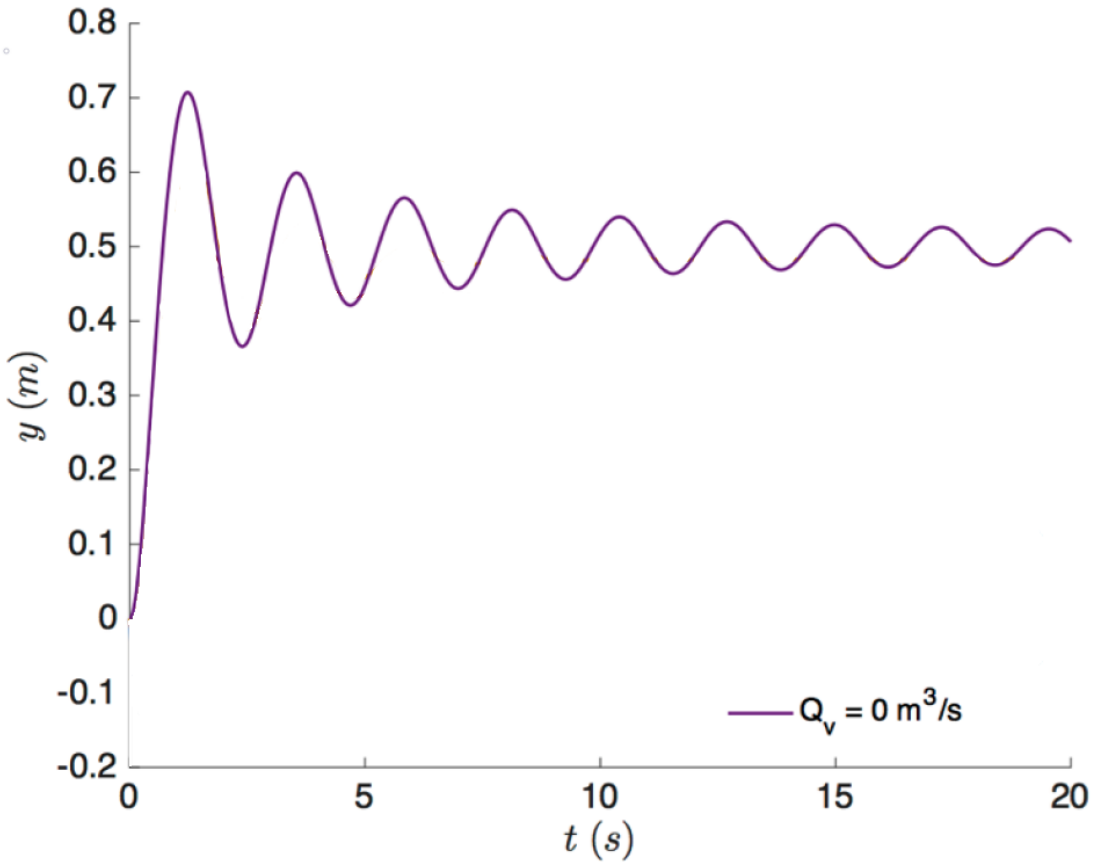

Figure 40 Y pipe fluid oscillations after valve closure (Roberts 2017).

The input signal for the Roberts code was a sawtooth wave and this modelled the closing of the ram valve. Using this waveform, the model was compared to the experimental data and the results are shown in Figure 10 in the literature review.

4.2. Alterations made to the Roberts model

For the Roberts model to resemble the Ocean Current Power patent, certain alterations were made. The reservoir needed to be replaced by an inclined pipe of various lengths and height. In addition, the terminal velocity of the fluid during the acceleration phase of the cycle was also calculated. These changes stem from the Darcy-Weisbach head loss equation.

To calculate the head loss associated with the pipe, the Darcy-Weisbach equation (4.1) was used where the velocity is embedded. The friction factor used in this equation is dependent on the Reynolds number and this is shown in equation (4.2). In the Roberts code, the friction factor was a user defined input value which was confirmed with experimental data, however, this needed to be calculated with long lengths of pipe.

Darcy-Weisbach equation

$$H_f = \frac{f v_p^2 l}{2gD} \quad (4.1)$$

(Roberts 2017)

H_f-Head loss (m)
f-Friction factor
v_p-fluid velocity (ms^{-1})
l -pipe length (m)
g-acceleration due to gravity (ms^{-2})
D-Diameter of pipe (m)

Reynolds number

$$Re = \frac{\rho u D}{\mu} = \frac{uD}{\upsilon} = \frac{QD}{\upsilon A} \quad (4.2)$$

(Roberts 2017)

A-pipe cross sectional area (m^2)
υ-kinematic viscosity (μ/ ρ)
D_H-hydraulic diameter (m)
Q-volumetric flow rate (m^3s^{-1})
μ-Dynamic viscosity (Pa·s)
ρ-Density ($kg{\cdot}m^{-3}$)

Due to the implicit friction factor term of the Colebrook-White equation (4.3), the approximated Haaland equation (4.4) was used. This approximation is used when the fluid is flowing in a circular pipe (Brkic, 2012). The full code with all alterations is shown Appendix C.

Colebrook-white Equation

$$\frac{1}{\sqrt{f}} = -2\log_{10}\left(\frac{2.51}{Re\sqrt{f}} + \frac{\varepsilon}{3.71D}\right) \quad (4.3)$$

(Roberts 2017)

ε-pipe relative roughness
Re-Reynolds Number

Haaland Equation

$$\frac{1}{\sqrt{f}} = \mathrm{l} - 1.8\log_{10}\left[\left(\frac{\varepsilon/_D}{3.7}\right)^{1.11} + \frac{6.9}{Re}\right] \quad (4.4)$$

(Brkic, 2012)

4.3. MATLAB results

The revised code was initially used to calculate the terminal velocity at various pipe lengths with the input shown in Table 11. The head was fixed at 10m with no flow. The dynamic head of 1 ms^{-1} was calculated previously at 0.05m therefore was negligible. The maximum velocity reached with the above variables is shown in the 3D plot in Figure 41. The fluid took up to 60 seconds to reach terminal velocity; however, after 7 seconds it had reached over 95% of the terminal velocity.

Table 11 Input variables for calculating the terminal velocity

variables	size	unit
Pipe diameter	1.5	m
Total head	10	m
Water Viscosity @ 5 degrees	1.5182	mPa.s
Pipe length (variable)	10-100	m

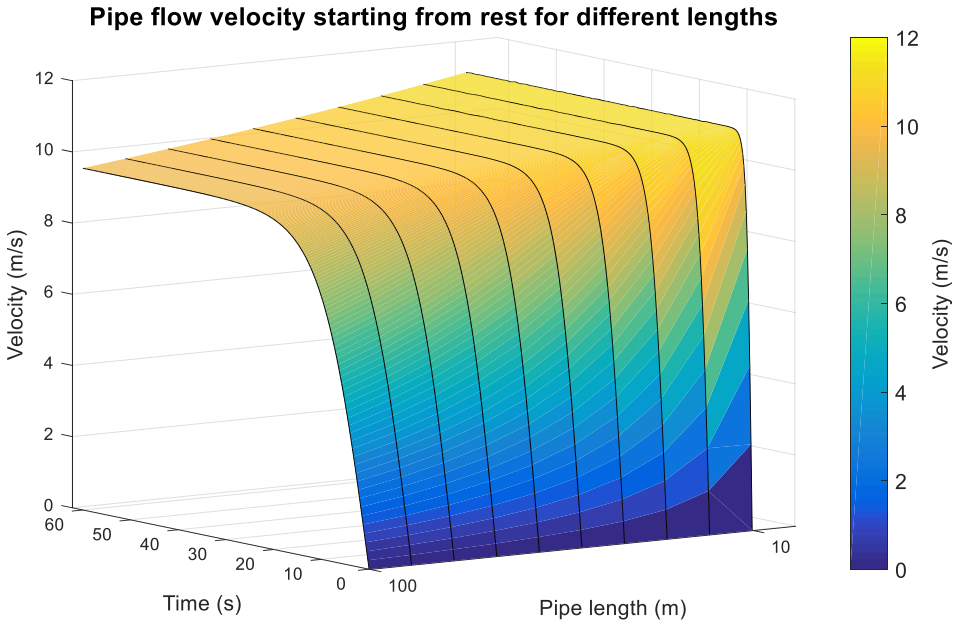

Figure 41 Maximum velocity at various pipe lengths

The frequency of the valve closing in the Roberts code was set within the sawtooth waveform. However, the valve open, closed and closing times were altered to find the maximum power output with the initial variables shown in Table 12.

Table 12 Variables used to determine the valve open and closed times to obtain the maximum power output

variables	size	unit
Length of pipe	40	m
Inlet pipe diameter	1.5	m
Y direction off-shoot pipe diameter	1	m
Total head	10	m
Time to close valve	1	sec

The results of these variables inserted into the code are shown in the 3D plot in Figure 42. To gain the maximum hydraulic power output of 153.86 kW, the valve needed to be open for 7 seconds to gain the required velocity of the fluid. The valve then needed to be closed for a further 6.5 seconds to achieve this power. A nominal time of 1 second was used to close the valve. However, if the valve is closed almost instantaneously with a valve closing time of 0.01 seconds (keeping within the limit of incompressible liquids), the power output was 159.77kW as shown in Figure 43. This accounted for a 3% increase in power. The power was calculated within the Roberts code using equation (5.5) at varying velocities calculated within the velocity function.

$$P = \rho * g * h * \mathrm{Q} \qquad (5.5)$$

P – Hydraulic power (W)
ρ -Fluid density ($kg \cdot m^{-3}$)
g- Acceleration due to gravity (ms^{-2})
Q-Volumetric Flowrate ($m^3 s^{-1}$)

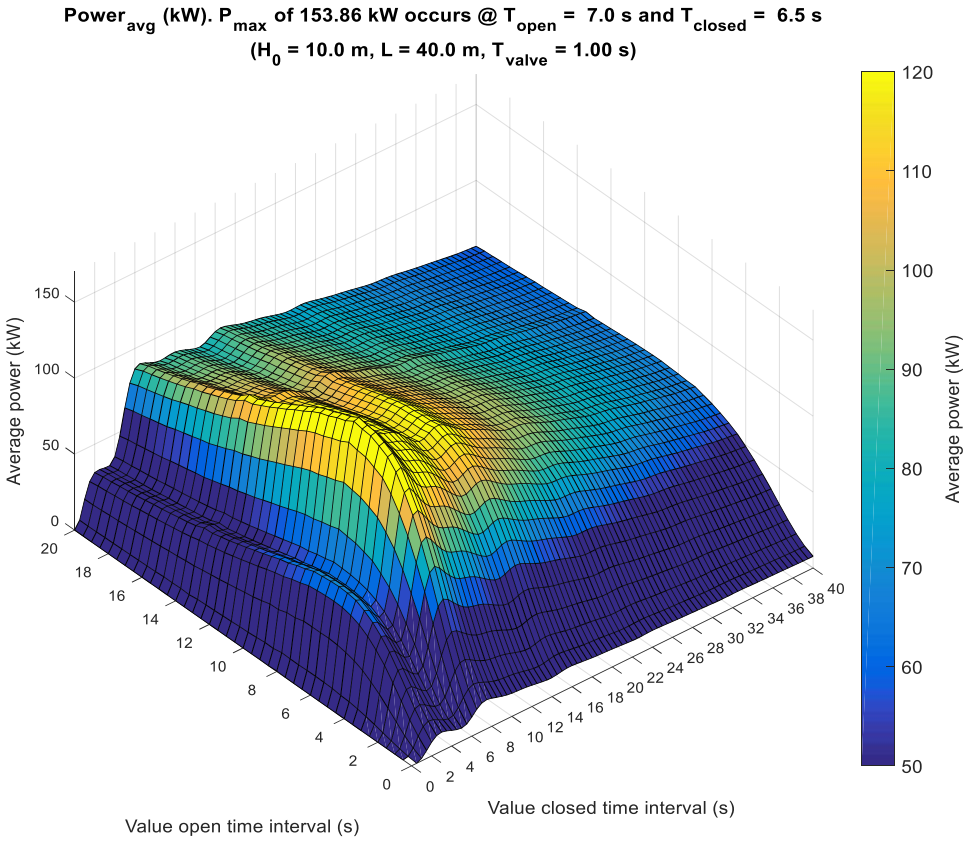

Figure 42 Hydraulic output power with varying valve opening and closing times. Valve closes in 1 second (1.5/1)

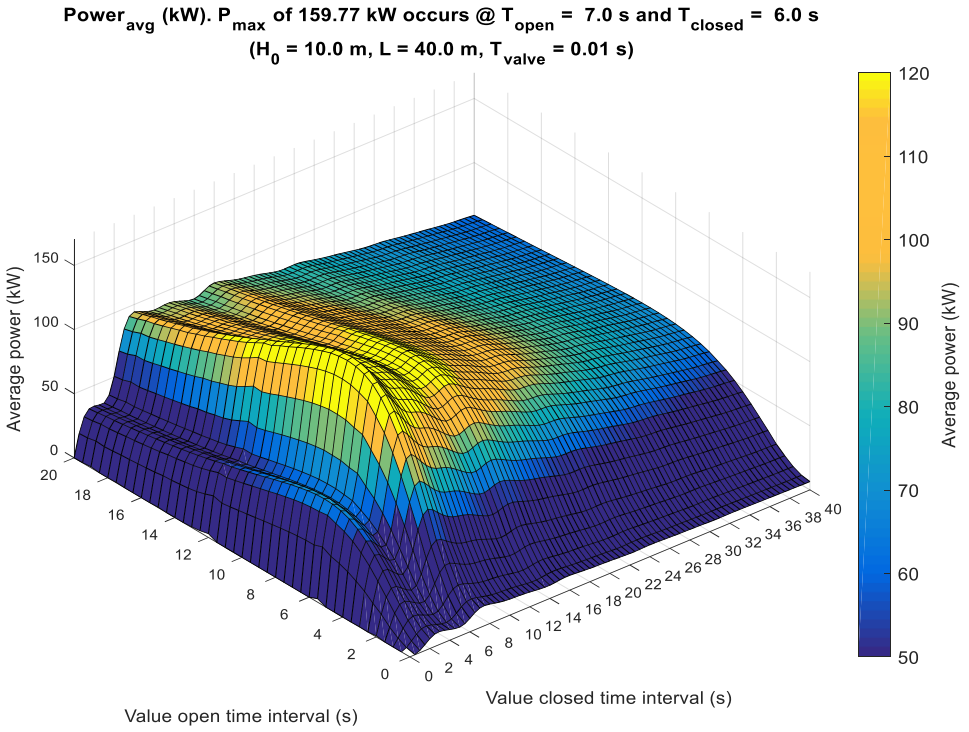

Figure 43 Hydraulic output power with varying valve opening and closing times. Valve closes in 0.01 second (1.5/1)

Using the data calculated previously the valve opening and closing times were added to the variable list and shown in Table 13. The volumetric flowrate of the inlet and Y direction off-shoot pipe is shown in Figure 44. The volumetric flow rate in the main pipe (Qp-blue line) started with the valve open at zero seconds. The flowrate in the Y direction pipe (Qy-Orange line) was zero through this phase of the cycle. The flow increases as the fluid velocity increases until 7 seconds where the valve begins to close. Through the closing phase the fluid flow started to increase in the Y-direction off-shoot pipe. This fluid in the off-shoot pipe then oscillated.

Table 13 Revised variables used to calculate the output power

variables	size	unit
Length of pipe	40	m
Inlet pipe diameter	1.5	m
Y off-shoot pipe diameter	1	m
Total head	10	m
Time valve open	7	sec
Time valve closed	6.5	sec
Time to close valve	1	sec

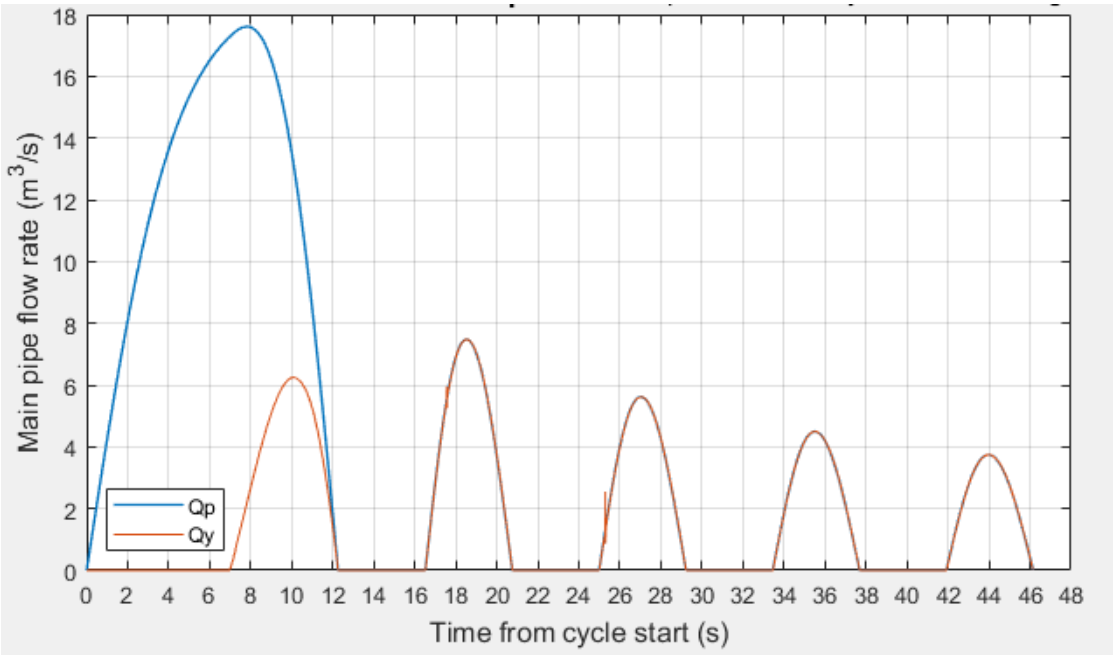

Figure 44 Flow rate in the main pipe and Y direction off-shoot pipe during cycle

The total head generated in the Y-direction off-shoot pipe through the closing of the valve is shown in Figure 45 with the hydraulic power generated in the oscillations shown in Figure 46. The average hydraulic power calculated was 147.1 kW with an efficiency of 27%. The power output calculated is hydraulic power and to convert this to electrical power a conversion factor needed to be applied. As the power is extracted from both the positive Y direction pipe fluid flow and the negative, a conversion factor of 30% was applied (Roberts, 2017). Therefore, if this rate is applied the power output would be 44.1 kW with an efficiency of 8.1%. The volumetric flow rate through the cycle was 3.77 m^3s^{-1}.

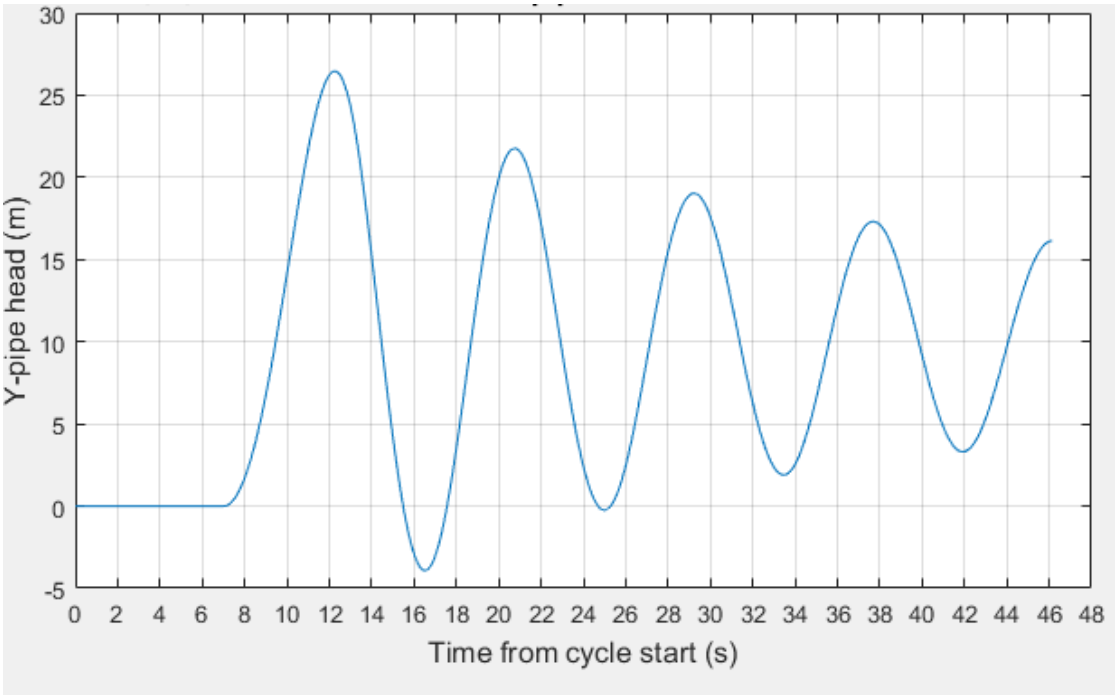

Figure 45 Head in the Y direction off-shoot pipe during the cycle

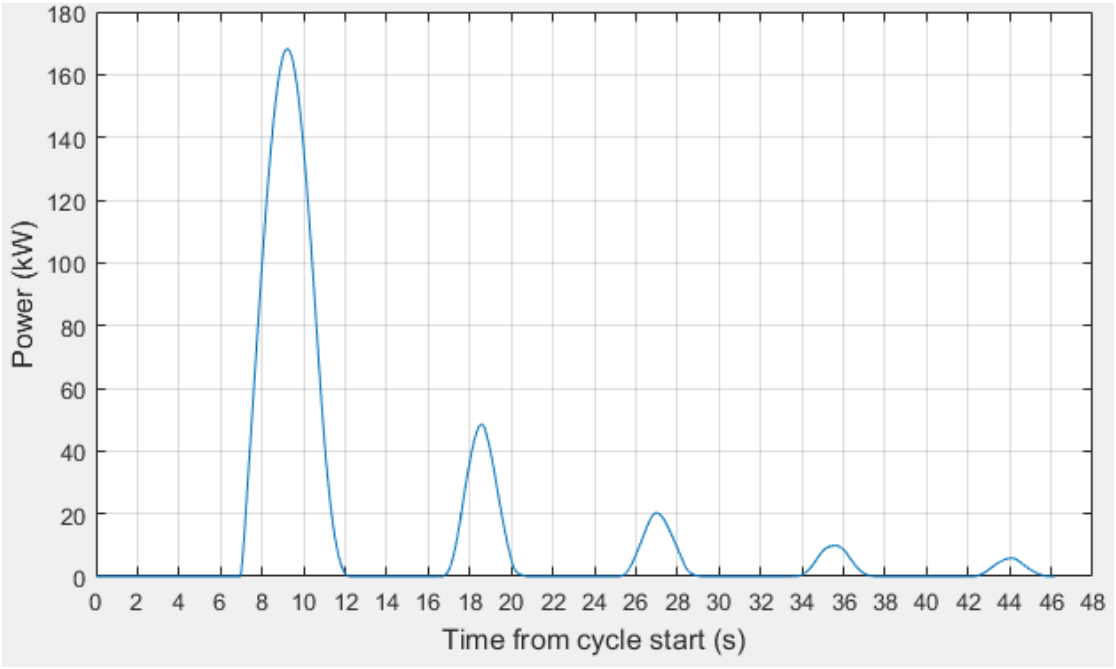

Figure 46 Hydraulic power created throughout the cycle

The above code calculated the hydraulic power from the amount of fluid that moved within the Y-direction off-shoot pipe. This code extracted power from both directions of the oscillations of the fluid in the off-shoot pipe. However, if the off-shoot pipe were to be

connected to a standard water turbine, only the positive movement of this fluid would be used in power generation. The code was altered to only allow the positive flow of the fluid to be incorporated into the power generation. This was to simulate single direction flow. Figure 47 and Figure 48 show the volumetric flow rate and the power throughout the ram pump cycle respectively.

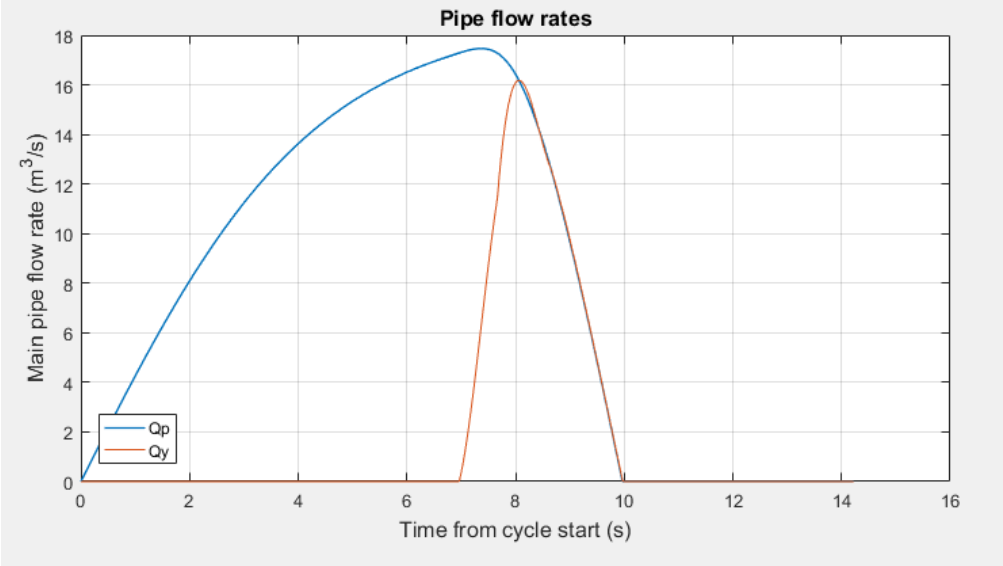

Figure 47 Single direction volumetric flow rate in the main and off-shoot pipe

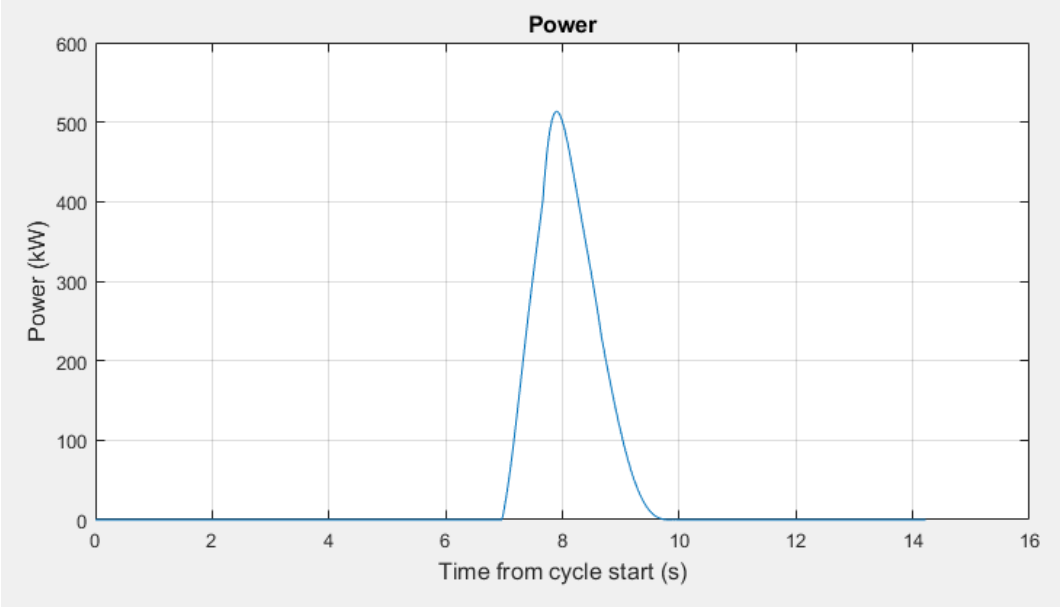

Figure 48 Single direction hydraulic power output throughout the ram pump cycle

As previously stated in the literature review, Conversion rates for fluid turbines from hydraulic to rotational power can be up to 83% in favourable conditions. With generator, transformer, and gear drive losses applied, this efficiency lowered to 79% for the latest turbines. As specified by Roberts (2017), for the oscillating water column, a 30% conversion factor should be applied due to the complexities of the flow in water. Therefore, models were completed in dual and single direction mode with different conversion factors applied for the electrical power output.

4.4. Matlab model conclusion

Previous work undertaken by Roberts (2017) positively compared an experimental model of a Ram pump system to MATLAB code. This mathematical model differed in how the fluid was delivered to the ram valve and how the power was extracted from the off-shoot pipe. This code was altered to simulate an inclined pipe of 10m head in accordance with the patent inlet. A range of variables (valve opening times; closing times, length of pipe, diameter of off-shoot and inlet pipe) were altered and the generated power was calculated. Initially, the power was calculated for only the oscillating off-shoot pipe as designed by Roberts, however, the single direction power generation was subsequently added.

The variables that gave the maximum power are detailed in Table 13. The velocity of the inlet took 7 seconds to reach 95% of the terminal velocity of approximately 9.5 ms^{-1}. The valve closing time was limited to 1 second as the maximum power developed was only decreased by 3% if a closing time of 0.01 second was used. This reduced the forces acting on the valve as it slammed shut. The power generated using these variables for the oscillating off-shoot pipe was approximately 150kW with a volumetric flow rate of 3.77 m^3s^{-1}.

As the inlet pipe had to be a circular due to the Haaland equation, this MATLAB model was limited in simulating the OCPL patent. To change the inlet into a complicated 3D geometry and to model the ram pump throughout its cycle, CFD using a transient solution had to be complete.

5. Computational fluid dynamic model (ANSYS)

The MATLAB model detailed in chapter 5 used governing fluid dynamic equations and therefore could only be used with simple geometry. The final inlet chosen by OCPL had complicated geometry and a new method was required to calculate the mechanical power generated. The computational fluid dynamic software ANSYS FLUENT was used. This software is fully supported by the University of Lancaster and can also be used on the Lancaster High-End Computing (HEC) network via the UNIX operating system. HEC allows the FLUENT solver to be shared over multiple nodes reducing the solving time. FLUENT also allows for multiple fluid zones to be created within the same model and these were used to simulate the closing of valves.

5.1. Constructed geometry of the ram pump

The Ram pump inlet sketches issued by OCPL are shown in Figure 49 and Figure 50. The inlet and ram valve were constructed in SOLIDWORKS with the dimensional drawings shown Appendix D

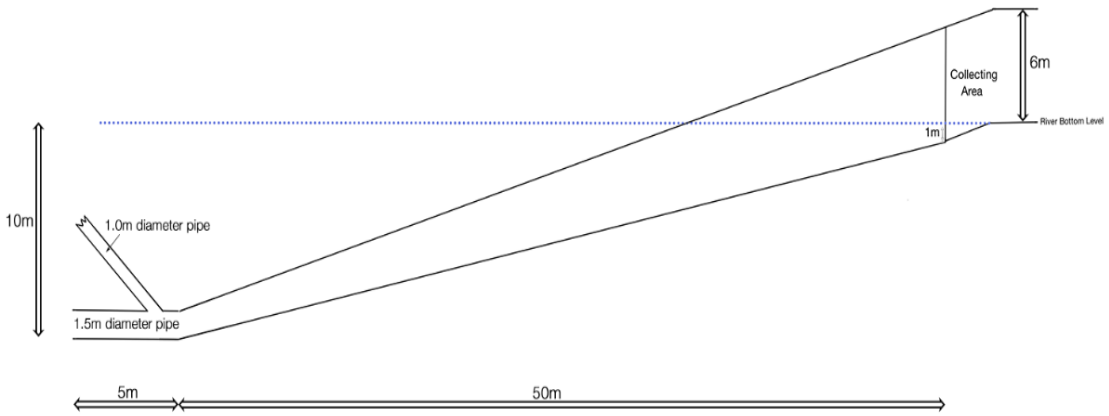

Figure 49 Inlet section view issued by OCP

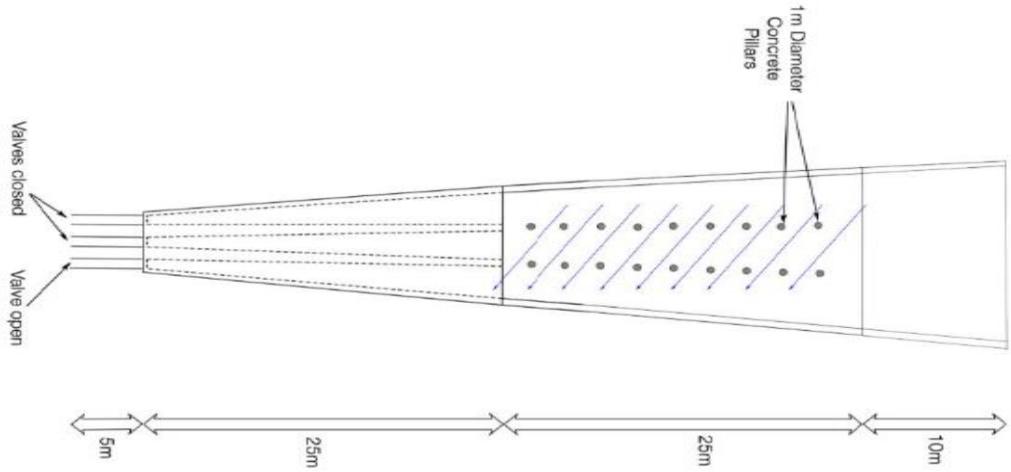

Figure 50 Inlet plan view issued by OCP

The actual valve plunger was removed from the model to allow for simpler calculations when using the ANSYS FLUENT calculation solver. The completed model is shown in Figure 51. This was then converted into the extension file ".IGS" which was then imported into ANSYS workbench for analysis.

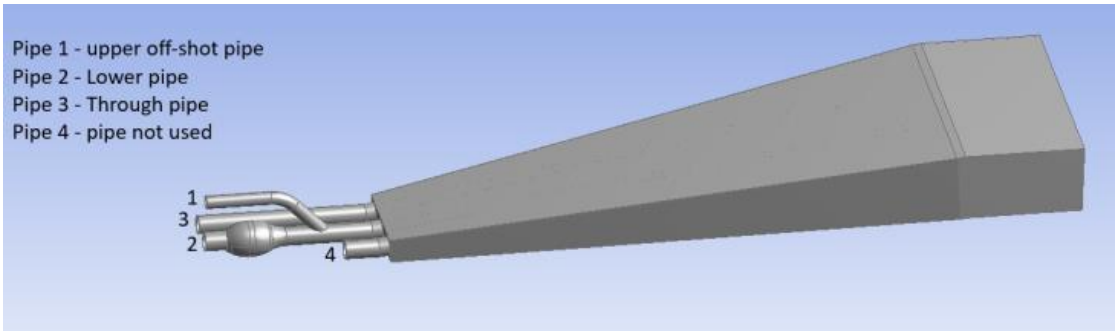

Figure 51 Full model including ram valve and outlet

The off-shoot pipe would be connected to a water turbine and generator, however, to reduce the computational time, only the mechanical power was calculated in this pipe using equation (5.1).

$$Mechanical\ power\ (w) = \rho ghQ \qquad (5.1)$$

ρ-density ($kg \cdot m^{-3}$)

g-acceleration due to gravity (ms^{-2})
h-pressure head (m)
Q-volumetric flow rate (m^3s^{-1}

The model has four main outlets: Pipe 1 is the upper off-shoot pipe, this is the where the fluid was monitored and the mechanical power calculated. Pipe 2, the lower pipe, this is where the Ram valve would be located and the fluid was accelerated up to terminal velocity. Pipe 3, the through pipe which allowed fluid flow. Pipe 4, another through pipe which did not allow fluid flow. Pipes 3 and 4 may have a ram pump and off-shoot pipe attached, however, these were removed to simplify the model thereby reducing the computational time. Pipe 3 was extended through the computational domain to allow fluid movement to determine if it had an overall effect on the system. All the pipes identifications are shown in Figure 51.

5.2. CFD Fluid domain method

The issues of CFD internal flow were demonstrated previously in chapter 3. This internal flow generated negative pressures required to maintain the outlet/inlet velocities. This implied a new CFD method was required to calculate the mechanical power output of the system. A large external fluid domain was constructed around the model allowing fluid to flow through and around the inlet of the Ram pump. The inlet face of the fluid domain had a boundary condition applied of 1 ms^{-1} (average river velocity). The face of the fluid domain was 10m away from the ram pump inlet allowing fluid to move freely throughout the domain. This caused the fluid to enter the ram pump inlet independent and without negative pressures present to maintain flow.

Using the ANSYS design modeller feature, the fluid domain was constructed around the imported 3D model in the form of a solid box. Using the Boolean feature, the model is extracted leaving the fluid domain ready for meshing and this is shown in Figure 52.

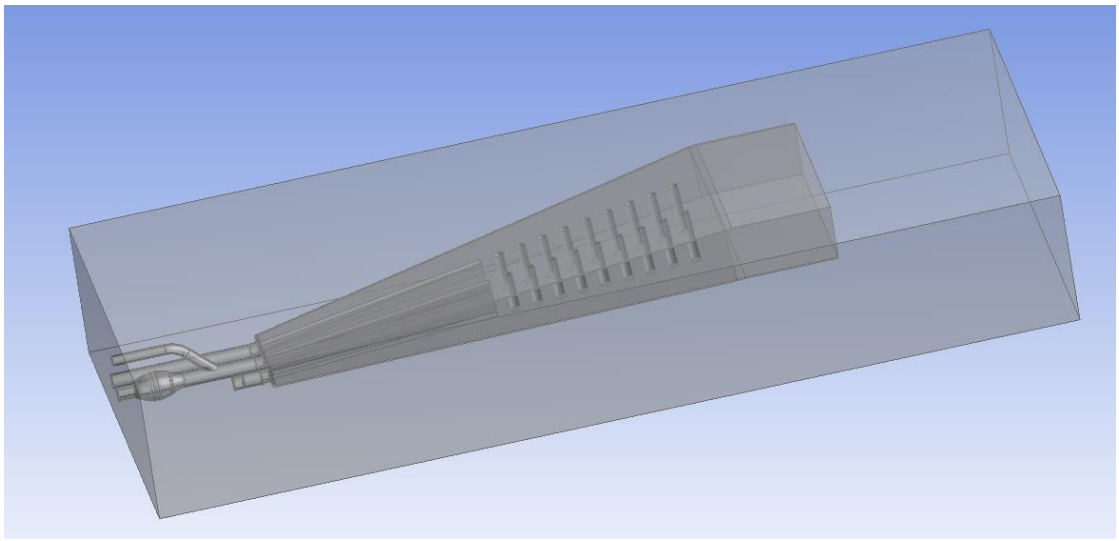

Figure 52 External fluid domain

5.3. CFD mesh method and verification

The fluid domain was split up into 3D tetrahedral elements of varying sizes. This allows for the governing equations to be discretised and solved through these smaller elements. The size of each individual element depends on its location within the fluid domain. The closer to boundaries, the smaller the element, as larger elements may overlook boundaries of the model. This also assists in reducing the total number of elements by having larger elements in the domain where no significant change has occurred. The cell sizes in the open section on the fluid domain are approximately 10m in size and reduce to 1mm in the areas close to the boundary walls.

The stability of the computation not only relies on the element size near the wall, but also the quality of the elements. An increase in the quality of the elements is represented as a decrease in the number of iterations required to achieve convergence. This reduces the overall computational time of the model. Through the ANSYS workbench, the mesh quality is monitored with the main metrics shown in Table 14.

Table 14 Fluid domain mesh metrics with ANSYS maximum and average required values

Mesh metric	Element quality	Aspect ratio	Skewness	Orthogonal quality
Minimum	0.0723	1.1527	0.0004	0.0542
Maximum	0.9997	25.8580	0.9458	0.9978
Average	0.8240	1.8755	0.2488	0.7501
Standard deviation	0.0898	0.4516	0.1134	0.1117
Fluent manual maximum value to obtain accuracy	N/A	35	0.95	>0.01
Fluent manual average value to obtain accuracy	>0.75	5	0.33	N/A

The element quality is the ratio of the volume of the element to the cube root of the sum of all the edge lengths squared, shown mathematically in equation (5.2). This element quality ranges from zero (worst quality) to 1 (best quality). The element quality for the total number of elements is shown in Figure 53.

$$Element\ Quality = C * \frac{volume}{\sqrt[3]{[\sum(edge\ length)^2]}} \qquad (5.2)\ (ANSYS, 2016)$$

C-constant required which differs for each type of element

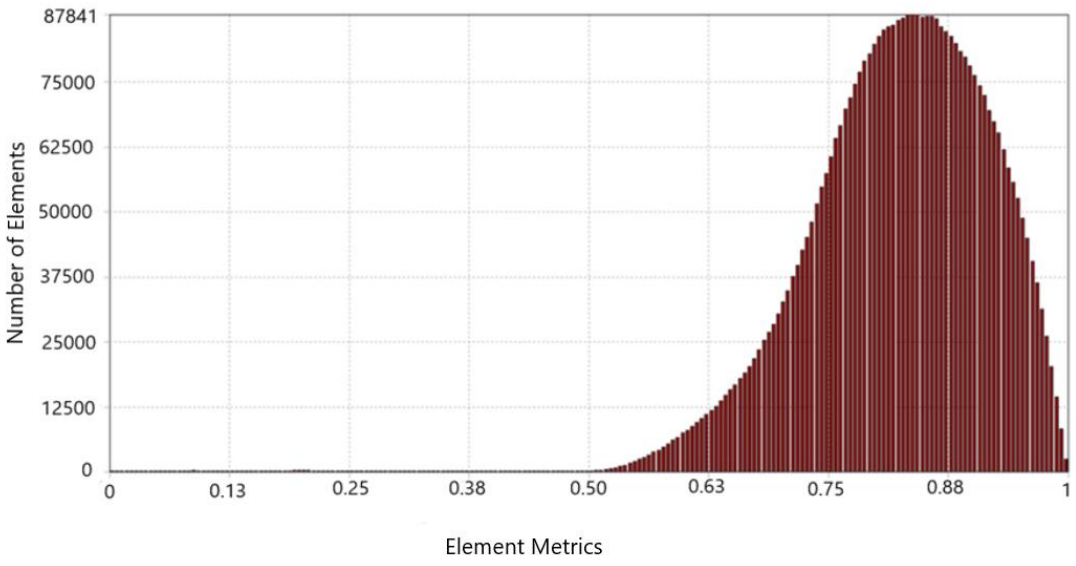

Figure 53 Element quality chart showing total number of elements and their quality metric

The aspect ratio is the correlation between the lengths of all the sides of the 3D tetrahedral cell. If the aspect ratio is too high, the element may distort or flatten out and this affects the precision of the calculations. Keeping the maximum aspect ratio to below 35 and the average to 5 is recommended by ANSYS (ANSYS, 2016). In Table 14 the maximum element aspect ratio of the model was 25.8 and the average was 1.9, which was in the acceptable range. The aspect ratio for the total number of elements is shown in Figure 54.

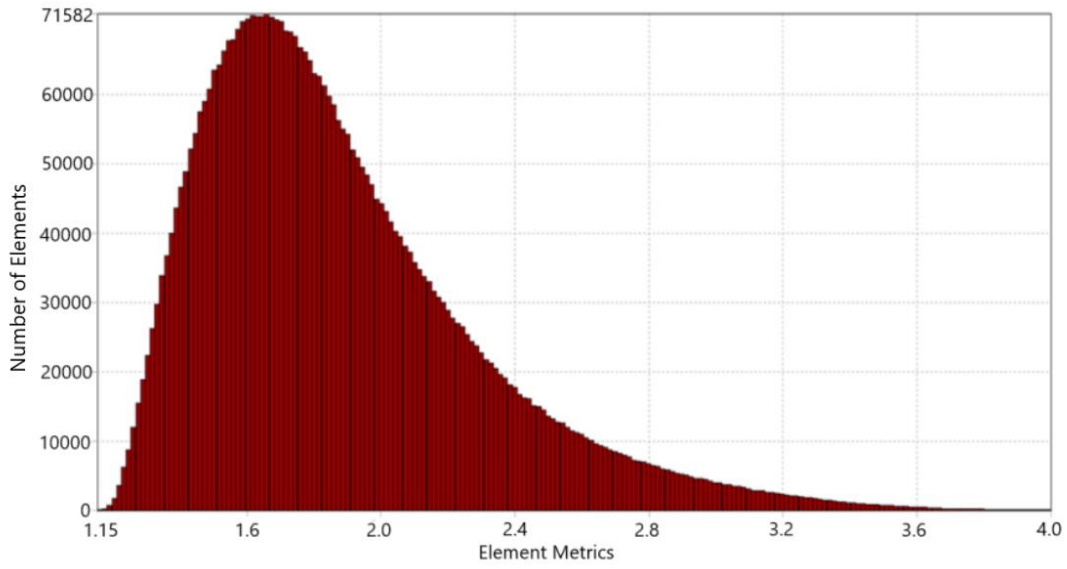

Figure 54 Aspect ratio chart showing the total number of cells and their aspect ratio metric

Skewness is the difference between the shape of the 3D tetrahedral and an equilateral 3D tetrahedral of the same volume. ANSYS recommend the maximum skewness to be less than 0.95 and the average to be 0.33 (ANSYS, 2016). In Table 14, the maximum skewness element is 0.95 and the average is 0.25 and is shown in the element skewness distribution chart in Figure 55.

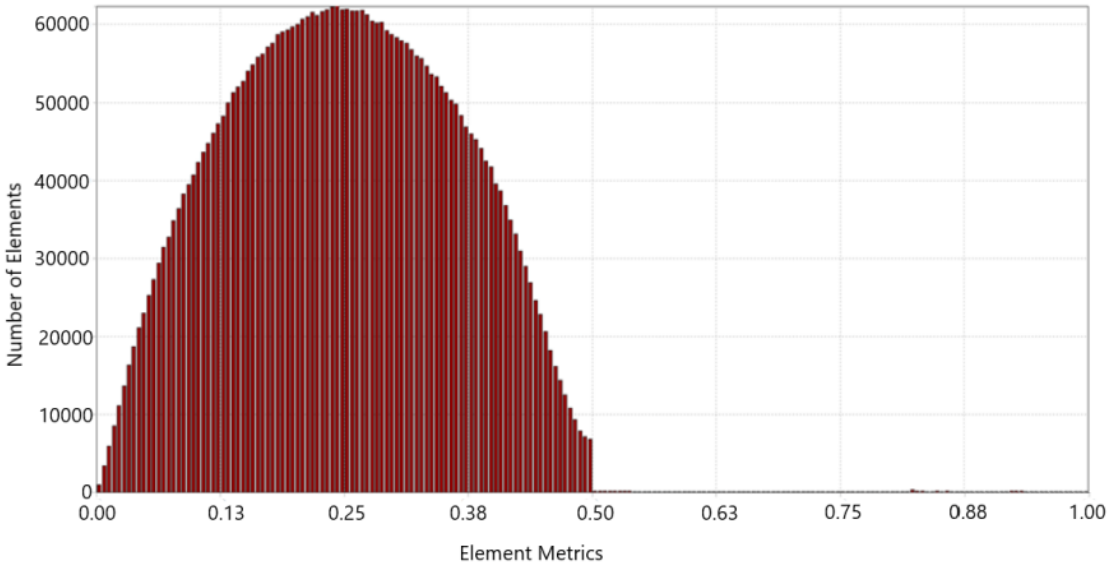

Figure 55 Skewness chart showing the total number of element and their skewness rating

The vectors shown in Figure 56 are used to calculate the orthogonal quality. This is achieved by using equations (5.3) and (5.4) with the lowest value of these two calculations used as the value for that element. The orthogonal quality ranges from 0 (worst) to 1 (best) and the element distribution is shown in Figure 57. As shown in Table 14, the minimum value for the model is 0.05 with an average value of 0.75, which are both higher than the acceptable minimum of >0.01 advised by ANSYS.

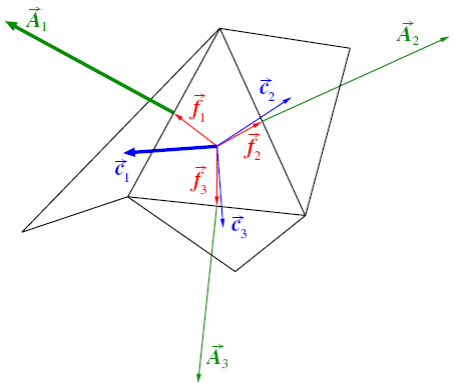

Figure 56 Vectors used to calculate element orthogonal quality (ANSYS, 2016)

$$OQ = \frac{\vec{A} \cdot \vec{f}}{|\vec{A}|\,|\vec{f}|} \qquad (5.3)\ (ANSYS, 2016)$$

$$OQ = \frac{\vec{A} \cdot \vec{c}}{|\vec{A}|\,|\vec{c}|} \qquad (5.4)\ (ANSYS, 2016)$$

OQ-Orthogonal Quality
$\vec{A}$-face normal vector
$\vec{f}$-vector from the centre of the element to the centre of the face of that element
$\vec{c}$-vector from the centre of the element to the centre of the adjacent element
$|\vec{A}|$-absolute face normal vector
$|\vec{f}|$-absolute distance from the centre of the element to the centre of the face of that element
$|\vec{c}|$-absolute distance from the centre of the element to the centre of the adjacent element

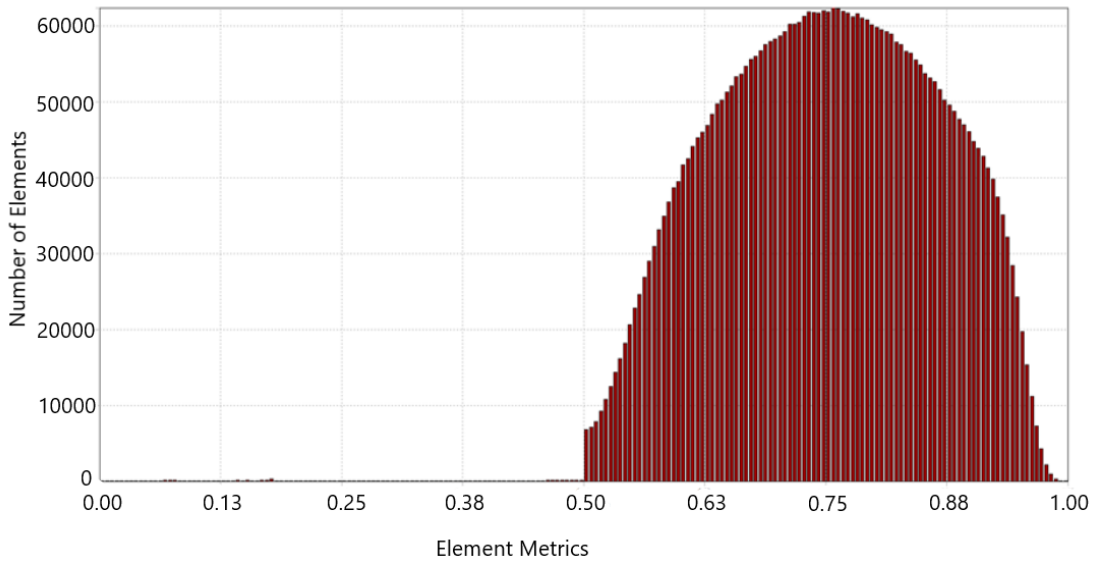

Figure 57 Chart showing the number of elements and their orthogonal quality rating

The final mesh chosen had 4.1 million elements and is shown in Figure 58. More elements would have increased the computational time for the model and fewer elements may have corrupted the calculations as the mesh metrics would not be within acceptable tolerances. The areas closer to the boundary wall of the Ram pump are more densely populated with elements as shown in the sectional view in Figure 59.

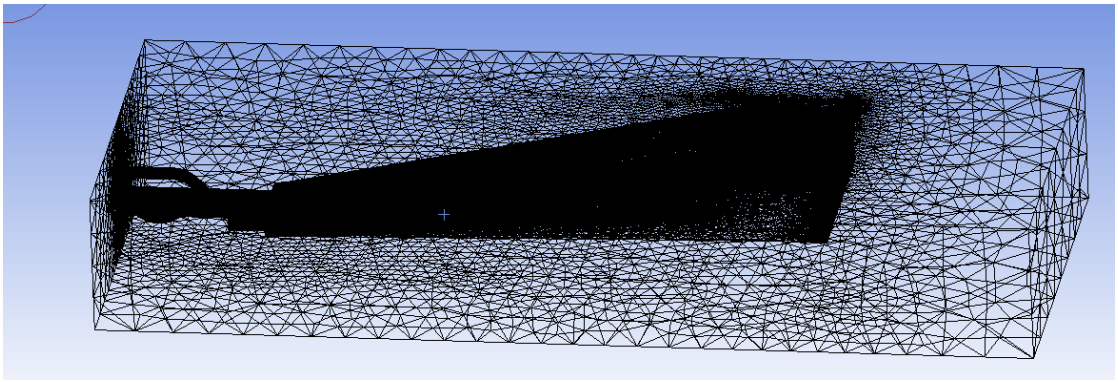

Figure 58 Final mesh with 4.1 million elements

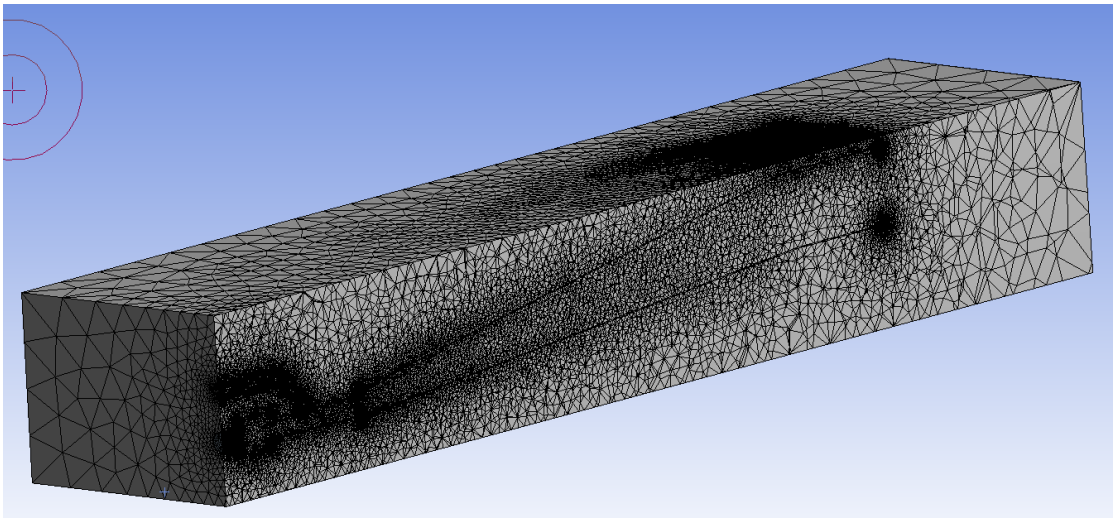

Figure 59 Section of the fluid domain mesh

5.4. CFD Solver (FLUENT)

FLUENT uses the Reynolds Averaged Naiver Stokes (RANS) equations to solve the fluid motion. These are predominantly used to express turbulent flows and are shown in equations 5.5 and 5.6 in their Cartesian form. These equations are taken derived from the N-S equations, but are time averaged approximations. This simplifies the calculations reducing the computational time.

$$\frac{\partial \rho}{\partial t}+\frac{\partial}{\partial x_i}(\rho u_i)=0$$ 5.5(ANSYS, 2013)

$$\frac{\partial}{\partial t}(\rho u_i)+\frac{\partial}{\partial x_j}\left(\rho u_i u_j\right)= -\frac{\partial p}{\partial x_i}+\frac{\partial}{\partial x_j}\left[\mu\left(\frac{\partial u_i}{\partial x_j}+\frac{\partial u_j}{\partial x_i}-\frac{2}{3}\delta_{ij}\frac{\partial u_l}{\partial x_l}\right)\right] +\frac{\partial}{\partial x_j}\left(-\rho\overline{u'_i u'_j}\right)$$ 5.6(ANSYS, 2013)

The k-omega Shear Stress Transport (SST) model initially developed by Menter (1993) was used to compute the turbulence and this gave rise to an additional two equations (5.7 and 5.8) for the solver to calculate. The k-omega SST solver combines the benefits of both the k-epsilon and the k-omega models in predicting the fluid flow and these equations perform better with vortex flows near walls. The disadvantage to this greater level of accuracy was the solving of the additional two equations which required more computational time (Menter et al., 2003).

$$\frac{\partial}{\partial t}(\rho k)+\frac{\partial}{\partial x_i}(\rho k u_i)=\frac{\partial}{\partial x_j}\left(\Gamma_k\frac{\partial k}{\partial x_j}\right)+G_k-Y_k+S_k$$ 5.7(ANSYS, 2013)

$$\frac{\partial}{\partial t}(\rho\omega)+\frac{\partial}{\partial x_j}\left(\rho\omega u_j\right)=\frac{\partial}{\partial x_j}\left(\Gamma_\omega\frac{\partial \omega}{\partial x_j}\right)+G_\omega-Y_\omega+D_\omega+S_\omega$$ 5.8(ANSYS, 2013)

K(terms) – turbulance kinetic enegry
ω(terms)-Specific dissipation rate (omega)

5.5. Ram valve and non-return valve modelling

There are a number of ways to simulate closing a valve in FLUENT. Creating separate fluid zones and changing the porosity of these zones to mimic the closing of a valve was deemed the least computer intensive. The additional fluid zones were constructed outside the main fluid domain and are shown in Figure 60. The upper off-shoot fluid zone (blue) was used to simulate a non-return valve for the fluid entering the turbine. The lower pipe fluid zone

(orange) was used to simulate the closing of the Ram valve and the through pipe fluid zone (green) was altered to simulate fluid transferring to an additional Ram pump.

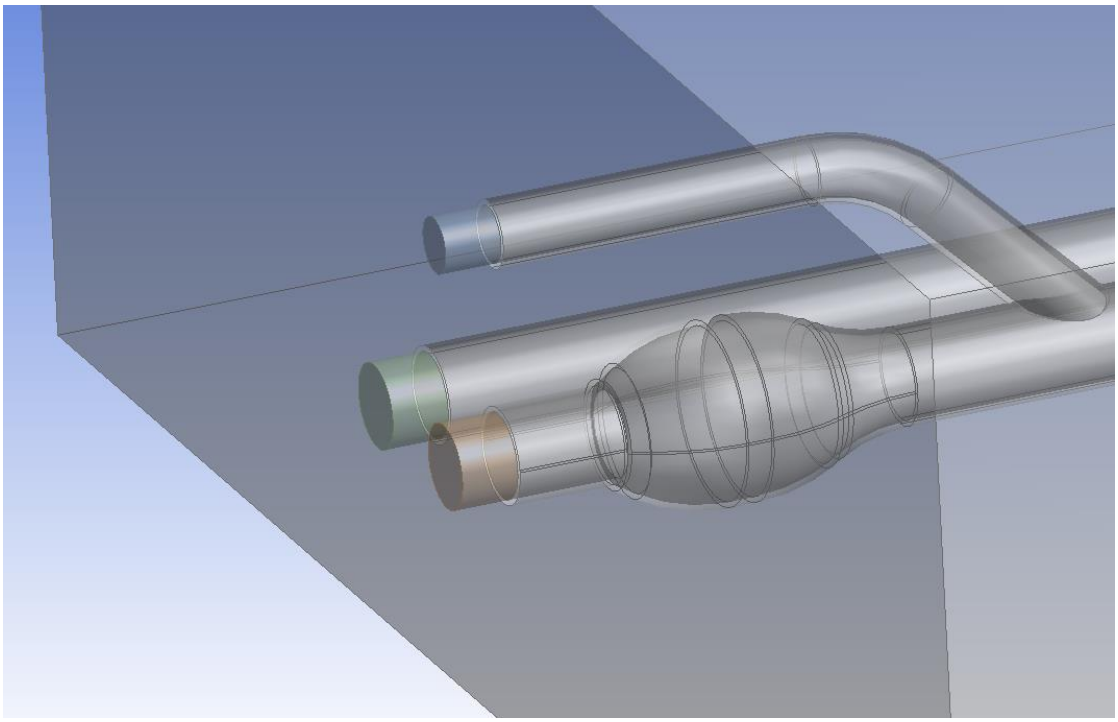

Figure 60 Additional fluid domains required to simulate valve operation. Blue: Upper off-shoot, Green: through pipe, Red: Main pipe

Using the information gathered from the MATLAB code in chapter 5, the total run time for the model was 20 seconds. This allowed for an initial phase of 1 second to steady the flow with both off-shoot and lower pipe closed. This is equivalent to zeroing the variables in MATLAB. Second phase was to allow the acceleration of the fluid and confirm the time it took to gain terminal velocity. The final phase was to rapidly close the Ram valve and open the off-shoot pipe. This was for the final 10 seconds to calculate the mechanical power generated.

It was determined in the MATLAB code chapter, that there was an opportunity to generate mechanical power by allowing the fluid to return from the off-shoot pipe during the acceleration phase.

As the fluid accelerates through the lower pipe, the fluid in the off-shoot is dragged back through by means of the Venturi effect. Theoretically, additional mechanical power may be

developed. Therefore, two types of power generation were modelled. One-way, where the off-shoot pipe fluid domain was closed during the acceleration phase thus modelling a non-return valve and two-way where the off-shoot pipe was not restricted during the whole 20 second cycle. The valve operation in the one-way cycle is shown in Table 15 and the two-way valve operation is shown in Table 16.

Table 15 One-way valve operation for the 20 second cycle

One-way power generation					
Time (s)		**Pipe 1**	**Pipe 2**	**Pipe 3**	**Action**
From	**To**	**Upper**	**Lower**	**Through pipe**	
0	1	closed	closed	open	start steady state
1	1.2	closed	opening	closing	divert water through ram pump (valve operation)
1.2	10	closed	open	closed	acceleration of water through Ram valve
10	10.2	opening	closing	closed	water hammer effect
10.2	20	open	closed	closed	power generation

Table 16 Two-way valve operation for the 20 second cycle

Two-way power generation					
Time (s)		**Pipe 1**	**Pipe 2**	**Pipe 3**	**Action**
From	**To**	**Upper**	**Lower**	**Through pipe**	
0	1	closed	closed	open	start steady state
1	1.2	opening	opening	closing	divert water through ram pump (valve operation)
1.2	10	open	open	closed	acceleration of water through Ram valve
10	10.2	open	closing	closed	water hammer effect
10.2	20	open	closed	closed	power generation

In FLUENT, the viscous resistance ($1/m^2$) of a fluid domain alters the porosity of the elements in that region. The viscous resistance of the porous fluid domain is zero ($1/m^2$) when fluid is allowed to flow freely and 10^{10} ($1/m^2$) when the fluid is fully restricted. The mathematical values for the open and closed elements are shown in Table 17 andTable 18 respectively. For

the closing of the valve, the ramp from zero to 10^{10} ($1/m^2$) was calculated using the standard straight-line equation (5.9).

$$y = m * x + c \qquad (5.9)$$

x- Time along the x-axis
y- Viscous resistance along the y axis
m- Gradient of the straight line
c- Point where it crosses the y axis

Table 17 Mathematical equations required to change the porosity of the fluid in one-way power generation simulating opening and closing valves

One-way power generation					
Time (s)		**Pipe 1**	**Pipe 2**	**Pipe 3**	**t=cycle time (s)**
From	**To**	**Upper**	**Lower**	**Through pipe**	**y=viscous resistance ($1/m^2$)**
0	1	10^{10}	10^{10}	0	start steady state
1	1.2	10^{10}	$y=-5*10^{10}*t + 6*10^{10}$	$y=5*10^{10}*t - 5*10^{10}$	divert water through ram pump (valve operation)
1.2	10	10^{10}	0	10^{10}	acceleration of water through ram valve
10	10.2	$y=-5*10^{10}*t + 5.1*10^{11}$	$y=5*10^{10}*t - 5*10^{11}$	10^{10}	water hammer effect
10.2	20	0	10^{10}	10^{10}	power generation

Table 18 Mathematical equations required to change the porosity of the fluid in two-way power generation simulating opening and closing valves

Two-way power generation					
Time (s)		**Pipe 1**	**Pipe 2**	**Pipe 3**	
From	**To**	**Upper**	**Lower**	**Through pipe**	
0	1	10^{10}	10^{10}	0	start steady state
1	1.2	$y=-5*10^{10}*t + 6*10^{10}$	$y=-5*10^{10}*t + 6*10^{10}$	$y=5*10^{10}*t - 5*10^{10}$	divert water through ram pump (valve operation)
1.2	10	0	0	10^{10}	acceleration of water through ram valve
10	10.2	0	$y=5*10^{10}*t + 5*10^{11}$	10^{10}	water hammer effect
10.2	20	0	10^{10}	10^{10}	power generation

It can be seen in Figure 61 the porosity change required to simulate the closing pipe 1 (upper off-shoot pipe) for the one-way valve operation in Table 17.

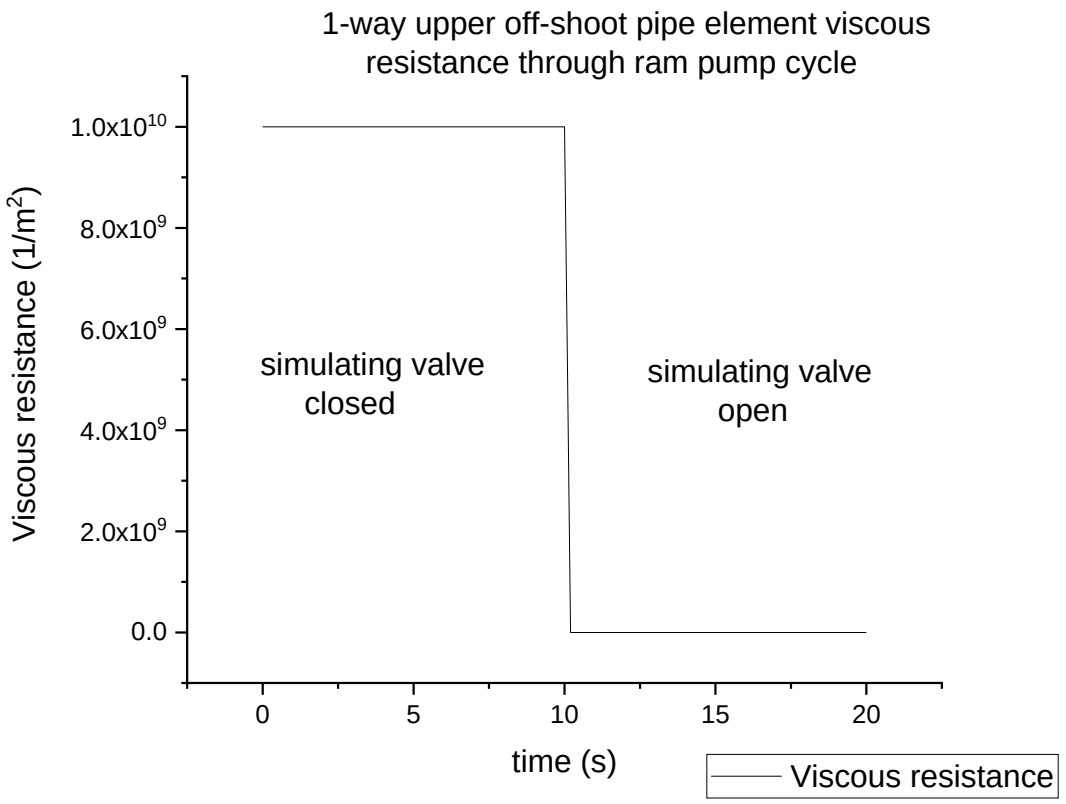

Figure 61 Element porosity change simulating the off-shoot non-return valve through the generation cycle

To change the porosity of a cell in a transient time study, a User Defined Function (UDF) was required to be written. This is a piece of code that the CFD solver checks when running through each time step. This code is written in the programming language 'C' and is compiled within FLUENT via visual studio. The flow chart of the UDF for the upper off-shoot pipe (pipe 1) is shown in Figure 62. There are 5 'IF' statements, which relate to the five time segments in the 20 second cycle shown in Table 17. The first three 'IF' statements run from zero to 10 seconds maintaining the viscous resistance at 10^{10} ($1/m^2$) which does not allow fluid to flow through the elements. The fourth 'IF' statement allows fluid to go from zero flow to full flow in 0.2 seconds simulating the opening of the non-return valve. The three user defined functions used for the 3 pipe outlets for both 1-way and 2-way are shown in Appendix D.

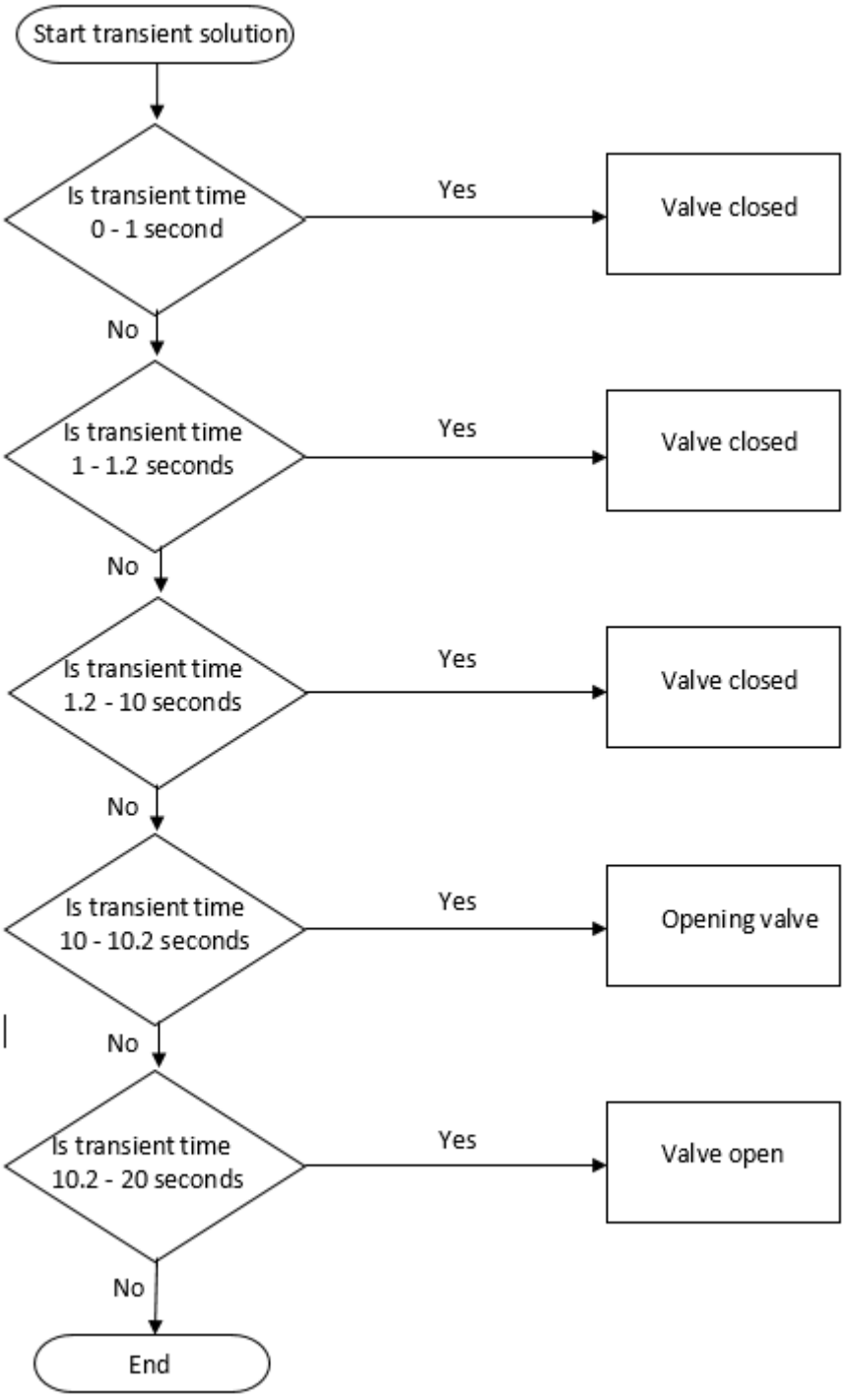

Figure 62 one-way upper off-shoot pipe flow chart of the UDF

5.6. Formulas used to calculate power output

The velocity (ms^{-1}), mass flow rate ($Kg{\cdot}s^{-1}$) and pressure (Pa) were monitored through each of the time steps for all of the outlets. Pressure was monitored in Pascals and this was converted

into another monitor in FLUENT using equation (5.10). The power was calculated using equation (5.11). This was rearranged using the general equations (5.12) and (5.13).

$$Head = \frac{P}{\rho * g} \qquad (5.10)$$

Head-pressure (m)
P-pressure (Pa)
ρ -Fluid density (kg·m^{-3})
g- Acceleration due to gravity (ms^{-2})

$$P = MFR * head * g \qquad (5.11)$$

P – Hydraulic power (W)
MFR- Mass flow rate (kg·s^{-1})
Head- Pressure calculated in equation (6)

$$P = \rho * g * h * \mathrm{Q} \qquad (5.12)$$

Q̇-Volumetric flow rate (m^{3}s^{-1})

$$\rho = \frac{\dot{\mathrm{m}}}{\mathrm{Q}} \qquad (5.13)$$

ṁ-mass flow rate (kg·s^{-1})

5.7. Geometrical models used

The geometry of the model above used pillars in the inlet as per the OCPL design as shown in Figure 63. This was to provide support for the roof of the inlet. Another model was constructed without these pillars (Figure 64) to establish if they restricted the flow and therefore reduce the power output. Finally, a third model was constructed with the off-shoot pipe diameter reduced to 0.1m (Figure 65). This was to investigate the increased pressure of the fluid and to establish if power output was increased.

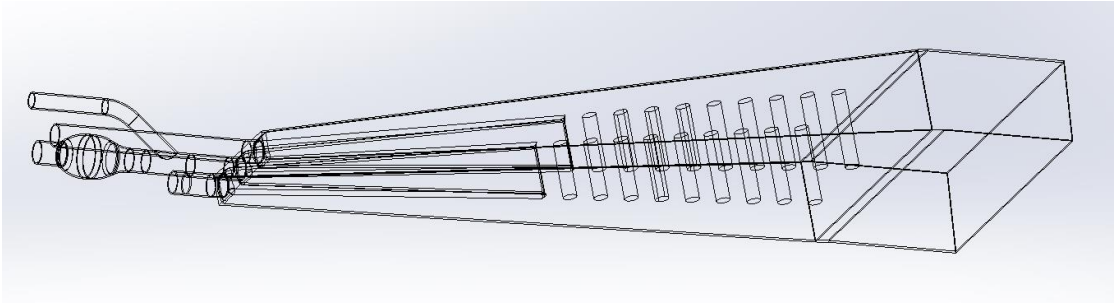

Figure 63 Model with pillars

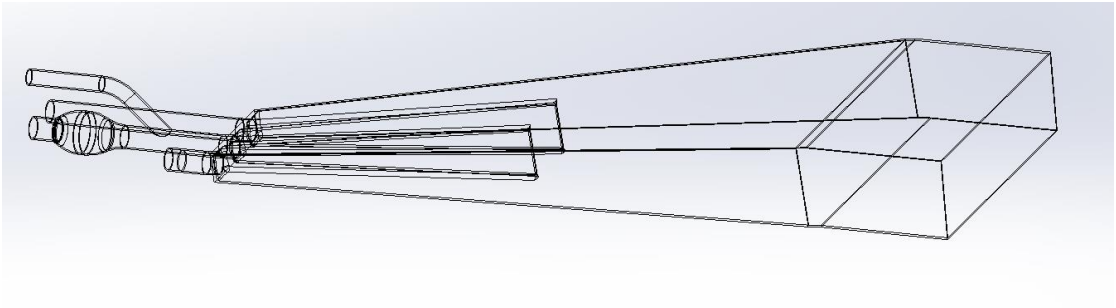

Figure 64 Model without pillars

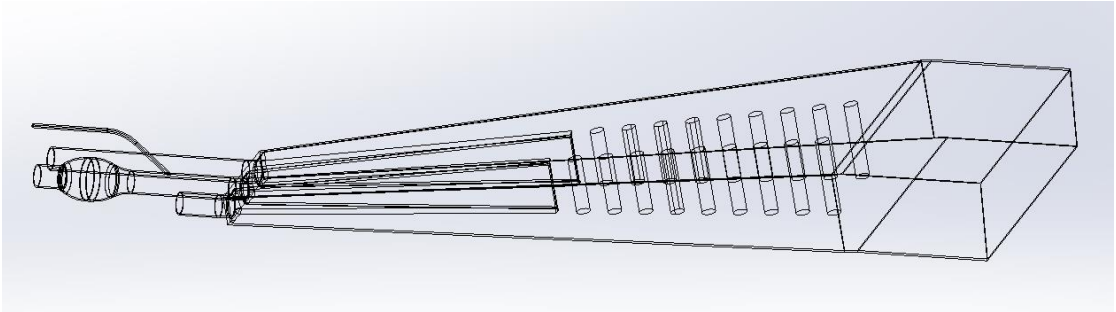

Figure 65 0.1m diameter off-shoot pipe model

5.8. Fluent model results

Within these results are the calculations to confirm the most cost-effective time step to use, confirming geometry modifications and to calculate 1-way/2-way power generation. The 1-way velocity cut plots at 3, 10 and 11 seconds are shown in Figure 66. The velocity in the main pipe peaks at 10 seconds when the valve is closed. At 11 seconds the fluid is moving through the upper pipe where the power is calculated. The detailed view of the velocity magnitude before and after the closing of the ram valve is shown in Figure 67.

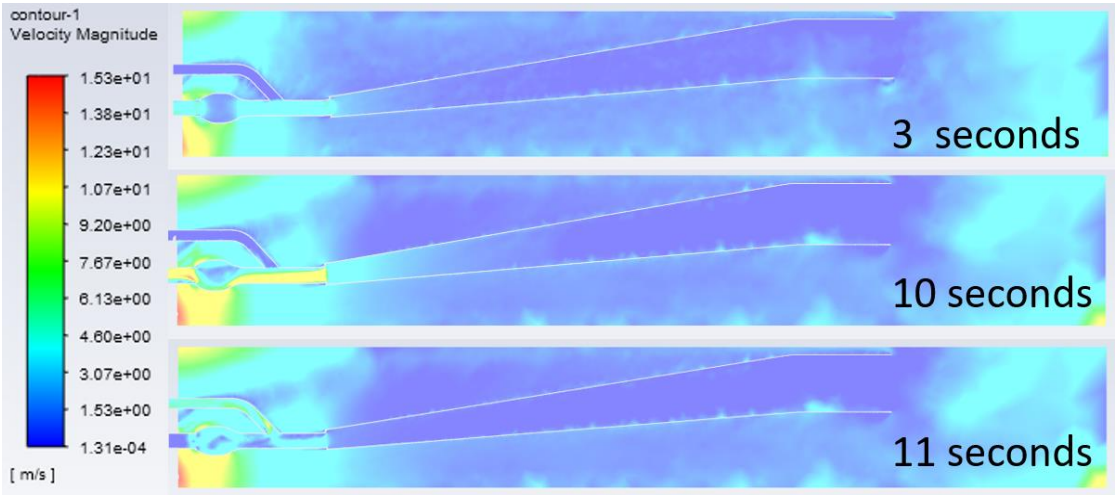

Figure 66 Velocity magnitude at 3, 10 and 11 seconds

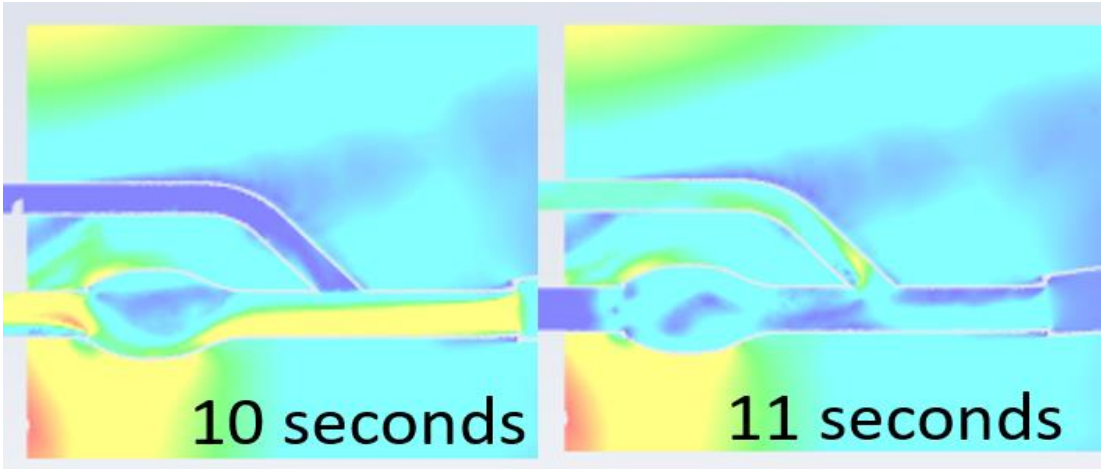

Figure 67 velocity magnitude at 10 and 11 seconds

5.8.1. Time step calculations

The transient model has a total run time of 20 seconds. This total time was split up into incremental changes in time (time steps) for the governing equations to be solved. Generally, the smaller the time step the greater the accuracy, however this increased computational time. The run times for all models are shown in Table 19 with the first three model examining the 0.01, 0.001 and 0.0001 second time steps.

Multiple computer cores were used when completing the FLUENT model calculations. To compare the run times equally, the total run time was multiplied by the number of computer

cores to give a total time taken if a single core was used and this is also shown in Table 19. When a time step of 0.01 seconds was used, the total number of transient steps was 2000 (20 seconds/0.01) and the total run time if one core was used was 75 hours and 20 minutes. For a time step of 0.001s, the total number of transient steps was 20,000 and the total run time for one core was 168 h. Finally, for a 0.0001s time step, 200,000 transient steps and a run time of 3969 h and 30 min were calculated for a single core.

Table 19 Computational models and calculation times

Model No	models	power generation type	time steps	pipe	Comments	Cores used	time to complete (H:M:S)	time if only 1 core was used (D:H:M:S)
1	no pillars	1-way	0.01	variable	to confirm adequate time steps	16	05:45:01	3:20:0:16
2	no pillars	1-way	0.001	variable		16	10:30:03	7:0:0:48
3	no pillars	1-way	0.0001	variable		48	82:41:53	165:9:30:24
4	no pillars	1-way	0.001	variable	to see if the pipe letting fluid through affects the power output	16	10:30:03	7:0:0:48
5	no pillars	1-way	0.001	closed		16	17:05:36	11:9:29:36
6	no pillars	1-way	0.001	open		16	N/A	
7	no pillars	2-way	0.001	variable	compare 1-way and 2-way power generation (no pillars)	16	11:54:52	7:22:37:52
8	with pillars	1-way	0.001	variable	compare 1-way and 2-way power generation (with pillars)	16	N/A	
9	with pillars	2-way	0.001	variable		16	12:51:11	8:13:38:56
10	reduced outlet	1-way	0.001	variable	OCP asked to look at the pressure using a greatly reduced outlet	16	17:38:56	11:18:22:56
11	reduced outlet	2-way	0.001	variable		16	20:33:29	13:16:55:44

The velocity of the lower pipe for the three different time steps are shown in Figure 68. The blue line is the 0.01 second time step with the quickest computational time, however, during the acceleration phase of 4 - 10 seconds the acceleration is erratic compared to the 0.001 second and 0.0001 second time steps.

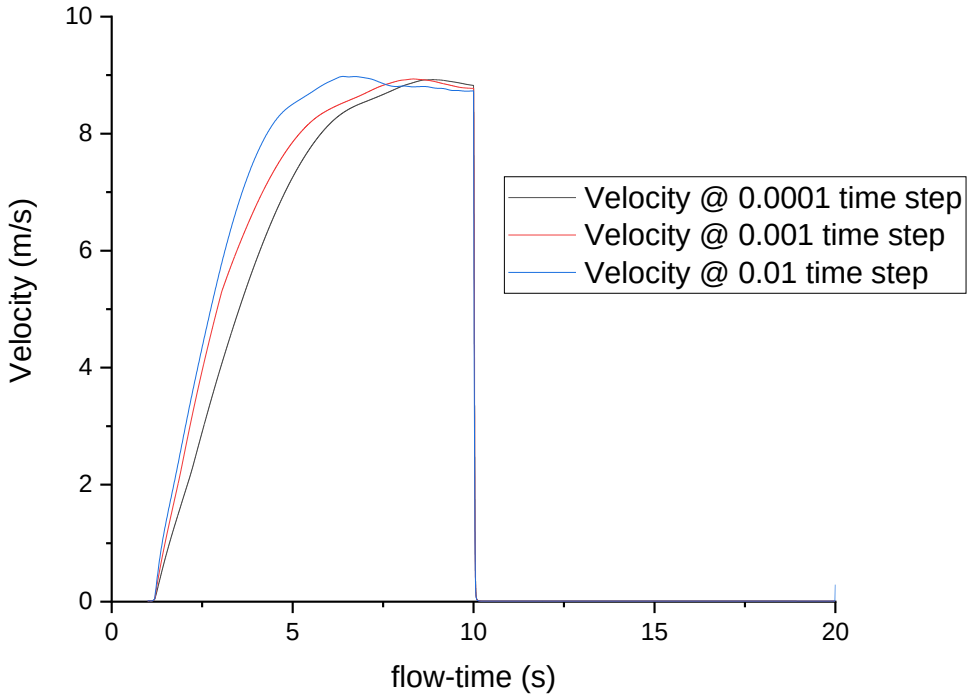

Figure 68 Velocity through the lower pipe with no pillars and 1-way power generation at 0.01, 0.001 and 0.0001 second time steps

Upper off-shoot pipe pressure (metres head) for the three different time steps are shown in Figure 69. The maximum pressure once the ram valve was closed was 9.14m with 0.01 seconds time step, 12.15m with 0.001 and 12.61m for the 0.0001s time step.

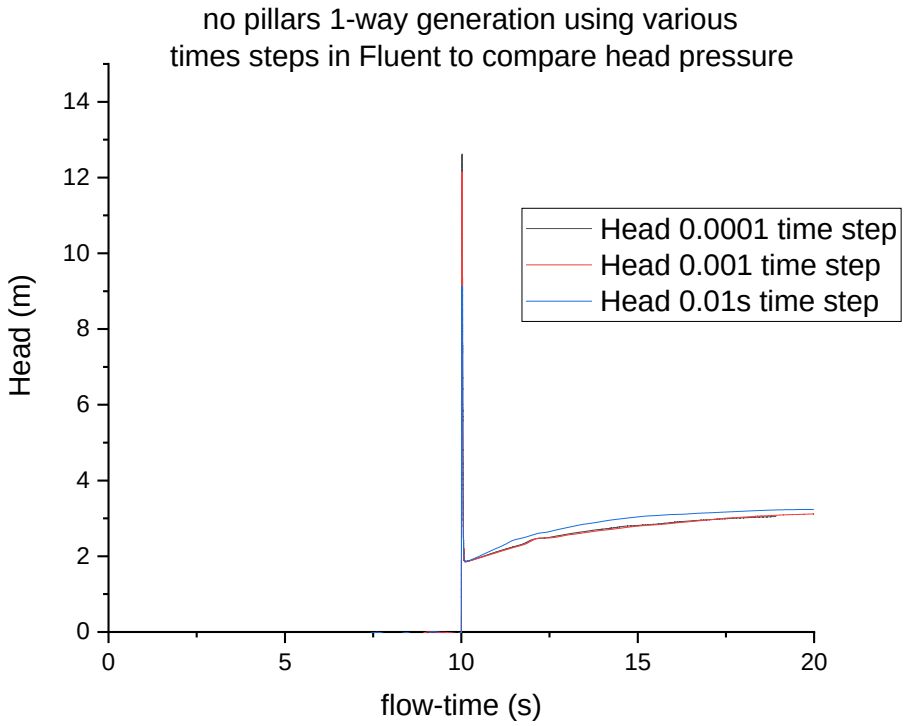

Figure 69 Pressure (metres head) in the upper off-shoot with no pillars 1-way power generation at 0.01, 0.001 and 0.0001 second time steps.

The mechanical power calculated through the total cycle for the three different time steps are shown in Figure 70 with Figure 71 showing the mechanical power generated through the hydraulic shock phase from 10 - 10.2 seconds. The maximum peak power generated through this phase is 246.9kW with 0.01s, 303.6kW with 0.001s and 312.8kW with the 0.0001s time step.

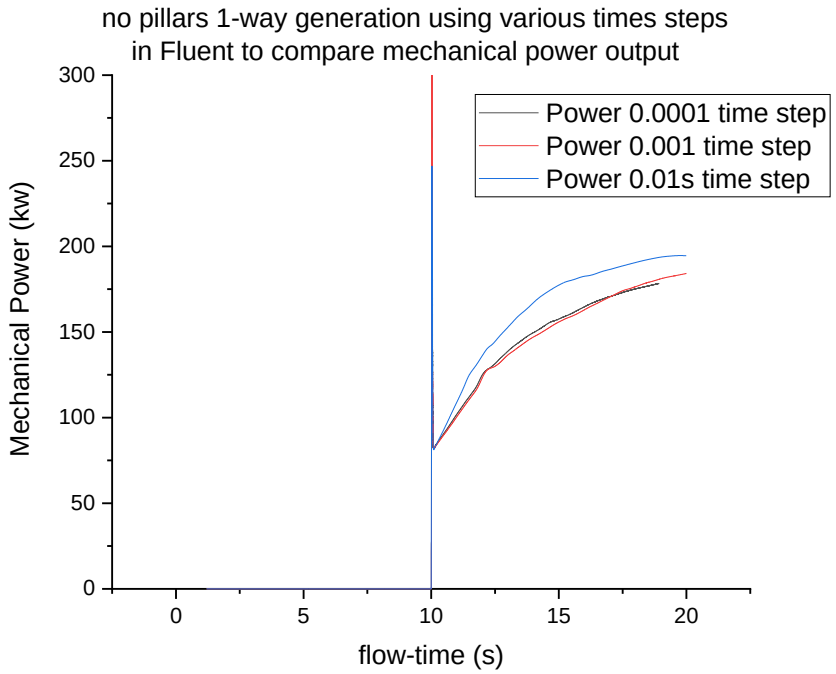

Figure 70 Mechanical power generated in the upper off-shoot pipe with no pillars and 1-way power generation at 0.01, 0.001 and 0.0001 second time steps

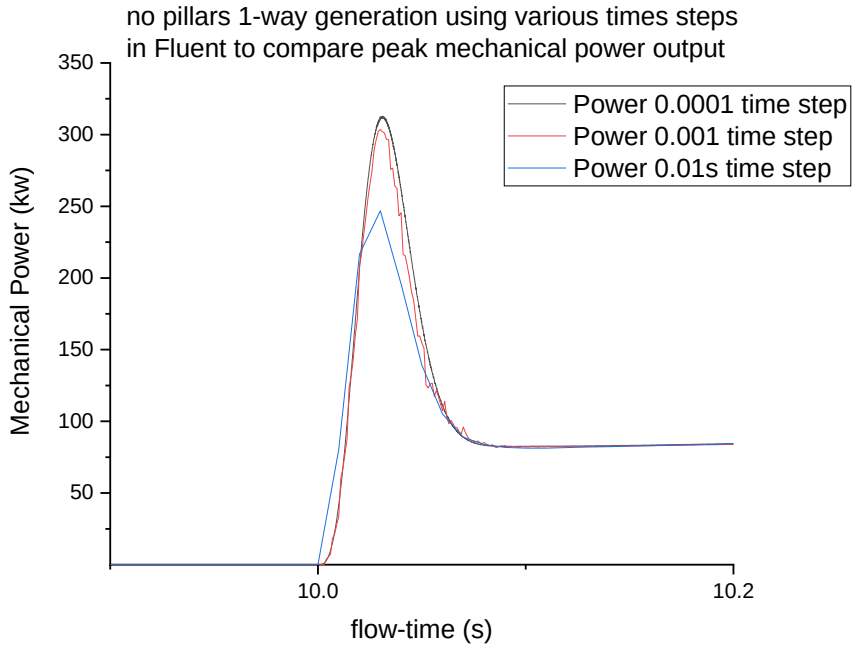

Figure 71 Mechanical power generated in the upper off-shoot pipe during the ram valve closing using 0.01, 0.001 and 0.0001 second time steps (no pillars and 1-way power generation)

As shown in Table 20, there was an increase of the power of 23% between the 0.01 and the 0.001 second time steps with a 123% increase in computational time. There was an increase of the power of 3% between the 0.001 and 0.0001 second time step with a 2263% increase in computational time.

Table 20 Percentage increase of hydraulic power and computational time (no pillars and 1-way generation)

	Time step (s)		Percentage increase
	0.01	**0.001**	
Peak power during hydraulic show phase (kw)	246.9	303.6	22.96%
Time to calculate 20 second run (hours)	75.3	168	123.11%
	Time step (s)		**Percentage Increase**
	0.001	**0.0001**	
Peak power during hydraulic show phase (kw)	303.6	312.8	3.03%
Time to calculate 20 second run (hours)	168	3969	2262.50%

The 0.0001 second time step gave the smoothest power curves; however, this took the longest to compute. Therefore, with only a 3% decrease in hydraulic power output and a heavily reduced computational time the 0.001 second time step was used for all future FLUENT models.

5.8.2. Confirmation of whether the fluid flowing through the through pipe reduces power output

The through pipe shown in Figure 51 was installed to allow fluid to flow through to a potential secondary Ram pump and generation system. Three different user defined functions were written to simulate fluid flowing throughout the 20 second cycle, no fluid flow throughout the cycle and fluid flow up until the start of the Ram valve closing and then closed for the remaining cycle. The hydraulic power generated for all three simulations are shown in Figure **72** and the initial valve closing phase in Figure 73.

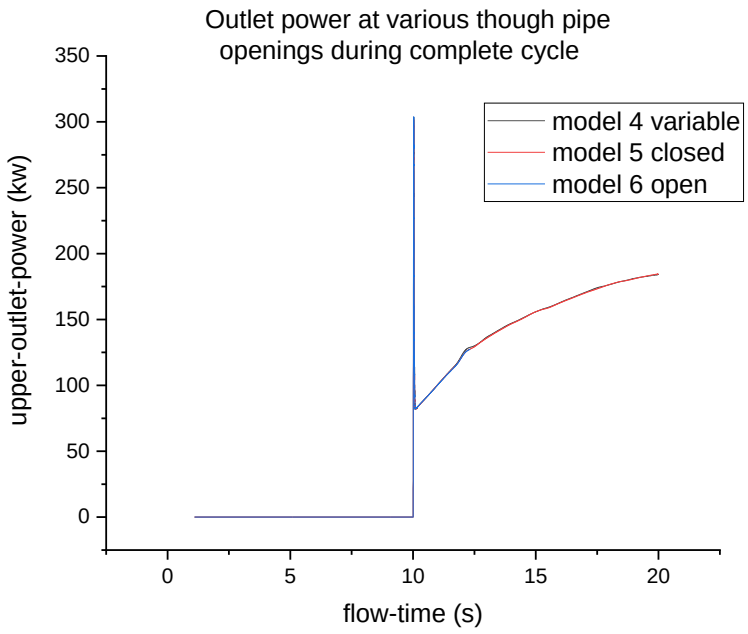

Figure 72 **Off-shoot outlet hydraulic power generation during various through pipe operations**

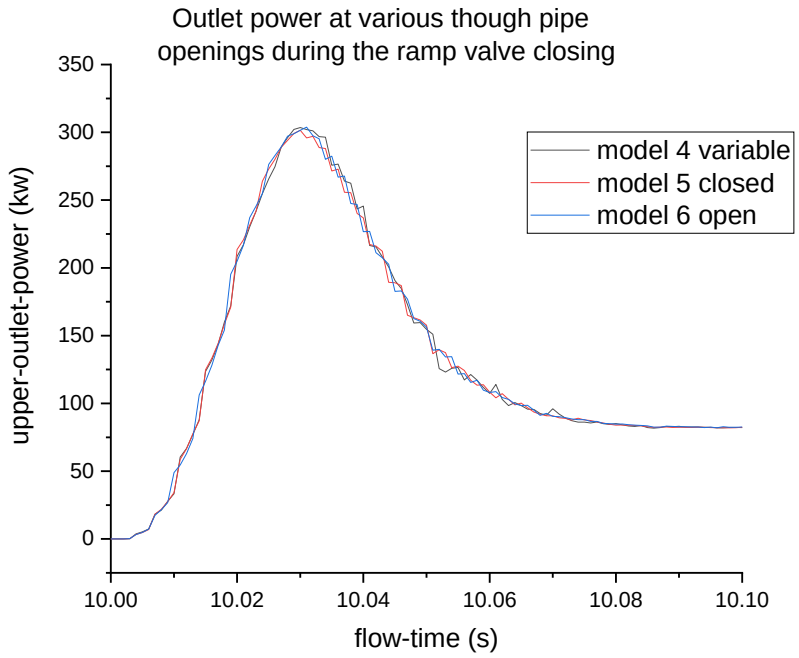

Figure 73 Off-shoot outlet hydraulic power generation at various through pipe operations during the Ram valve closing

5.8.3. Comparison of power generated using geometry with and without inlet pillars

Computational models were completed using the geometries with or without pillars. The power generated through the off-shoot pipe is shown in Figure 74 with the Ram valve closing shown in Figure 75. These graphs show there was an increase of 3.75% increase in power output when the pillars were included in the geometry. This increase was not expected as the momentum of the fluid was altered after interacting with the pillars. One explanation could be the guide vanes funnel that fluid through to the ram valve are extended to the inlet via the pillars. However, a new model with guide vanes along the length of the inlet would need to be produced to confirm if this was achieved. As the two models were similar in the power output, no further action was taken.

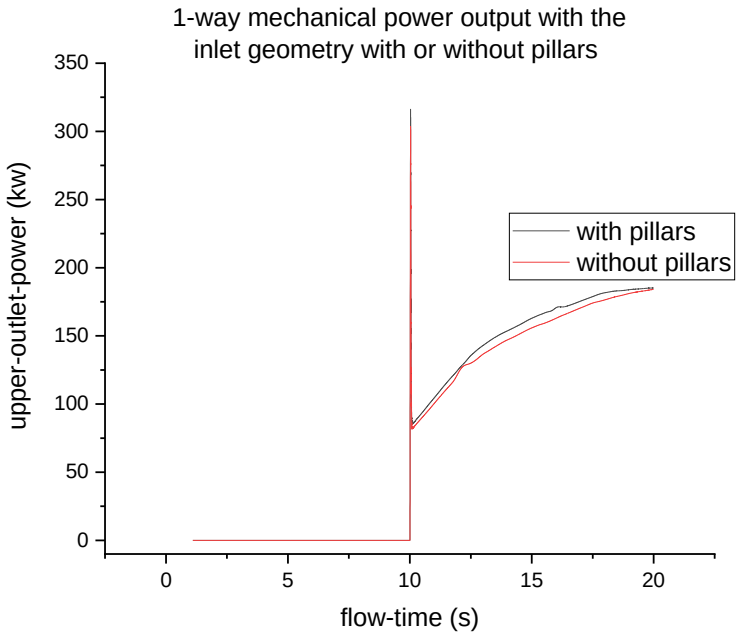

Figure 74 1-way power output for both with and without pillars

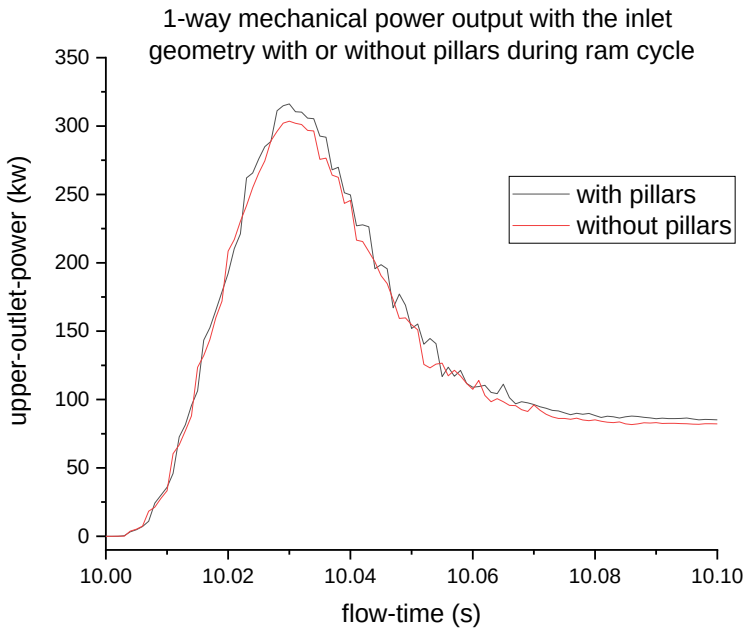

Figure 75 1-way power generation during Ram valve closing phase for both with pillars and without pillars

5.8.4. 1-way and 2-way power generation comparison

The velocity through the acceleration phase between 1 - 10 seconds of the cycle is shown in Figure 76. There is velocity difference just before it reaches terminal velocity and this is shown in the last 5 seconds of the acceleration phase in Figure 77. In the 2-way power generation, there is a reversed flow in the off-shoot pipe, which acts as drag on the fluid exiting the lower pipe thus slowing it down.

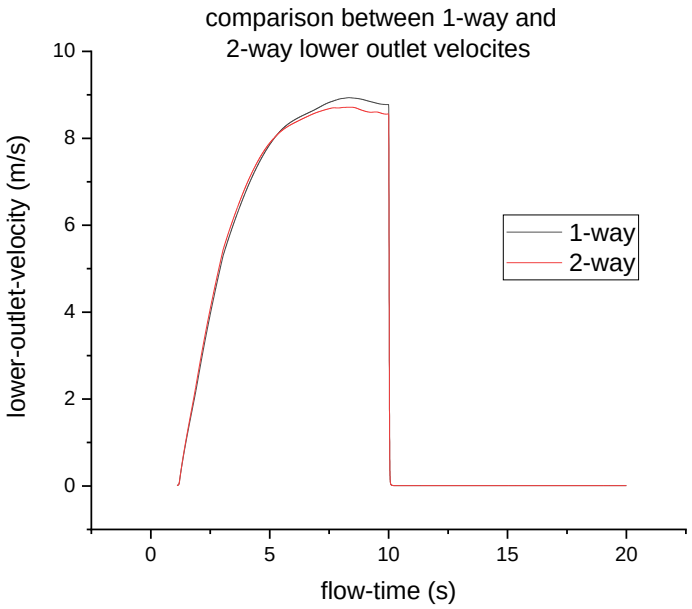

Figure 76 Velocity through the lower pipe during the acceleration phase

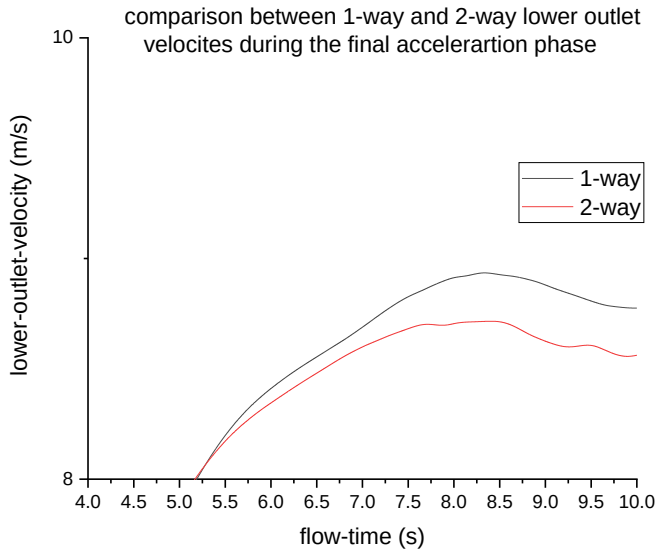

Figure 77 Velocity through the lower outlet pipe during the last 5 seconds of the acceleration phase

The mass flow rate of the upper off-shoot pipe is shown in Figure 78 for both the 1-way and 2-way cycle. The 1-way modelled a non-return valve on the off-shoot pipe using a UDF and does not allow fluid to reverse flow. The 2-way model allowed the reverse flow and this was used to generate mechanical power. However, this reversed mass flow rate in the off-shoot

pipe acts against the fluid when the Ram valve is closed and does not peak as high as the 1-way model.

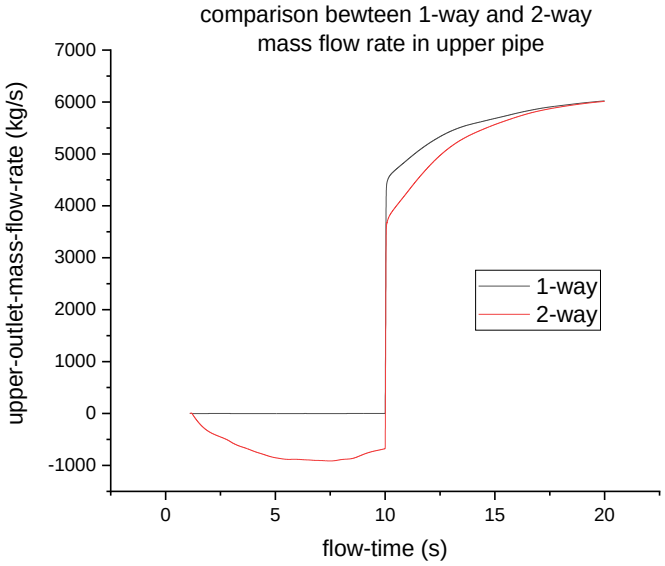

Figure 78 Mass flow rate in the off-shoot pipe for 1-way and 2-way generation

The hydraulic power is shown in Figure **79**, where after the Ram valve has closed, the power generation is reduced. This is due to the reverse flow of the off-shoot pipe acting against the hydraulic shock. Once the Ram valve has been shut, the power output generated in the off-shoot pipe is shown in Figure 80. The confirmed power generated in the 2-way model during the acceleration phase is shown in Figure 81. The average power developed during the 20 second cycle is 149.1 kW for the 1-way model and 72.2 kW for the 2-way model.

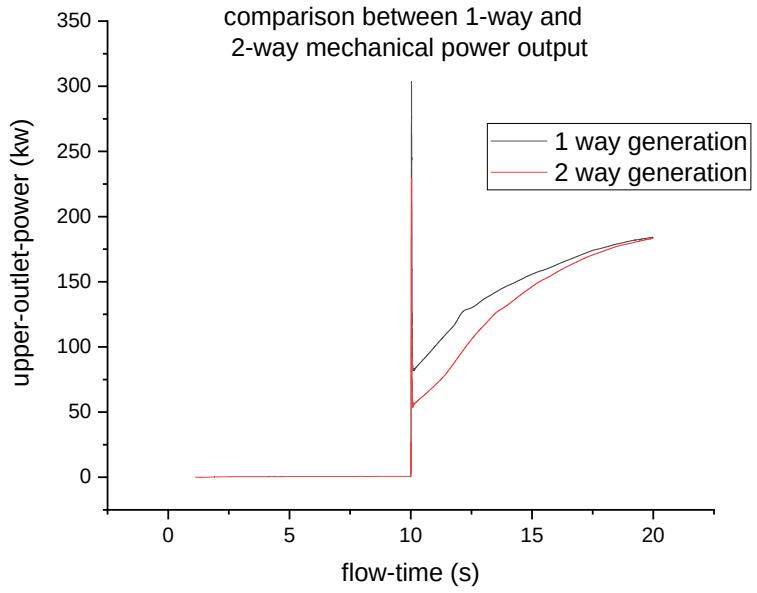

Figure 79 **Hydraulic power in the off-shoot pipe for 1-way and 2-way generation**

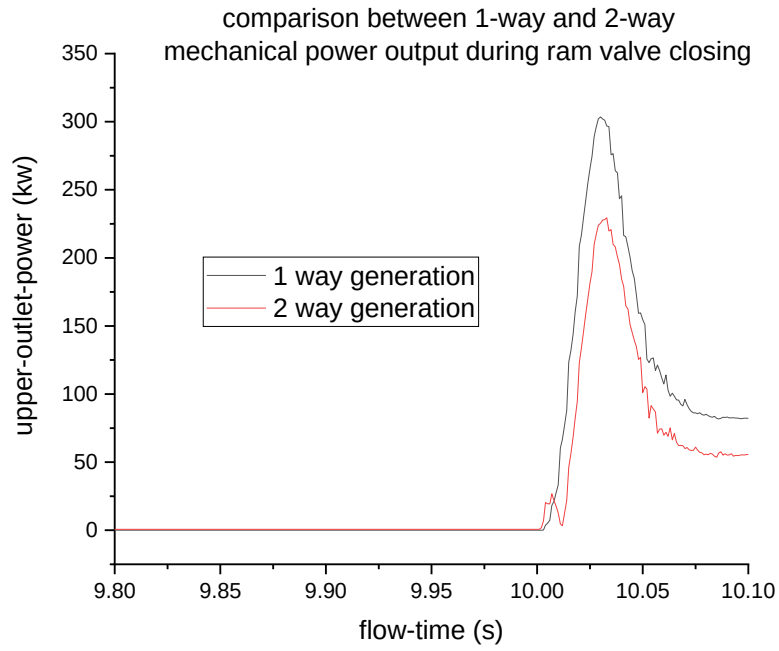

Figure 80 Hydraulic power in the off-shoot pipe for 1-way and 2-way generation for the acceleration phase through to the end of Ram phase

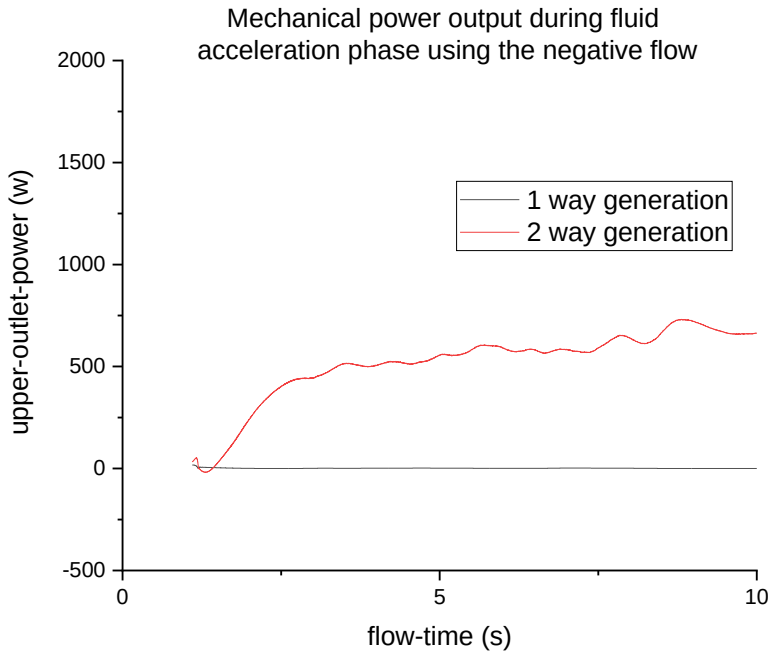

Figure 81 Hydraulic power in the off-shoot pipe for 1-way and 2-way generation through the acceleration phase

5.8.5. Reduced off-shoot pipe

The off-shoot pipe was reduced to 0.1m diameter to confirm the increase of head and to establish the power output. In addition, both 1-way and 2-way system models were applied. The pressure head for the reduced off-shoot pipe was raised to 16.1m in the instant the Ram valve was closed as shown in both Figure 82 and Figure 83. The previous off-shoot outlet with a 1m diameter pipe had a maximum head of 12.49m. Therefore, the reduced off-shoot outlet has an increased 3.61m of head. The hydraulic power generated is shown in Figure 84 and Figure 85 with a maximum power spike for 1-way power generation of 5.1kW and an average of 0.73kW. The 2-way power generation had a maximum of 1.6kW with an average of 0.6kW.

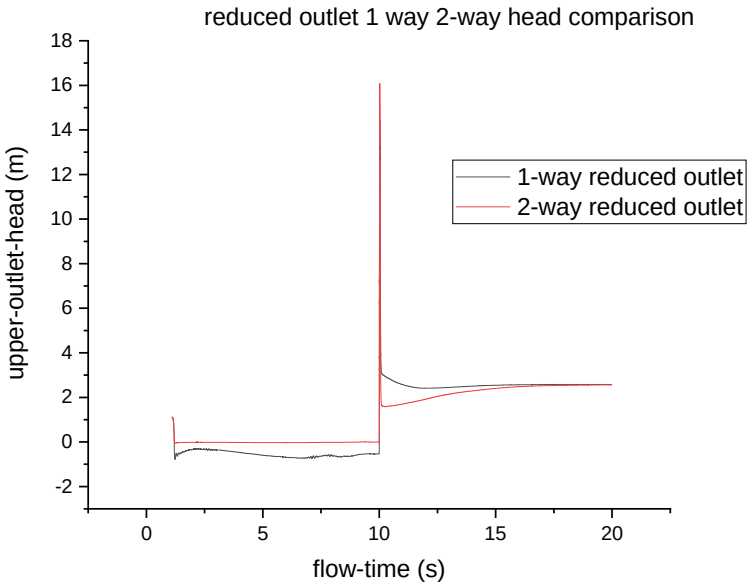

Figure 82 Reduced off-shoot pipe pressure head for 1-way and 2-way generation

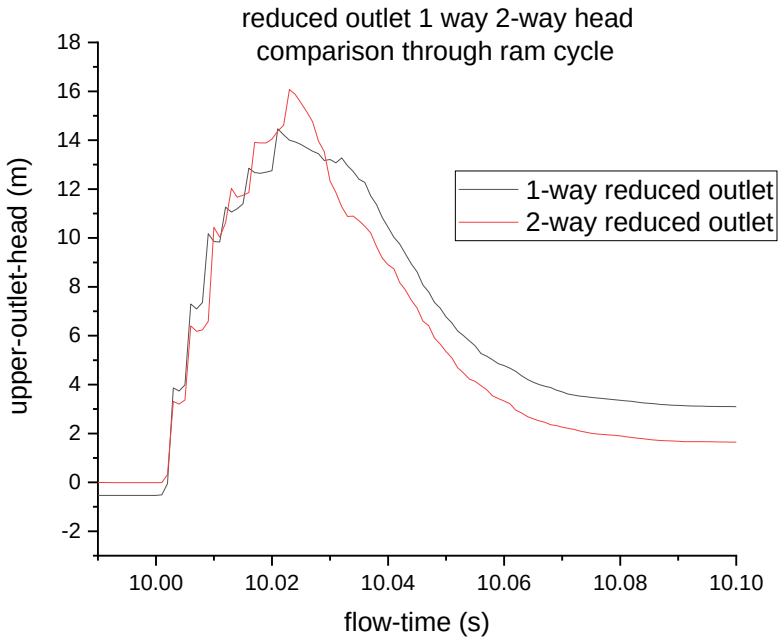

Figure 83 Reduced off-shoot pipe pressure head for 1-way and 2-way generation after the Ram valve was closed

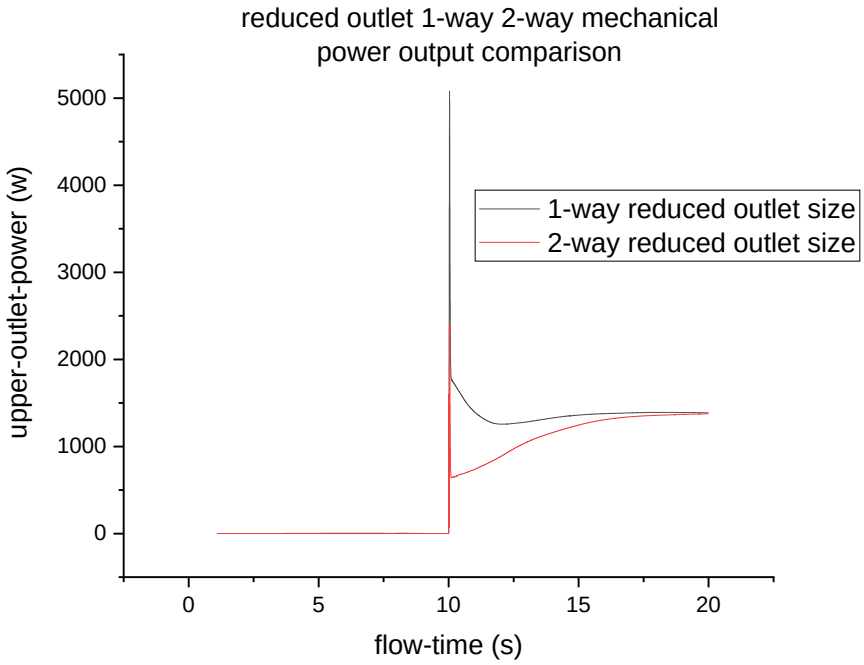

Figure 84 Reduced off-shoot pipe hydraulic power for 1-way and 2-way generation

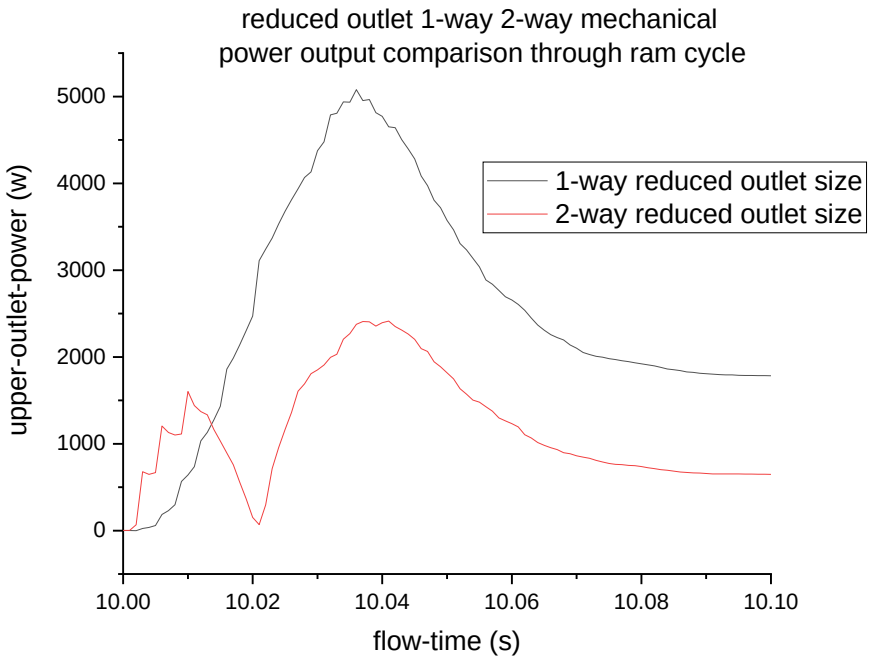

Figure 85 Reduced off-shoot pipe hydraulic power for 1-way and 2-way generation after the Ram valve was closed

5.9. Fluent model conclusion

The average and maximum power output for all models tested are shown in Table 21. The model that gave the highest average mechanical output power was the 1-way model with pillars at 81.7kW. This also gave the highest maximum power of 316.2 kW. The reduced off-shoot pipe diameter offered both the lowest average and maximum power of 0.61kW and 1.6kW respectively. The mass flow rate for all models was between 5821 and 8587 $Kg \cdot s^{-1}$ through the completed cycle.

Table 21 Average and maximum power output for all main models

Model No.	model	type	Total mass flow rate ($Kg \cdot s^{-1}$)	Mechanical power output (kW)	
				Average	max
2	no pillars	1-way	8566	78.51	303.58
7	no pillars	2-way	8088	71.32	229.50
8	with pillars	1-way	8587	81.57	316.20
9	with pillars	2-way	8104	75.30	242.99
10	reduced off-shoot	1-way	5845	0.73	5.08
11	reduced off-shoot	2-way	5821	0.61	1.60

The three alterations to the fluid flow in the through pipe did not change the power output in the off-shoot pipe. This suggested the inlet is capable of adding another Ram valve power generation system. However, for each additional system installed, the total fluid used will also increase by the same amount.

6. Current state of the art technology

To confirm whether electricity generation using Ram pump technology is viable, a mathematical model was constructed of a Kaplan bulb turbine. As discussed in the literature review (chapter 2), the Kaplan turbine performs well at low heads. The latest Andritz Hydro Kaplan bulb turbine performance charts were used in creating this model. This type of turbine is not the cheapest; however, it is the best performing turbine at low heads.

6.1. Kaplan Bulb performance charts "hill charts"

Turbine manufacturing is a competitive market and obtaining the performance data can be challenging. The most informative information circulated by manufacturers are known as hill charts. These charts are graphs created by the manufacturer which represent the turbine characteristics throughout its operation. The numbers with the graph are non-dimensional and are derived from the affinity laws. Initially the turbine manufacturer obtains empirical data from a scale model of the turbine (normally around Ø300mm), and the data is then used to compile the hill chart. The graph plots specific discharge against unit speed. The affinity laws allow the turbine to be scaled up to a much larger size whilst still giving accurate data. The hill chart indicates how the specific discharge changes with the unit speed as well as with differing heights of head (Barker, 2018).

Until the Andritz Hydro hill chart was published in 2012, the main hill chart used was by Sulzer Esher Wyss and is shown in Figure 86. This chart was altered by the manufacturer prior to publishing in order to maintain intellectual property rights (Aggidis and Feather, 2012). Turbine efficiencies were substituted with maximum efficiency values, resulting in the hill chart giving inaccurate solutions to power calculations (Aggidis and Feather, 2012).

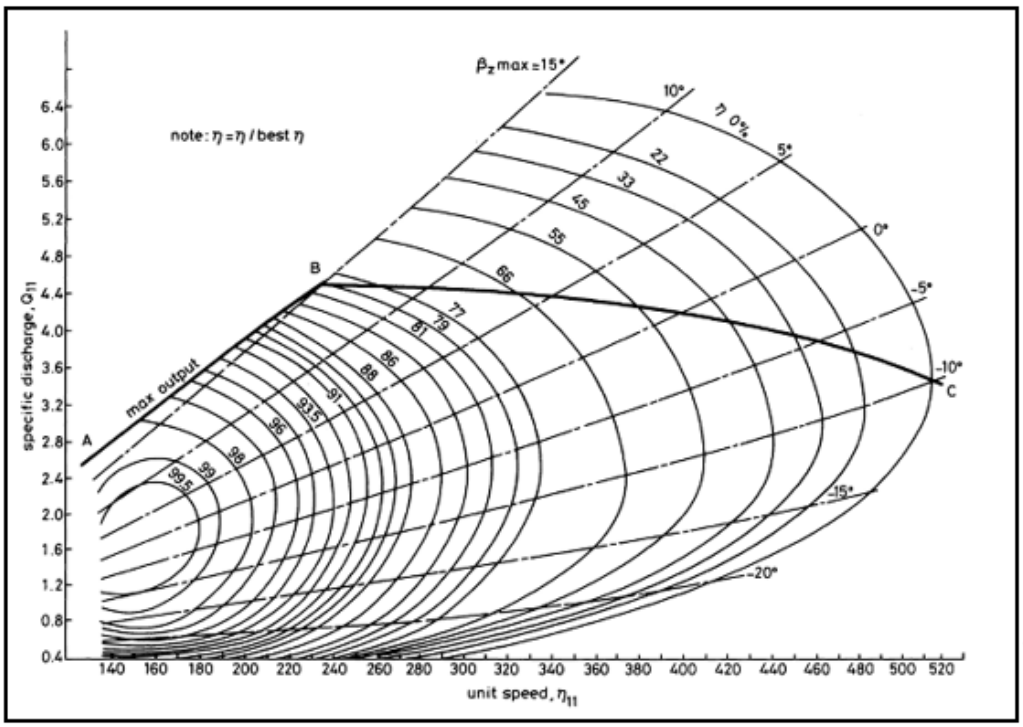

Figure 86 Performance Chart for a Sulzer Esher Wyss Turbine (Aggidis and Feather, 2012)

Andritz Hydro used a state of the art, double regulated, bulb Kaplan turbine to complete a new hill chart. Since its introduction, this chart has been extensively used (Aggidis and Benzon, 2013, Aggidis and Feather, 2012, Petley and Aggidis, 2016) and is shown in Figure 87, with the maximum output given by the blue line. It should be noted that the chart was constructed in the same way as the Sulzer Esher Wyss hill chart using cutting edge turbine technology, however the efficiencies were not altered (Aggidis and Feather, 2012).

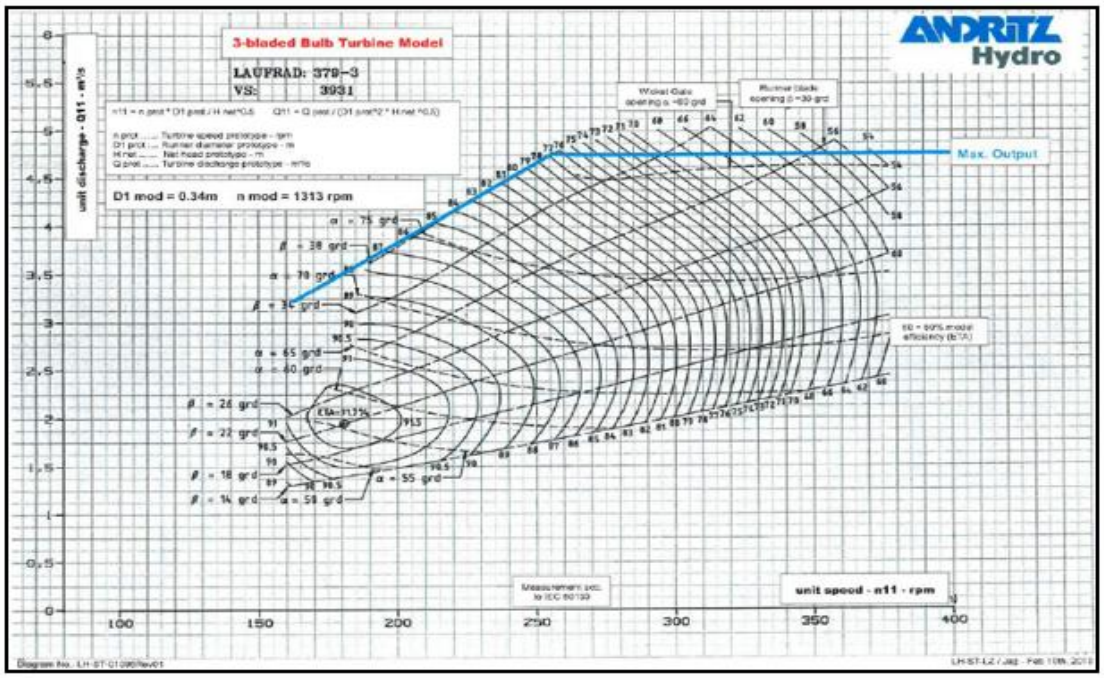

Figure 87 Performance chart for an Andritz Hydro Turbine (Aggidis and Feather, 2012)

6.1.1. Application of performance charts

To calculate the output power of the turbine, formulae need to be applied to the information obtained from the hill chart. The three crucial bits of information obtained from the graph are: Unit speed (n11), Unit discharge (Q11) and turbine efficiency (eta). Equations (6.1), (6.2), (6.3), (6.4) and (6.5) are used to obtain the power output. Each term in the equations are variables that can be altered to change the output power (Aggidis and Feather, 2012).

$$Q_{11} = \frac{Q}{D^2 H^{0.5}}$$

(6.1) Specific Discharge of the Turbine (Aggidis and Feather, 2012)

Q_{11} - Specific discharge of the turbine (Vertical axis on Figure 86) (m^3s^{-1})
Q - Fluid flow (m^3s^{-1})
D - Runner Diameter (m)
H – Head (m)

$$n_{11} = \frac{Sp * D}{H^{0.5}}$$

(6.2) Unit speed of the turbine (Aggidis and Feather, 2012)

n_{11} – Unit speed of the turbine (Horizontal axis on Figure 86) (RPM)
SP– Synchronous Speed (RPM)

$$\eta = \eta_h * \eta_p * \eta_t * \eta_w * \eta_g * eta$$ (6.3) Total Loss Efficiencies (Aggidis and Feather, 2012)

η – Total system efficiency
η_h – Hydraulic or turbine efficiency
η_p – Generator efficiency
η_t – Transformer efficiency
η_w – water friction efficiency
η_g – Drive train efficiency
eta – Turbine efficiency

$$Q = A_s C_d (2gH)^{0.5}$$ (6.4) Volumetric Flow rate filling Lagoon (Aggidis and Feather, 2012)

Q – Volumetric flow rate (m^3s^{-1})
As – Area of sluice gate (m^2)
Cd – Coefficient of drag (scalar number)
g – Acceleration due to gravity (ms^{-2})

$$P = \rho g Q H \eta$$ (6.5) Output Power (Aggidis and Feather, 2012)

P – Power (MW)
P – Density of fluid (tonne*m^{-3})
η – Overall Efficiency (%)

6.2. MATLAB code to calculate output power

In addition to the computational model shown in chapter 5, MATLAB was also used to model the Kaplan bulb turbine.

6.2.1. Digitising the Andritz performance chart

In order to calculate the maximum output within the model, the Andritz hill chart was required to be digitised. Measurements were taken along the hill chart (Figure 87) and a table of these values was produced (Table 22). A graph was produced showing the maximum output of the Unit speed (n11) against the Unit discharge (Q11) shown in Figure 88.

Table 22 Information Measured Directly from the Andritz Hill Chart

Information from the Andritz Hill Chart					
n11	**Q11**	**Efficiency**	**n11**	**Q11**	**Efficiency**
150		0.8820	280	4.75	0.7265
160	3.2	0.8820	290	4.75	0.7091
173.2		0.8820	300	4.75	0.6920
180	3.5	0.8820	310	4.75	0.6748
200		0.8666	320	4.75	0.6569
210	4	0.8542	330	4.75	0.6376
220		0.8389	340	4.75	0.6164
230		0.8215	350	4.75	0.5931
240	4.5	0.8026	360	4.75	0.5678
250		0.7831	370	4.75	0.5415
255	4.75	0.7733	380	4.75	0.5160
260	4.75	0.7637	390	4.75	0.4947
270	4.75	0.7447	400	4.75	0.4822

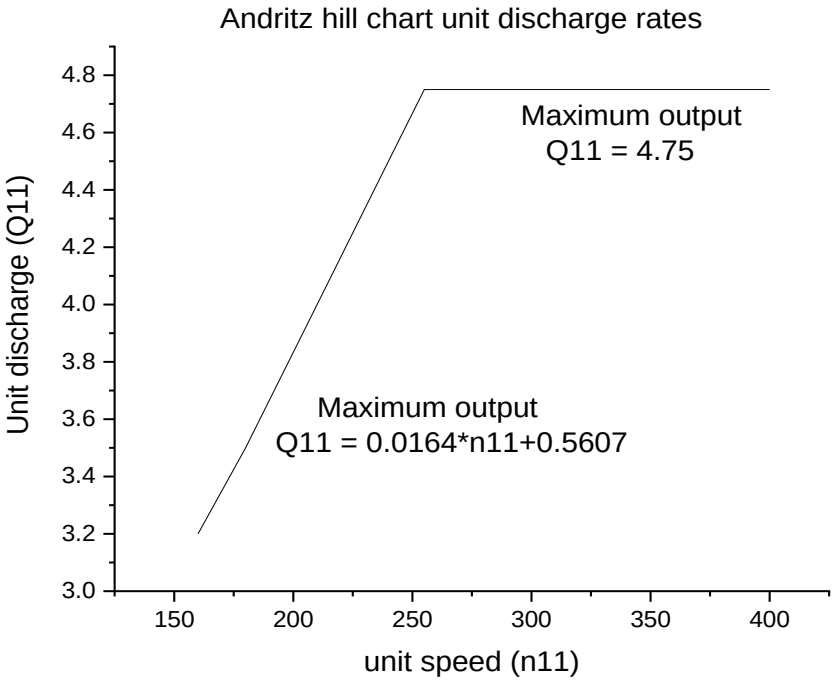

Figure 88 Andritz hill chart rates of Unit discharge with trendline equations

The unit discharge increased linearly when the unit speed was between 150 and 255, therefore, to define this rise, the equation of a straight line was used. Using the data from Table 22 and the straight-line equation y=mx+c, the unit discharge was calculated and is shown in equation (6.6). If the unit speed was greater than 255 the unit discharge was a constant 4.75.

$$Q11 = 0.0164*n11 + 0.5607 \quad (6.6)$$

Using the unit discharge equations, an 'IF statement' script was constructed and is shown in Figure 89 which was required to complete the MATLAB code.

```
if n11(n) < 255;
    Q11(n) = (n11(n)*0.0164)+0.5607;
 else n11(n)> 255;
    Q11(n)=4.75;

end;
```

Figure 89 MATLAB script for unit discharge (Q11) for varying unit input speed (n11)

The unit efficiency (η) was completed using a similar method. Points were taken when the efficiency crossed the blue maximum line and inserted into Table 22. A graph was produced of the efficiency and is shown in Figure 90. The unit efficiency was not a straight line therefore a polynomial was required. A 6th order polynomial was calculated and is shown in equation (7.7)

$$\eta=0.000000000000043175739746 0819*n11^6 - 0.000000000070129382041258 6*n11^5 + 0.000000046339908802 73*n11^4 - 0.000015904035364132 4*n11^3 + 0.002978758037031 02*n11^2 - 0.28884127232470 6*n11 + 12.251101104331 6 \quad (7.7)$$

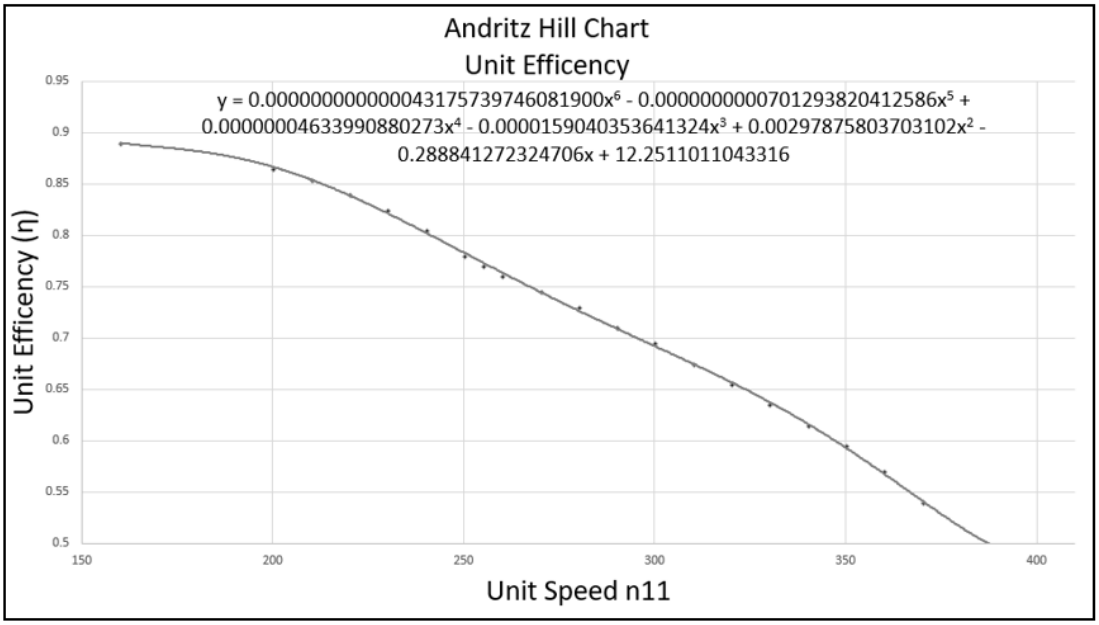

Figure 90 Andritz hill chart of Unit efficiency with trendline equations

The reduction of unit speed increases the unit efficiency, which gives rise to an error when the unit speed drops below 100. When this happens, the unit efficiency increases above 100%. To counteract this, a ceiling of 88.2% which originated from the Andritz empirical testing is added to the unit efficiency chart (Figure 91).

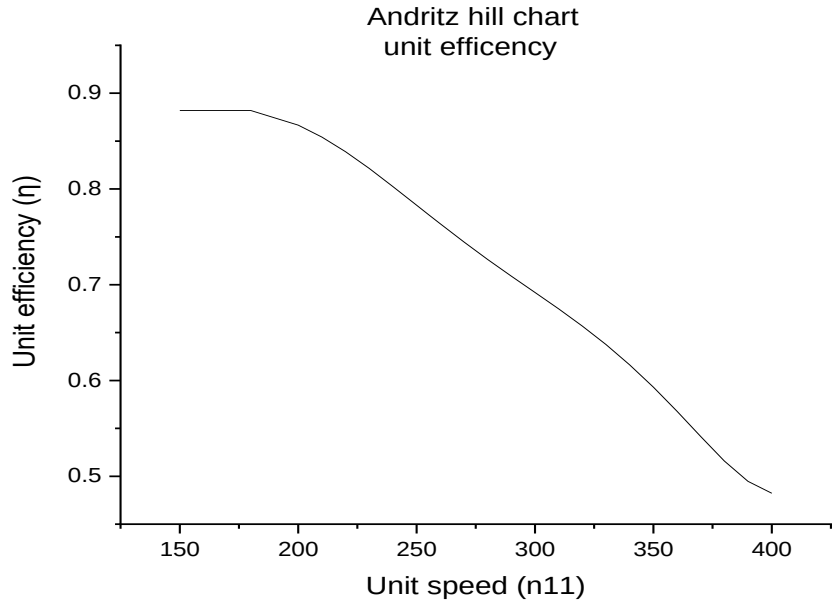

Figure 91 Supplementary Maximum efficiency added to the unit efficiency hill chart

Using the efficiency equations in (3.2) and the 88.2% efficiency ceiling, an 'IF statement' script was constructed in MATLAB and is shown in Figure 92.

```
if n11(n) > 173.2;

            eta(n) = 0.000000000000043175739746081900*(n11(n))^6 - ...
                0.000000000070129382041258 6*(n11(n))^5 + ...
                0.000000046339908802 73*(n11(n))^4 - ...
                0.000015904035364132 4*(n11(n))^3+ ...
                0.002978758037031 02*(n11(n))^2 - ...
                0.288841272324706*(n11(n)) + 12.2511011043316;

                else n11(n) < 180;
            eta(n)=0.88196;
```

Figure 92 MATLAB IF statement for the Unit Efficiency

From the turbine to the national grid, additional efficiencies need to be applied to confirm the annual power output. These efficiencies were researched by Aggidis and Benzon (2013) and are shown in Table 23. The related efficiency variables used within the MATLAB code are shown in Figure 93. The full MATLAB code is shown in Appendix E.

Table 23 All Losses Associated with Generating Electricity (Aggidis and Benzon, 2013)

Efficiency	Percentage
Turbine	Unit Efficiency from Hill Chart
Generator	98%
Transformer	99.50%
Water Friction	95%
Gearbox/Drive chain	97.2
Turbine availability	95%

```
np=0.98;        % Generator Efficiency For turbining and pumping (Aggidis/Benzon)
nt=0.995;       % Transfromer Losses (Aggidis/Benzon)
ng=0.972;       % Gear Drive Train Losses (Aggidis/Benzon)
nw=0.95;        % Water friction losses and turbine availability (Aggidis/Benzon)
na=0.95;        % Turbine Availability (Aggidis/Benzon)
```

Figure 93 Efficiency variables in MATLAB Code

6.3. Current state of the art technology results

The power generated, efficiency and volumetric flowrate at turbine diameters ranging from 0.5m to 2m are shown in Table 24. The hydraulic power and the electrical power were plotted against turbine diameters and are shown in Figure 94 and the volumetric flowrate is shown in Figure 95. The synchronous speed of the turbine was set to 60RPM in the model. This reduced the amount of fluid and set the unit speed to below 180. Therefore, from the Andritz hill chart, the efficiency for all diameters of turbine used was 79.41%.

Table 24 Hydraulic power, electrical power, efficiency and volumetric flow rate at various turbine diameters

Diameter Kaplan bulb turbine	Hydraulic Power kW	Electrical power kW	efficiency	Q (m^3s^{-1})
0.5	55.22	43.85	79.41%	0.56
0.6	83.00	65.91	79.41%	0.85
0.7	117.72	93.48	79.41%	1.2
0.8	159.94	127.01	79.41%	1.63
0.9	210.28	166.98	79.41%	2.14
1	269.27	213.83	79.41%	2.74
1.1	337.54	268.04	79.41%	3.44
1.2	415.64	330.06	79.41%	4.24
1.3	504.16	400.35	79.41%	5.14
1.4	603.61	479.33	79.41%	6.15
1.5	714.78	567.61	79.41%	7.29
1.6	838.04	665.49	79.41%	8.54
1.7	974.06	773.50	79.41%	9.93
1.8	1123.38	892.08	79.41%	11.45
1.9	1286.63	1021.71	79.41%	13.12
2	1464.35	1162.84	79.41%	14.93

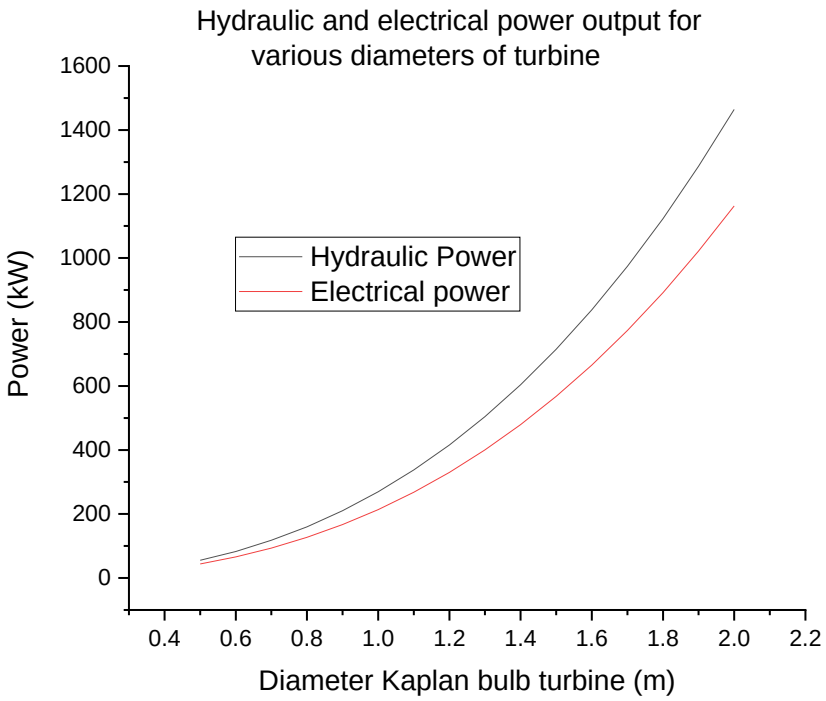

Figure 94 Hydraulic and electrical power generated at various turbine diameters

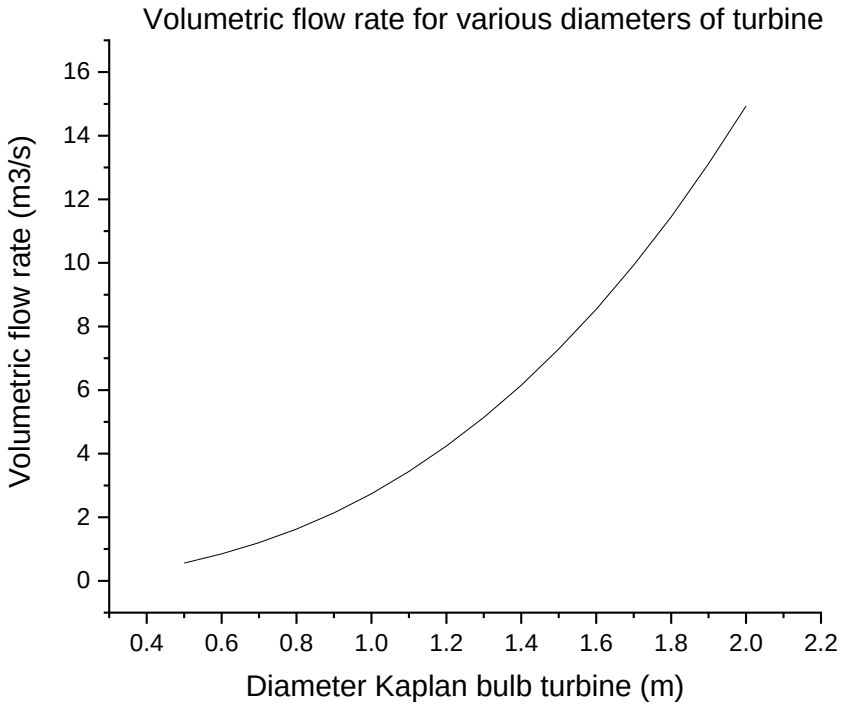

Figure 95 Volumetric flow rate at various turbine diameters

6.4. Current state of the art technology conclusion

The aim of this chapter was to determine the viability of Ram pump technology for electricity generation through comparison with current available technologies. Using a model of a Kaplan Bulb turbine and extrapolated efficiency values from Andritz hill charts, a range of turbine diameters were tested.

Through running the model at various diameters, the MATLAB code established increasing the turbine diameter increased the power generated. However, increasing the diameter of the turbine also increased the volumetric flowrate. To reduce the volumetric flow rate of the system, the synchronous speed of the turbine model was lowered to 60RPM.

If the turbine was set at 1.5m in diameter as in the previous models within this project, the Kaplan turbine generated 567kW of electrical power. This power was generated using $7.3m^3s^{-1}$ of fluid. The MATLAB and ANSYS Ram pump models used around $4m^3s^{-1}$ of fluid due to the closing of the valve reducing the amount of fluid used. If the volumetric flowrate was restricted to 4 m^3s^{-1} in this model a 1.2m diameter turbine would be used and this would generate approximately 415 kW of hydraulic power.

7. Conclusion

This project completed all the tasks set out in the aims and objectives in chapter 1. The MATLAB code using the governing equations gave a maximum power output of 150kW. The MATLAB model was altered from code verified with empirical data from a working model at the University of Bournemouth (Roberts 2017). The ANSYS model offered 82kW of mechanical power, however, this model did take the turbulence of the fluid around the complicated geometry into account. Therefore, using the input variables throughout this project, a lower boundary of approximately 80kW would be expected with the maximum power output of 150kW in ideal conditions.

There was an increase of around 4m of additional head during the Ram phase of the power generation cycle in the ANSYS calculations. However, this was only present for a fraction of the 20 second cycle. This pressure head gained appeared to not be enough to compensate for the power lost during the acceleration phase.

The Kaplan turbine model generated more power than both Ram pump models. Power was generated by the Kaplan throughout the cycle. However, the Ram pump only generated power after the fluid reached terminal velocity and the Ram valve was closed. Therefore, there was between 7 and 9 seconds during the 20 second cycle where no power was generated. The work completed in this project confirmed that the patent would be able to generate power, however, with more efficient methods available on the market it would not be a viable option at present.

Further work

During the literature review, Ram pumps in remote locations to irrigate land appeared to be financially viable. Increasing the reliability and wear on the Ram valve would benefit the farmers in these areas. When using the MATLAB code, it was found that reducing the velocity when the Ram valve was closing greatly reduced the force on the valve with only a small reduction in pressure. A working model could therefore be produced that varies the damping effect of the Ram valve and record the pressure loss. From this model, the life span of the Ram valve may potentially be increased without the loss of pumped water.

Further development of the FLUENT model would be to remove the pillars and increase the guide vanes. The addition of the pillars increased the power output of the ram valve, which appeared counter intuitive. Investigation into the guide vane lengths may alter the power output of the ram valve. In addition, increasing the slope angle of the ram pump inlet may increase the power output and should also be investigated.

References

ACHARYA, N., KIM, C.-G., THAPA, B. & LEE, Y.-H. 2015. Numerical analysis and performance enhancement of a cross-flow hydro turbine. *Renewable Energy,* 80**,** 819-826.

AGGIDIS, G. A. & BENZON, D. S. 2013. Operational optimisation of a tidal barrage across the Mersey estuary using 0-D modelling. *Ocean Engineering,* 66**,** 69-81.

AGGIDIS, G. A. & FEATHER, O. 2012. Tidal range turbines and generation on the Solway Firth. *Renewable Energy,* 43**,** 9-17.

ALIMAN, I., KURNIAWATI, I., WULANDARI, J. A. & SUTIKNO, P. 2018. Evaluation design and simulation of three-way nozzle and control flow vane nozzle on cross flow water turbine for various head.

ANSYS 2013. ANSYS Fluent Theory Guide *In:* ANSYS (ed.).

ANSYS 2016. *ansys fluent 18 tutorial guide,* Southpointe, 2600 ANSYS Drive, Canonsburg, PA 15317, Author.

BARKER, N. 2018. SOLWAY Offshore Tidal Lagoon Power Estimation. University of Lancaster.

BRKIC, D. 2012. Determining friction factors in Tubulant pipe flow. *Chemical Engineering***,** 6.

CHEN, J., YANG, H. X., LIU, C. P., LAU, C. H. & LO, M. 2013. A novel vertical axis water turbine for power generation from water pipelines. *Energy,* 54**,** 184-193.

CHEN, Z. & CHOI, Y.-D. 2015. Influence of air supply on the performance and internal flow characteristics of a cross flow turbine. *Renewable Energy,* 79**,** 103-110.

DE CARVALHO, M., DINIZ, A. & NEVES, F. 2012. Resonant behavior of a Hydraulic ram pump.pdf. *International Review of Mechanical Engineering*.

DEPARTMENT FOR BUISINESS, E. A. I. S. 2013. Harnessing hydroelectric power. *In:* DEPARTMENT FOR BUISINESS, E. A. I. S. (ed.).

DEPARTMENT FOR BUSINESS, E. A. I. S. 2019. DUKES_2019_MASTER_COPY. *In:* DEPARTMENT FOR BUISINESS, E. A. I. S. (ed.). The national Archives: Open Government Licence.

DEPARTMENT OF ENERGY, A. C. C. 2008. Climate Change Act 2008. *In:* CHANGE, D. O. E. A. C. (ed.). UK Government.

GOYAL, R. & GANDHI, B. K. 2018. Review of hydrodynamics instabilities in Francis turbine during off-design and transient operations. *Renewable Energy,* 116**,** 697-709.

GUO, P., WANG, Z., SUN, L. & LUO, X. 2017. Characteristic analysis of the efficiency hill chart of Francis turbine for different water heads. *Advances in Mechanical Engineering,* 9.

INTHACHOT, M., SAEHAENG, S., MAX, J., MÜLLER, J. & SPREER, W. 2015. Hydraulic ram pumps for irrigation in Northern Thailand. *Agriculture and Agricultural Science Procedia,* 5**,** 7.

KADIER, A., KALIL, M. S., PUDUKUDY, M., HASAN, H. A., MOHAMED, A. & HAMID, A. A. 2018. Pico hydropower (PHP) development in Malaysia: Potential, present status, barriers and future perspectives. *Renewable and Sustainable Energy Reviews,* 81**,** 2796-2805.

KARWATA, D. 2003. Lester Pelton and the Pelton waterwheel. *Technologies past.* University of Microfilms.

KAYA, A. M., KANDEMIR, İ., AKŞIT, M. F. & YIĞIT, K. S. 2015. Investigation of optimum working conditions of a micro cross flow turbine. *Environmental Progress & Sustainable Energy,* 34**,** 1506-1511.

KOUGIAS, I., AGGIDIS, G., AVELLAN, F., DENIZ, S., LUNDIN, U., MORO, A., MUNTEAN, S., NOVARA, D., PÉREZ-DÍAZ, J. I., QUARANTA, E., SCHILD, P. & THEODOSSIOU, N. 2019. Analysis of emerging technologies in the hydropower sector. *Renewable and Sustainable Energy Reviews,* 113.

MARTINEZ, J. J., DENG, Z. D., TITZLER, P. S., DUNCAN, J. P., LU, J., MUELLER, R. P., TIAN, C., TRUMBO, B. A., AHMANN, M. L. & RENHOLDS, J. F. 2019. Hydraulic and biological characterization of a large Kaplan turbine. *Renewable Energy,* 131**,** 240-249.

MENTER, F. R., KUNTZ, M. & LANGTRY, R. 2003. Ten years of industrial experience with the SST turbulence model. *Turbulence, Heat and Mass Transfer,* 4.
OKOT, D. K. 2013. Review of small hydropower technology. *Renewable and Sustainable Energy Reviews,* 26**,** 515-520.
PAISH, O. 2002. Small hydro power technology and current status. *Renewable and Sustainable Energy Reviews,* 6**,** 19.
PETLEY, S. & AGGIDIS, G. 2016. Swansea Bay tidal lagoon annual energy estimation. *Ocean Engineering,* 111**,** 348-357.
REIHANI, A., OJAGHI, A., DERAKHSHAN, S. & BEIGZADEH, B. 2014. Shaft fatigue life and efficiency improvement of a micro cross flow turbine. *Engineering Solid Mechanics***,** 1-14.
ROBERTS, A., THOMAS, B., SEWELL, P. & HOARE, E. 2018. Generating renewable power from water hammer pressure surges. *Renewable Energy*.
ROBERTS, A. D. 2017. *The hydrodynamics of the water hammer energy system.* Doctor of Philosophy, Bournemouth University.
VARUN, PRAKASH, R. & BHAT, I. K. 2010. Life Cycle Energy and GHG Analysis of Hydroelectric Power Development in India. *International Journal of Green Energy,* 7**,** 361-375.
VIOLLET, P.-L. 2017. From the water wheel to turbines and hydroelectricity. Technological evolution and revolutions. *Comptes Rendus Mécanique,* 345**,** 570-580.
WATERS, S. & AGGIDIS, G. 2016. A World First: Swansea Bay Tidal lagoon in review. *Renewable and Sustainable Energy Reviews,* 56**,** 916-921.
YOUNG, B. W. 1995. Design of hydraulic ram pump systems. *Proceedings of The Institution of Mechanical Engineers Part A-journal of Power and Energy***,** 9.
ZHANG, H., CHEN, D., XU, B., PATELLI, E. & TOLO, S. 2018. Dynamic analysis of a pumped-storage hydropower plant with random power load. *Mechanical Systems and Signal Processing,* 100**,** 524-533.
ZHANG, M., VALENTÍN, D., VALERO, C., EGUSQUIZA, M. & EGUSQUIZA, E. 2019. Failure investigation of a Kaplan turbine blade. *Engineering Failure Analysis,* 97**,** 690-700.

Appendix A OCPL Patent (CONFIDENTIAL DO NOT PUBLISH)

Intellectual Property Office

Concept House
Cardiff Road, Newport
South Wales
NP10 8QQ
United Kingdom

Telephone +44 (0)1633 814000

Website https://www.gov.uk/ipo

Electronic Filing Receipt

Marks & Clerk LLP
Alpha Tower
Suffolk Street Queensway
Birmingham
United Kingdom
B1 1TT

Your Ref: PB154336GB

29 May 2018

PATENT APPLICATION NUMBER 1808702.3

We have received your request for grant of a patent and recorded its details as follows:

Filing date(*)	29 May 2018	
Earliest priority date (if any)		
Applicant(s) / contact point	Ocean Current Power Ltd.	
Application fee paid	Yes	
Description (number of pages or reference)	13	
Certified copy of referenced application	Not applicable	
If description not filed	Not applicable	
Claims (number of pages)	2	
Drawings (number of pages)	38	
Abstract (number of pages)	No, file by 29 May 2019	
Statement of inventorship (Form 7)	No, file by 30 September 2019	
Request for search (Form 9A)	Yes	
Request for examination (Form 10)	Yes	
Priority Documents	None	
Other Attachments Received	Pre-conversion archive	PB154336GB - Specification & Drawings as filed.zip
	PDAS Registration Form	PDASRegistration.pdf

	Fee Sheet	FeeSheet.pdf
	Validation Log	ValidLog.pdf
Signed by	CN=Thomas Somervell 33933	
Submitted by	CN=Bryan Davies 29196	
Timestamp of Receipt	29 May 2018, 10:45:55 (BST)	
Digest of Submission	F3:B4:13:A9:EB:49:99:DF:5C:42:32:C7:CA:98:85:34:B4:DA:95:C2	
Received	/Intellectual Property Office, Newport/	

Please quote the application number in the heading whenever you contact us about this application.

As requested your application as filed will be lodged in the Priority Document Access Service (PDAS) at WIPO. For further information relating to PDAS please see our website https://www.gov.uk/government/publications/how-to-file-documents-with-the-intellectual-property-office/how-to-file-documents-with-the-intellectual-property-office#file-on-line or contact our e-filing section on 01633 814870.

If you have any queries about the accuracy of this receipt, please phone the Document Reception Manager on +44 (0) 1633 814570. For all other queries, please phone our Information Centre on 0300 300 2000 if you are calling from the UK, or +44 (0) 1633 814000 if you are calling from outside the UK. Or e-mail information@ipo.gov.uk

* This date is provisional. We may have to change it if we find during preliminary examination that the application does not satisfy section 15(1) of the Patents Act 1977 or if we re-date the application to the date when we get any later filed documents.

Apparatus and Method for Extracting Energy from Moving Water

Field of the Invention

[0001] The present invention relates to an apparatus and method for extracting energy from moving water.

Background

[0002] The principle of having an inlet, and outlet and a constriction there-between to increase flow velocity in the region of a turbine to extract energy from moving water is well-known. However, to date, only low inlet to constriction ratios have been successful (with limited increase in velocity and therefore limited energy extraction) since water will naturally avoid flowing through a high ratio constriction in favour of an easier path around it.

[0003] It is therefore an aim of the present invention to provide an improved apparatus and method for extracting energy from moving water that helps to ameliorate the above problems.

Summary of the invention

[0004] Aspects of the present invention relate to extracting energy from moving water, for example, river water or tidal water.

[0005] In accordance with a first aspect of the invention there is provided an apparatus for extracting energy from moving water comprising:

an inlet;

an outlet;

a constriction in a flow path between the inlet and the outlet;

a turbine positioned in the region of the constriction and arranged for extraction of energy from water flowing through the constriction, when in use; and

wherein the constriction comprises at least two parallel flow branches and each branch comprises a valve configured for selective control of flow through each branch.

[0006] The valves may be arranged to operate in sequence to maximise velocity of flow through a single branch at a time.

[0007] In some embodiments, three or more parallel flow branches may be employed, each having a valve configured for selective control of flow through each branch.

[0008] The valves may be in the form of ram valves, water pressure valves, oil-operated valves, electro-magnetically operated valves or other valves.

[0009] The inlet may be configured to capture relatively fast flowing water from an outer curvature portion of a bend in a second flow path.

[0010] Thus, embodiments of present invention provide an apparatus for extracting energy from moving water which is configured to capitalise on fast flowing water which is naturally present at an outer curvature portion of a bend in a second flow path to overcome resistance to flow entering an inlet in favour of an easier path around the inlet.

[0011] The second flow path may be defined by a river bank or a tidal wall or another structure, which may be natural (e.g. a land mass or island) or man-made.

[0012] The outlet may be configured to discharge water from the apparatus at a desired location and/or orientation. For example, the outlet may be configured to discharge water so as to generate a back-flow of water upstream of the outlet. This can help to retard flow of the water past the inlet thereby maximising flow into the inlet and minimising environmental effects which may result from a reduced amount of water downstream of the inlet.

[0013] The apparatus may be configured to provide a high inlet to constriction ratio (e.g. of at least 10:1; at least 15:1; or at least 20:1). In some embodiments, the inlet to constriction ratio is 22.5:1, 27.5:1 or 37.5:1.

[0014] A section of the flow path between the inlet and the constriction may be inclined downwardly so as to utilise gravity to overcome a resistance to flow through the constriction. The section may be inclined downwardly in the direction of flow by a height to length ratio of 1:20; 1:15; 1:10; 1:5; 1:1, 1:0.75 or 1:0.5.

[0015] A second aspect of the invention relates to use of an apparatus for extracting energy from moving water, the apparatus having an inlet arranged to capture relatively fast flowing water from an outer curvature portion of a bend in a water flow path.

[0016] In accordance with a third aspect of the invention there is provided a method of extracting energy from moving water comprising:

capturing flowing water via an inlet;

accelerating the flowing water using a constriction between the inlet and an outlet, wherein the constriction comprises at least two parallel flow branches and each branch comprises a valve;

selectively controlling the flowing water through each branch by operation of the valves;

using the flowing water once accelerated to drive a turbine; and

extracting energy from the turbine.

Brief description of the drawings

[0017] Embodiments of the invention will now be described, by way of example only, with reference to the drawings.

Detailed description

[0018] Some embodiments of the invention concern using bends in rivers to deliver high velocity river water into a tapering channel device to accelerate water flow in order to efficiently drive a turbine and an electrical generator.

[0019] It is known to dam rivers and create a high head flow from that dam to drive a turbine. However, the environmental impact of dams is severe.

[0020] It is known to insert the inlet of a turbine device into a river to get a run of the river power device without use of a dam. There are problems with these run of the river devices, namely they act as an obstruction to river boat traffic and importantly water 'choses' to flow around the device inlet rendering the device inefficient and generating relatively small amounts of electricity.

[0021] Bends on rivers raise problems that are well understood. A problem with bends is that there is a natural tendency for meandering to increase and oxbow lakes eventually form. The velocity of water flow in a river is not uniform around bends in rivers.

[0022] As can be seen in Fig. 1 the highest water velocity is around the outer curvature of bends with the lowest velocity around the inner curvature of bends. This leads to constant erosion on the outer bend and sediment deposition on the inner bend.

[0023] Fig. 2 shows that the river floor is sloped with the deepest part of the floor on the outer bend and the shallowest part of the river on the inner bend.

[0024] The applicant has had computational fluid dynamics (CFD) carried out on a tapered tube device to investigate increasing water velocity. Water velocity in large and medium sized rivers is typically between 0.5 and 1.5 m/s. Turbines are most efficiently driven with a water velocity of 150 m/s.

[0025] Fig 3 shows a tapered channel power device with inlet area ratio to constriction area 150:1. The inlet water velocity of 0.5 m/s was accelerated at the constriction and turbine inlet to 150 m/s. A major limitation of this CFD modelling was that all the incoming water was directly channeled into the device inlet. This is of course unrealistic and only a dammed river can deliver all the incoming water into the device inlet.

[0026] Tapered channels and tubes have been used to accelerate water flow through sea turbines, but only single figure ratios of inlet area to constriction area have been used otherwise sea water would simply bypass the inlet of a high ratio channel or tube.

[0027] It is therefore desirable to utilise the high velocity of water on the outer curvature of a bend on a river to direct water into the inlet of a high ratio tapered channel power device.

[0028] The device of Fig. 3 was designed as a sea device. However, as explained above, only low ratio tubes can be used to increase flow through a sea turbine since, in the open sea, water would not flow through a high ratio tube.

[0029] The curved upward rising centre of the device in Fig. 3 was designed to get the turbine and generator above the water and make maintenance etc. easier. However, embodiments of the invention may be better suited for use in a very narrow high

flowing gap e.g. between islands, rather than in open ocean where water is more likely to divert around a high tapering inlet.

[0030] Fig. 4 shows two bends on the river Severn in Worcester, England, but any bend on any river (or other body of flowing water) can be utilised.

[0031] Fig. 5 shows one device iteration where the inlet of the device is on the outer bend of the river. The channel depth in the device matches the maximum depth of the river on the outer bend, in this case 3.5m. A row of vertically disposed poles with gaps between guard the device inlet from accidental entry into the device of a river boat or floating objects such as broken branches or swimmers. An alternative is a row of buoys on a cable across the inlet mouth. In the example drawn the width of the inlet is 75m and the depth is 3.5m. The example drawn is a curved device but any shape of tapered device can be used with the outlet into any point further down the river. In the curved example drawn the device outlet returns water to the river at the next bend. With power devices drawing a large volume of water from a medium sized river, relative starvation of water from the 'at risk' river between inlet and outlet is a real possibility. In the example drawn, a small river and a canal entering the 'at risk' stretch of river minimises the possibility of water starvation. In addition, some back flow of water from the device outlet into the 'at risk' stretch of river can occur to allow a constant river depth thus allowing unobstructed river traffic.

[0032] The inlet section of the device is generally U shaped (although it may have flat bottom) and the open stretch of inlet allows filtering and manual extraction of smaller debris that has passed through the vertical row of inlet poles or row of buoys on a cable. This device is sited in a flood plane and recently recorded river height in Worcester during severe flooding was 5.67m. The side walls of the device should extend above the flood water level, in this case, the sidewalls should be 6m above river floor height.

[0033] The device gradually tapers to 0.5m width at the constriction. The whole length of the constriction will be covered by a strong roof, typically reinforced concrete as this is an area of high pressure. At the centre of the constriction there is an adjustable vertically descending steel valve. When the river level is high, the valve is relatively open, when the river level is low the valve is relatively closed. The valve is only fully closed as an emergency stop or a planned shut-down.

[0034] One or more pipe(s) are connected to the inlet side of the channel just before the steel valve. This pipe ascends and transmits high velocity water to a turbine(s) which is positioned well above the flood level such that the bottom of the attached electrical generator(s) is well above the maximum ever recorded flood level. The outflow of the turbine has a pipe which feeds into the channel beyond the central steel valve. The central closed constriction area is covered by a power house containing the turbine(s), inlet and outlet pipe(s), electrical generator(s) and all associated electrical apparatus. Electrical wires are either overhead or underground from the powerhouse to a substation and national electrical grid.

[0035] Outside the powerhouse, the outlet channel gradually widens but not as wide as the inlet so throughput water velocity is kept high to clear sediment back into the river. Widening of the channel past the constriction is useful to 'drag' water through the constriction. At the outlet into the river, this is guarded by vertical poles or buoys. Since the outlet may be onto an inner curvature bend, the river floor sediment needs initial excavation. High device outflow velocity keeps the outflow channel clear of sediment.

[0036] The Fig. 5 device outlet may be able to generate some back-flow to assist in filling the at risk section of river.

[0037] Fig. 6 shows a substantially straight device channel. An advantage of this design is that the straightness will encourage increased velocity at the channel constriction. A major disadvantage however is the length of river 'at risk' of water starvation is increased. In addition, because the distance from the device outlet to the inlet is great, significant back-flow of water from the outlet is unlikely.

[0038] The straight device of Fig. 6 could be used e.g. higher up the river where no boats travel, so if the at risk section of river is rendered dry or nearly dry it is of much less concern.

[0039] Fig. 7 shows a hybrid device between the devices of Fig. 5 and Fig. 6. There is a straight section from the inlet initially encouraging acceleration of water velocity. However, the channel then enters an approximately 170m diameter U-shaped bend with the outlet only 125m approximately from the inlet. This minimises the length of the 'at risk' river. In addition, the water from the device outlet is directed upstream at high velocity. This assists backfilling of the river in the 'at risk' section. Additionally, it is

advantageous that the high velocity backward flowing water from the device outlet retards the velocity of downstream river water that has by-passed the channel inlet. The intention here is that local retardation of downstream river water velocity after the inlet position will encourage a greater volume of river water to flow into the device inlet. In effect the backflow of water from the outlet will create a 'functional' dam to maximise flow into the device inlet without actually damming the river, thereby avoiding all the environmental problems associated with a dam.

[0040] For comparison, huge power can be obtained from a dammed river and reservoir with a pipe some 500m downstream from the reservoir (head) driving turbines. However, to avoid damming rivers it is necessary to work with little or no head of water and embodiments of the present invention attempt to substitute a head of water with a flow of water.

[0041] Tapering structures are attractive for increasing water velocity. The downside of this is that the more aggressive the taper, the more resistance there is to flow of water through the device. With little head to drive water past the resistance of the device, an aggressive taper effectively blocks water flow.

[0042] Accordingly, in some embodiments of the present invention further features have been included to compensate for only a moderate acceleration of water flow through a more gently tapering device.

[0043] Fig. 8 shows one such device on the River Severn just North of Worcester. The device entry is on a bend and the outlet is beyond the weir and lock to get a head of 3m. This is presented as typical of a medium sized river. However, any river can be used.

[0044] Fig. 9 shows how the device could be positioned on the outer bend of a river such that the momentum of water will tend to cause flow of water into the device inlet.

[0045] Fig.'s 10a and 10b show more details of the device. From the turbine outlet a pipe returns water to the river just downstream of the inlet. This return flow minimises water abstraction from the river.

[0046] Fig. 11 shows the symmetrical part of the tapered concrete device with three 1.5m diameter pipe branches emerging from the sharp constriction end. There are two internal walls to support the roof of the tapered structure. The device inlet is open

topped and filters are inserted here. The combined cross-sectional area of the emerging pipes is 3 x 1.33m^2.

[0047] Fig. 12 shows the equation that governs velocity through tapered devices: area of inlet x velocity of water at inlet = area of outlet x velocity of water at outlet. However, this equation only holds true assuming zero losses. There are however finite losses from friction of moving water on device walls and resistance of tapering device to water flow.

[0048] Both inlet area and inlet water velocity vary according to river height. As can be seen from Fig. 12, when river height is 1.5m the inlet area = 20 x 1.5 m^2 and the river velocity is 0.75m/s. When the river height is 5.5m (i.e. flooding) the inlet area = 20 x 5.5m^2 and the river velocity is 1.5m/s. The typical river height is 3.5m so the device taper ratio is 20 x 3.5 : 3 x 1.33 (with all three constriction pipes open), which equates to 17.5 : 1.

[0049] There are alternatives to an open construction of a large concrete inlet structure. For example, to obtain an area ratio of inlet to outlet of 17.5 : 1 Underground Directional Drilling (UDD) could be employed. Thus, instead of a large open construction, each 1.5m diameter flexible plastic or rigid metal pipe extending from a conical tapered inlet of 5.5m diameter (i.e. maximum river height) could be inserted underground using UDD from a comparatively smaller collecting area on the river bank. In some embodiments, three drillings would be employed giving a total of three pipes each with conical tapered inlets.

[0050] Fig. 13 shows that the ratio of inlet to constriction can be altered by closing one or two of the pipes. This will be explained in more detail below.

[0051] Fig. 14 shows the complete device including the tapering inlet, three constriction branches or pipes, each of which is provided with a valve downstream of a take-off pipe which leads to a pressure tank before passing through a turbine to generate energy and then to an outlet.

[0052] Fig.'s 15a, 15b 15c and 15d show more detail of the ram valves used in each branch in Fig. 14. Fig. 15a shows two radial pipes emerging from the side of the valve. These carry compressed air actuated by a computer controlled on/off switching system. These two pipes travel along apertures in one of the three vanes which support the

central cylinder and double acting piston which opens and closes the valve rapidly. Other options are water pressure operated valves, oil operated valves or electro-magnetically controlled valve opening / closing.

[0053] Fig.'s 16a to 16h show a sequence of operation of the valves to maximise high pressure flow through the turbine.

[0054] Fig. 16a shows the starting state with the left pipe ram valve open and full cross-hatching across the pipe indicating maximum velocity water flowing through the open valve in the left pipe and flowing down the downstream outlet pipe. The middle and right ram valves are closed at this time and no water is flowing through these branches.

[0055] Fig. 16b shows the moment the ram valve in the left pipe is closed (at 0s). At the same time the valve in the central pipe is opened. When the left ram valve is suddenly shut, the momentum of water causes water to surge up the connected vertically rising 1.0m diameter take-off pipe. These three vertically rising take-off pipes each have an emergency stop valve and a non-return valve. Because the water rushes under the influence of momentum from a 1.5m pipe into a 1m diameter pipe there is an acceleration of water velocity. This water 1) feeds a vertical shaft six jet Pelton turbine which rotates the generator above and 2) drives water into a 250 cubic meter pressure tank. It is estimated that the surge following valve closure will last 3 seconds. Note that the turbine outlet water is fed back into the river close to the inlet, as explained previously. As shown in Fig. 16b a thin cross-hatched line represents low velocity water beginning to flow at this moment in the central pipe as it takes a certain recovery time for water to accelerate from zero velocity to maximum velocity.

[0056] Fig. 16c shows the system state 3 seconds later when there is no longer surge water from the left pipe feeding the turbine. Instead the turbine is being fed by water from the pressure tank. The velocity of water in the left pipe is now zero and the left ram valve stays closed to conserve water flowing away in the downstream outlet. The velocity of water in the central pipe is increasing. This stage is estimated to last 3 seconds.

[0057] Fig. 16d shows the system state after 6 seconds when water in the central pipe has now achieved maximum velocity and the central ram valve is shut and the right ram valve is opened. As explained in relation to Fig. 16b, the momentum of water

causes water to surge up the connected vertically rising 1.0m diameter take-off pipe to feed the turbine and drive water into the pressure tank. At the same time, low velocity water is beginning to flow in the right pipe.

[0058] Fig. 16e shows the system state after 9 seconds when there is no longer surge water from the central pipe feeding the turbine. Instead the turbine is being fed by water from the pressure tank. The velocity of water in the central pipe is now zero and the central ram valve stays closed to conserve water flowing away in the downstream outlet. The velocity of water in the right pipe is increasing.

[0059] Fig. 16f shows the system state after 12 seconds when water in the right pipe has now achieved maximum velocity and the right ram valve is shut and the left ram valve is opened. As explained in relation to Fig. 16b, the momentum of water causes water to surge up the connected vertically rising 1.0m diameter take-off pipe to feed the turbine and drive water into the pressure tank. At the same time, low velocity water is beginning to flow in the left pipe.

[0060] Fig. 16g shows the system state after 15 seconds when there is no longer surge water from the right pipe feeding the turbine. Instead the turbine is being fed by water from the pressure tank. The velocity of water in the right pipe is now zero and the right ram valve stays closed to conserve water flowing away in the downstream outlet. The velocity of water in the left pipe is increasing.

[0061] Fig. 16h shows the system state after 18 seconds when water in the left pipe has now achieved maximum velocity and the left ram valve is shut and the central ram valve is opened. As explained in relation to Fig. 16b, the momentum of water causes water to surge up the connected vertically rising 1.0m diameter take-off pipe to feed the turbine and drive water into the pressure tank. At the same time, low velocity water is beginning to flow in the central pipe. This state is the same as that shown in Fig. 16b and the cycle outlined above is continued to maximise flow through the turbine. In this embodiment, the water is returned to the river close to the inlet with minimal flow through the downstream outlet. However, in another example described below, the cycle is altered to maximise downstream outlet flow in times of flooding.

[0062] Fig. 16i shows a view similar to that of Fig. 16h wherein each take-off pipe has an area of $0.5m^2$ compared to the area of each branch pipe which is $1.33m^2$.

[0063] Fig.'s 17 to 24 show calculations for different river conditions. These calculations are illustrative and assume no losses. Different turbine jet diameters are also considered. When water flows from the 1m diameter feed pipes through the smaller diameter jets, the final velocity of water depends on the jet diameter and the velocity of water flow in the 1m diameter pipe. Fig. 24 shows calculations for a valve cycle optimised for power production.

[0064] For context, it has been reported that the total cost associated with the 2007 floods in England was £3.2bn.

[0065] Fig. 25 shows calculations with the valve opening and closing cycle optimised for maximum downstream outlet flow (e.g. to divert water away from a town/city to avoid catastrophic flooding). In this example, all 3 constriction pipes are open. In practice, the valves may be shut as described above to cause flow through the turbine. However, with the valve settings set to maximise downstream outlet flow, the flow through the turbine is consequently reduced.

[0066] Fig. 26 shows a proposed under-river pipe going right through the centre of Worcester exiting into the river south of the city. There is a green flood plane right through the centre of Worcester so an alternative would be a straight pipe inserted by underground directional drilling (UDD) through the centre of Worcester. This UDD requires open insertion holes digging approximately every 200m.

[0067] Other towns subject to flooding would need specific solutions. For example, Shrewsbury would be suited to an outflow pipe from North of the town to South of the town by a pipe sited to the South-West of the town.

[0068] In the embodiment described above, the difference in water level between device inlet and outlet beyond the weir is 3m. Fig.'s 27a, 27b and 27c show a variant device which uses this 3m head to slope the concrete inlet structure. It remains to be seen whether a 3m head will overcome all of the resistance to flow described above.

[0069] Fig.'s 28a, 28b and 28c therefore show a further variant device which uses a 10m head or drop to slope the concrete inlet structure. Since gravity acts on a mass of water, the aim is that gravity will have a greater effect on the huge mass in the concrete tapered structure thus overcoming resistance to flow through the constriction.

[0070] Fig.'s 29a, 29b and 29c show a yet further variant device which uses a more extreme inclined slope for the concrete inlet structure to obtain a larger gravitational effect.

[0071] Fig. 30 shows a modification of the device for use in a tidal lagoon, according to an embodiment of the invention. The main modification is to have the facility to use bi-directional flow depending on the state of the tide and height of seawater on either side of the tidal wall. The arrangement is slightly modified to make use of the same turbine and generator with flow in both directions. In addition the turbine has two outlets with on/off valves. This allows turbine outflow in the most advantageous direction. For example, when the lagoon is full and the tide going out reduces the seawater height on the ocean side of the wall, it is advantageous to have the turbine outflow into the lagoon to prolong the duration of generator production. When the tide comes in and the ocean side of the wall has high water and the lagoon water level is low, it is advantageous to have the turbine discharging onto the ocean side - again to prolong the duration of electricity generation as clearly the limited volume of water in the lagoon is a limiting factor in electricity generation.

[0072] Another advantage of using this device in a tidal wall is that the ram valves in parallel with the optimum sequence of opening / closing dramatically increases water velocity through the turbine thus increasing power generation.

[0073] Other embodiments of the present invention, may be used on existing or new low head hydro systems - again to accelerate water velocity through the turbine and increase power generation.

[0074] Although only certain embodiments of the present invention have been described in detail, many variations are possible in accordance with the appended claims. For example, features described in relation to one embodiment may be incorporated into one or more other embodiments and vice versa.

References

[0075] The following references are incorporated herein by reference, with regards to the background of the invention.

1. WO 00/28210

2. EP1654457 B1

3. GB 2503104 B

4. EP 2331811 B1

Claims

1. An apparatus for extracting energy from moving water comprising:

an inlet;

an outlet;

a constriction in a flow path between the inlet and the outlet;

a turbine positioned in the region of the constriction and arranged for extraction of energy from water flowing through the constriction, when in use; and

wherein the constriction comprises at least two parallel flow branches and each branch comprises a valve configured for selective control of flow through each branch.

2. The apparatus according to claim 1 wherein the valves are arranged to operate in sequence to maximise velocity of flow through a single branch at a time.

3. The apparatus according to claim 1 or 2 wherein three or more parallel flow branches are employed, each having a valve configured for selective control of flow through each branch.

4. The apparatus according to any preceding claim wherein the valves are in the form of ram valves, water pressure valves, oil-operated valves, electro-magnetically operated valves or other valves.

5. The apparatus according to any preceding claim wherein the inlet is configured to capture relatively fast flowing water from an outer curvature portion of a bend in a second flow path.

6. The apparatus according to claim 5 wherein the second flow path is defined by a river bank or a tidal wall or another structure.

7. The apparatus according to any preceding claim wherein the outlet is configured to discharge water from the apparatus at a desired location and/or orientation.

8. The apparatus according to claim 7 wherein the outlet is configured to discharge water so as to generate a back-flow of water upstream of the outlet.

9. The apparatus according to any preceding claim wherein the apparatus is configured to provide an inlet to constriction ratio of at least 10:1; at least 15:1; or at least 20:1.

10. The apparatus according to any preceding claim wherein a section of the flow path between the inlet and the constriction is inclined downwardly so as to utilise gravity to overcome a resistance to flow through the constriction.

11. The apparatus according to claim 10 wherein the section is inclined downwardly in the direction of flow by a height to length ratio of 1:20; 1:15; 1:10; 1:5; 1:1, 1:0.75 or 1:0.5.

12. Use of an apparatus according to any preceding claim for extracting energy from moving water, the apparatus having an inlet arranged to capture relatively fast flowing water from an outer curvature portion of a bend in a water flow path.

13. A method of extracting energy from moving water comprising:

capturing flowing water via an inlet;

accelerating the flowing water using a constriction between the inlet and an outlet, wherein the constriction comprises at least two parallel flow branches and each branch comprises a valve;

selectively controlling the flowing water through each branch by operation of the valves;

using the flowing water once accelerated to drive a turbine; and

extracting energy from the turbine.

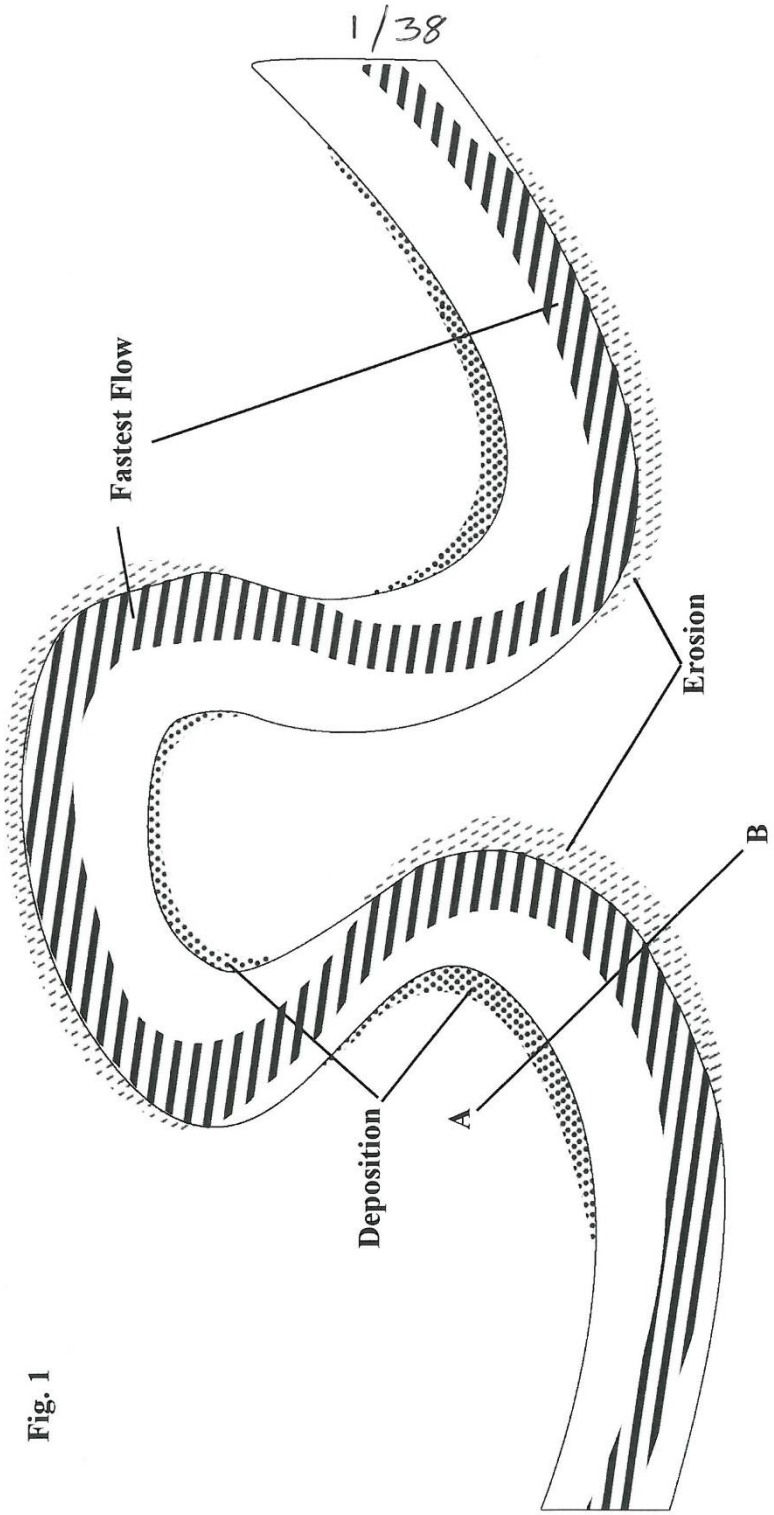

Fig. 1

Fig.2

Cross-section

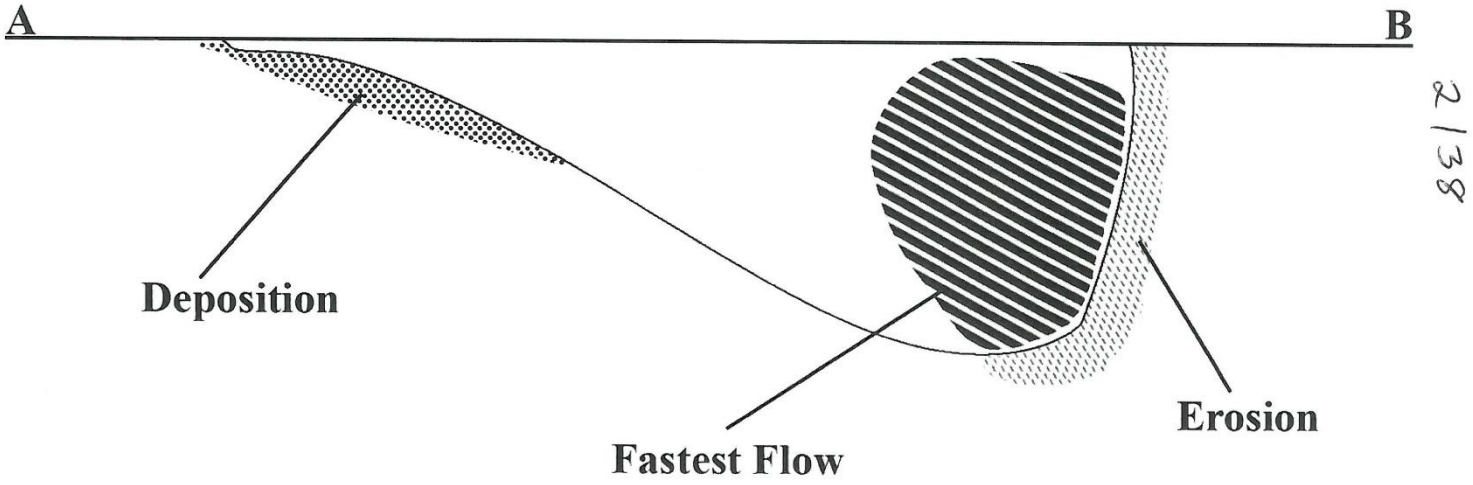

2 | 38

3/38

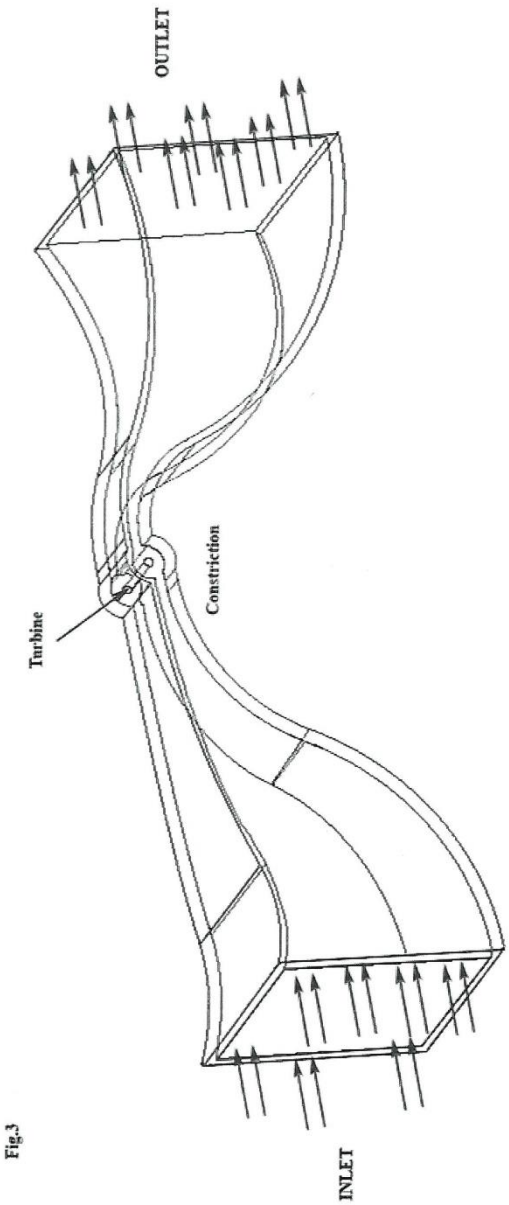

Fig.3

4/38

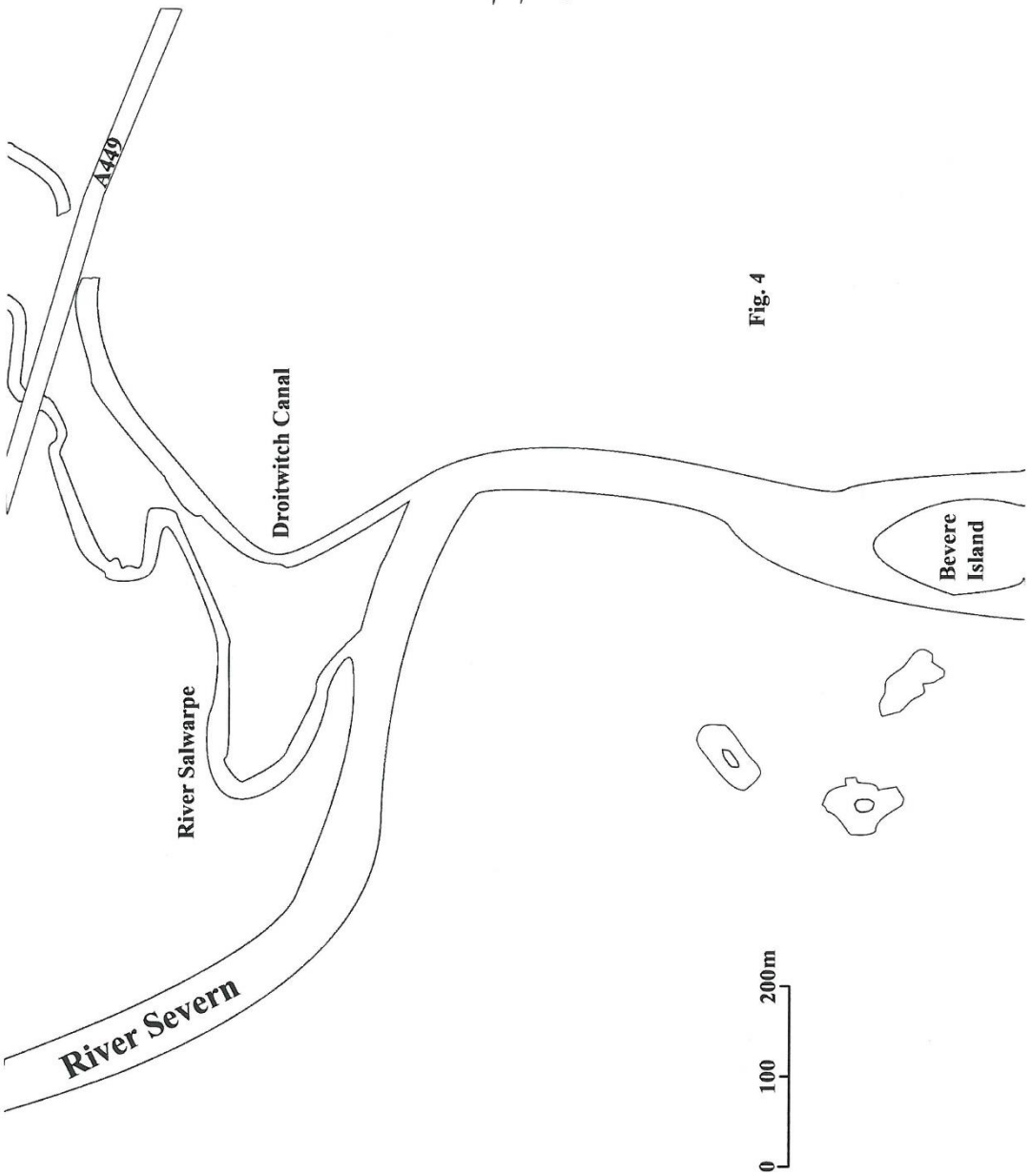
A449
Droitwitch Canal
River Salwarpe
River Severn
Bevere Island
0
100
200m

Fig. 4

5/38

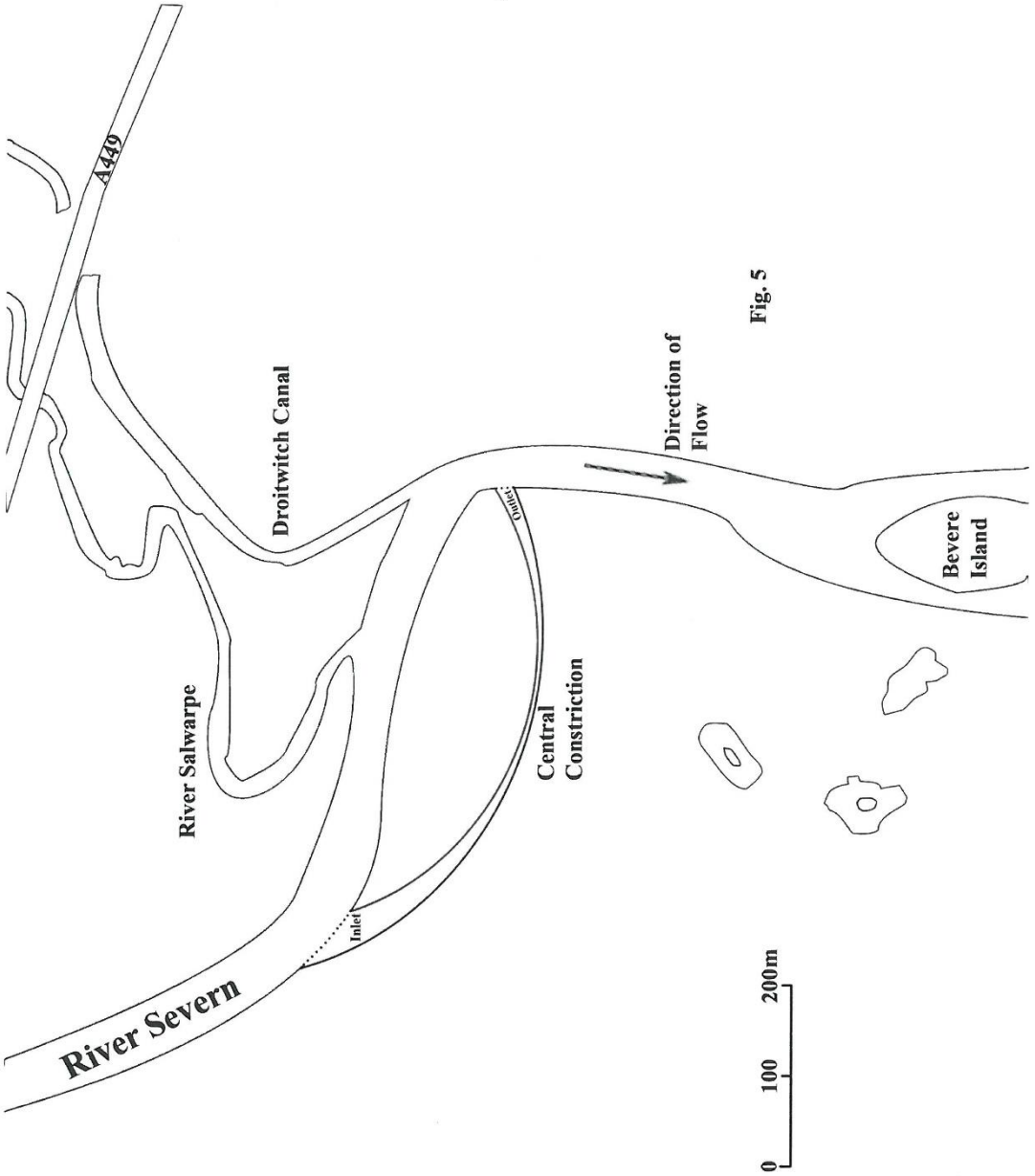
A449
Droitwitch Canal
River Salwarpe
River Severn
Inlet
Outlet
Central Constriction
Direction of Flow
Bevere Island
0
100
200m

Fig. 5

6/38

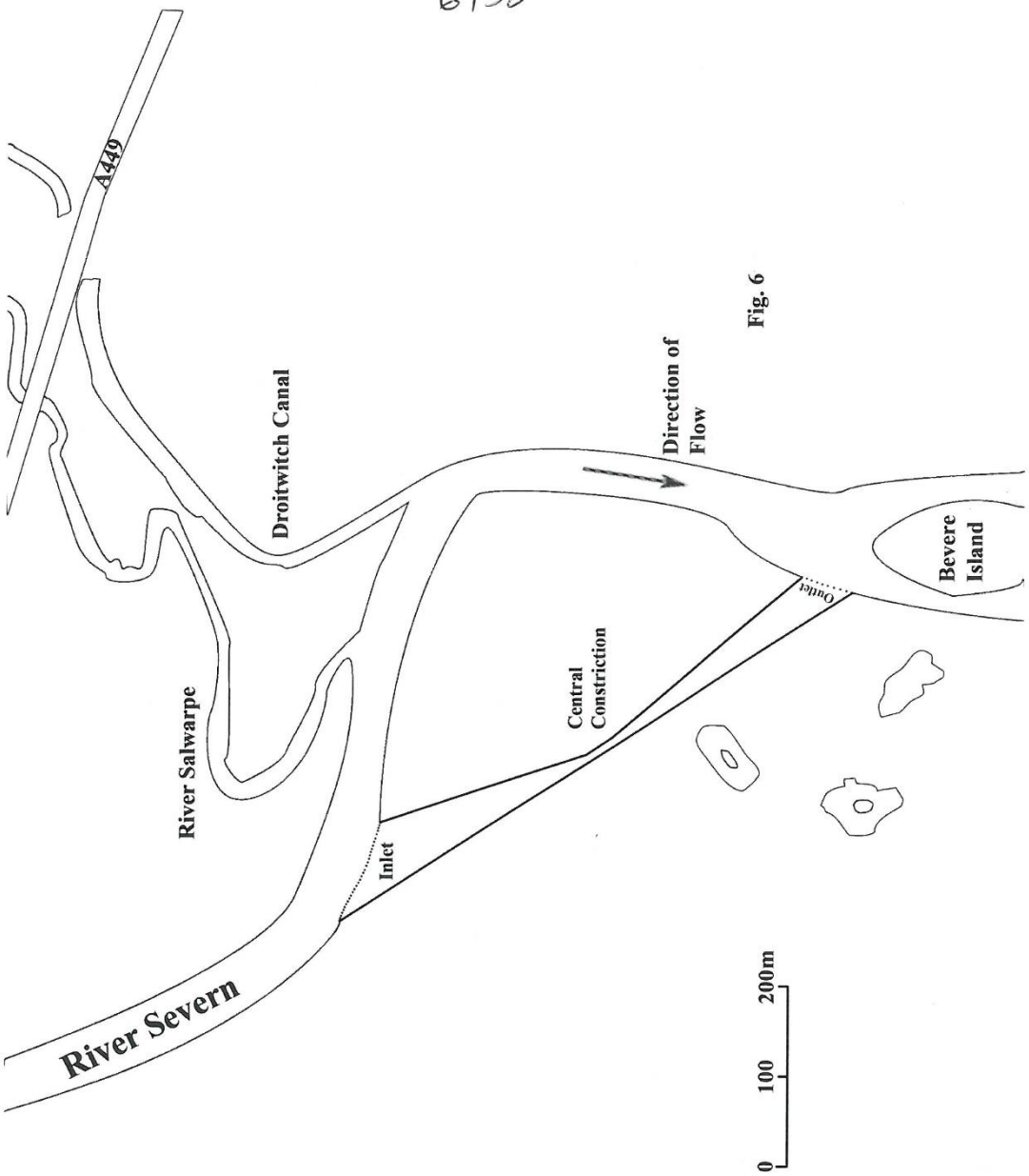
A449
Droitwitch Canal
Direction of Flow
Bevere Island
Outlet
Central Constriction
River Salwarpe
Inlet
River Severn
0
100
200m

Fig. 6

7/38

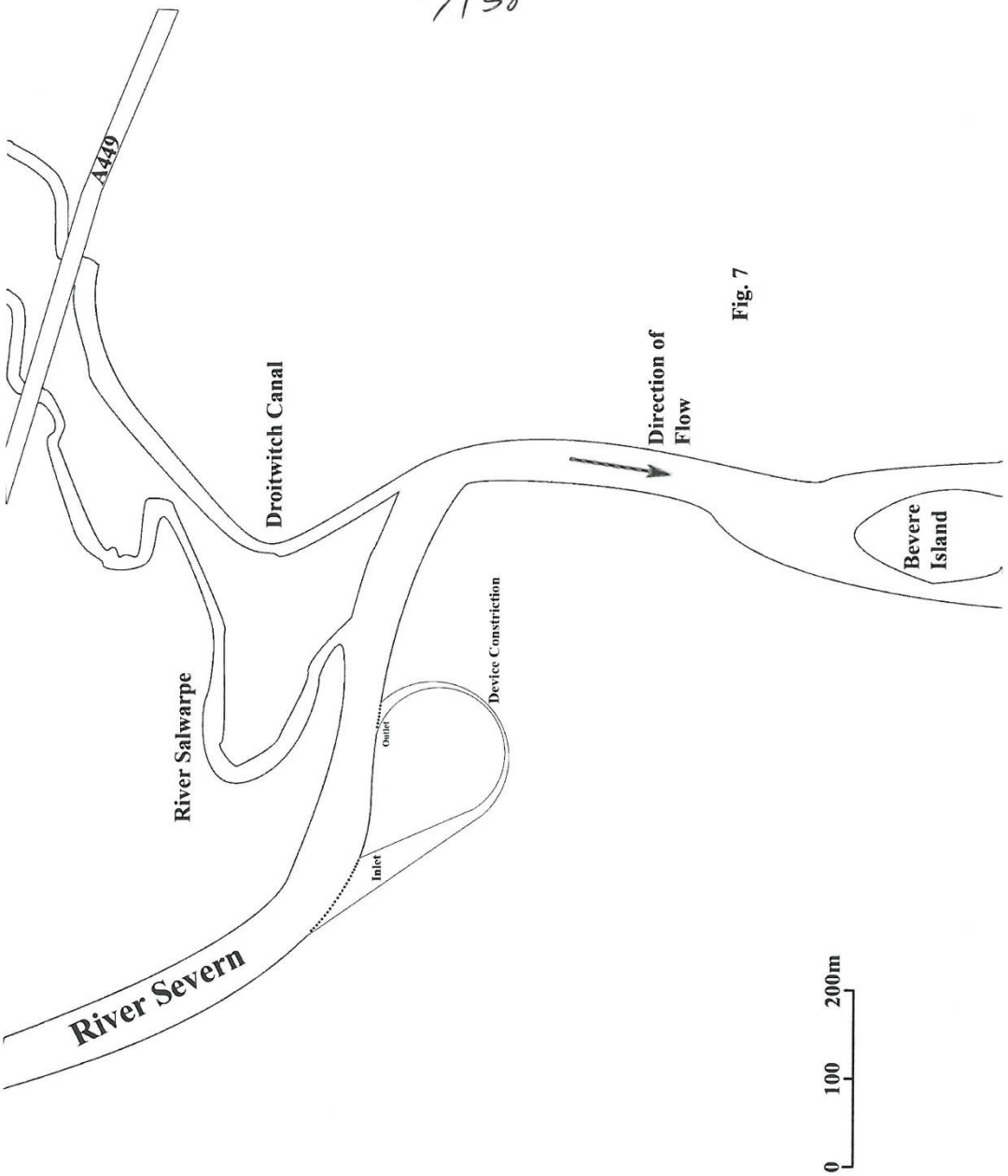
A449
Droitwitch Canal
River Salwarpe
River Severn
Inlet
Outlet
Device Constriction
Direction of Flow
Bevere Island
0
100
200m

Fig. 7

Power device sited on River Severn just North of Worcester

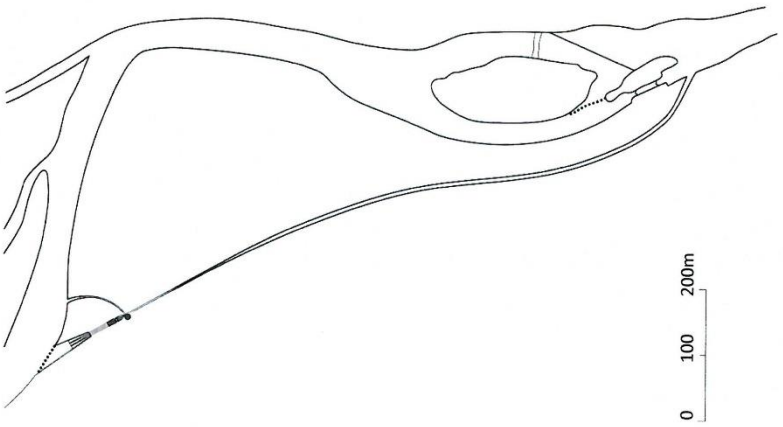

Fig. 8

9/38

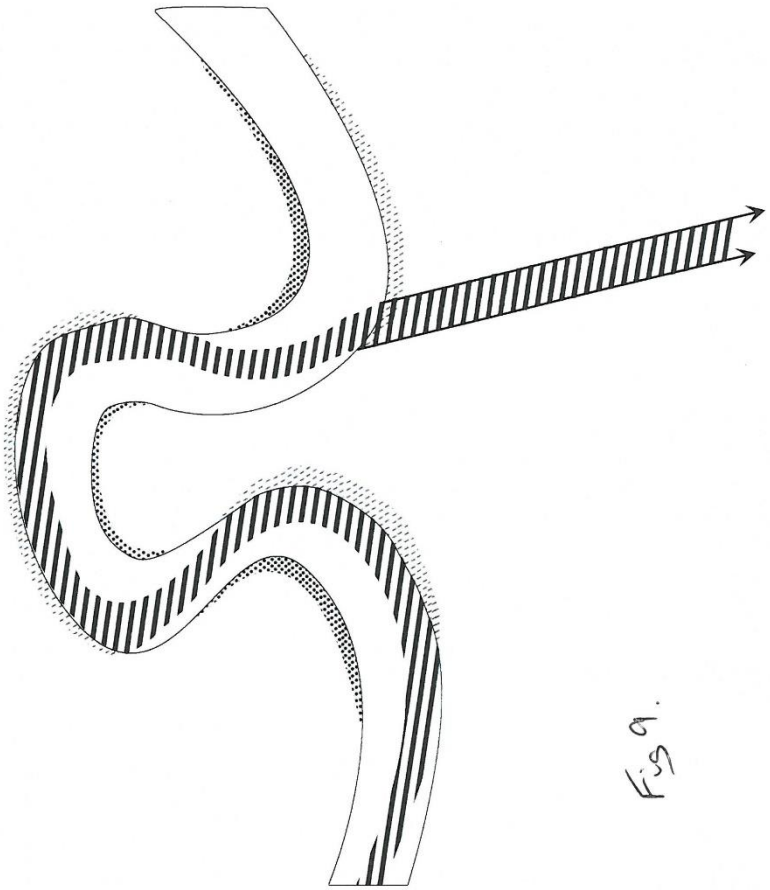

Fig 9.

10/38

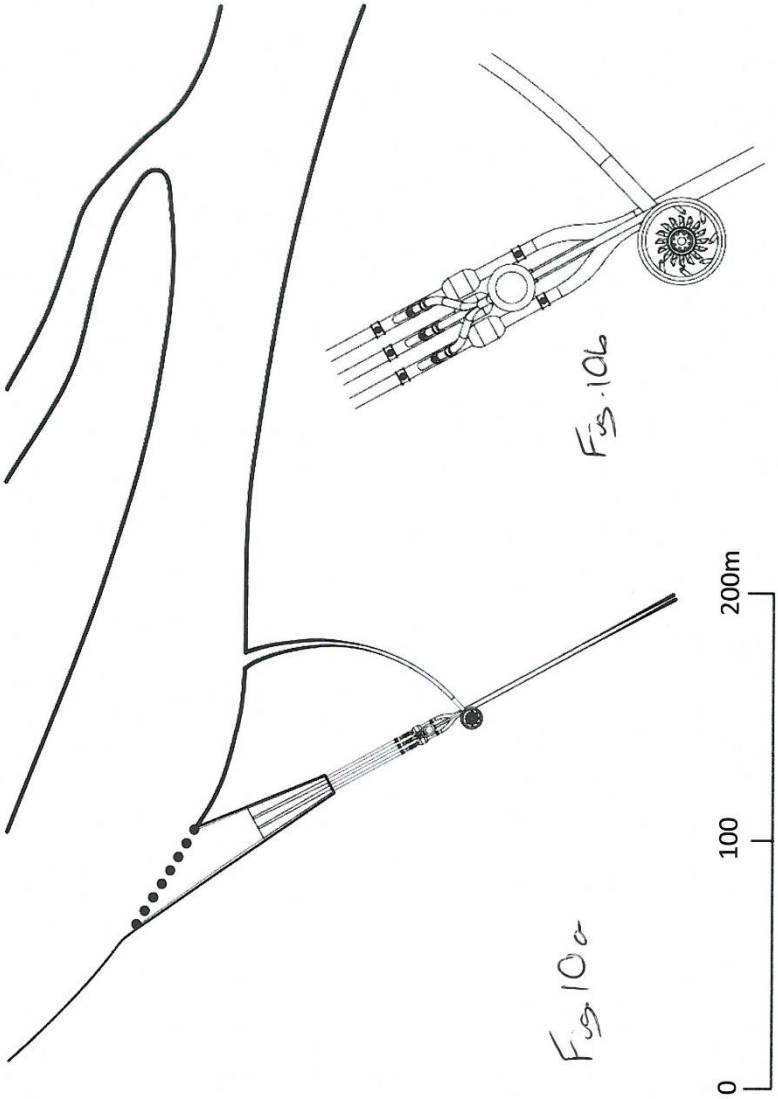

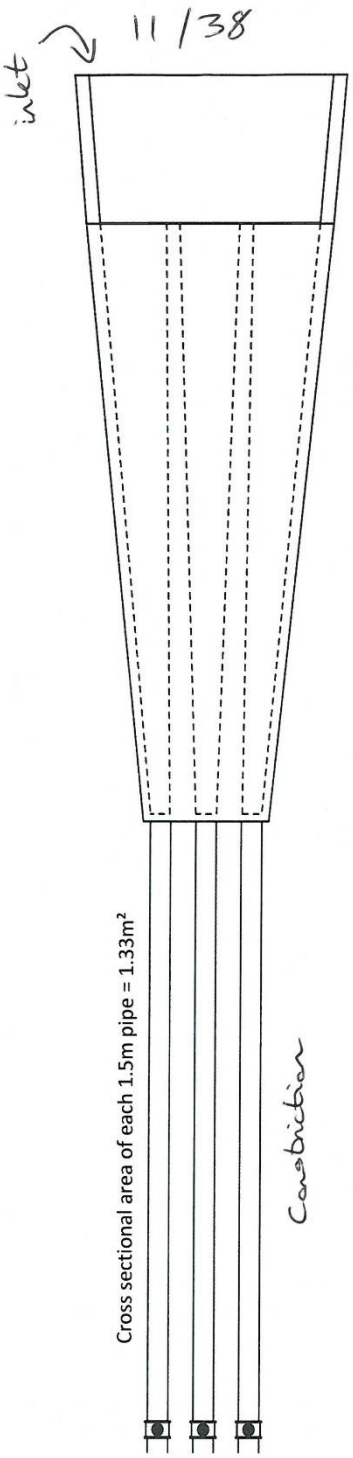
inlet
11/38
Cross sectional area of each 1.5m pipe = 1.33m²
Constriction

Fig. 11

Area at inlet x Velocity at inlet = Area at outlet x Velocity at outlet.

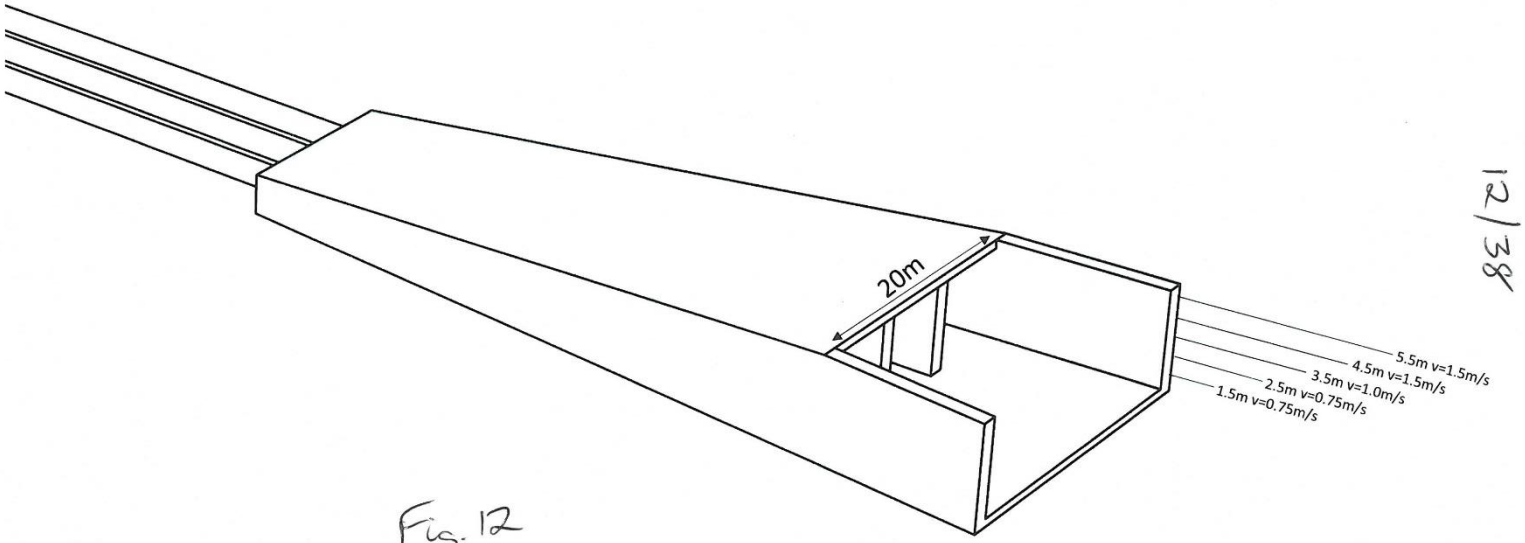

Fig. 12

12/38

River height 1.5m, Velocity 0.75 m/s

Area at inlet x Velocity at inlet = Area at outlet x Velocity at outlet.

Close two pipes to get better taper ratio.

- 20m x 1.5m : 1.33 m^2
- 22.5 : 1

In 1.3m ID pipe Velocity = 0.75 x 22.5 = 16.9 m/s

Fig. 13

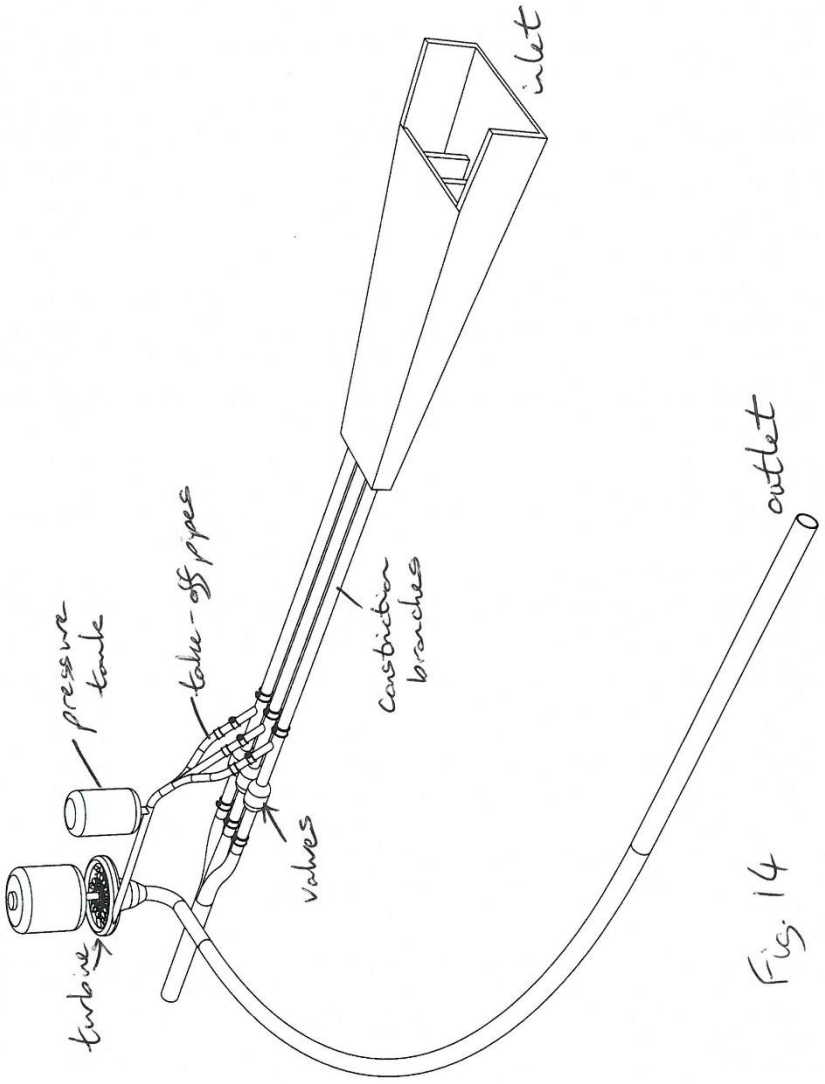
inlet
outlet
constriction branches
valves
take-off pipes
pressure tank
turbine

Fig. 14

15/38

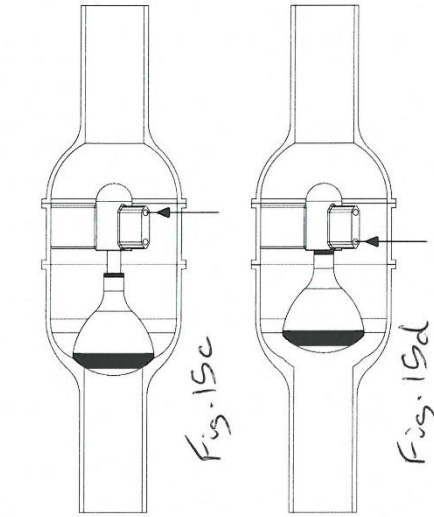

Fig. 15c

Fig. 15d

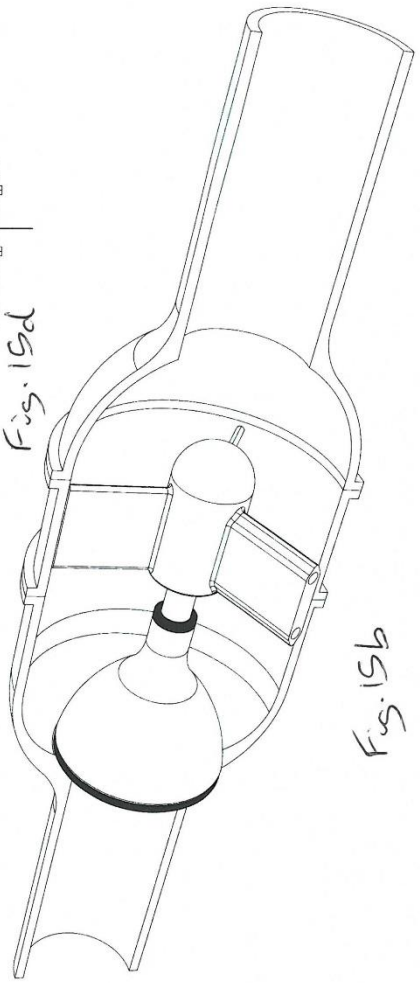

Fig. 15b

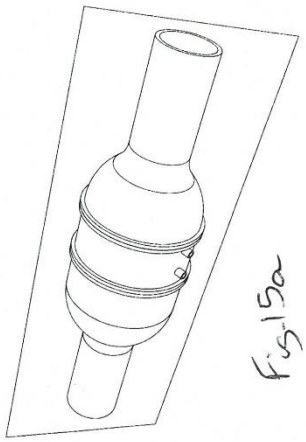

Fig. 15a

16/38

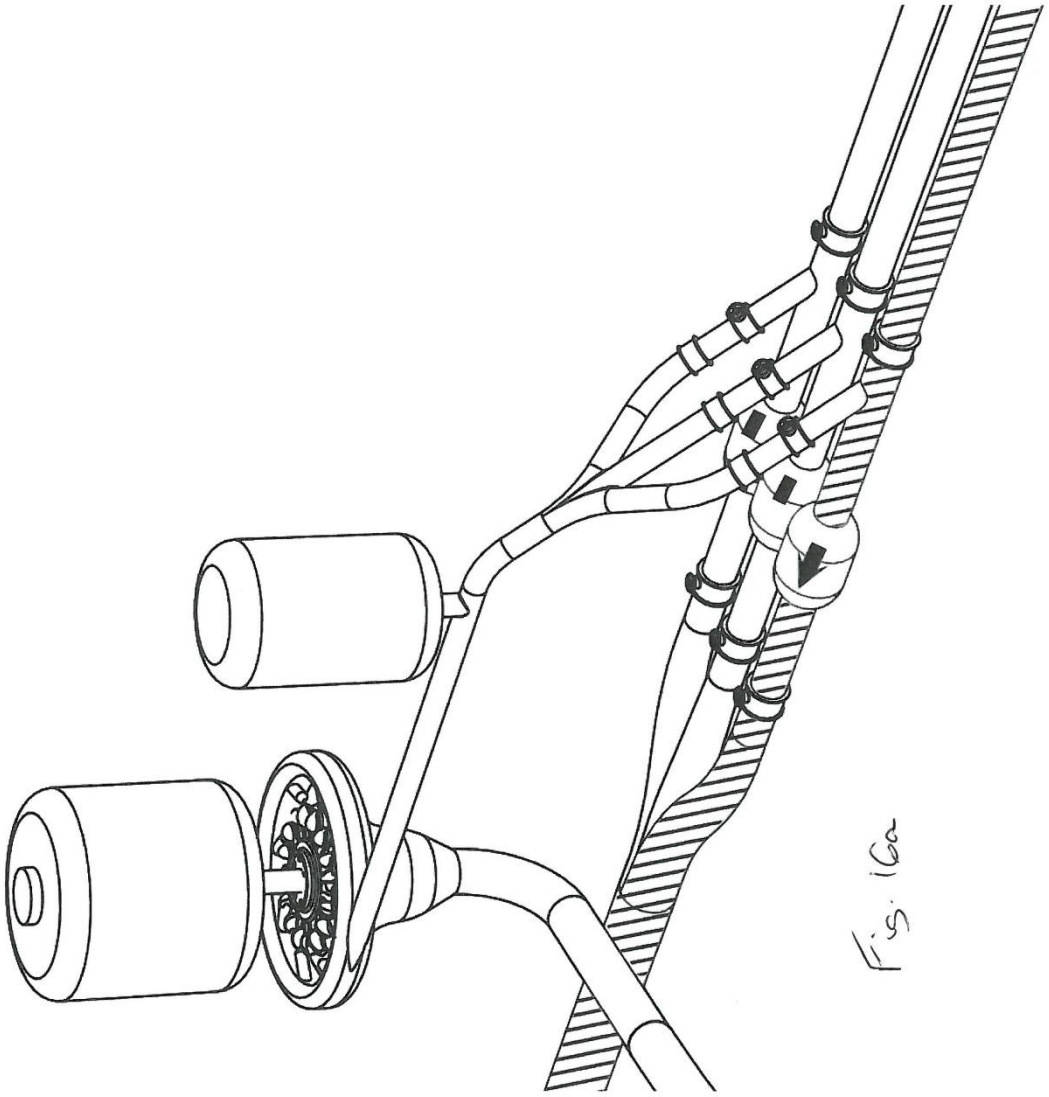

Fig. 16a

17/38

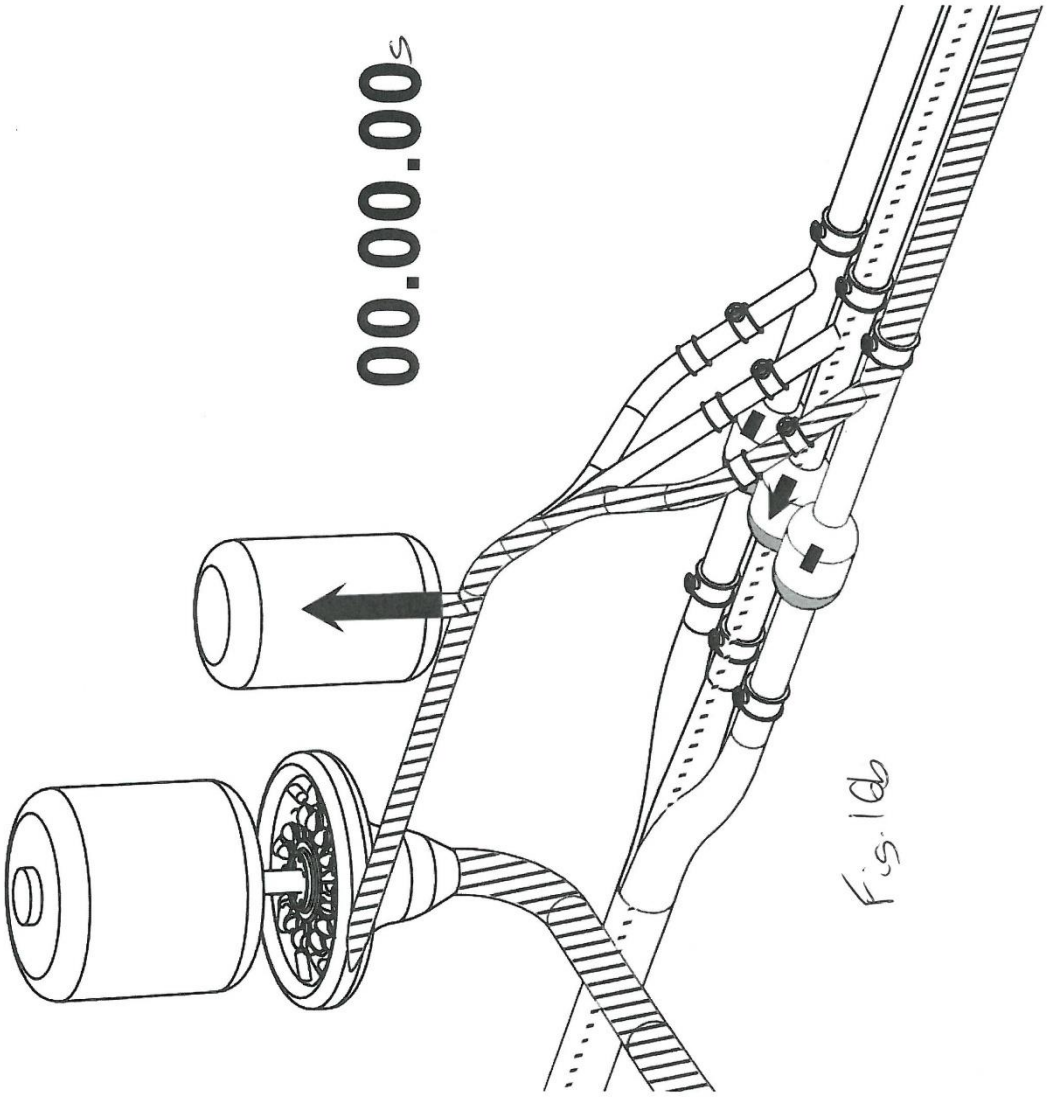

Fig. 10

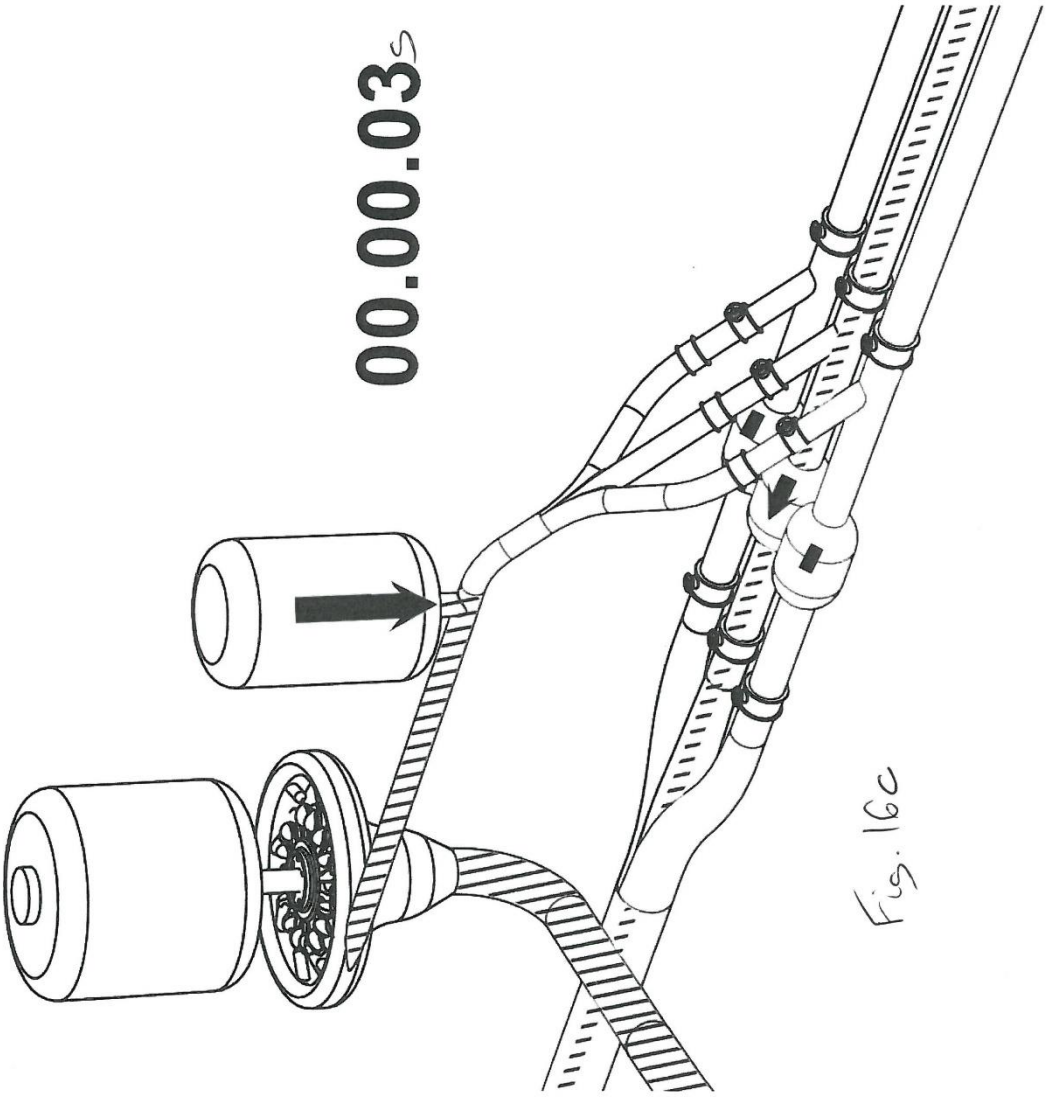

Fig. 16c

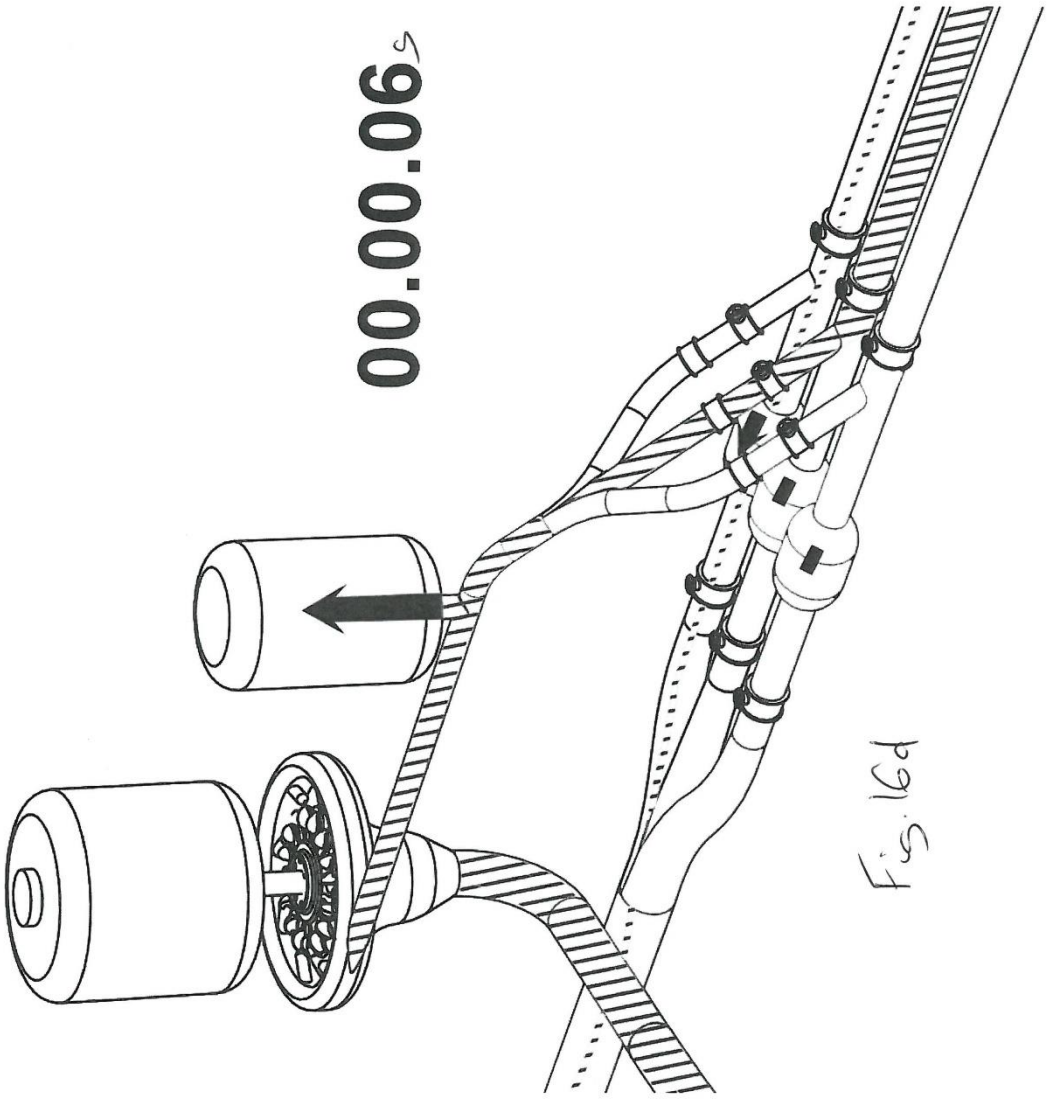

Fig. 16d

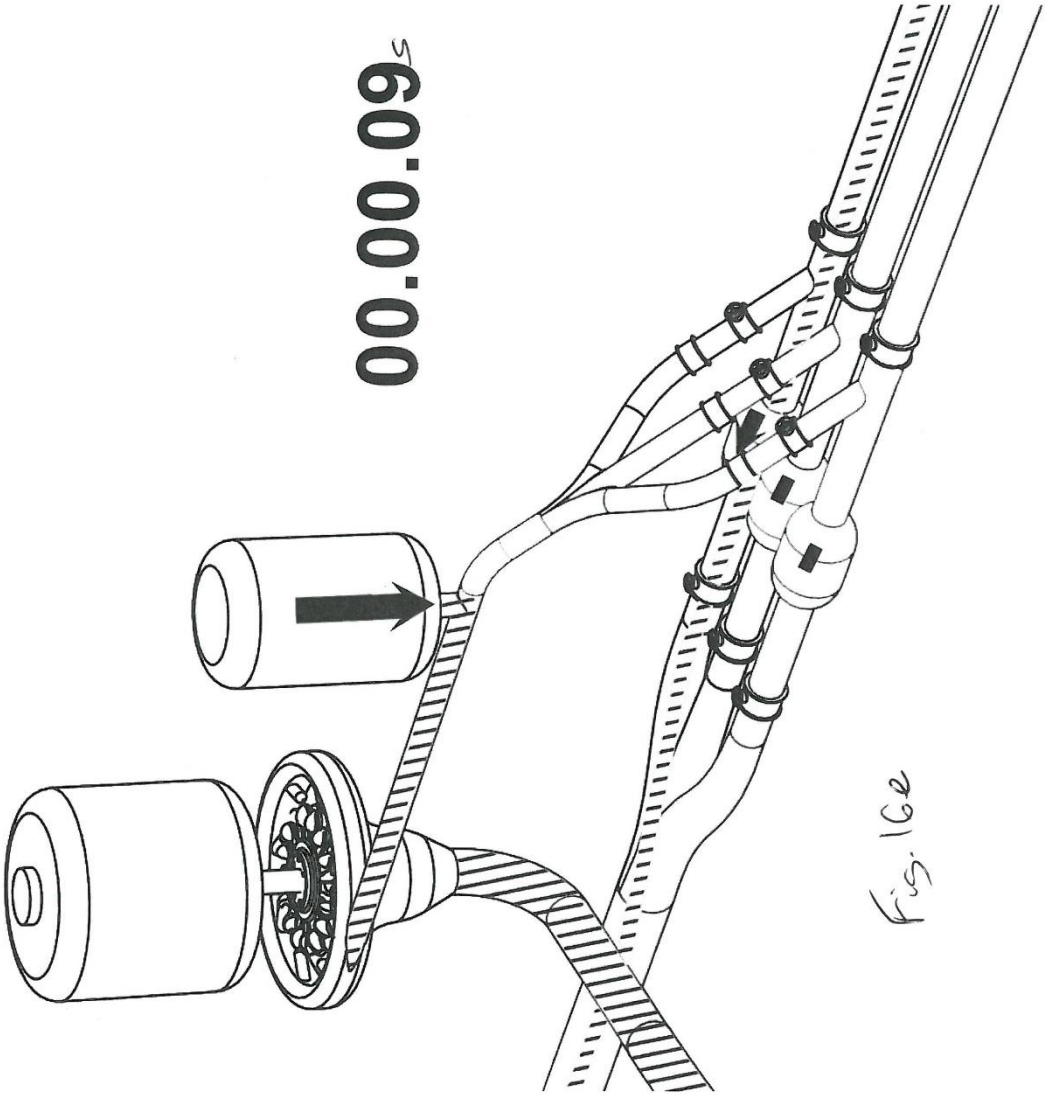

Fig. 16e

21/38

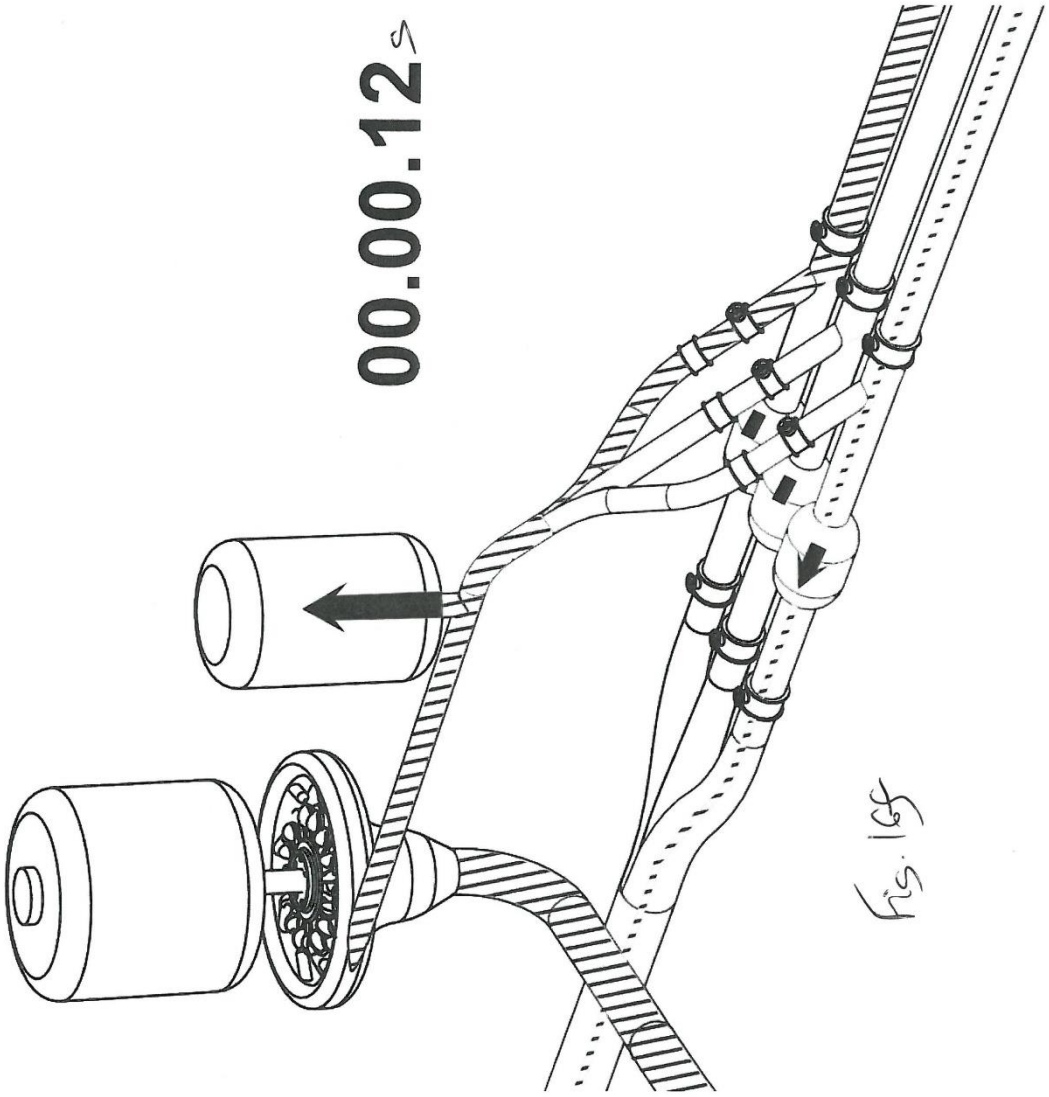

Fig. 16F

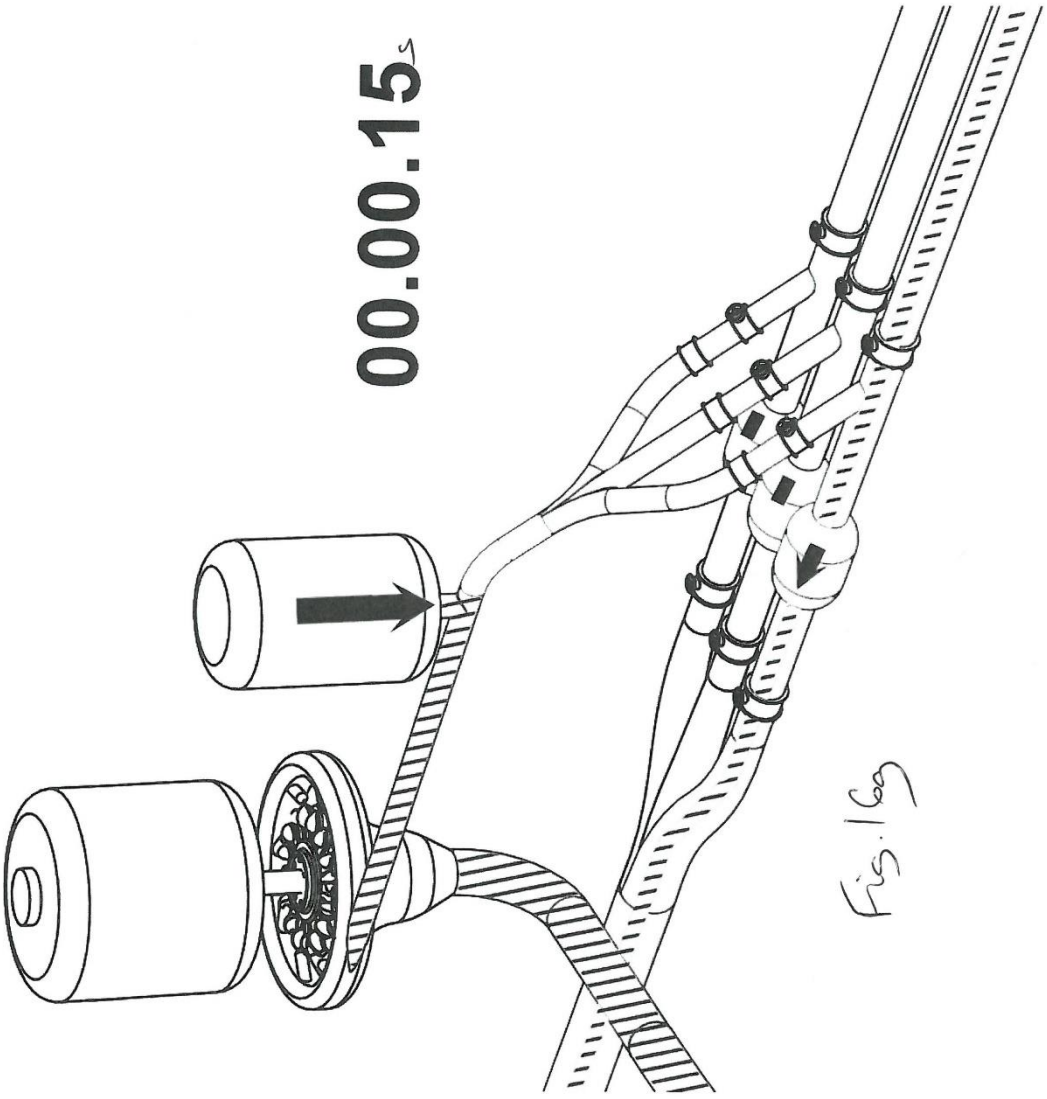

Fig. 16a

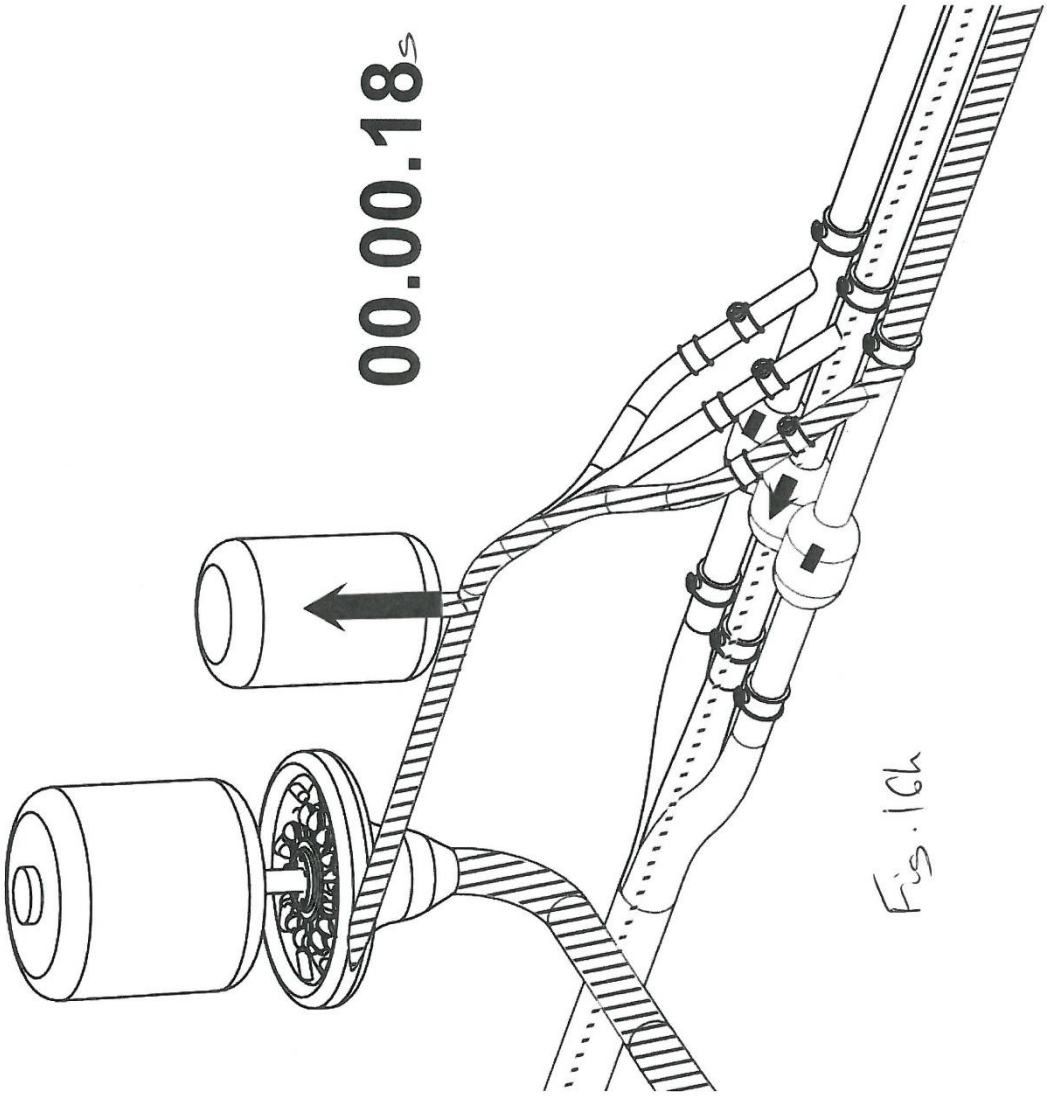

Fig. 16

24/38

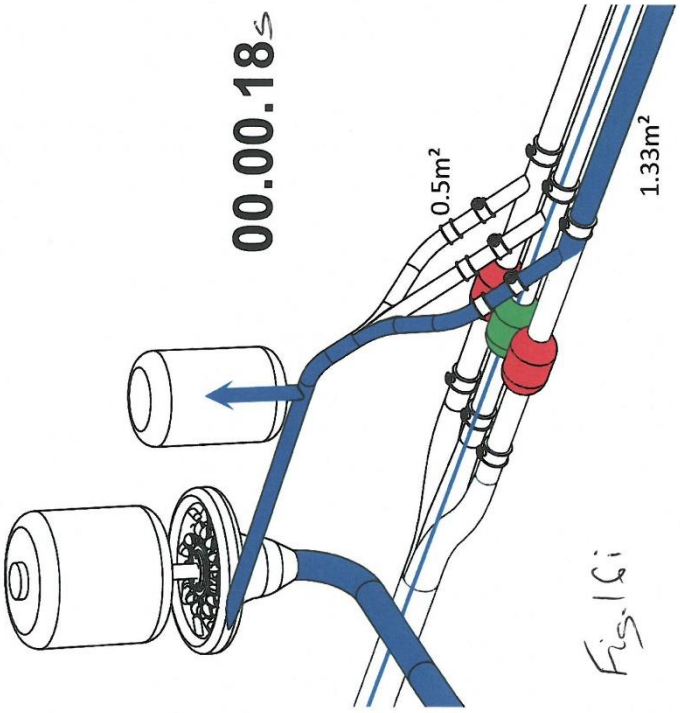

Fig. 16

River height 1.5m, Velocity 0.75 m/s

Area at inlet x Velocity at inlet = Area at outlet x Velocity at outlet.

Close two pipes to get better taper ratio.

- 20m x 1.5m : 1.33 m^2
- 22.5 : 1

In 1.3m ID pipe Velocity = 0.75 x 22.5 = 16.9 m/s

After ram valve Velocity =16.9 x 2.66 (1.33:0.5) = 45 m/s

Fig. 17

25/38

River height 1.5m, Velocity 0.75 m/s

Area at inlet x Velocity at inlet = Area at outlet x Velocity at outlet.

Close two pipes to get better taper ratio.

- 20m x 1.5m : 1.33 m^2
- 22.5 : 1

In 1.3m ID pipe Velocity = 0.75 x 22.5 = 16.9 m/s

After ram valve Velocity = 16.9 x 2.66 (1.33:0.5) = 45 m/s

Velocity with 1 jet (10cm diameter) 45/2 x 63 = 1417 m/s

Fig. 18

26/38

River height 1.5m, Velocity 0.75 m/s

Area at inlet x Velocity at inlet = Area at outlet x Velocity at outlet.

Close two pipes to get better taper ratio.

- 20m x 1.5m : 1.33 m^2
- 22.5 : 1

In 1.3m ID pipe Velocity = 0.75 x 22.5 = 16.9 m/s

After ram valve Velocity =16.9 x 2.66 (1.33:0.5) = 45 m/s

Velocity with 1 jet (10cm diameter) 45/2 x 63 = 1417 m/s

Velocity with 6 jets = 1417/ 6 = 236 m/s

Fig. 19

27/38

River height 1.5m, Velocity 0.75 m/s

Area at inlet x Velocity at inlet = Area at outlet x Velocity at outlet.

Close two pipes to get better taper ratio.

- 20m x 1.5m : 1.33 m^2
- 22.5 : 1

In 1.3m ID pipe Velocity = 0.75 x 22.5 = 16.9 m/s

After ram valve Velocity =16.9 x 2.66 (1.33:0.5) = 45 m/s

Velocity with 1 jet (10cm diameter) 45/2 x 63 = 1417 m/s

Velocity with 6 jets = 1417/ 6 = 236 m/s

Flow through turbine and returned to the river = (45/2) x 0.5 = 11.25 m^3/s

Fig. 20

28/38

River height 2.5m, Velocity 0.75m/s

Again close two pipes to improve taper ratio

Taper ratio 20 x 2.5 : 1.33
37.5 : 1
In 1.3m ID pipe Velocity = 37.5 x 0.75 = 28.1 m/s
After ram valve Velocity = 28.1 x 2.66 = 74.8 m/s

Velocity with 1 jet (13cm diameter) = 74.8 /2 x 37.6 = 1406 m/s
Velocity with 6 jets = 1406/6 = 234 m/s

Flow through turbine and returned to the river = (74.8/2) x 0.5 = 18.7 m^3/s

Fig. 21

29/38

River height 3.5m, Velocity = 1.0m/s

Close two pipes

Velocity with 6 jets (19cm diameter) = 241m/s

Flow through turbine and returned to the river = 35m³/s

Fig. 22

30/38

River height 4.5m, Velocity = 1.5 m/s

Close two pipes

Velocity with 6 jets (25cm diameter) = 229.5 m/s

Flow through turbine and returned to river = 67.5 m^3/s

Fig. 23

31/38

River height 5.5m Velocity = 1.5 m/s

Close two pipes

Velocity with 6 jets (28cm diameter) = 222 m/s

Flow through turbine and returned to river = 82.5 m^3/s

Flow downstream (174 x 1.3 /2) - 82.5 = 30.6 m^3/s

Fig. 24

32/38

A river height of 5.5m = flooding in Worcester.

Can we use this device as a flood prevention mechanism?

Leave all three pipes open to increase downstream output.
Create an under-river high velocity pipe right through Worcester ending south of the city

However, this sacrifices some flow through turbine as taper ratio is decreased.
Taper ratio = 20 x 5.5 : 3 x 1.33 = 27.5 : 1
In 1.3m diameter pipes, Velocity = 27.5 x 1.5 = 41.3 m/s
After ram valve, Velocity = 41.3 x 2.66 = 109.7 m/s

Velocity with one jet (17cm diameter) = 109.7 x 0.5 x 28 = 1,206 m/s

Velocity with six jets = 1,206 / 6 = 201 m/s

Flow through turbine and returned to river (109.7/2) x 0.5 = 27.4m^3/s

Flow downstream = (41.3 x 4) - 27.4 = 137.8 m^3/s

Fig. 25

33/38

34/38

Fig. 26

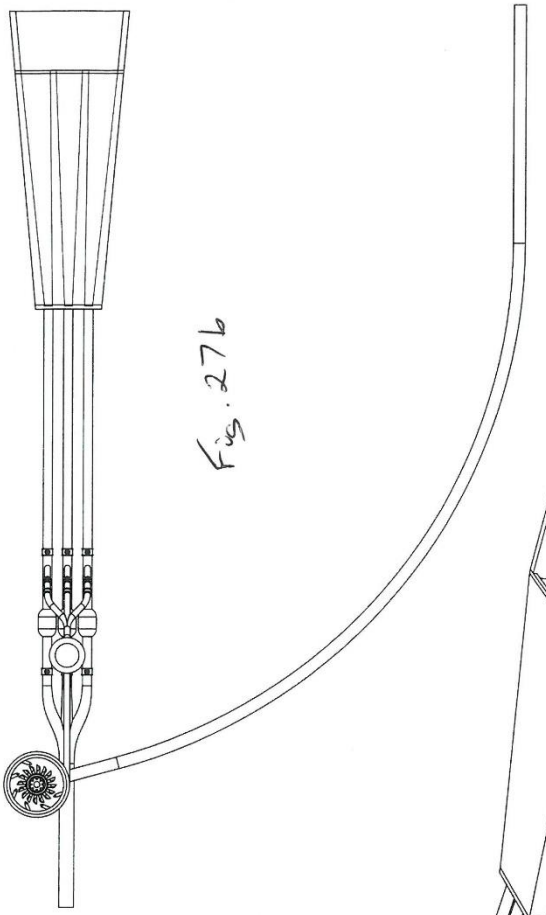

Fig. 27b

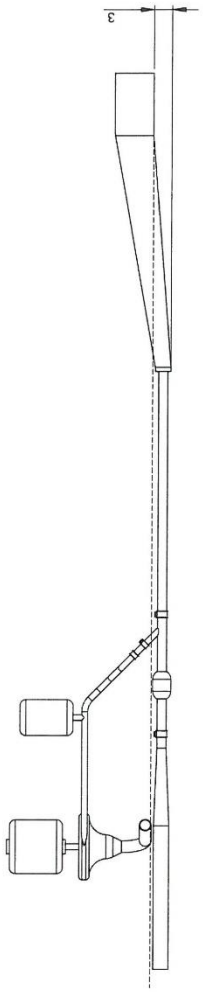

Fig. 27c

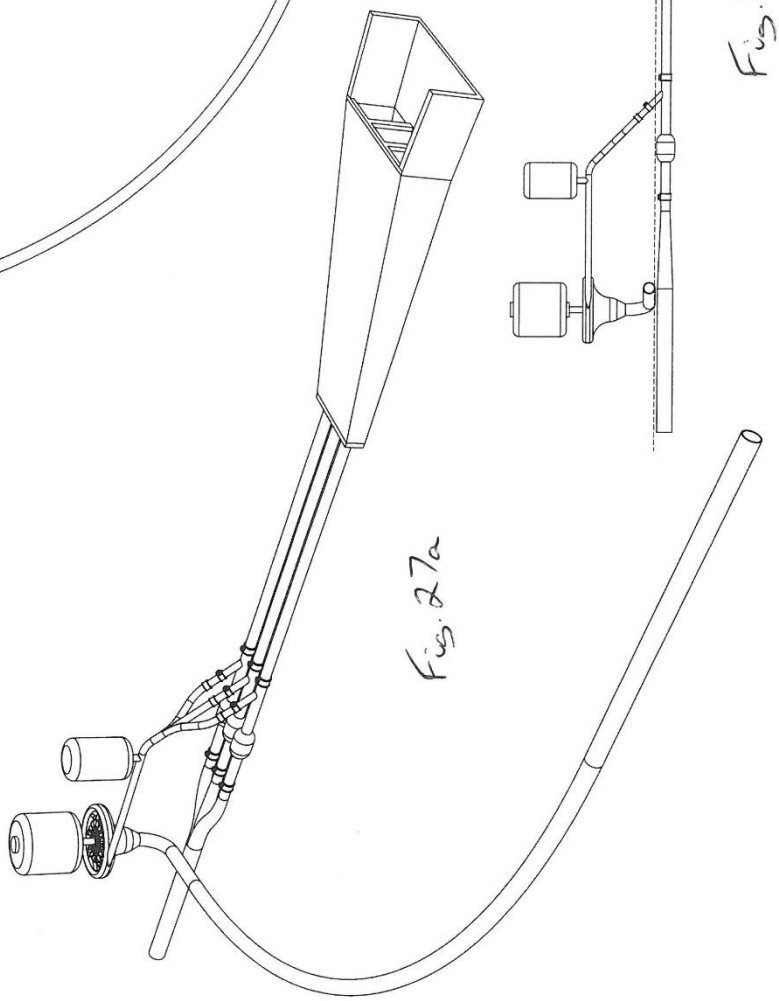

Fig. 27a

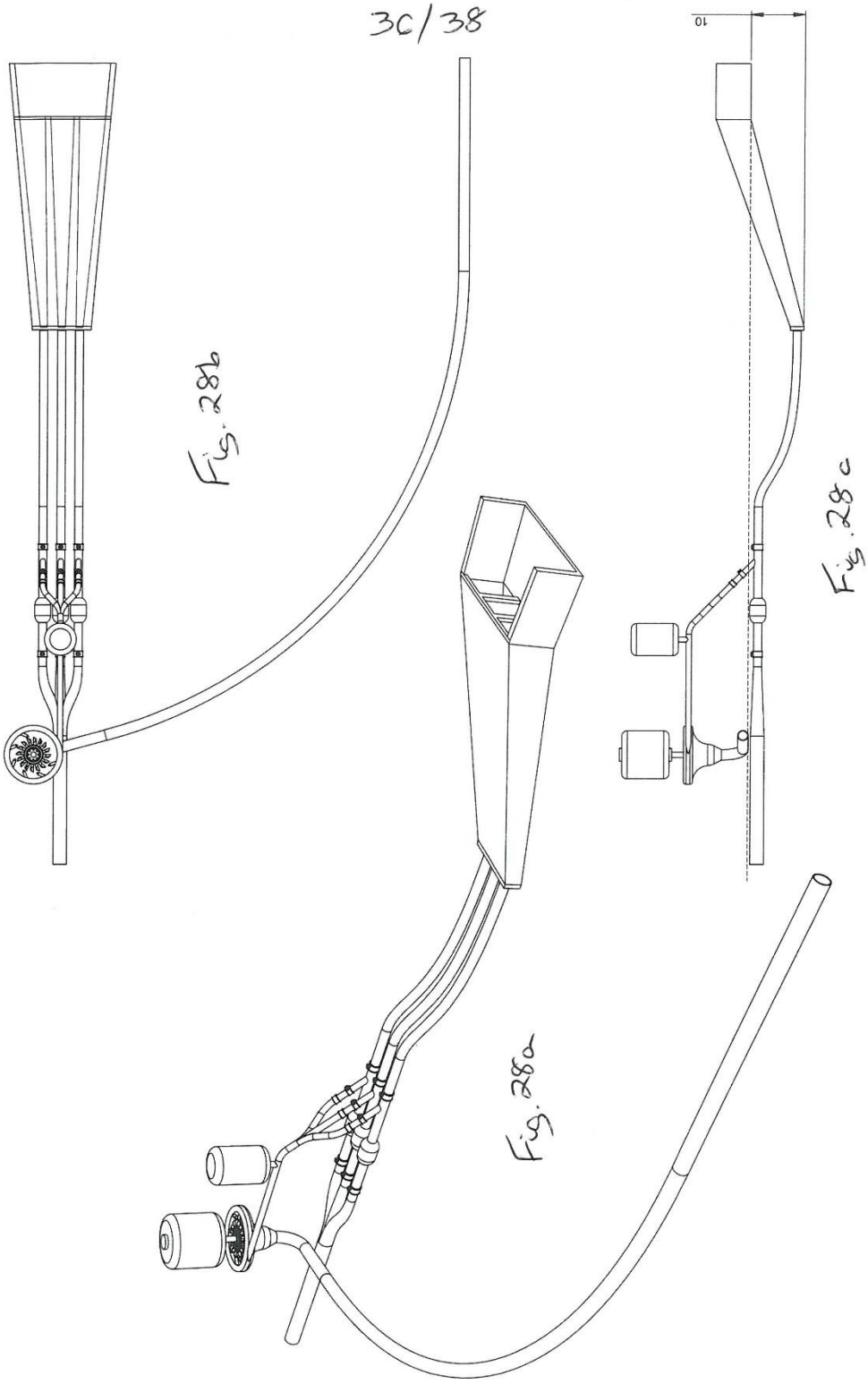
Fig. 28b
Fig. 28c
Fig. 28a

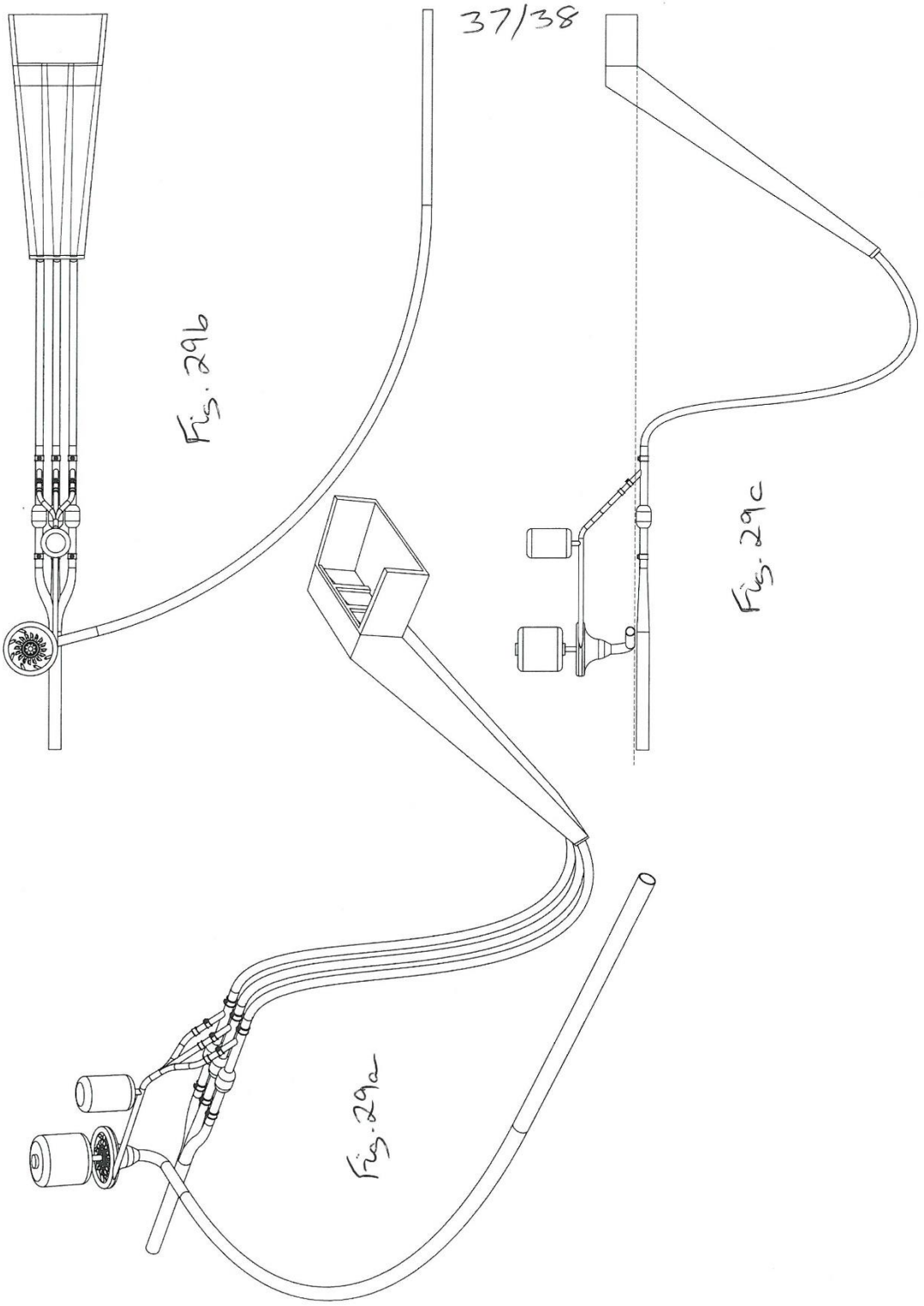
Fig. 29b
Fig. 29c
Fig. 29a

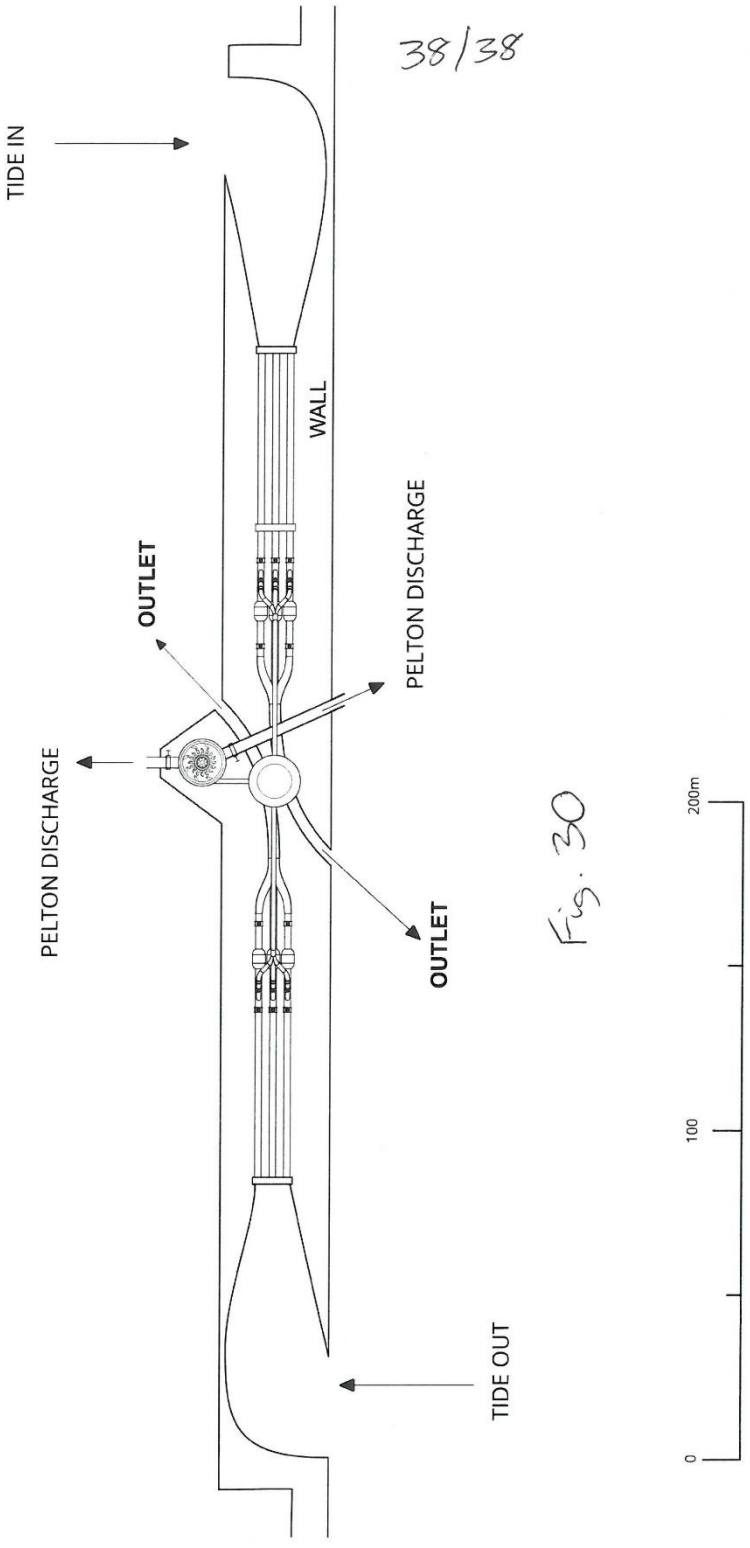
38/38
TIDE IN
WALL
OUTLET
PELTON DISCHARGE
PELTON DISCHARGE
OUTLET
TIDE OUT
0
100
200m

Fig. 30

Appendix B- Initial hand calculations

0m static head applied

		Water density	rho=	1000	kg/m^3				From the Patent	Hand Calcs							
		Acceleration due to gravity	g=	9.81	m/s^2				Using continuity equation					from Bernoulli's			If no additional head is required the exit pressure is 1 Pa
		meters of static head		0	m				m=rho*u*A	p=0.5*rho*u^2				P1-P2=0.5*rho*(V2^2-V1^2)	p=rho*g*h	P=rho*g*h	
Funnel Number	Patent	inlet width (m)	river height (m)	inlet surface area (m^2)	inlet velocity (m/s)	outlet internal diameter (m)	number of pipes	outlet surface area (m^2)	outlet velocity (m/s)	dynamic inlet pressure (Pa)	static inlet pressure (Pa)	total inlet pressure (Pa)	inlet head (m)	outlet pressure (Pa)	Addition head required to achieve outlet velocity (m)		Actual exit velocity (m/s)
1	fig 13	20	1.5	30	0.75	1.3	1	1.33	16.95	281.25	0	281.25	0.03	-143112.96	14.59		1.06
2		20	1.5	30	0.75	1.3	2	2.65	8.48	281.25	0	281.25	0.03	-35356.37	3.60		1.06
3		20	1.5	30	0.75	1.3	3	3.98	5.65	281.25	0	281.25	0.03	-15401.44	1.57		1.06
4	fig 21	20	2.5	50	0.75	1.3	1	1.33	28.25	281.25	0	281.25	0.03	-398536.01	40.63		1.06
5		20	2.5	50	0.75	1.3	2	2.65	14.13	281.25	0	281.25	0.03	-99212.13	10.11		1.06
6		20	2.5	50	0.75	1.3	3	3.98	9.42	281.25	0	281.25	0.03	-43781.78	4.46		1.06
7	fig 22	20	3.5	70	1	1.3	1	1.33	52.74	500	0	500	0.05	-1389636.57	141.66		1.41
8		20	3.5	70	1	1.3	2	2.65	26.37	500	0	500	0.05	-346659.14	35.34		1.41
9		20	3.5	70	1	1.3	3	3.98	17.58	500	0	500	0.05	-153515.17	15.65		1.41
10	fig 23	20	4.5	90	1.5	1.3	1	1.33	101.71	1125	0	1125	0.11	-5170066.63	527.02		2.12
11		20	4.5	90	1.5	1.3	2	2.65	50.85	1125	0	1125	0.11	-1290829.16	131.58		2.12
12		20	4.5	90	1.5	1.3	3	3.98	33.90	1125	0	1125	0.11	-572451.85	58.35		2.12
13	fig 24	20	5.5	110	1.5	1.3	1	1.33	124.31	1125	0	1125	0.11	-7724297.07	787.39		2.12
14		20	5.5	110	1.5	1.3	2	2.65	62.16	1125	0	1125	0.11	-1929386.77	196.68		2.12
15		20	5.5	110	1.5	1.3	3	3.98	41.44	1125	0	1125	0.11	-856255.23	87.28		2.12

			Boundary conditions set in Ansys		Results from CFD Analysis		
Funnel Number	Patent	inlet velocity (m/s)	outlet velocity (m/s)	total inlet pressure (Pa)	outlet pressure (Pa)	exit velocity (m/s)	
1	fig 13	0.75	16.95	281.25	-145421		
2		0.75	8.48	281.25	-35571		
3		0.75	5.65	281.25	-15663		
4	fig 21	0.75	28.25	281.25	-393658		
5		0.75	14.13	281.25	-98700		
6		0.75	9.42	281.25	-43818		
7	fig 22	1	52.74	500	-1.37E+06		
8		1	26.37	500	-343098		
9		1	17.58	500	-152565		
10	fig 23	1.5	101.71	1125	-5068070		
11		1.5	50.85	1125	-1.27E+06		
12		1.5	33.90	1125	-566420		
13	fig 24	1.5	124.31	1125	-7.55E+06		
14		1.5	62.16	1125	-1.90E+06		
15		1.5	41.44	1125	-845014		

Validation of CFD/Hand calculations				
outlet pressure CFD	outlet pressure hand calc	Pressure difference (Pa)	pressure difference (m)	% difference
-145421.00	-143112.96	-2308.04	-0.24	1.59
-35571.00	-35356.37	-214.63	-0.02	0.60
-15663.00	-15401.44	-261.56	-0.03	1.67
-393658.00	-398536.01	4878.01	0.50	-1.24
-98700.00	-99212.13	512.13	0.05	-0.52
-43818.00	-43781.78	-36.22	0.00	0.08
-1367110.00	-1389636.57	22526.57	2.30	-1.65
-343098.00	-346659.14	3561.14	0.36	-1.04
-152565.00	-153515.17	950.17	0.10	-0.62
-5068070.00	-5170066.63	101996.63	10.40	-2.01
-1272910.00	-1290829.16	17919.16	1.83	-1.41
-566420.00	-572451.85	6031.85	0.61	-1.06
-7552540.00	-7724297.07	171757.07	17.51	-2.27
-1899000.00	-1929386.77	30386.77	3.10	-1.60
-845014.00	-856255.23	11241.23	1.15	-1.33

5m static head applied

		Water density	rho=	1000	kg/m^3				From the Patent	Hand Calcs						
		Acceleration due to gravity	g=	9.81	m/s^2				Using continuity equation					from Bernoulli's		If no additional head is required the exit pressure is 1 Pa
		meters of static head		5	m				m=rho*u*A	p=0.5*rho*u^2			p=rho*g*h	P1-P2=0.5*rho*(V2^2-V1^2)	P=rho*g*h	
Funnel Number	Patent	inlet width (m)	river height (m)	inlet surface area (m^2)	inlet velocity (m/s)	outlet Internal diameter (m)	number of pipes	outlet surface area (m^2)	outlet velocity (m/s)	dynamic inlet pressure (Pa)	static inlet pressure (Pa)	total inlet pressure (Pa)	inlet head (m)	outlet pressure (Pa)	Addition head required to achieve outlet velocity (m)	Actual exit velocity (m/s)
1	fig 13	20	1.5	30	0.75	1.3	1	1.33	16.95	281.25	49050	49331.25	5.03	-94062.96	9.59	9.96
2		20	1.5	30	0.75	1.3	2	2.65	8.48	281.25	49050	49331.25	5.03	13693.63	0.00	8.48
3		20	1.5	30	0.75	1.3	3	3.98	5.65	281.25	49050	49331.25	5.03	33648.56	0.00	5.65
4	fig 21	20	2.5	50	0.75	1.3	1	1.33	28.25	281.25	49050	49331.25	5.03	-349486.01	35.63	9.96
5		20	2.5	50	0.75	1.3	2	2.65	14.13	281.25	49050	49331.25	5.03	-50162.13	5.11	9.96
6		20	2.5	50	0.75	1.3	3	3.98	9.42	281.25	49050	49331.25	5.03	5268.22	0.00	9.42
7	fig 22	20	3.5	70	1	1.3	1	1.33	52.74	500	49050	49550	5.05	-1340586.57	136.66	10.00
8		20	3.5	70	1	1.3	2	2.65	26.37	500	49050	49550	5.05	-297609.14	30.34	10.00
9		20	3.5	70	1	1.3	3	3.98	17.58	500	49050	49550	5.05	-104465.17	10.65	10.00
10	fig 23	20	4.5	90	1.5	1.3	1	1.33	101.71	1125	49050	50175	5.11	-5121016.63	522.02	10.13
11		20	4.5	90	1.5	1.3	2	2.65	50.85	1125	49050	50175	5.11	-1241779.16	126.58	10.13
12		20	4.5	90	1.5	1.3	3	3.98	33.90	1125	49050	50175	5.11	-523401.85	53.35	10.13
13	fig 24	20	5.5	110	1.5	1.3	1	1.33	124.31	1125	49050	50175	5.11	-7675247.07	782.39	10.13
14		20	5.5	110	1.5	1.3	2	2.65	62.16	1125	49050	50175	5.11	-1880336.77	191.68	10.13
15		20	5.5	110	1.5	1.3	3	3.98	41.44	1125	49050	50175	5.11	-807205.23	82.28	10.13

			Boundary conditions set in Ansys			Results from CFD Analysis		
Funnel Number	Patent	inlet velocity (m/s)	outlet velocity (m/s)	total inlet pressure (Pa)		outlet pressure (Pa)	exit velocity (m/s)	
1	fig 13	0.75	16.95	49331.25		-93953		
2		0.75	8.48	49331.25		13389		
3		0.75	5.65	49331.25		33377		
4	fig 21	0.75	28.25	49331.25		-344466		
5		0.75	14.13	49331.25		-49652		
6		0.75	9.42	49331.25		5231		
7	fig 22	1	52.74	49550		-1.32E+06		
8		1	26.37	49550		-294016		
9		1	17.58	49550		-103467		
10	fig 23	1.5	101.71	50175		-5.02E+06		
11		1.5	50.85	50175		-1.22E+06		
12		1.5	33.90	50175		-5.17E+05		
13	fig 24	1.5	124.31	50175		-7.50E+06		
14		1.5	62.16	50175		-1.85E+06		
15		1.5	41.44	50175		-795858		

Validation of CFD/Hand calculations				
outlet pressure CFD	outlet pressure hand calc	Pressure difference (Pa)	pressure difference (m)	% difference
-93953.00	-94062.96	109.96	0.01	-0.12
13389.00	13693.63	-304.63	-0.03	-2.28
33377.00	33648.56	-271.56	-0.03	-0.81
-344466.00	-349486.01	5020.01	0.51	-1.46
-49652.00	-50162.13	510.13	0.05	-1.03
5231.00	5268.22	-37.22	0.00	-0.71
-1317840.00	-1340586.57	22746.57	2.32	-1.73
-294016.00	-297609.14	3593.14	0.37	-1.22
-103467.00	-104465.17	998.17	0.10	-0.96
-5017360.00	-5121016.63	103656.63	10.57	-2.07
-1223540.00	-1241779.16	18239.16	1.86	-1.49
-517329.00	-523401.85	6072.85	0.62	-1.17
-7501380.00	-7675247.07	173867.07	17.72	-2.32
-1849590.00	-1880336.77	30746.77	3.13	-1.66
-795858.00	-807205.23	11347.23	1.16	-1.43

		Water density	rho=	1000	kg/m^3				From the Patent	Hand Calcs						
		Acceleration due to gravity	g=	9.81	m/s^2				Using continuity equation					from Bernoulli's		If no additional head is required the exit pressure is 1 Pa
		meters of static head		10	m				m=rho*u*A	p=0.5*rho*u^2			p=rho*g*h	P1-P2=0.5*rho*(V2^2-V1^2)	P=rho*g*h	
Funnel Number	Patent	inlet width (m)	river height (m)	inlet surface area (m^2)	inlet velocity (m/s)	outlet Internal diameter (m)	number of pipes	outlet surface area (m^2)	outlet velocity (m/s)	dynamic inlet pressure (Pa)	static inlet pressure (Pa)	total inlet pressure (Pa)	inlet head (m)	outlet pressure (Pa)	Addition head required to achieve outlet velocity (m)	Actual exit velocity (m/s)
1	fig 13	20	1.5	30	0.75	1.3	1	1.33	16.95	281.25	98100	98381.25	10.03	-45012.96	4.59	14.05
2		20	1.5	30	0.75	1.3	2	2.65	8.48	281.25	98100	98381.25	10.03	62743.63	0.00	8.48
3		20	1.5	30	0.75	1.3	3	3.98	5.65	281.25	98100	98381.25	10.03	82698.56	0.00	5.65
4	fig 21	20	2.5	50	0.75	1.3	1	1.33	28.25	281.25	98100	98381.25	10.03	-300436.01	30.63	14.05
5		20	2.5	50	0.75	1.3	2	2.65	14.13	281.25	98100	98381.25	10.03	-1112.13	0.11	14.05
6		20	2.5	50	0.75	1.3	3	3.98	9.42	281.25	98100	98381.25	10.03	54318.22	0.00	9.42
7	fig 22	20	3.5	70	1	1.3	1	1.33	52.74	500	98100	98600	10.05	-1291536.57	131.66	14.08
8		20	3.5	70	1	1.3	2	2.65	26.37	500	98100	98600	10.05	-248559.14	25.34	14.08
9		20	3.5	70	1	1.3	3	3.98	17.58	500	98100	98600	10.05	-55415.17	5.65	14.08
10	fig 23	20	4.5	90	1.5	1.3	1	1.33	101.71	1125	98100	99225	10.11	-5071966.63	517.02	14.17
11		20	4.5	90	1.5	1.3	2	2.65	50.85	1125	98100	99225	10.11	-1192729.16	121.58	14.17
12		20	4.5	90	1.5	1.3	3	3.98	33.90	1125	98100	99225	10.11	-474351.85	48.35	14.17
13	fig 24	20	5.5	110	1.5	1.3	1	1.33	124.31	1125	98100	99225	10.11	-7626197.07	777.39	14.17
14		20	5.5	110	1.5	1.3	2	2.65	62.16	1125	98100	99225	10.11	-1831286.77	186.68	14.17
15		20	5.5	110	1.5	1.3	3	3.98	41.44	1125	98100	99225	10.11	-758155.23	77.28	14.17

			Boundary conditions set in Ansys			Results from CFD Analysis		
Funnel Number	Patent	inlet velocity (m/s)	outlet velocity (m/s)	total inlet pressure (Pa)		outlet pressure (Pa)	exit velocity (m/s)	
1	fig 13	0.75	16.95	98381.25		-44016		
2		0.75	8.48	98381.25		62437		
3		0.75	5.65	98381.25		82421		
4	fig 21	0.75	28.25	98381.25		-295244		
5		0.75	14.13	98381.25		-1211		
6		0.75	9.42	98381.25		54293		
7	fig 22	1	52.74	98600		-1.27E+06		
8		1	26.37	98600		-244815		
9		1	17.58	98600		-54397		
10	fig 23	1.5	101.71	99225		-4.96E+06		
11		1.5	50.85	99225		-1.17E+06		
12		1.5	33.90	99225		-467995		
13	fig 24	1.5	124.31	99225		-7.44E+06		
14		1.5	62.16	99225		-1.80E+06		
15		1.5	41.44	99225		-746403		

Validation of CFD/Hand calculations				
outlet pressure CFD	outlet pressure hand calc	Pressure difference (Pa)	pressure difference (m)	% difference
-44016.00	-45012.96	996.96	0.10	-2.26
62437.00	62743.63	-306.63	-0.03	-0.49
82421.00	82698.56	-277.56	-0.03	-0.34
-295244.00	-300436.01	5192.01	0.53	-1.76
-1211.00	-1112.13	-98.87	-0.01	8.16
54293.00	54318.22	-25.22	0.00	-0.05
-1267960.00	-1291536.57	23576.57	2.40	-1.86
-244815.00	-248559.14	3744.14	0.38	-1.53
-54397.00	-55415.17	1018.17	0.10	-1.87
-4963440.00	-5071966.63	108526.63	11.06	-2.19
-1173720.00	-1192729.16	19009.16	1.94	-1.62
-467995.00	-474351.85	6356.85	0.65	-1.36
-7443830.00	-7626197.07	182367.07	18.59	-2.45
-1799280.00	-1831286.77	32006.77	3.26	-1.78
-746403.00	-758155.23	11752.23	1.20	-1.57

15m of static head applied

		Water density	rho=	1000	kg/m^3				From the Patent	Hand Calcs						
		Acceleration due to gravity	g=	9.81	m/s^2				Using continuity equation					from Bernoulli's		If no additional head is required the exit pressure is 1 Pa
		meters of static head		15	m				m=rho*u*A	p=0.5*rho*u^2			p=rho*g*h	P1-P2=0.5*rho*(V2^2-V1^2)	P=rho*g*h	
Funnel Number	Patent	inlet width (m)	river height (m)	inlet surface area (m^2)	inlet velocity (m/s)	outlet Internal diameter (m)	number of pipes	outlet surface area (m^2)	outlet velocity (m/s)	dynamic inlet pressure (Pa)	static inlet pressure (Pa)	total inlet pressure (Pa)	inlet head (m)	outlet pressure (Pa)	Addition head required to achieve outlet velocity (m)	Actual exit velocity (m/s)
1	fig 13	20	1.5	30	0.75	1.3	1	1.33	16.95	281.25	147150	147431.25	15.03	4037.04	0.00	16.95
2		20	1.5	30	0.75	1.3	2	2.65	8.48	281.25	147150	147431.25	15.03	111793.63	0.00	8.48
3		20	1.5	30	0.75	1.3	3	3.98	5.65	281.25	147150	147431.25	15.03	131748.56	0.00	5.65
4	fig 21	20	2.5	50	0.75	1.3	1	1.33	28.25	281.25	147150	147431.25	15.03	-251386.01	25.63	17.19
5		20	2.5	50	0.75	1.3	2	2.65	14.13	281.25	147150	147431.25	15.03	47937.87	0.00	14.13
6		20	2.5	50	0.75	1.3	3	3.98	9.42	281.25	147150	147431.25	15.03	103368.22	0.00	9.42
7	fig 22	20	3.5	70	1	1.3	1	1.33	52.74	500	147150	147650	15.05	-1242486.57	126.66	17.21
8		20	3.5	70	1	1.3	2	2.65	26.37	500	147150	147650	15.05	-199509.14	20.34	17.21
9		20	3.5	70	1	1.3	3	3.98	17.58	500	147150	147650	15.05	-6365.17	0.65	17.21
10	fig 23	20	4.5	90	1.5	1.3	1	1.33	101.71	1125	147150	148275	15.11	-5022916.63	512.02	17.29
11		20	4.5	90	1.5	1.3	2	2.65	50.85	1125	147150	148275	15.11	-1143679.16	116.58	17.29
12		20	4.5	90	1.5	1.3	3	3.98	33.90	1125	147150	148275	15.11	-425301.85	43.35	17.29
13	fig 24	20	5.5	110	1.5	1.3	1	1.33	124.31	1125	147150	148275	15.11	-7577147.07	772.39	17.29
14		20	5.5	110	1.5	1.3	2	2.65	62.16	1125	147150	148275	15.11	-1782236.77	181.68	17.29
15		20	5.5	110	1.5	1.3	3	3.98	41.44	1125	147150	148275	15.11	-709105.23	72.28	17.29

		Boundary conditions set in Ansys			Results from CFD Analysis		
Funnel Number	Patent	inlet velocity (m/s)	outlet velocity (m/s)	total inlet pressure (Pa)	outlet pressure (Pa)	exit velocity (m/s)	
1	fig 13	0.75	16.95	147431.25	4150		
2		0.75	8.48	147431.25	111412		
3		0.75	5.65	147431.25	131467		
4	fig 21	0.75	28.25	147431.25	-246403		
5		0.75	14.13	147431.25	48438		
6		0.75	9.42	147431.25	103328		
7	fig 22	1	52.74	147650	-1.22E+06		
8		1	26.37	147650	-195937		
9		1	17.58	147650	-5383		
10	fig 23	1.5	101.71	148275	-4.92E+06		
11		1.5	50.85	148275	-1.13E+06		
12		1.5	33.90	148275	-419271		
13	fig 24	1.5	124.31	148275	-7.40E+06		
14		1.5	62.16	148275	-1.75E+06		
15		1.5	41.44	148275	-697841		

Validation of CFD/Hand calculations				
outlet pressure CFD	outlet pressure hand calc	Pressure difference (Pa)	pressure difference (m)	% difference
4150.00	4037.04	112.96	0.01	2.72
111412.00	111793.63	-381.63	-0.04	-0.34
131467.00	131748.56	-281.56	-0.03	-0.21
-246403.00	-251386.01	4983.01	0.51	-2.02
48438.00	47937.87	500.13	0.05	1.03
103328.00	103368.22	-40.22	0.00	-0.04
-1219920.00	-1242486.57	22566.57	2.30	-1.85
-195937.00	-199509.14	3572.14	0.36	-1.82
-5383.00	-6365.17	982.17	0.10	-18.25
-4919790.00	-5022916.63	103126.63	10.51	-2.10
-1125560.00	-1143679.16	18119.16	1.85	-1.61
-419271.00	-425301.85	6030.85	0.61	-1.44
-7404640.00	-7577147.07	172507.07	17.58	-2.33
-1751720.00	-1782236.77	30516.77	3.11	-1.74
-697841.00	-709105.23	11264.23	1.15	-1.61

20m of static head applied

		Water density	rho=	1000	kg/m^3				From the Patent	Hand Calcs						
		Acceleration due to gravity	g=	9.81	m/s^2				Using continuity equation					from Bernoulli's		If no additional head is required the exit pressure is 1 Pa
		meters of static head		20	m				m=rho*u*A	p=0.5*rho*u^2			p=rho*g*h	P1-P2=0.5*rho*(V2^2-V1^2)	P=rho*g*h	
Funnel Number	Patent	inlet width (m)	river height (m)	inlet surface area (m^2)	inlet velocity (m/s)	outlet Internal diameter (m)	number of pipes	outlet surface area (m^2)	outlet velocity (m/s)	dynamic inlet pressure (Pa)	static inlet pressure (Pa)	total inlet pressure (Pa)	inlet head (m)	outlet pressure (Pa)	Addition head required to achieve outlet velocity (m)	Actual exit velocity (m/s)
1	fig 13	20	1.5	30	0.75	1.3	1	1.33	16.95	281.25	196200	196481.25	20.03	53087.04	0.00	16.95
2		20	1.5	30	0.75	1.3	2	2.65	8.48	281.25	196200	196481.25	20.03	160843.63	0.00	8.48
3		20	1.5	30	0.75	1.3	3	3.98	5.65	281.25	196200	196481.25	20.03	180798.56	0.00	5.65
4	fig 21	20	2.5	50	0.75	1.3	1	1.33	28.25	281.25	196200	196481.25	20.03	-202336.01	20.63	19.84
5		20	2.5	50	0.75	1.3	2	2.65	14.13	281.25	196200	196481.25	20.03	96987.87	0.00	14.13
6		20	2.5	50	0.75	1.3	3	3.98	9.42	281.25	196200	196481.25	20.03	152418.22	0.00	9.42
7	fig 22	20	3.5	70	1	1.3	1	1.33	52.74	500	196200	196700	20.05	-1193436.57	121.66	19.86
8		20	3.5	70	1	1.3	2	2.65	26.37	500	196200	196700	20.05	-150459.14	15.34	19.86
9		20	3.5	70	1	1.3	3	3.98	17.58	500	196200	196700	20.05	42684.83	0.00	17.58
10	fig 23	20	4.5	90	1.5	1.3	1	1.33	101.71	1125	196200	197325	20.11	-4973866.63	507.02	19.92
11		20	4.5	90	1.5	1.3	2	2.65	50.85	1125	196200	197325	20.11	-1094629.16	111.58	19.92
12		20	4.5	90	1.5	1.3	3	3.98	33.90	1125	196200	197325	20.11	-376251.85	38.35	19.92
13	fig 24	20	5.5	110	1.5	1.3	1	1.33	124.31	1125	196200	197325	20.11	-7528097.07	767.39	19.92
14		20	5.5	110	1.5	1.3	2	2.65	62.16	1125	196200	197325	20.11	-1733186.77	176.68	19.92
15		20	5.5	110	1.5	1.3	3	3.98	41.44	1125	196200	197325	20.11	-660055.23	67.28	19.92

			Boundary conditions set in Ansys			Results from CFD Analysis		
Funnel Number	Patent	inlet velocity (m/s)	outlet velocity (m/s)	total inlet pressure (Pa)		outlet pressure (Pa)	exit velocity (m/s)	
1	fig 13	0.75	16.95	196481.25		53417		
2		0.75	8.48	196481.25		160521		
3		0.75	5.65	196481.25		180525		
4	fig 21	0.75	28.25	196481.25		-197177		
5		0.75	14.13	196481.25		97516		
6		0.75	9.42	196481.25		152388		
7	fig 22	1	52.74	196700		-1.17E+06		
8		1	26.37	196700		-146749		
9		1	17.58	196700		43705		
10	fig 23	1.5	101.71	197325		-4.87E+06		
11		1.5	50.85	197325		-1.08E+06		
12		1.5	33.90	197325		-370006		
13	fig 24	1.5	124.31	197325		-7.35E+06		
14		1.5	62.16	197325		-1.70E+06		
15		1.5	41.44	197325		-648458		

Validation of CFD/Hand calculations				
outlet pressure CFD	outlet pressure hand calc	Pressure difference (Pa)	pressure difference (m)	% difference
53417.00	53087.04	329.96	0.03	0.62
160521.00	160843.63	-322.63	-0.03	-0.20
180525.00	180798.56	-273.56	-0.03	-0.15
-197177.00	-202336.01	5159.01	0.53	-2.62
97516.00	96987.87	528.13	0.05	0.54
152388.00	152418.22	-30.22	0.00	-0.02
-1170010.00	-1193436.57	23426.57	2.39	-2.00
-146749.00	-150459.14	3710.14	0.38	-2.53
43705.00	42684.83	1020.17	0.10	2.33
-4866870.00	-4973866.63	106996.63	10.91	-2.20
-1075880.00	-1094629.16	18749.16	1.91	-1.74
-370006.00	-376251.85	6245.85	0.64	-1.69
-7349880.00	-7528097.07	178217.07	18.17	-2.42
-1701720.00	-1733186.77	31466.77	3.21	-1.85
-648458.00	-660055.23	11597.23	1.18	-1.79

Appendix C Inlet drop variation sketches and models

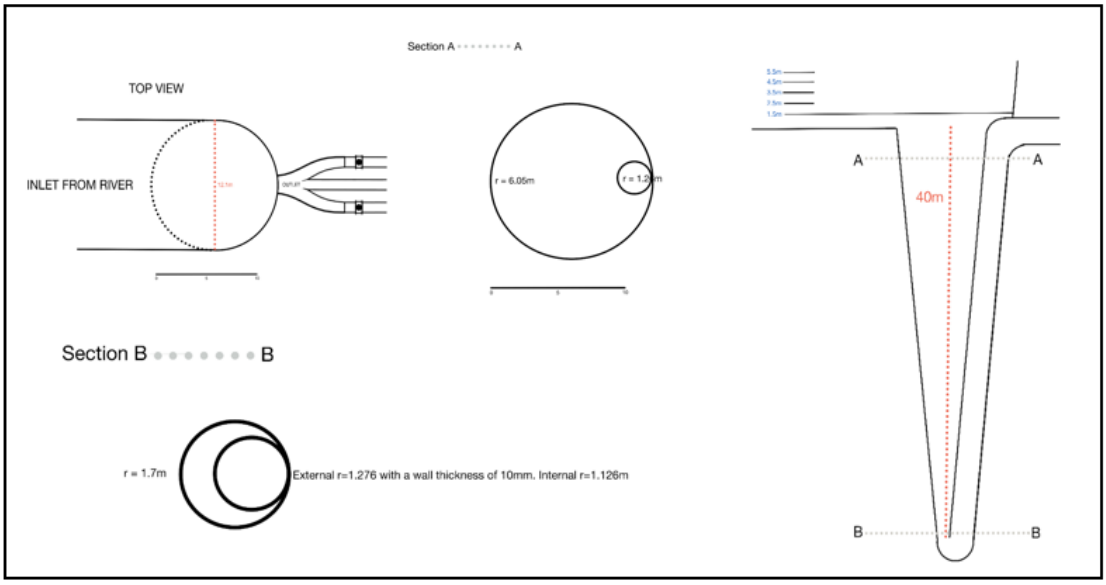

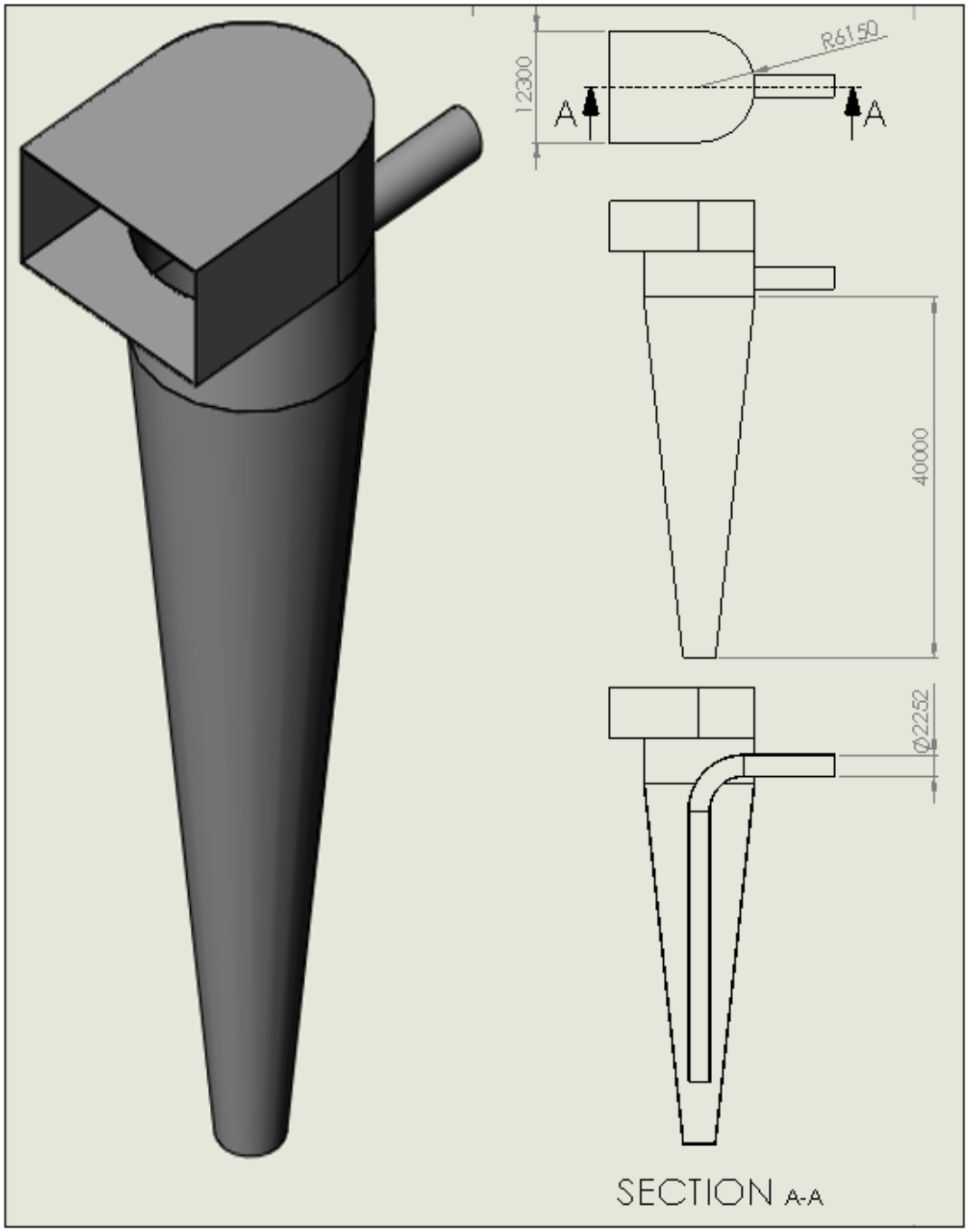
R6150
12300
A
A
40000
Ø2252
SECTION A-A

Appendix D Ram valve and inlet model

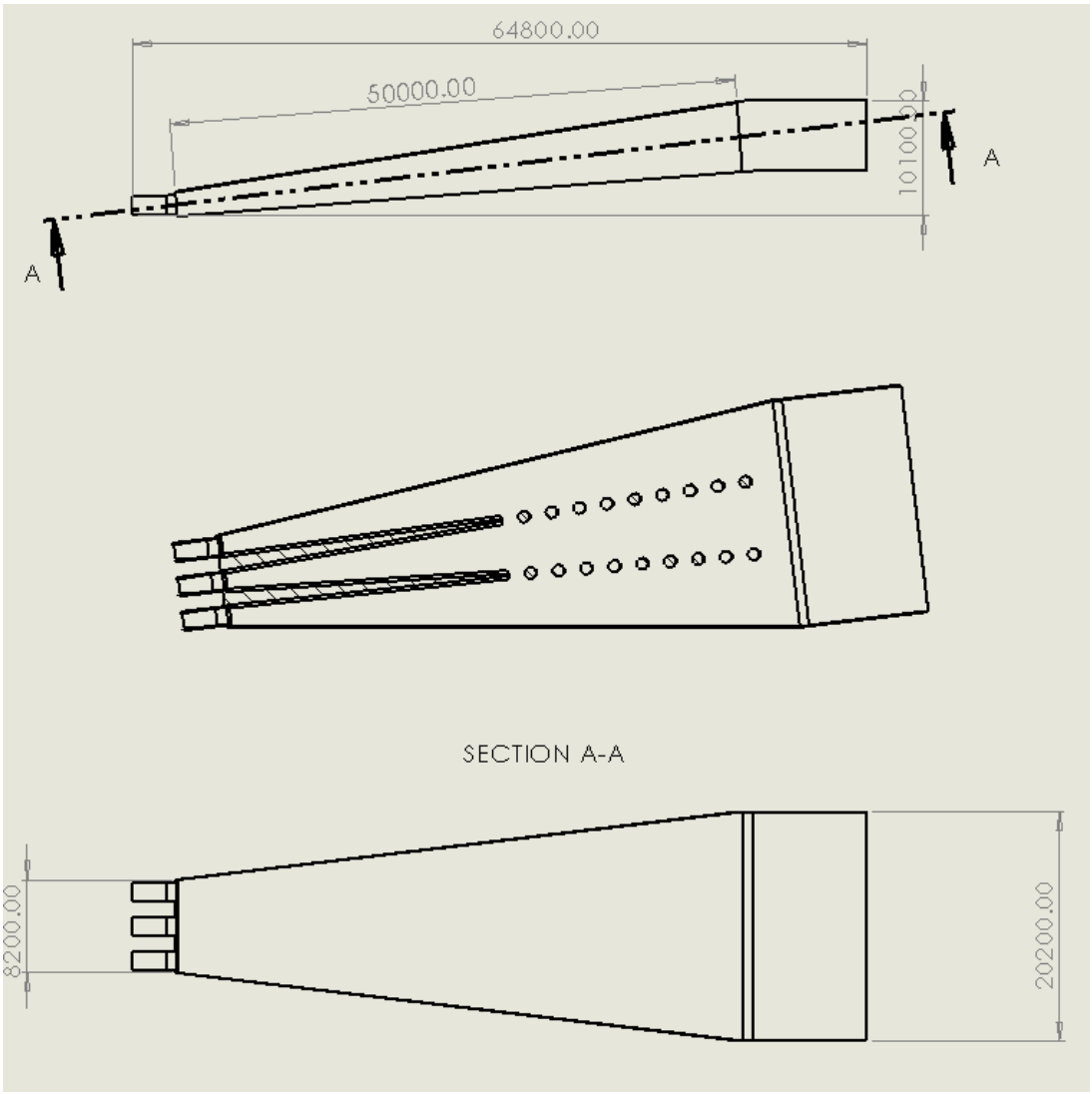

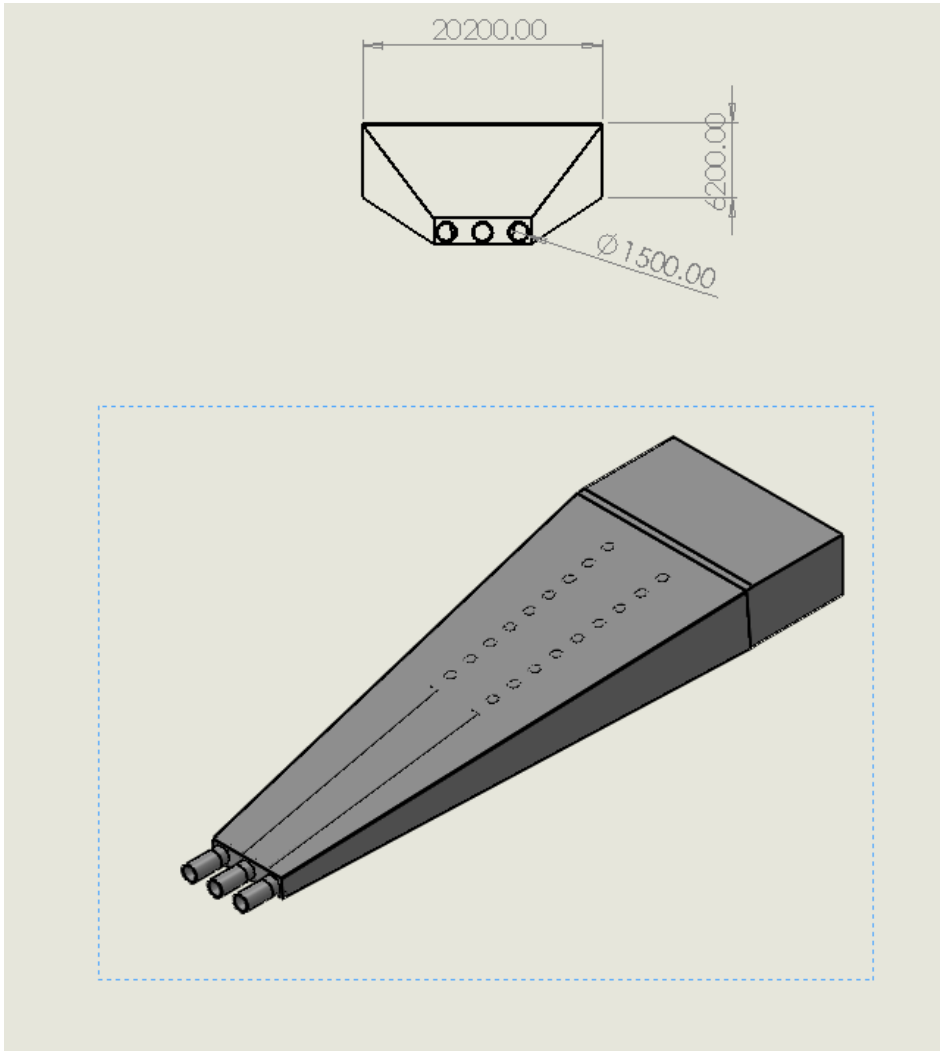
20200.00
6200.00
Ø1500.00

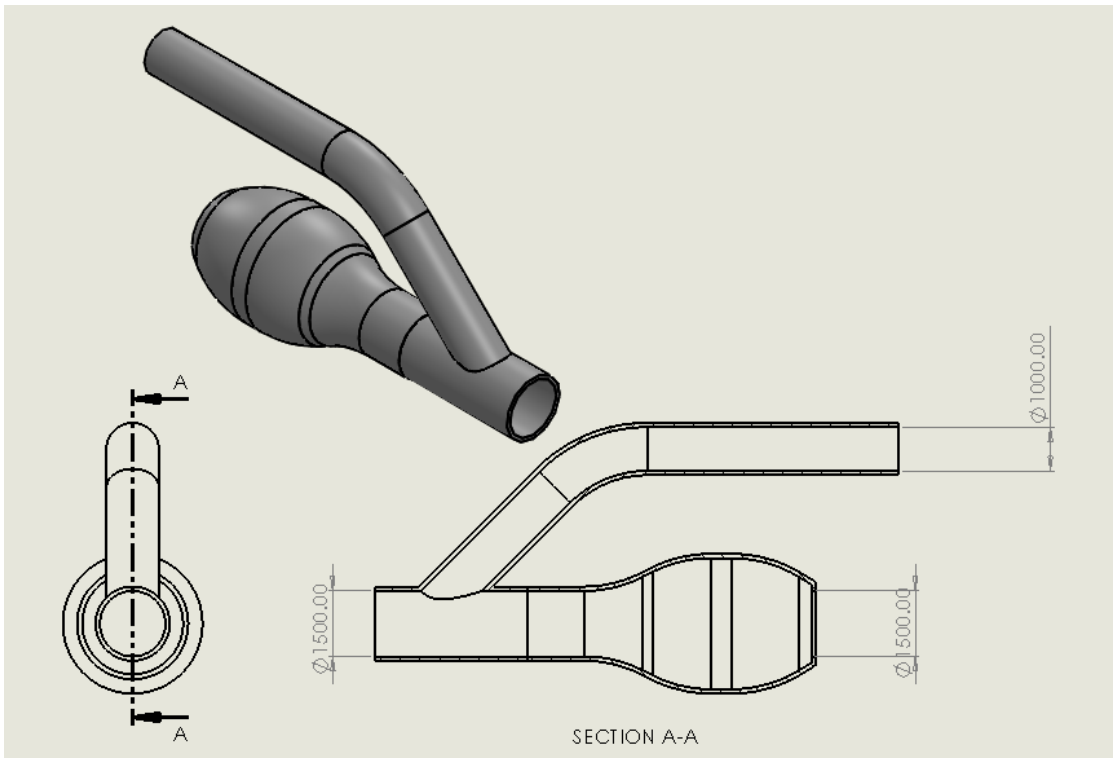
A
A
Ø1000.00
Ø1500.00
Ø1500.00
SECTION A-A

Appendix E Ram pump MATLAB code

Power and Surface plots

```
function Eff_Pow_surface_plots_2(L,Dp,Dc,H0,t3)
k = 0.025;                  % Concrete - New, very smooth, smooth
joints
K = 0.5;                    % pipe inlet coefficient
rho = 1000;
g = 9.81;
visc = 0.001520;            % viscosity at 5 degrees
Ap  = pi*Dp^2/4;            % cross sectional area main pipe
Ac  = pi*Dc^2/4;            % cross sectional area Y pipe

%%% Solve differential equations
t = 0.01; tt = 0:t:60;      % time step and run span
tinc = 0.5;
y0  = 0;                    % initial condition: Y = 0 - ignores time
to empty Y pipe!!!
Qp0 = 0;                    % initial condition: main pipe flow rate
is zero
m = 0;
for t1=0:tinc:20;
    m = m+1;
    [x,Y] = ode45(@(x,Y)
ode_Qp_Yc(x,Y,H0,Dp,Dc,L,k,K,visc,rho,t1,t3),tt,[Qp0;y0]);
    Qp = sign(real(Y(:,1))).*abs(Y(:,1));
    Yc = sign(real(Y(:,2))).*abs(Y(:,2));
    Vp  = Qp/Ap;
    Vc  = [zeros(1,1);(diff(Yc)/t)];
    dQp = [zeros(1,1);(diff(Qp)/t)];
    P2   = rho * ( g*(H0-Yc) - (Qp.^2/(2*Ap^2)) - (L.*dQp/Ap) );
% Pressure
    Pw = Ac.*Vc.*P2;    Pw(Ap.*Vc.*P2<0) = 0;
% Power
    CSQp = cumsum(Qp).*t;                          % cumulative volume
of water in m^3
    Engy_in = rho*g*H0*CSQp;                       % cumulative energy
    Engy_out = cumsum(abs(Pw)*t);
    n = 0;
    for t2 = 0:tinc:40;
        n = n+1;
        it2 = int16((t1+t2)/t)+1;                  % array index of end
of t1 + t2 time window
        Pwr(m,n) = Engy_out(it2)/(t1+t2);
        Eff(m,n) = Engy_out(it2)/Engy_in(it2);
    end;
end;

[M I] = max(Pwr);
[N J] = max(max(Pwr));
Fig1=figure;
clf;
hold on;
s=surf(Pwr/1000);
set(s,'EdgeColor','black','MeshStyle','both');
% contour_intervals = 0:5:50;
% contour3(Pwr/1000,contour_intervals,'black');
grid on;
```

```
fmt1 = 'Power_{avg} (kW). P_{max} of %5.2f kW occurs @ T_{open} =
%4.1f s and T_{closed} = %4.1f s';
fmt2 = '(H_0 = %4.1f m, L = %4.1f m, T_{valve} = %3.2f s)';
title_str1 = sprintf(fmt1,N/1000,(I(J)-1)*tinc,(J-1)*tinc);
title_str2 = sprintf(fmt2,H0,L,t3);
title({title_str1;title_str2},'FontSize', 13),
xlabel('Value closed time interval (s)','FontSize',12);
ylabel('Value open time interval (s)','FontSize',12);
zlabel('Average power (kW)','FontSize',12);
cb = colorbar; caxis([0 70]); cb.Label.String = 'Average power (kW)';
cb.FontSize = 12;
axis([1 n 1 m 0 170]);
set(gcf,'position',[200 200 880 480]);
view([-40 50]);
ax1=gca;
ax1.XTick=1:2/tinc:n; ax1.YTick=[1:2/tinc:m];
xText=(ax1.XTick-1)*tinc; ax1.XTickLabel = xText;
yText=(ax1.YTick-1)*tinc; ax1.YTickLabel = yText;

Fig2=figure;
clf;
hold on;
s=surf(Eff);
set(s,'EdgeColor','black','MeshStyle','both');
% contour_intervals = 0:5:50;
% contour3(Pwr/1000,contour_intervals,'black');
grid on;
fmt3 = 'Energy efficiency. \\eta = %4.2f at P_{max} @ T_{open} =
%4.1f s and T_{closed} = %4.1f s';
Eff(I,J);
title_str3 = sprintf(fmt3,Eff(I(J),J),(I(J)-1)*tinc,(J-1)*tinc);
title({title_str3;title_str2},'FontSize', 13);
xlabel('Value closed time interval (s)','FontSize',12);
ylabel('Value open time interval (s)','FontSize',12);
zlabel('Efficiency','FontSize',12);
cb = colorbar; caxis([0 0.7]); cb.Label.String = 'Efficiency';
cb.FontSize = 12;
axis([1 n 1 m 0 0.7]);
set(gcf,'position',[200 200 880 480]);
view([-40 50]);
ax2=gca;
ax2.XTick=1:2/tinc:n; ax2.YTick=[1:2/tinc:m];
xText=(ax2.XTick-1)*tinc; ax2.XTickLabel = xText;
yText=(ax2.YTick-1)*tinc; ax2.YTickLabel = yText;

end
```

Ordinary differential equation function

```
function dYdt = ode_Qp_Yc(x,Y,H0,Dp,Dc,L,k,K,visc,rho,t1,t3)
g  = 9.81;
% Qv = 0;                                                    %
valve completely closed - zero flow
Ap = pi*Dp^2/4;                                            % Pipe
cross-sectional area
Ac = pi*Dc^2/4;                                            % Y
pipe cross-sectional area
```

```
Re = rho*Y(1)/Ap*Dp/visc;                                          %
Reynolds number - Y(1)/Ap is velocity
ff = 1/((-1.8*log10(6.9/Re+(k/1000/3.71/Dp)^1.11))^2);             %
Friction factor - Uses the Haaland equation
valve=(x-t1)/t3; valve(x>=t1+t3)=1; valve(x<=t1)=0;                %
create ramp after t1 seconds over t3 seconds for valve closing time
dYdt = [g/L*Ap*(H0-Y(2)-
((1./(2*g*Ap^2))*(1+K+(L*ff/Dp)))*Y(1)*abs(Y(1)));(1/Ac)*(Y(1)*valve)
];
          % Y(1) is the pipe flow rate - Qp      % Y(2) is the fluid
level in the Y pipe

 Data = [ff];

end
```

pipe length and velocity function

```
function Pipe_length_vel_time_plot_2(Dp,H0)
k = 0.025;                  % Concrete - New, very smooth, smooth
joints
K = 0.5;                    % pipe inlet coefficient
rho = 1000;
visc = 0.001520;            % viscosity at 5 degrees
Ap  = pi*Dp^2/4;            % cross sectional area main pipe

%%% Solve differential equations - Part 1 - when valve is closed
t = 0.25; tt = 0:t:60;      % time step and run span - needs to be
long enough to cover t1 and 2nd zero crossing
Qp0 = 0;                    % initial condition: main pipe flow rate
is zero at the time the valve is opened
y0  = 0;                    % initial condition: Y = 0 - ignores time
to empty Y pipe!!!
t1 = 60;  t3 =0;            % t1 same length as time window to ensure
the valve is open all the time
Dc = Dp;                    % effectively not used in the ode
solution
for L=10:10:100;
    [x,Y] = ode45(@(x,Y)
ode_Qp_Yc(x,Y,H0,Dp,Dc,L,k,K,visc,rho,t1,t3),tt,[Qp0;y0]);
    vels(L/10,:)=Y(:,1)./Ap;
end;

Fig1=figure;
clf;
hold on;
s=surf(vels);
set(s,'EdgeColor','black','MeshStyle','row');
grid on;
title('Pipe flow velocity starting from rest for different
lengths','FontSize', 14),
xlabel('Time (s)','FontSize',12);
ylabel('Pipe length (m)','FontSize',12);
zlabel('Velocity (m/s)','FontSize',12);
cb = colorbar;
caxis([0 12]);
cb.Label.String = 'Velocity (m/s)'; cb.FontSize = 12;
% axis([1 241 1 100 0 12]);
set(gcf,'position',[200 200 780 480]); view([-125 10]);
```

```
ax1=gca;
ax1.XTick=1:40:241; ax1.YTick=[1,10:10:10];
xText=(ax1.XTick-1)/4; yText=(ax1.YTick)*10;
ax1.XTickLabel = xText; ax1.YTickLabel = yText;
end
```

line plots

```
function Line_plots(L,Dp,Dc,H0,t1,tc,t3)
% l = drive pipe length
% Dp = drive pipe diameter
% Dc = off-shoot pipe diameter
% H0 = total head
% t1 = how long the valve is closed
% tc = 3
% t3 = how quick the valve closes

k = 0.025;                  % Concrete - New, very smooth, smooth
joints
K = 0.5;                    % pipe inlet coefficient
rho = 1000;
g = 9.81;
visc = 0.001520;            % viscosity at 5 degrees
Ap  = pi*Dp^2/4;            % cross sectional area main pipe
Ac  = pi*Dc^2/4;            % cross sectional area Y pipe

%%% Solve differential equations
t = 0.01; tt = 0:t:60;      % time step and run span
y0  = 0;                    % initial condition: Y = 0 - ignores time
to empty Y pipe!!!
Qp0 = 0;                    % initial condition: main pipe flow rate
is zero
[x,Y] = ode45(@(x,Y)
ode_Qp_Yc(x,Y,H0,Dp,Dc,L,k,K,visc,rho,t1,t3),tt,[Qp0;y0]);
Qp = sign(real(Y(:,1))).*abs(Y(:,1));
ZC = ZeroX(tt,Qp);
t2 = t * round(ZC(tc)/t);   % nearest time increment to nth zero
crossing
it2 = int16(t2/t)+1;        % array index of nth zero crossing
tp = tt(1:it2)             % truncate to nearest time of nth zero
crossing
Qp = Qp(1:it2);       % NB      % truncate to nearest time of nth
zero crossing
% Qp = max(0,Qp(1:it2)); % NB
Yc = sign(real(Y(1:it2,2))).*abs(Y(1:it2,2));
Vp  = Qp/Ap;
Vc  = [zeros(1,1);(diff(Yc)/t)];
Qy  = Vc*Ac; %NB
% Qy = max(0,(Vc*Ac)); % NB
dQp = [zeros(1,1);(diff(Qp)/t)];
P2   = rho * ( g*(H0-Yc) - (Qp.^2/(2*Ap^2)) - (L.*dQp/Ap) );      %
Pressure
PH2  =  ones(1,length(tp))'*rho * g * H0;                          %
Pressure
PY2  = -rho * g * Yc;                                              %
Pressure
PV2  = -rho * Qp.^2/(2*Ap^2);                                     %
Pressure
```

```
PA2  = -rho * L.*dQp/Ap;                                                    %
Pressure
Pw = Ac.*Vc.*P2;    Pw(Ap.*Vc.*P2<0) = 0;    % NB
% Power
% Pw = Qy.*P2;    Pw(Qy.*P2<0) = 0; % NB
Engy_out = cumsum(abs(Pw)*t);
Pwr = Engy_out(end)/t2;
CSQp = cumsum(Qp).*t;     % cumulative volume of water in m^3
Engy_in = rho*g*H0*CSQp;       % cumulative energy
Eff = Engy_out(end)/Engy_in(end);
%
fig1=figure;
set(gcf,'position',[100 50 1200 700]);
fmt = 'H_{0}= %d m, L = %d m, \\oslash_{p}=%4.2f m,
\\oslash_{y}=%4.2f m, P_{avg}= %4.1f kW, \\bf\\eta\\rm = %4.2f,
T_{open|vlv|cl}= %4.1f|%3.1f|%4.1f s, Q_{avg}= %5.2f m^3/s';
title_str = sprintf(fmt,H0,L,Dp,Dc,Pwr/1000,Eff,t1,t3,t2-t1-
t3,CSQp(end)/(t1+t2));
suptitle(title_str);
% subplot(2,2,1,'Position',[0.07,0.54,0.4,0.34]); grid on; hold on;
box;
subplot(2,2,1); grid on; hold on; box;
xlimit = [0;2*ceil(t2(end)/2)];
plot(tp,Qp,'DisplayName','Qp','LineWidth',1);
plot(tp,Qy,'DisplayName','Qy');
title('Pipe flow rates','FontSize',12);
ax=gca; ax.XTick = 0:2:xlimit(end); ax.XLim = xlimit;
xlabel('Time from cycle start (s)','FontSize',12); ylabel('Main pipe
flow rate (m^3/s)','FontSize',12);
legend('show','Location','southwest','Orientation','vertical');
%
% subplot(2,2,2,'Position',[0.55,0.54,0.4,0.34]); grid on; hold on;
box;
subplot(2,2,2); grid on; hold on; box;
plot(tp,Yc);
title('Y-pipe head','FontSize',12);
ax=gca; ax.XTick = 0:2:xlimit(end); ax.XLim = xlimit;
xlabel('Time from cycle start (s)','FontSize',12); ylabel('Y-pipe
head (m)','FontSize',12);
%
% subplot(2,2,3,'Position',[0.07,0.08,0.4,0.34]); grid on; hold on;
box;
subplot(2,2,3); grid on; hold on; box;
plot(tp,P2/1000,'DisplayName','Total','LineWidth',2);
plot(tp,PH2/1000,'DisplayName','H_0 term');
plot(tp,PY2/1000,'DisplayName','Y_c term');
plot(tp,PV2/1000,'DisplayName','velocity term');
plot(tp,PA2/1000,'DisplayName','acceleration term');
title('Pressure','FontSize',12);
ax=gca; ax.XTick = 0:2:xlimit(end); ax.XLim = xlimit;
xlabel('Time from cycle start (s)','FontSize',12); ylabel('Pressure
(kPa)','FontSize',12);
legend('show','Location','southwest','Orientation','vertical');
%
% subplot(2,2,4,'Position',[0.55,0.08,0.4,0.34]); grid on; hold on;
box;
subplot(2,2,4); grid on; hold on; box;
plot(tp,Pw/1000);
title('Power','FontSize',12);
ax=gca; ax.XTick = 0:2:xlimit(end); ax.XLim = xlimit;
```

```
xlabel('Time from cycle start (s)','FontSize',12); ylabel('Power
(kW)','FontSize',12);

end



function ZC = ZeroX(tx,ty)                                  % function
to determine zero crossing points in x,y list
zci = @(v) find(v(:).*circshift(v(:), [-1 0]) <= 0);      % Returns
Approximate Zero-Crossing Indices Of Argument Vector
zxidx = zci(ty);
for k1 = 1:numel(zxidx)
    idxrng = max([1 zxidx(k1)-1]):min([zxidx(k1)+1 numel(ty)]);
    xrng = tx(idxrng);
    yrng = ty(idxrng);
    ZC(k1) = interp1( yrng(:), xrng(:), 0, 'linear', 'extrap' );
end
end
```

Appendix F User defined function code

One-way off-shoot pipe code

```
#include "udf.h"
DEFINE_PROFILE(viscosity_upper_1w, thread, index)
{
real viscous_resistance;
face_t f;
real t=RP_Get_Real("flow-time");
if ((t>=0) && (t<1))
    viscous_resistance=pow(10,10);
if ((t>=1) && (t<1.2))
    viscous_resistance=pow(10,10);
if ((t>=1.2) && (t<10))
    viscous_resistance=pow(10,10);
if ((t>=10) && (t<10.2))
    viscous_resistance=(t*-5*pow(10,10))+(5.1*pow(10,11);
if ((t>=10.2) && (t<20))
    viscous_resistance=0;
begin_f_loop(f,thread)
{
F_PROFILE(f, thread, index) = viscous_resistance;
}
end_f_loop(f, thread)
}
```

One-way lower pipe code

```
#include "udf.h"
DEFINE_PROFILE(viscosity_lower_1w, thread, index)
{
real viscous_resistance;
face_t f;
real t=RP_Get_Real("flow-time");
if ((t>=0) && (t<1))
    viscous_resistance=pow(10,10);
if ((t>=1) && (t<1.2))
    viscous_resistance=(t*-5*pow(10,10))+(6*pow(10,10));
if ((t>=1.2) && (t<10))
    viscous_resistance=0;
if ((t>=10) && (t<10.2))
    viscous_resistance=(t*5*pow(10,10))-(5*pow(10,11));
if ((t>=10.2) && (t<20))
    viscous_resistance=pow(10,10);
begin_f_loop(f,thread)
{
F_PROFILE(f, thread, index) = viscous_resistance;
}
end_f_loop(f, thread)
}
```

One-way through pipe

```
#include "udf.h"
DEFINE_PROFILE(viscosity_pipe_1w, thread, index)
{
real viscous_resistance;
face_t f;
real t=RP_Get_Real("flow-time");
if ((t>=0) && (t<1))
    viscous_resistance=0;
if ((t>=1) && (t<1.2))
    viscous_resistance=(t*5*pow(10,10))-(5*pow(10,10));
if ((t>=1.2) && (t<10))
    viscous_resistance=pow(10,10);
if ((t>=10) && (t<10.2))
    viscous_resistance=pow(10,10);
if ((t>=10.2) && (t<20))
    viscous_resistance=pow(10,10);
begin_f_loop(f,thread)
{
F_PROFILE(f, thread, index) = viscous_resistance;
}
end_f_loop(f, thread)
}
```

Two-way off-shoot pipe code

```
#include "udf.h"
DEFINE_PROFILE(viscosity_upper_2w, thread, index)
{
real viscous_resistance;
face_t f;
real t=RP_Get_Real("flow-time");
if ((t>=0) && (t<1))
    viscous_resistance=pow(10,10);
if ((t>=1) && (t<1.2))
    viscous_resistance=(t*-5*pow(10,10))+(6*pow(10,10));
if ((t>=1.2) && (t<10))
    viscous_resistance=0;
if ((t>=10) && (t<10.2))
    viscous_resistance=0;
if ((t>=10.2) && (t<20))
    viscous_resistance=0;
begin_f_loop(f,thread)
{
F_PROFILE(f, thread, index) = viscous_resistance;
}
end_f_loop(f, thread)
}
```

Two-way lower pipe code

```
#include "udf.h"
DEFINE_PROFILE(viscosity_lower_2w, thread, index)
{
real viscous_resistance;
face_t f;
real t=RP_Get_Real("flow-time");
if ((t>=0) && (t<1))
    viscous_resistance=pow(10,10);
if ((t>=1) && (t<1.2))
```

```
    viscous_resistance=(t*-5*pow(10,10))+(6*pow(10,10));
if ((t>=1.2) && (t<10))
    viscous_resistance=0;
if ((t>=10) && (t<10.2))
    viscous_resistance=(t*5*pow(10,10))-(5*pow(10,11));
if ((t>=10.2) && (t<20))
    viscous_resistance=pow(10,10);
begin_f_loop(f,thread)
{
F_PROFILE(f, thread, index) = viscous_resistance;
}
end_f_loop(f, thread)
}
```

Two-way through pipe

```
#include "udf.h"
DEFINE_PROFILE(viscosity_pipe_2w, thread, index)
{
real viscous_resistance3;
face_t f;
real t=RP_Get_Real("flow-time");
if ((t>=0) && (t<1))
    viscous_resistance3=0;
if ((t>=1) && (t<1.2))
    viscous_resistance3=(t*5*pow(10,10))-(5*pow(10,10));
if ((t>=1.2) && (t<10))
    viscous_resistance3=pow(10,10);
if ((t>=10) && (t<10.2))
    viscous_resistance3=pow(10,10);
if ((t>=10.2) && (t<20))
    viscous_resistance3=pow(10,10);
begin_f_loop(f,thread)
{
F_PROFILE(f, thread, index) = viscous_resistance3;
}
end_f_loop(f, thread)
}
```

Appendix G Kaplan bulb MATLAB code

MATLAB code for the Kaplan bulb fluid turbine

```
%% Kaplan bulb MATLAB code
Dp = 1.5;    % diameter of the turbine/pipe
g = 9.81;    % acceleration due to gravity
rho = 1000; % Density
Ho = 10;     % total head of the river
Sp = 60;     % synchronous speed of the turbine
N = 1;       % number of turbines

%%% efficiencies
np=0.98; % Generator efficiency
nt=0.995; % Transformer Losses
ng=0.972; % Gear Drive Train Losses
nw=0.95; % Water friction losses and turbine availability
visc = 0.001520; % viscosity of water @ 5 degrees
k = 0.025; % Roughness factor - Concrete - New, very smooth, smooth
joints
K = 0.5; % Pipe inlet coefficient
Ap = pi*Dp^2/4; % cross sectional area of the pipe
n11 = (Sp*Dp)/sqrt (Ho); % Calculate unit speed
 Q11 = (n11*0.016447368421) +0.555921; % Calculate unit discharge
(m^3/s)

            if Q11 > 4.75; Q11 = 4.75; end; % Limit to 4.75 m^3/s
            eta = 0.000000000000043175739746O819*(n11)^6 -...
                0.000000000070129382041258 6*(n11)^5 + ...
                0.000000046339908802 73*(n11)^4 - ...
                0.000015904035364132 4*(n11)^3+ ...
                0.002978758037031 02*(n11)^2 - ...
                0.288841272324706*(n11) + 12.2511011043316;
% Efficiency following max output curve

            if n11 < 180; eta = 0.88196; end;% Set to 88.2% for low
n11 -
            Q = sign(Ho)*(Dp^2)*Q11*sqrt(Ho);% Calculate discharge
(m^3/s) for single full size turbine
            Qdt  = Q*N;% discharge through all turbine
            Pw1  = rho*g*Q*Ho*eta*np*nw*ng*nt; % Turbine power j/s =
watt
            kW = Pw1/(1000); % kiloWatts
            TotalEff = eta*np*nw*ng*nt;
            vel = Q/Ap;

fprintf('Total Head = %3.2f m; Volumetric flow rate = %3.2f m^3/s;
Turbine kW = %5.2f; Efficency = %3.2f %%; ', Ho,Q,kW,TotalEff*100)
```